UNIVERSITY OF LJUBLJANA
BIOTECHNICAL FACULTY

Anja BLAŽIČ

CHANGES IN TRANSMEMBRANE VOLTAGE REGULATION DUE TO CELL ELECTROPORATION

DOCTORAL DISSERTATION

Ljubljana, 2025

UNIVERSITY OF LJUBLJANA
BIOTECHNICAL FACULTY

Anja BLAŽIČ

CHANGES IN TRANSMEMBRANE VOLTAGE REGULATION DUE TO CELL ELECTROPORATION

DOCTORAL DISSERTATION

SPREMEMBE V URAVNAVANJU TRANSMEMBRANSKE NAPETOSTI PO ELEKTROPORACIJI CELIC

DOKTORSKA DISERTACIJA

Ljubljana, 2025

Based on the Statute of the University of Ljubljana and the decision of the Biotechnical Faculty senate, as well as the decision of the Commission for Doctoral Studies of the University of Ljubljana adopted on 27th September 2023 it has been confirmed that the candidate meets the requirements for pursuing a PhD in the interdisciplinary doctoral programme in Biosciences, Scientific Field Cell Sciences. Assist. Prof. Lea Rems is appointed as supervisor.

Doctoral dissertation was conducted at the Laboratory of Biocybernetics, Faculty of Electrical Engineering, University of Ljubljana.

Supervisor:	Assist. Prof. Lea REMS, Ph.D.

Commission for assessment and defence:

President:	Prof. Marko KREFT, Ph.D. University of Ljubljana, Biotechnical Faculty, Department of Biology
Member:	Prof. Gregor SERŠA, Ph.D. Institute of Oncology, Department of Experimental Oncology
Member:	Assoc. Prof. Alenka MAČEK LEBAR, Ph.D. University of Ljubljana, Faculty of Electrical Engineering, Department of Biomedical Engineering

Anja Blažič

KEY WORDS DOCUMENTATION

ND Dd
DC 602.621:644.725.2(043.3)
CX electroporation, transmembrane voltage changes, cell membrane permeability, cell survival, cell invasion, ion channels
AU BLAŽIČ, Anja
AA REMS, Lea (supervisor)
PP SI-1000 Ljubljana, Jamnikarjeva 101
PB University of Ljubljana, Biotechnical Faculty, Interdisciplinary Doctoral Programme in Biosciences, scientific field Cell Sciences
PY 2025
TI CHANGES IN TRANSMEMBRANE VOLTAGE REGULATION DUE TO CELL ELECTROPORATION
DT Doctoral dissertation
NO X, 140 p., 15 fig, 2 ann., 196 ref.
LA sl
AL sl/en

Electroporation enables the increase in cell membrane permeability by exposing cells to high-voltage electric pulses and is widely used in medical procedures such as electrochemotherapy, non-thermal tumour ablation, and most recently for ablation of arrhythmogenic cardiac tissue. Despite its broad applications, the regulation of transmembrane voltage following electroporation remains incompletely understood. This dissertation aims to investigate how TMV is shaped and modulated after electroporation, and how these changes influence downstream cellular processes. It builds on three complementary studies. The first study examined alterations in TMV over 30 min after pulse exposure, demonstrating that post-pulse TMV dynamics are governed by an interplay between nonselective leak current due to membrane permeabilization and ion channel activation. The second study examined reversible electroporation in patient-derived glioblastoma cells, showing that electric field exposure can alter the invasive behaviour of surviving cells, with evidence implicating ion channels in this adaptive response. The third study explored pharmacological inhibition of voltage-gated sodium channels using lidocaine during electroporation, revealing that lidocaine can affect cell survival outcome through mechanisms that extend beyond simple ion channel modulation. Taken together, these studies provide an integrated view of how electrical stress translates into functional and phenotypic cellular changes. By linking TMV regulation to ion channel activity, invasive behaviour, and pharmacological modulations, the findings extend the mechanistic understanding of electroporation and suggest novel opportunities for therapeutic modulation, particularly in the context of glioblastoma.

KLJUČNA DOKUMENTACIJSKA INFORMACIJA

DN Dd
DK 602.621:644.725.2(043.3)
KG elektroporacija, spremembe transmembranske napetosti, prepustnost plazemske membrane, preživetje celic, invazija celic, ionski kanali
AV BLAŽIČ, Anja, mag. mikrobiol.
SA REMS Lea (mentorica)
KZ SI-1000 Ljubljana, Jamnikarjeva 101
ZA Univerza v Ljubljani, Biotehniška fakulteta, Interdisciplinarni doktorski študijski program Bioznanosti, znanstveno področje Znanosti o celici
LI 2025
IN SPREMEMBE V URAVNAVANJU TRANSMEMBRANSKE NAPETOSTI PO ELEKTROPORACIJI CELIC
TD Doktorska disertacija
OP X, 140 str., 15 sl., 2 pril., 196 vir.
IJ sl
JI sl/en
AI Elektroporacija je pojav, pri katerem pride do povečane prepustnosti celične membrane zaradi izpostavitve celic visokonapetostnim električnim pulzom. Pogosto se uporablja v medicini, med drugim pri elektrokemoterapiji, netermični ablaciji tumorjev ter v zadnjem času tudi pri ablaciji aritmogenega srčnega tkiva. Kljub široki uporabi pa regulacija transmembranske napetosti po elektroporaciji ostaja nepopolno pojasnjena. Namen te disertacije je bil raziskati spremembe in mehanizme transmembranske napetosti po elektroporaciji ter ugotoviti, kako te spremembe vplivajo na nadaljnje celične procese. Delo temelji na treh medsebojno dopolnjujočih se študijah.

V prvi študiji smo preučevali spremembe transmembranske napetosti v času 30 minut po izpostavitvi celic električnemu pulzu in pokazali, da dinamiko teh sprememb uravnava tako neselektivni tok ionov, ki nastane zaradi povečane prepustnosti membrane, kot tudi aktivacija ionskih kanalov. V drugi študiji smo ovrednotili vpliv reverzibilne elektroporacije na primarne humane glioblastomske celice ter pokazali spremembe v invazivnem vedenju preživelih celic, pri čemer je bilo nakazano, da so v te prilagoditvene odzive vključeni tudi ionski kanali.V tretji študiji pa smo raziskovali vpliv lidokaina, modulatorja napetostno odvisnih natrijevih kanalov, na elektroporacijo in pokazali, da lahko lidokain vpliva na preživetje celic prek mehanizmov, ki presegajo zgolj modulacijo ionskih kanalov. Skupaj rezultati teh študij ponujajo poglobljen vpogled v to, kako izpostavitev električnemu polju vpliva na spremembe v celičnih procesih in odzivu celic po elektroporaciji. Z razkrivanjem povezav med regulacijo transmembranske napetosti, delovanjem ionskih kanalov, invazivnostjo celic in farmakološko modulacijo odzivov na izpostavitev celic električnemu polju, ugotovitve v doktorski nalogi poglabljajo dosedanje razumevanje mehanizmov elektroporacije. S tem se odpirajo nove možnosti za terapevtsko modulacijo, zlasti pri zdravljenju glioblastoma.

TABLE OF CONTENTS

LIST OF SCIENTIFIC PAPERS

Blažič A., Guinard M., Leskovar T., O'Connor R. P., Rems L. 2025a. Long-term changes in transmembrane voltage after electroporation are governed by the interplay between nonselective leak current and ion channel activation. Bioelectrochemistry, 161: 108802, https://doi.org/10.1016/j.bioelechem.2024.108802

Blažič A., Majc B., Novak M., Breznik B., Rems L. Reversible electroporation enhances invasive properties of patient-derived glioblastoma cells. Radiology and Oncology, accepted for publication

Blažič A., Šmerc R., Polajžer T., Miklavčič D., Rems L. 2025b. Reassessing lidocaine as an electroporation sensitizer in vitro. Scientific Reports, 15, 1: 25593, https://doi.org/10.1038/s41598-025-11695-3

LIST OF FIGURES

LIST OF ANNEXES

ABBREVIATIONS

ATP	Adenosine triphosphate
DNA	Deoxyribonucleic acid
ECT	Electrochemotherapy
GB	Glioblastoma
GEVI	Genetically encoded voltage indicator
GET	Gene electrotransfection
H-FIRE	High-frequency irreversible electroporation
IRE	Irreversible electroporation
K_{Ca}	Calcium-activated potassium channel
MD	Molecular dynamics
PI	Propidium iodide
PFA	Pulsed field ablation
REC	Recurrent lesion
RNA	Ribonucleic acid
TMV	Transmembrane voltage
TEA	Tetraethylammonium
TRP	Transient receptor potential
V_{Ca}	Voltage-gated calcium channels
VSD	Voltage-sensing domain

1 INTRODUCTION

Understanding how cells generate and regulate electrical signals is essential for interpreting their behaviour in both physiological and non-physiological contexts. The transmembrane voltage (TMV) is a fundamental biophysical property that governs cellular homeostasis, signal transduction, and responsiveness to environmental stimuli. Additionally, supraphysiological TMV changes, induced by an external electric field, lead to the process of electroporation, which transiently disrupts membrane integrity and enhances molecular transport across the membrane. This introduction first outlines the fundamental principles of TMV generation and regulation under physiological conditions and highlights the connection between TMV and cellular responses. A detailed overview of electroporation mechanisms then follows, which describes how electroporation can affect the TMV dynamics through increased membrane permeability and ion channel activation. The chapter concludes by presenting the research objectives related to underpinning the mechanisms of electroporation-induced TMV changes and its downstream functional consequences, as well as exploring the effects of ion channel modulators on shaping electroporation outcomes.

1.1 TRANSMEMBRANE VOLTAGE: GENERATION, MAINTENANCE AND CELLULAR RESPONSE

1.1.1 Cellular electrophysiology

The TMV refers to the difference in electric potential across the cell plasma membrane. Since an electric potential difference is by definition termed voltage, “transmembrane voltage” more accurately describes this physical quantity than the commonly used alternatives “transmembrane potential” or "membrane potential". Throughout the text, we thus use the term TMV. However, when referring to transient changes in TMV in excitable cells, known as “action potentials”, we retain this conventional term due to its established use in the literature.

As a fundamental electrical property of all living cells, TMV plays a critical role in maintaining cellular function. TMV arises from the unequal distribution of ions, primarily sodium (Na^+), potassium (K^+), chloride (Cl^-), and calcium (Ca^{2+}), on either side of the plasma membrane and from the selective permeability of the membrane to these ions (Alberts, 2015; Kotnik et al., 2019). By convention, the transmembrane voltage is measured from the inside towards the outside of the cell; thus, a negative TMV indicates that the cell interior is electrically more negative than the exterior. In normal physiological state, the TMV in cells at rest can range between approximately –95 mV and –10 mV, depending on the cell type and its cell cycle phase (Hille, 2001; Neuroscience, 2004; Wright, 2004).

In non-excitable cells, TMV is involved in processes such as volume regulation, vesicle trafficking, and cell cycle progression, while in excitable cells (e.g., neurons, muscle and neuroendocrine cells), it is essential for action potential generation and electrical signalling. The interplay between ion gradients, membrane permeability, and cell signalling pathways enables TMV to serve as a sensitive indicator of the cell's physiological state and its response to changes in the intracellular and extracellular environment. Importantly, TMV also acts as a

regulatory signal influencing cellular behaviour (Blackiston et al., 2009; Hille, 2001; Sachs et al., 1974).Variations in TMV, whether transient or sustained, play a central role in regulating diverse aspects of cellular communication and adaptive responses, such as proliferation, differentiation, migration, and apoptosis (Alberts, 2015; Blackiston et al., 2009; Hille, 2001).

1.1.2 Cellular mechanisms of TMV generation and maintenance

The resting TMV is established and maintained through a combination of active and passive mechanisms. Central to this process is the sodium/potassium ATPase (Na^+/K^+-ATPase), which actively transports three sodium ions (Na^+) out of the cell and two potassium ions (K^+) in, consuming adenosine triphosphate (ATP) and generating a net negative charge inside the cell. This pump creates the electrochemical gradients that serve as the foundation for TMV. Additionally, the selective permeability of the membrane, particularly to potassium ions (K^+), plays an important role in setting the resting TMV. Potassium leak channels allow potassium ions (K^+) to move out of the cell down its concentration gradient, leaving behind negatively charged intracellular compartments, which contribute to the negative resting TMV, shown in Figure 1 (Alberts, 2015; Kotnik et al., 2019; Wright, 2004).

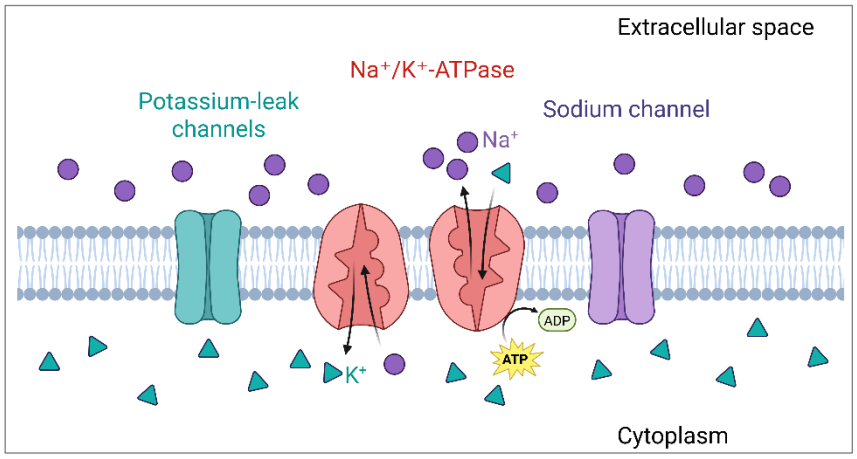

Figure 1: Membrane transport mechanisms underlying the resting TMV. The Na^+/K^+-ATPase maintains ionic gradients by exporting three Na^+ ions and importing two K^+ ions for each ATP molecule consumed. Additionally, passive efflux of K^+ through potassium-leak channels also contributes to the negative resting TMV. Although membrane permeability to Na^+ is low at rest, a minor inward sodium current may still occur. Created in BioRender.

Another important mechanism involves inwardly rectifying potassium (K_{ir}) channels, which favour inward over outward potassium movement. They conduct efficiently during membrane hyperpolarization, allow limited outward current near the resting TMV, and become progressively blocked at more depolarized voltages. Through this voltage-dependent behaviour, K_{ir} channels help stabilize the resting TMV and counteract depolarizing shifts (Alberts, 2015; Hille, 2001; Kotnik et al., 2019; Wright, 2004).

The resting TMV is most accurately described by the Goldman–Hodgkin–Katz equation:

$$\Delta V_m = \frac{RT}{F} ln \left(\frac{P_{K^+} [K^+]_o + P_{Na^+} [Na^+]_o + P_{Cl^-} [Cl^-]_o}{P_{K^+} [K^+]_i + P_{Na^+} [Na^+]_i + P_{Cl^-} [Cl^-]_i} \right) \quad \ldots (1)$$

In this equation, the following symbols are used:

V_m resting transmembrane voltage (V),
P_x relative membrane permeability for the major ions — K^+, Na^+ and Cl^-,
$[X]_i$ intracellular concentration of these ions — K^+, Na^+ and Cl^- (mM),
$[X]_o$ extracellular concentration of these ions — K^+, Na^+ and Cl^- (mM),
R universal gas constant (8.314 J/(K·mol)),
T absolute temperature (K),
F Faraday constant (96485 C/mol).

Whereas the Nernst equation defines the equilibrium TMV for a single ion species, the Goldman–Hodgkin–Katz equation integrates the contributions of several ions and thus provides a quantitative description of the resting TMV (Hille, 2001). Because the membrane at rest is most permeable to potassium ions (K^+), the potassium gradient has the strongest influence on the resting TMV, while the contributions of sodium (Na^+) and chloride (Cl^-) ions are less pronounced. Under resting conditions, the contribution of calcium ions (Ca^{2+}) is considered negligible because of its considerably lower extracellular and cytoplasmic concentrations compared with sodium (Na^+), potassium (K^+), and chloride (Cl^-) ions. Nevertheless, calcium plays a crucial role in intra- and intercellular communication, and it therefore serves as a second messenger.

The electrical properties of the plasma membrane are shaped by both its capacitance and resistance. Membrane capacitance, determined by the insulating nature of the lipid bilayer, influences the amount of charge required to change the TMV. In contrast, membrane resistance is governed primarily by the number and functional state of ion channels, which control the ease and speed of ion flow across the membrane. Together, these parameters regulate the dynamics and help stabilize the resting TMV. This stability is essential for maintaining the responsiveness of the cell to external signals, preserving internal homeostasis, and ensuring efficient transport and signal transduction (Hille, 2001; Neuroscience, 2004; Wright, 2004).

1.1.3 Cellular responses to changes in TMV

TMV is not only a passive electrical property but also a critical regulator of cellular activity. The most rapid and well-characterized changes in TMV are known as action potentials, which are the foundation of electrical signalling in excitable cells such as neurons, muscle and neuroendocrine cells. These brief, transient voltage spikes result from the coordinated opening and closing of voltage-gated ion channels, particularly those for sodium (Na^+), potassium (K^+), and calcium (Ca^{2+}) ions. Action potentials enable fast, long-distance communication within and between tissues, allowing for essential physiological functions such as nerve conduction, muscle contraction, and cardiac rhythm regulation. The timing of these events is tightly linked to the precise regulation of TMV, highlighting its central role in excitable tissue function (Armstrong and Hille, 1998; Hille, 2001).

Beyond rapid electrical signals, sustained or gradual changes in TMV can significantly influence cellular behaviour. In proliferating cells, membrane depolarization is often linked to cell cycle entry (Blackiston et al., 2009; Sachs et al., 1974; Yang and Brackenbury, 2013), while hyperpolarization is typically associated with cell cycle exit or differentiation (Sachs et al., 1974; Sundelacruz et al., 2009). During apoptosis, TMV destabilizes, and shifts in ion concentrations, particularly the efflux of potassium ions (K^+) and the influx of calcium ions (Ca^{2+}), act as early signals that initiate downstream cell death pathways. These voltage-dependent mechanisms highlight the importance of TMV in processes ranging from fast cellular signalling to long-term regulation of gene expression, metabolic processes, and signal transduction (Blackiston et al., 2009; Bortner and Cidlowski, 2007; Franco et al., 2006).

TMV also contributes to the control of cell migration and polarity, especially in dynamic processes like embryonic development, wound healing and tumour migration. Electrical gradients across tissues or within the local environment can direct cell orientation and movement, in part through their influence on cytoskeletal dynamics and ion transport at the leading and trailing edges of migrating cells (McCaig et al., 2009; Schwab and Stock, 2014; Zhao, 2009).

In the context of cancer, persistent membrane depolarization has been increasingly linked to a more invasive and metastatic phenotype. Depolarized TMV can promote epithelial-to-mesenchymal transition, enhance motility, and increase extracellular matrix remodelling, thereby facilitating tumour progression. These effects are often mediated or modulated by specific ion channels, which play critical roles in regulating cell volume, intracellular pH, and focal adhesion turnover — key processes in cellular invasion (Yang and Brackenbury, 2013).

More broadly, ion channels serve as essential integrators of intracellular and environmental signals, linking TMV fluctuations with diverse downstream responses. They regulate electrical excitability as well as key aspects of cell fate decisions, intercellular communication, and adaptive responses to stress. Dysregulation of ion channel expression or function is increasingly associated with pathological conditions, including cancer, neurodegeneration, epilepsy, and cardiovascular diseases (Amin et al., 2010; Lerche et al., 2013; Yang and Brackenbury, 2013).

Together, these observations emphasize that TMV is not only an electrical gradient, but a dynamic signalling pathway shaped by ion channel activity. Given its central role in regulating cellular function, external modulation, such as with electroporation, may profoundly affect cell behaviour and viability.

1.2 ELECTROPORATION AND ITS MOLECULAR MECHANISMS

Electroporation, also called electropermeabilization, is associated with the transient disruption of the cell membrane integrity caused by a strong electric field. Electroporation is a versatile technique applicable to virtually all cell types, including eukaryotic cells, bacteria, and archaea (Rems and Miklavčič, 2016). The cell membrane electrically behaves as a thin dielectric sheet; thus, exposure to an electric field induces a TMV, which, when sufficiently high, promotes the formation of nanoscale membrane defects or pores that increase the transport of ions and

various molecules (including dyes, antibodies, oligonucleotides, ribonucleic acid – RNA and deoxyribonucleic acid – DNA) across the cell membrane (Kotnik et al., 2019). In eukaryotic cells, the resting TMV typically ranges from -10 to -95 mV (depending on the cell type); meaning that the cell interior is electrically more negative than its exterior (Hille, 2001; Neuroscience, 2004). However, during electric field exposure, the induced voltage can exceed hundreds of millivolts, leading to structural perturbations in the cell membrane (Benz and Zimmermann, 1980). Whether electroporation is reversible or irreversible depends on the pulse parameters — electric field strength, duration, number, and frequency of the applied electric pulses, as well as other experimental factors. In reversible electroporation, cells recover and remain viable, while in irreversible electroporation, membrane damage leads to loss of homeostasis and cell death, as presented in Figure 2 (Kotnik et al., 2019).

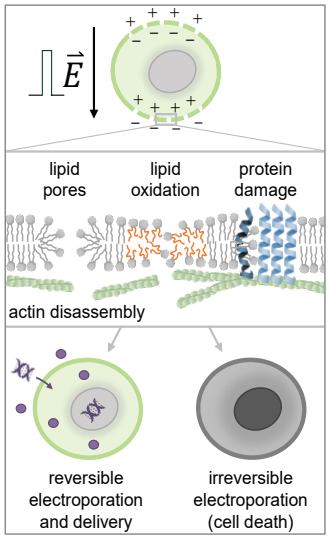

Figure 2: Schematic representation of electroporation – induced effects, including lipid pore formation in the cell membrane, lipid oxidation, disruption of the cytoskeleton, and protein damage. The outcome of electroporation, whether reversible or irreversible, depends on multiple parameters. Created in BioRender.

Electroporation can be achieved with pulses of various shapes and durations. Most often, monophasic or biphasic rectangular pulses are used, although exponentially decaying, sinusoidal, and triangular pulses achieve electroporation as well (Kotnik et al., 2003). The pulse duration can range from hundreds of picoseconds to hundreds of milliseconds. Important pulse parameters influencing electroporation also include pulse number and repetition rate. The extent of membrane permeabilization generally increases with electric field strength, pulse duration and the number of pulses, shifting the outcome from reversible towards irreversible electroporation (Rems and Miklavčič, 2016).

Electroporation induces effects on the membrane, including oxidative damage to membrane lipids, cytoskeletal disruptions, and modifications of transmembrane proteins (Kotnik et al., 2019; Vižintin and Miklavčič, 2022). This section outlines the fundamental mechanisms of electroporation, beginning with pore formation in the lipid bilayer and further addressing changes to membrane lipids, the cytoskeleton, and proteins, as illustrated in Figure 2.

1.2.1 Molecular mechanisms of electroporation

Historically, the first suggested mechanism underlying electroporation-induced membrane permeability was the formation of aqueous pores in the lipid bilayer (Neumann et al., 1982). When a cell is exposed to an external electric field, the TMV increases in absolute value due to the build-up of charged ions at the two sides of the cell membrane. If the TMV exceeds a certain value (reported between 0.2 and 1 V) (Tsong, 1991), pores are formed in the lipid bilayer and its permeability transiently increases. Molecular dynamics simulations reveal that pore formation begins with the alignment of water dipoles in the direction of the electric field, a process that occurs within picoseconds. This rapid molecular rearrangement is followed by a charge redistribution on both sides of the cell membrane. Water molecules then form hydrogen-bonded clusters, termed water fingers (Figure 3, b), which penetrate the hydrophobic core of the lipid bilayer from both intracellular and extracellular sides. As these structures grow, they eventually connect and form a continuous water column spanning the membrane (Figure 3, c). As a result, phospholipids reorganize themselves, orienting their polar head groups toward the water column to stabilize the pore structure and enable molecular transport (Casciola and Tarek, 2016; Vernier et al., 2013). Pore formation has also been experimentally visualized using TIRF microscopy in lipid bilayers (Sengel and Wallace, 2016), and more recently in cell membranes following the application of millisecond pulses (Silkunas et al., 2024). However, the exact nature and origin of these pores, whether they arise within the lipid bilayer or involve other membrane components, remains to be elucidated.

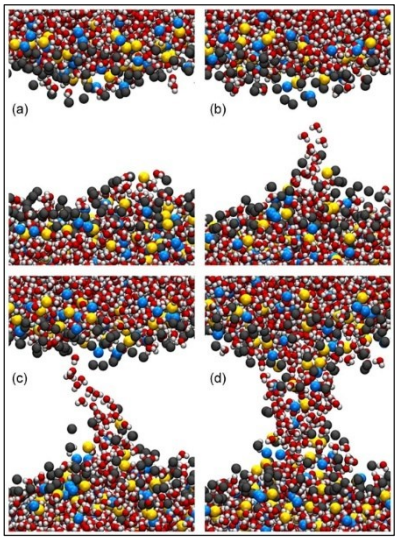

Figure 3: Molecular dynamics simulation of pore formation in a POPC bilayer. Water molecules (red/white), phosphorus (gold) and nitrogen (blue) atoms of the headgroups, and phospholipid acyl oxygens (gray) are shown; hydrocarbon chains are omitted for clarity. Electric field exposure triggers water entry into the bilayer (b), followed by its extension across the membrane (c), ultimately resulting in a hydrophilic pore stabilized by aligned headgroups (d). Complete pore formation occurs within 5 ns (Vernier et al., 2013).

To better understand the mechanisms of electroporation on a molecular and cellular level, it is important to emphasize that different processes are understood by the term electroporation, as discussed for many years (Abidor et al., 1993; Kinosita and Tsong, 1979; Pavlin et al., 2007; Pucihar et al., 2008; Teissié and Ramos, 1998; Weaver and Chizmadzhev, 1996) and then clearly experimentally demonstrated in 2015, when carefully designed electrophysiological

measurements were able to distinguish between transient electroporation and long-term sustained permeabilization of the cell membrane (Wegner et al., 2015). For the transient electroporation (detected during pulse application and within ~100 ms after the pulse), the researchers suggested that it is well explained by the classical electroporation theory – the formation of pores in the lipid domains of the cell membrane. On the contrary, the underlying mechanisms for sustained permeabilization, as well as prolonged membrane depolarization, occurring minutes after the pulse delivery, remain poorly understood and are likely to involve lipid oxidation, membrane protein damage, cytoskeletal rearrangement, enhanced endocytotic-like processes and the activation of ion channels and/or other membrane proteins (Burke et al., 2017; Dermol-Černe et al., 2018; Kotnik et al., 2019; Wegner et al., 2015).

The recovery of the membrane following electroporation is governed by mechanisms more complex than those predicted by existing theoretical models. While molecular dynamics simulations suggest that pores close within nanoseconds (Vernier et al., 2013), experimental studies show that increased membrane permeability can persist for minutes to hours after treatment (Dermol-Černe et al., 2018; Lopez et al., 1988; Pakhomov et al., 2007a). This prolonged duration varies with temperature and pulse parameters (Lopez et al., 1988; Pucihar et al., 2008), suggesting that additional biological processes contribute to membrane resealing, stabilization, and overall cellular recovery.

Extended membrane permeability following electroporation is accompanied by significant disruptions in ion homeostasis. The resulting influx of calcium (Ca^{2+}) and sodium (Na^{+}) ions, along with efflux of potassium (K^{+}) ions and ATP, alter TMV, trigger depolarization, and disturb osmotic balance, often leading to cell swelling. Beyond these immediate effects, electroporation initiates a broader cellular response known as the electropermeome, which includes the release of damage-associated molecular pattern molecules, activating signalling pathways, changes in gene expression, and initiating repair mechanisms. Together, these processes shape how cells respond to electroporation, determining whether they recover or undergo further stress-related changes (Vižintin and Miklavčič, 2022).

While some cells recover after electroporation, the molecular determinants that drive others toward cell death are still not fully elucidated (Batista Napotnik et al., 2021). Gene expression profiling has revealed that electroporation triggers a time-dependent sequence of cellular responses: genes associated with cell injury are activated immediately, followed by transient upregulation of apoptotic markers within hours, and later by expression of genes related to inflammation, regeneration, and immunogenic forms of cell death (Ringel-Scaia et al., 2019). A parallel *in vitro* study using viability, membrane integrity, and apoptosis assays further confirmed that the onset and type of cell death depend not only on pulse parameters but also on the specific cell type and timing of assessment (Peng et al., 2024). Together, these findings emphasize that electroporation-induced cell death or recovery is a dynamic, multistep process, shaped by both early biophysical damage and delayed cellular responses.

1.2.2 Chemical effects on the membrane lipids

The impact of electroporation on membrane lipids is an important aspect of the broader cellular response. Exposure to electric pulses during electroporation can generate reactive oxygen species (ROS), which may contribute to lipid oxidation and subsequent changes in membrane structure and function (Gabriel and Teissié, 1994). The cell membrane is composed of a phospholipid bilayer, embedded with proteins, sterols (such as cholesterol), and other biomolecules, all of which can be affected by oxidative stress (Kotnik et al., 2019).

The oxidation of membrane lipids, commonly referred to as lipid peroxidation, has been proposed as one of the mechanisms underlying prolonged membrane permeability following electroporation. During this process, lipid hydroperoxides are formed as primary products, which can further degrade into secondary reactive species, including aldehydes, ketones, alcohols, hydrocarbons, esters, furans, lactones, and peroxides (Balantič et al., 2023). These byproducts can interact not only with lipids but also with proteins, DNA, and other cellular structures, potentially contributing to broader functional alterations.

Although molecular dynamics simulations suggest that lipid hydroperoxides contribute to membrane destabilization, this may not fully account for the extent of electroporation-induced permeabilization observed experimentally (Rems et al., 2019). More recent studies have shown that secondary oxidation products, particularly lipid aldehydes, can accumulate at sufficient concentrations to directly induce pore formation, thereby providing a mechanistic link between oxidative damage and sustained membrane permeability (Wiczew et al., 2021).

In addition to phospholipids, sterols, particularly cholesterol, play a critical role in maintaining membrane integrity and organization. Cholesterol regulates lipid packing, contributes to membrane rigidity at physiological temperatures, and modulates the diffusion of water, ions, and small molecules (Chakraborty et al., 2020). Oxidation of cholesterol, either enzymatic or ROS-mediated, alters its structural and functional properties. The resulting oxidized derivatives, known as oxysterols, affect membrane behaviour differently depending on their specific modifications. For example, oxysterols with oxidized tails tend to reduce bilayer condensation while preserving overall membrane structure, whereas those with an oxidized tetracyclic ring have a more pronounced effect on membrane fluidity and permeability by disturbing phospholipid tail arrangement (Maxfield and Tabas, 2005).

Supporting the relevance of sterol oxidation in electroporation, it was demonstrated that the formation of oxysterols increases with the number of applied pulses, suggesting a dose-dependent relationship between electroporation intensity and cholesterol oxidation (Kaźmierska et al., 2012). This finding reinforces the notion that electroporation-induced oxidative processes may contribute to long-lasting changes in membrane permeabilization.

1.2.3 Cytoskeletal disruption and its consequences

Electroporation affects not only the plasma membrane but also internal cellular structures, including the cytoskeleton. This highly dynamic network, including actin filaments,

microtubules, and intermediate filaments, plays a critical role in maintaining cellular architecture, mechanical stability, intracellular transport, and membrane-cytoskeleton interactions. Experimental observations indicate that all major cytoskeletal components undergo transient structural disruptions upon exposure to electroporation pulses, with recovery occurring within a few hours (Graybill and Davalos, 2020; Kotnik et al., 2019).

The precise mechanisms behind this disruption remain under investigation. While some studies suggest that depolymerization of filamentous structures is secondary to ATP leakage, calcium (Ca^{2+}) ions influx, or cell swelling (Xiao et al., 2011), others provide evidence for a direct impact of the electric field on cytoskeletal proteins (Perrier et al., 2019). Disruption of cortical actin significantly decreases membrane stiffness following electroporation, attributed not only to filament breakdown but also to weakened attachment of actin to the membrane (Chopinet et al., 2014).

Within the cytoplasm, electroporation can disturb the structure and function of proteins involved in homeostasis, such as cytoskeletal elements, chaperones, and metabolic enzymes (Graybill and Davalos, 2020). Molecular dynamics (MD) simulations and experimental data (11 ns long pulses, 20 kV/cm, 1 Hz) suggest that nanosecond pulses can modify the conformation of β-tubulin and disrupt the interaction between tubulin and motor proteins like kinesin, potentially affecting intracellular trafficking and cell division (Chafai et al., 2019; Marracino et al., 2019). However, the simulated electric field is higher than typically used for electroporating cells.

Collectively, these findings emphasize that cytoskeletal disruption is a complex and multifactorial process, influenced by both the direct effects of the electric field and secondary consequences resulting from membrane permeabilization. This cytoskeletal disruption can compromise cell shape, mechanical properties, intracellular organization, and recovery capacity, making it a key aspect of the broader cellular response to electroporation.

1.2.4 Effects on the membrane proteins and their function

Exposure to pulses used for electroporation can activate or disable certain membrane proteins, including ion channels and transporters (Burke et al., 2017; Teissie and Tsong, 1980), which are essential for regulating ion gradients, signal transduction, and molecular transport. For instance, electric field strengths required to achieve electroporation are typically higher than those required for activation of voltage-gated sodium channels and the triggering of action potentials. Thus, electroporation treatments are often accompanied by pain and muscle contraction due to unwanted stimulation of nerves that are in the vicinity of the treated area (Cvetkoska et al., 2023). Electric field exposure can also trigger the opening of voltage-gated calcium channels, leading to a rapid influx of calcium (Ca^{2+}) ions and activation of downstream signalling pathways (Burke et al., 2017; Casciola et al., 2017, 2019; Craviso et al., 2010; Kotnik et al., 2019; Muratori et al., 2017; Pakhomov et al., 2017; Semenov et al., 2015a, 2015b). Apart from voltage-gated ion channels, many membrane proteins exhibit voltage sensitivity (Kasimova et al., 2018); thus, we can presume that their function could also be modulated during electroporation as well.

Additionally, the intense electric field used for electroporation can cause structural damage to membrane proteins. Electrophysiological measurements suggest that strong electric fields can induce electroconformational changes in voltage-gated ion channels (Chen W. and Lee, 1994a), leading to reduced channel conductance (Chen W. and Lee, 1994b; Nesin and Pakhomov, 2012). This has been reported for both sodium and potassium channels, occurring at field strengths above those required for electroporation but still below the thresholds for thermal injury (Chen W. et al., 1998). In this context, the disruption of ion channel function is considered a crucial mechanism of electrical injury, particularly in excitable tissues, where impaired excitability and altered ionic selectivity may persist long after the pulse has ended. A growing body of experimental studies shows that exposure to electroporating electric fields perturbs the function of certain types of ion channels (Azarov et al., 2019; Burke et al., 2017; Casciola et al., 2017, 2019; Chen W. and Lee, 1994b, 1994a; Chen W. et al., 1998; Craviso et al., 2010; Hristov et al., 2018; Huang et al., 2013; Muratori et al., 2017; Nesin and Pakhomov, 2012; Nesin et al., 2012; Pakhomov et al., 2017; Semenov et al., 2015a; Wang et al., 2009) as well as sodium-potassium ATPase (Teissie and Tsong, 1980).

Recent molecular dynamics simulations have revealed that the TMV induced by electroporating pulses can trigger pore formation not only in lipid bilayers but also within the voltage-sensing domains (VSDs) of voltage-gated ion channels (Rems et al., 2020; Ruiz-Fernández et al., 2021, 2023), as shown in Figure 4. These protein-associated pores — formed by lipid headgroup reorientation around destabilized VSD helices — tend to be more stable than lipid-only pores, providing an additional mechanism contributing to the persistent increase in membrane permeability associated with electroporation. While these denatured channels can contribute to the leak current across the permeabilized membrane, they also likely become dysfunctional, thereby altering voltage-dependent currents. This mechanistic insight is supported by various electrophysiological measurements (Chen W. and Lee, 1994b, 1994a, 1994a; Chen W. and Wu, 2006; Chen W. et al., 1998, 2006; Hristov et al., 2018; Nesin and Pakhomov, 2012; Nesin et al., 2012; Yang et al., 2017).

Together, these findings underscore the dual nature of electric field effects on membrane proteins, where low to moderate fields may lead to (electro)physiological ion channel activation, but stronger fields may cause functional damage of ion channels and contribute to long-lasting physiological disruptions.

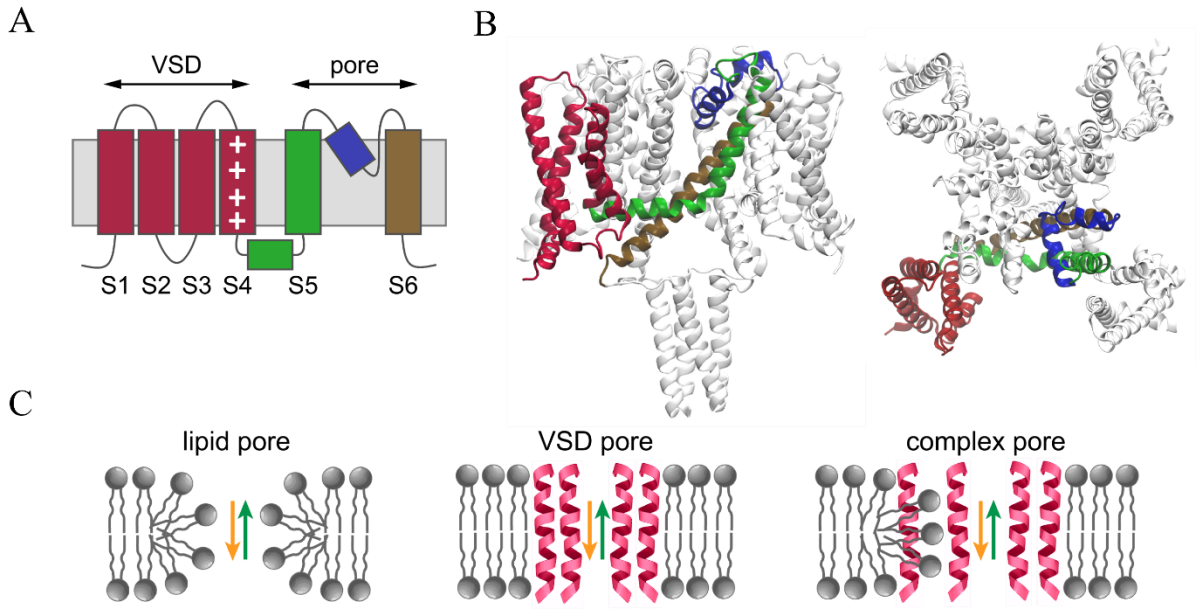

Figure 4: Voltage-gated ion channels as protein targets of pulsed electric fields: insights from molecular dynamics simulations. (A) Simplified schematic of a single subunit of a voltage-gated ion channel, showing the six transmembrane helices (S1–S6). The voltage-sensing domain (VSD) includes helices S1–S4, with S4 carrying positively charged residues that respond to transmembrane voltage changes. (B) Side view and extracellular view of the Na_VMs channel, indicating the segments of a single subunit: VSD (S1–S4) coloured in red, S5 together with S4–S5 linker in green, pore helix coloured in blue, and S6 in ochre. (C) Schematic representations of pore types observed in simulations: lipid pores, pores formed within the VSD, and complex pores involving both protein and lipid components. Simulations showed that VSD pores form when lipid headgroups penetrate and stabilize the disrupted helical structure, allowing ion conduction through the VSD. Notably, such VSD-associated pores appeared more stable than lipid pores. These MD findings provide a mechanistic explanation for experimental observations that electric fields can modulate or disrupt voltage-gated ion channel function. Figure 4 was assembled and adapted based on Figures 1 and 2 from Rems et al., 2020.

1.3 APPLICATIONS OF ELECTROPORATION

Electroporation, which can temporarily increase cell membrane permeability, is utilized across various fields for multiple applications. In biotechnology, it enables electro-transformation, microbial inactivation, biomolecule extraction, and accelerated biomass drying (Kotnik et al., 2015). It also plays a significant role in the food industry, where it enhances juice extraction, improves recovery of valuable compounds, and optimizes processes such as dehydration, cryopreservation, biorefinery applications, and meat processing (Mahnič-Kalamiza et al., 2014).

In the field of medicine, electroporation has introduced new therapeutic possibilities known as gene electrotransfer, electrochemotherapy, and non-thermal tissue ablation using irreversible electroporation (Chun et al., 2024; Geboers et al., 2020; Lambricht et al., 2016; Sardesai and Weiner, 2011; Sugrue et al., 2018; Yarmush et al., 2014). Its precision and minimally invasive nature have contributed to its growing use in clinical settings. The following sections explore electroporation-based medical applications, highlighting their underlying mechanisms, clinical advantages, and evolving therapeutic potential.

1.3.1 Electrochemotherapy (ECT)

Electrochemotherapy (ECT) combines chemotherapeutic agents, such as bleomycin or cisplatin, with electroporation to enhance intracellular drug accumulation and thereby increase drug cytotoxicity. ECT treatment is performed at moderate electric field strengths to achieve permeabilization while retaining high cell viability. In addition to its primary effect (i.e., enhanced chemotherapeutic uptake), ECT involves vascular changes and immune responses, contributing to long-lasting tumour protection (Bianchi et al., 2016; Kesar et al., 2023). In electroporation-based treatments, ECT was the first to reach clinical trials for melanoma, squamous cell carcinoma and basal cell carcinoma (Mir et al., 2006). Currently, it is implemented for the treatment of cutaneous and subcutaneous tumours in over 200 clinical institutions in the EU and is increasingly used for the treatment of deep-seated tumours, such as liver metastases (Geboers et al., 2020).

1.3.2 Gene electrotransfer (GET)

Gene electrotransfer (GET) is a non-viral method for introducing foreign nucleic acids into cells, enabling genetic modification without the use of viral vectors or chemical carriers. This technique has shown considerable promise due to its adaptability, efficiency, and cost-effectiveness (Geboers et al., 2020; Lambricht et al., 2016). It typically involves the application of monopolar millisecond (ms) electric pulses, which transiently increase cell membrane permeability and simultaneously generate an electrophoretic force driving negatively charged nucleic acids toward the membrane — thereby enhancing their uptake. Nevertheless, other types of pulses have been shown to achieve efficient GET (Potočnik et al., 2022). Although not yet part of standard clinical practice, GET is being actively investigated in over 100 clinical trials, particularly in the fields of cancer gene therapy and vaccine development.

1.3.3 Non-thermal ablation

Irreversible electroporation (IRE) is a non-thermal tumour ablation method that uses high-voltage electric pulses to induce cell death. Unlike thermal techniques, IRE preserves nearby critical structures such as blood vessels, bile ducts, and nerves, making it suitable for treating tumours in anatomically sensitive areas (Aycock and Davalos, 2019; Zhang et al., 2022). Clinically, IRE has been used to treat tumours in the liver, pancreas, kidney, and prostate (Aycock and Davalos, 2019; Ruarus et al., 2018). Additionally, IRE has established its potential role in the treatment of brain tumours, with encouraging results reported in preclinical animal models (Latouche et al., 2018; Rossmeisl et al., 2015).

Beyond oncology, the principles of IRE have also been adapted for use in cardiology through pulsed field ablation (PFA), a non-thermal approach to target abnormal heart tissue. PFA is recognized for its precision and safety, particularly in treating atrial fibrillation, as it minimizes damage to adjacent structures such as the oesophagus, phrenic nerve, and pulmonary veins, structures often at risk with traditional thermal methods like radiofrequency and cryoablation (Ekanem et al., 2024; Howard et al., 2020). Approved by the U.S. FDA in December 2023 and used in Europe since 2021 (Schmidt et al., 2023), PFA has demonstrated effective arrhythmia

control with minimal side effects. Its use in cardiology is expanding to treat various arrhythmias, including ventricular fibrillation, septal ablation, targeting the Purkinje network. Currently, PFA is rapidly emerging as a preferred technique for cardiac ablation (Chun et al., 2024).

1.4 RESEARCH OBJECTIVES

When a cell is exposed to an external electric field, the lipid bilayer behaves as a capacitor, resulting in rapid accumulation of charged ions on both sides of the membrane and a corresponding increase in TMV. This induced TMV develops with a characteristic membrane charging time (τ_m), which ranges from hundreds of nanoseconds to microseconds, depending on cell geometry and conductivity of the extracellular and intracellular media, and persists only during the presence of the external field (Kotnik et al., 2010; Pucihar et al., 2009). For an isolated spherical cell placed in a homogenous electric field, the induced TMV (ΔV_m) can be estimated using Schwan's equation:

$$\Delta V_m = \frac{3}{2} E R_{cell} \cos\theta \left(1 - exp(-t/\tau_m)\right) \quad \ldots (2)$$

In this equation, the following symbols are used:

ΔV_m induced transmembrane voltage (V),
E applied electric field strength (V/m),
R_{cell} cell radius (m),
θ angle between the direction of the electric field and the point on the cell membrane,
t time after electric field onset (s),
τ_m membrane charging time constant (s).

Equation (2) has been derived in a spherical coordinate system, where θ is the angle measured from the centre of the cell with respect to the direction of the electric field. As can be seen from equation (2), the induced TMV is proportional to the applied electric field strength and cell radius. Furthermore, it has the highest absolute values at the poles where the electric field is parallel to the membrane normal, i.e., at $\theta = 0^\circ$ and $\theta = 180^\circ$ (the "poles" of the cell) and in-between these poles it varies proportionally to the cosine of θ. It should be noted that the induced TMV is superimposed on the resting TMV. If the absolute value of TMV exceeds a critical threshold — typically between 0.2 and 1 V (Tsong, 1991) — transient aqueous pores form in the membrane, enabling nonselective transport of ions and molecules across the membrane and causing a rapid loss of membrane barrier function. This phenomenon is central to electroporation. Although the induced TMV dissipates rapidly after pulse exposure on the timescale of membrane discharge, the resulting increase in membrane permeability and its physiological consequences can persist considerably longer after the external field is removed (Kotnik et al., 2010, 2019). These consequences include the disruption of ionic gradients and consequently membrane depolarization. In other words, the TMV remains perturbed beyond the electric field exposure.

Several studies have investigated the dynamics of TMV change and recovery following exposure to intense pulsed electric fields. Electrophysiological recordings have shown that non-excitable cells require over 15 minutes to recover their resting TMV following exposure to nanosecond electric pulses (Pakhomov et al., 2007b). Similarly, prolonged membrane depolarization, lasting even more than 30 minutes, has been observed after exposure to pulses ranging from 10 ns to 10 ms in various cell types using a potentiometric dye (Dermol-Černe et al., 2018). Membrane depolarization and altered generation of action potentials have also been shown in cultured neurons (Pakhomov et al., 2017), primary cardiomyocytes (Chaigne et al., 2022; Neunlist and Tung, 1997), and cardiac tissue (Nikolski and Efimov, 2005). Initially, the observed membrane depolarization was mainly attributed to the nonselective leak current through pores formed in the plasma membrane by the electric field. Then, subsequent experiments in U-87 glioblastoma cells demonstrated that ion channels play an important role in prolonged membrane depolarization; by blocking different ion channels (voltage-gated potassium, calcium and TRPM8 channels) with drugs, it was possible to significantly inhibit membrane depolarization following exposure to a single 10 ns, 34 kV/cm pulse (Burke et al., 2017).

Understanding the mechanisms of TMV regulation after electroporation is important to decipher the functional response of cells to electroporation, since TMV acts as a critical regulator of cellular activity, as explained in Section 1.1.3. To this end, it is also crucial to develop a suitable methodology for monitoring prolonged changes in TMV due to electroporation. The patch clamp technique remains the gold standard for directly measuring TMV with high precision (Liu and Miller, 2020). However, it is an invasive and time-consuming (Liu and Miller, 2020), but its application in electroporation research is limited due to gigaseal disruption by high-voltage pulses and restrictions in pulse parameters that can be delivered without damaging the patch clamp amplifiers (Pakhomov et al., 2007a, 2009; Wegner et al., 2015). Voltage-sensitive dyes have been developed to allow non-invasive, real-time monitoring of TMV dynamics. These dyes were first introduced in the 1970s and have since been refined to improve their sensitivity, speed, and compatibility with various imaging modalities (Cohen et al., 1974; Ross et al., 1977). Based on their response mechanism, potentiometric dyes are generally divided into two classes: (i) slow-response dyes, which are translocated across the membrane via an electrophoretic mechanism altering their fluorescence, and (ii) fast-response dyes, which incorporate into the membrane and exhibit TMV-mediated fluorescence changes. The fast dyes typically operate through electric field-induced spectral shifts and voltage-dependent orientation or dimerization when bound to the membrane (Nikolaev et al., 2023). Compared to patch clamp, these optical techniques enable high-throughput, spatially resolved assessment of TMV changes across cell populations, making them especially useful in electroporation studies. Nevertheless, the measurements can be influenced by membrane damage, dye redistribution, and photobleaching, which must be carefully considered during experimental design (Jensen, 2012).

If ion channels play an important role in TMV regulation after electroporation, it is of particular interest to explore whether electroporation changes the ion channel expression profile and alters cells at a functional level. Electroporation has been shown to cause either downregulation or

upregulation of crucial sarco/endoplasmic reticulum Ca^{2+}-ATPase and Na^{+},K^{+}-ATPase isoforms in a cardiac cell line H9c2 (Jan et al., 2024). Additionally, it is important to evaluate how ion channel modulators may influence the cellular responses to electroporation. Understanding this influence is essential not only for elucidating the mechanisms governing TMV regulation but also has clinical relevance – particularly in patients receiving ion channel-targeting drugs such as sodium or calcium channel blockers (Lei et al., 2018; Moller and Covino, 1988; Pan et al., 2020). The presence of such pharmacological agents could potentially alter TMV dynamics, calcium uptake, or membrane permeability, and consequently cell viability following electroporation.

Given the background above, the following three objectives were defined within the disposition of the doctoral dissertation:

→ **Objective I:** To identify potentiometric dyes for monitoring transmembrane voltage alterations following electroporation using fluorescence microscopy.
→ **Objective II:** To assess the influence of ion channel modulators on changes in transmembrane voltage and associated cell responses after electroporation and vice versa.
→ **Objective III:** To identify whether and how electroporation induces changes in the expression of ion channels and/or pumps.

Objective I was addressed in the first publication titled: *"Long-term changes in transmembrane voltage after electroporation are governed by the interplay between nonselective leak current and ion channel activation"*. While this study primarily focused on characterizing the dynamics of TMV restoration up to 30 minutes after electroporation, we performed measurements with three fluorescent dyes: the slow-response FMP dye and two fast-response dyes, ElectroFluor630 and FluoVolt. We identified limitations of all tested dyes but found the slow-response FMP dye most suitable under our experimental conditions.

Objective II was partially addressed in the first publication, where we used inhibitors of voltage-gated calcium channels and calcium-activated potassium (K_{Ca}) channels, together with a theoretical model, to demonstrate that the TMV dynamics in U-87 MG glioblastoma cells are governed by activation of K_{Ca} channels after electroporation. **Objective II** was further addressed in the third publication, *"Reassessing lidocaine as an electroporation sensitizer in vitro"*, which examined the effect of lidocaine on electroporation outcomes across several cell lines. Lidocaine is primarily an inhibitor of voltage-gated sodium channels and is thus not expected to influence TMV considerably in non-excitable cells. However, it is commonly used as an anaesthetic in electroporation-based medical treatments. We chose lidocaine, since previous studies indicated that it could reduce the threshold electric field strengths required for both reversible and irreversible electroporation.

Objective III was addressed in the second publication *"Invasive properties of patient-derived glioblastoma cells after reversible electroporation"*. Building on findings from the first publication, this study explored whether reversible electroporation alters the invasive potential of patient-derived glioblastoma cells. We observed increased invasion and used transcriptomic analysis to confirm that this enhanced invasive behaviour was associated with changes in gene

expression. Notably, these expression changes included alterations in ion channel genes, supporting the connection between electroporation, ion channel modulation, and cellular function.

2 SCIENTIFIC PAPERS

2.1 LONG-TERM CHANGES IN TRANSMEMBRAN VOLTAGE AFTER ELECTROPORATION ARE GOVERNED BY THE INTERPLAY BETWEEN THE NONSELECTIVE LEAK CURRENT AND ION CHANNEL ACTIVATION

Blažič A., Guinard M., Leskovar T., O'Connor R. P., Rems L. 2025a. Long-term changes in transmembrane voltage after electroporation are governed by the interplay between nonselective leak current and ion channel activation. Bioelectrochemistry, 161: 108802, https://doi.org/10.1016/j.bioelechem.2024.108802

The induced transmembrane voltage during pulse delivery is well characterized, but less is known about how TMV behaves in the minutes following pulse exposure (Kotnik et al., 2010, 2019; Pucihar et al., 2009). A previous study suggested that prolonged TMV changes, particularly sustained membrane depolarization, may be influenced by ion channel activity (Burke et al., 2017). Therefore, our aim was to characterize the dynamics of TMV restoration up to 30 minutes after electroporation using two cell lines with distinct ion channel expression profiles: CHO-K1 and U-87 MG. 30-minute changes following electroporation were investigated through complementary approaches, including combined voltage-sensitive dye measurements with ion channel modulators, calcium and propidium iodide imaging, and theoretical modelling. We observed that CHO-K1 cells gradually repolarized as the membrane resealed, whereas U-87 MG glioblastoma cells exhibited a secondary hyperpolarization phase that depended on temperature and was consistent with the activation of calcium-activated potassium channels, suggesting that ion channel activity critically shapes long-term TMV recovery after electroporation.

Bioelectrochemistry 161 (2025) 108802

Contents lists available at ScienceDirect

Bioelectrochemistry

journal homepage: www.journals.elsevier.com/bioelectrochemistry

Long-term changes in transmembrane voltage after electroporation are governed by the interplay between nonselective leak current and ion channel activation

Anja Blažič [a], Manon Guinard [a], Tomaž Leskovar [a], Rodney P. O'Connor [b], Lea Rems [a,*]

[a] University of Ljubljana, Faculty of Electrical Engineering, SI-1000 Ljubljana, Slovenia
[b] Mines Saint-Etienne, Centre CMP, Département BEL, F-13541 Gardanne, France

ARTICLE INFO

Keywords:
Electroporation
Transmembrane voltage
Calcium
Temperature
Ion channels
Theoretical model

ABSTRACT

Electroporation causes a temporal increase in cell membrane permeability and leads to prolonged changes in transmembrane voltage (TMV) in both excitable and non-excitable cells. However, the mechanisms of these TMV changes remain to be fully elucidated. To this end, we monitored TMV over 30 min after exposing two different cell lines to a single 100 μs electroporation pulse using the FLIPR Membrane Potential dye. In CHO-K1 cells, which express very low levels of endogenous ion channels, membrane depolarization following pulse exposure could be explained by nonselective leak current, which persists until the membrane reseals, enabling the cells to recover their resting TMV. In U-87 MG cells, which express many different ion channels, we unexpectedly observed membrane hyperpolarization following the initial depolarization phase, but only at 33 °C and not at 25 °C. We developed a theoretical model, supported by experiments with ion channel inhibitors, which indicated that hyperpolarization could largely be attributed to the activation of calcium-activated potassium channels. Ion channel activation, coupled with changes in TMV and intracellular calcium, participates in various physiological processes, including cell proliferation, differentiation, migration, and apoptosis. Therefore, our study suggests that ion channels could present a potential target for influencing the biological response after electroporation.

1. Introduction

All cells maintain an electric potential difference across their plasma membranes, which results from the differences in membrane permeabilities for potassium, sodium, calcium and chloride ions. This potential difference is called the resting transmembrane voltage (TMV) and is maintained by a system of ion channels and pumps. In the normal physiological state, the resting TMV is negative, meaning that the cell interior is electrically more negative than its exterior. Changes in TMV have a fundamental biological function controlling the activity of various membrane proteins and act as an important biological signal closely associated with the cell cycle [1,2]. Furthermore, cells with less negative resting TMV (up to approximately −5 mV) tend to proliferate more, as observed in developing and cancerous cells [3]. Conversely, hyperpolarization (more negative TMV values, down to −90 mV) accelerates the cell differentiation process [4]. Therefore, changes in TMV can be used as an external signal to control cell proliferation, differentiation, and migration by continuous exposure (over hours) to low-intensity electric fields [1,5], a remarkable tool that is being actively explored for tissue engineering [6,7].

Long-term changes in TMV, persisting on the time scale of minutes, can also be observed after brief exposure to high-intensity pulsed electric field that result in electroporation. Electroporation is a phenomenon associated with increased plasma membrane permeability due to the creation of hydrophilic pores in the membrane lipid domains, lipid oxidation, and/or damage to certain membrane proteins, all promoted by the intense electric field [8]. Previous studies reported that electroporation is followed by prolonged membrane depolarization, lasting several minutes, both in excitable and non-excitable cells, as determined by potentiometric dyes [9] and electrophysiological measurements [10,11]. There is some evidence in the literature that these long-term changes in TMV might influence the progression of cells through the cell cycle. Electroporation with millisecond-duration electric pulses has been shown to initiate de-differentiation of cells in the limbs of newts, similar to that which occurs after limb amputation [12]. More recently, high-intensity nanosecond pulses have been shown to increase the

* Corresponding author.
E-mail address: lea.rems@fe.uni-lj.si (L. Rems).

https://doi.org/10.1016/j.bioelechem.2024.108802
Received 24 June 2024; Received in revised form 14 August 2024; Accepted 26 August 2024
Available online 30 August 2024

chondrogenic potential of mesenchymal stem cells and promote proliferation and differentiation of osteoblasts and myoblasts [13–16].

To systematically study the biological implications of long-term changes in TMV, it is of crucial importance to understand the underlying mechanisms by which electroporation alters the TMV. To this end, it is also important to establish or select an adequate methodology that allows one to monitor TMV after electroporation on a relevant time scale. While patch-clamp remains the golden standard for measuring the TMV [17], it has several limitations when it comes to electroporation research, including low throughput, perturbation of the gigaseal with high-voltage electroporation pulses and limitations on the pulse parameters that can be studied [18–20]. Another approach to measure changes in TMV is the use of voltage-sensitive fluorescent dyes. Based on their response mechanism, these dyes are divided into two classes: (i) slow-response dyes that translocate across the plasma membrane and consequently accumulate within the cells in a voltage-dependent manner, and (ii) fast-response dyes that incorporate into the membrane and have a voltage-dependent change in fluorescence emission. Fast-response dyes, such as FluoVolt and ElectroFluor630 (fluorinated version of the well-known ANEP dyes), were already used to monitor changes in action potential generation upon electroporation [21,22]. Slow-response indicators, such as the FLIPR Membrane Potential (FMP) dye, were used to detect long-term changes in TMV in excitable and non-excitable cells after exposure of cells to high-intensity pulsed electric field [9,23].

The FMP dye was originally developed for high throughput screening of ion channel activity using a plate reader [24–28]. The dye consists of two components, an anionic fluorescent voltage sensor molecule that enters the cells upon membrane depolarization and increases the cell fluorescence, and a quencher molecule that remains in the cell exterior and absorbs the fluorescence of the voltage sensor thus minimizing background fluorescence [9]. The FMP dye was demonstrated to be extremely sensitive showing a 50 % change in fluorescence per 10 mV [29]) with a large signal-to-noise ratio [30] and response time in seconds [29–31]. When compared with previously well-accepted dyes, like DiBAC4(3) [30,32–34] and dyes based on the FRET dye system [34], the FMP dye showed a greater sensitivity (response in fluorescence during membrane depolarization), a faster response time compared to DiBAC4 (3) and similar signal stability. Furthermore, an excellent correlation was shown between fluorescence changes and measurements made with the traditional patch clamp technique [29,30,33]. One of the limitations of the dye is that it can respond not only to changes in TMV at the plasma membrane but also to changes in TMV on the membranes of inner organelles [32].

Using the FMP dye, Burke et al. [23] demonstrated that prolonged membrane depolarization following pulse exposure was not solely associated with a nonselective leak current through pores in the plasma membrane, as previously thought [18,35,36]. Instead, they found that the observed depolarization may result from a more complex response involving the activation of multiple types of voltage-gated ion channels [23]. Their study exposed U-87 MG glioblastoma cells to a single 10 ns, 34 kV/cm pulse and monitored TMV changes over a 30-minute period. Inspired by this work, our primary objective was to further investigate mechanisms underlying long-term changes in TMV after exposing cells to 100 μs pulses. These longer pulses are more commonly employed in electroporation applications, including electrochemotherapy [37,38] and irreversible electroporation [39]. Following [23], we utilized the FMP dye to monitor TMV changes in U-87 MG cells, which express many different ion channels, and CHO-K1 cells, which express very low levels of endogenous ion channels. Our study delivers new insights into the mechanisms of TMV regulation after electroporation and identifies several challenges related to measuring electroporation-mediated long-term changes in TMV.

2. Materials and methods

2.1. Cell culture

Chinese hamster ovary cells (CHO-K1, #85051005) and human glioblastoma cells (U-87 MG, #9081402) were obtained from the European Collection of Authenticated Cell Cultures, Public Health England. They were grown in Ham-F12 (#N6658) and in EMEM (#51416C) medium, respectively. Both growth media were supplemented with 10 % fetal bovine serum (#F9665 for CHO-K1 and #F2442 for U-87 MG), L-glutamine (#G7513) and antibiotics (Penicillin-Streptomycin, #P0781, and Gentamicin, #G1397). All listed media and supplements were from Sigma-Aldrich, Germany. Cells were routinely passaged every 3 to 4 days, and passages between 5–30 were used for experiments. For experiments, cells were first trypsinized and counted. Afterwards 1.25×10^4 cells/3 days or 0.625×10^3 cells/4 days (CHO-K1) and 1×10^5 cells/3 days or 5×10^4 cells/4 days (U-87 MG) were seeded in Nunc Lab-Tek II chambered coverglass (Thermo Scientific™, #154461) and were grown in a humidified environment at 37 °C and 5 % CO_2.

2.2. Electric pulses

The cells were exposed to a single 100 μs electric pulse of chosen amplitude (70–630 V), delivered by a pulse generator B10 HV-LV (Leroy Biotech, France) or L-POR V0.1 (mPOR, Slovenia), through a pair of parallel Pt-Ir wire electrodes with wire diameter of 1 mm and the distance between inner edges of the electrodes of 2 mm. Delivered current and voltage were routinely monitored by the oscilloscope Wavesurfer 422, 200 MHz, the current probe CP030 and the differential probe ADP305 (all from LeCroy, USA), as per recommendations [40]. The electric field to which the cells were exposed was estimated as the ratio between the applied voltage and the interelectrode distance.

2.3. Electroporation buffer

Live Cell Imaging Solution (LCIS; Molecular Probes, #A14291DJ; composition: 140 mM NaCl, 2.5 mM KCl, 1.8 mM $CaCl_2$, 1.0 mM $MgCl_2$, 20 mM HEPES, pH 7.4, 300 mOsm), supplemented with 200 g/ml D-glucose (Gibco, #A2494001) in final 5.5 mM concentration, was selected as the electroporation buffer based on previous studies [9,23]. We did not use the growth medium for electroporation, since U-87 MG cells showed morphological changes (cell rounding and detachment) after several minutes of exposure to their growth medium (EMEM) at ambient conditions, likely due to the poor pH buffering capacity of the bicarbonate buffer at ambient CO_2 (Suppl. Material 1, Fig. S1.1a). Moreover, U-87 MG cells exhibited significantly lower cell survival when electroporated in EMEM compared with LCIS (Suppl. Material 1, Fig. S1.1b, c).

2.4. Temperature control

For experiments, the cells were first stained with selected dye (see sections 2.5-2.8), then the electrodes were positioned into the imaging chamber, and the chamber was placed on the microscope stage inside the microscope's incubator i8 Black (PeCon, Germany), as presented in Fig. 1a. Before time-lapse imaging, the cells were left for 5 min to equilibrate within the microscope's incubator. The incubator was either kept at room temperature, or at controlled temperature of 37 °C using the TempController 2000–2 (PeCon, Germany). The sample temperature was measured using a fiber optic temperature sensor (MPK-5, OpSens Solutions, Canada), see Suppl. Material 1, Fig. S1.3. At room temperature, the sample temperature was $T_{room} = 25.3 \pm 1.4$ °C (mean ± s.d.). At controlled temperature, the sample temperature was lower than 37 °C due to water evaporation from the open imaging chamber (the chamber could not be closed due to the presence of the electrodes). However, the

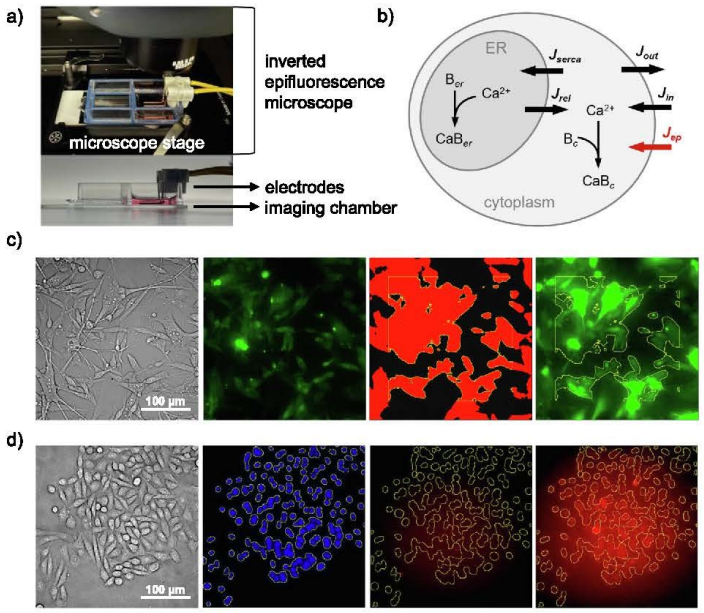

Fig. 1. Methodology. a) Experimental configuration – imaging chamber placed on the microscope stage (top) and side view of the position of electrodes within the chamber (bottom). b) Scheme of the theoretical model used to support experimental data. c) Image processing approach for determining the fluorescence of cells stained with FMP, Fluo4, and TMRE dye. An example is shown for U-87 MG cells stained with FMP dye. From left to right: brightfield image, baseline fluorescence, mask to determine the ROI corresponding to cells, maximum fluorescence reached after pulse application. d) Image processing approach for determining the fluorescence of cells stained with PI and Hoechst. Example is shown for CHO-K1 cells. From left to right: brightfield image, image of Hoechst-stained cell nuclei used to determine the ROI (yellow), baseline PI fluorescence, and PI fluorescence after pulse application at the end of 30 min time-lapse recording. Further details on the image analysis are given in Suppl. Material 2. Statistically significant differences (*: $p < 0.05$) were determined by *t*-test.

sample temperature was stable and repeatable and equal to $T_{ctrl} = 33.3 \pm 0.2$ °C.

2.5. Monitoring changes in transmembrane voltage (TMV)

For monitoring changes in TMV we used the FMP dye. FMP dye stock solution was prepared by dissolving the Component A of the FLIPR Membrane Potential Assay Red (Molecular Devices, #R7291) by adding 1 ml sterile distilled water (B.Braun, Germany) to the vial. The stock solution was mixed, aliquoted, and stored at −20 °C. To prepare the staining solution, 0.5 µL of the stock solution was dissolved in LCIS. Cells grown in the imaging chamber were stained for 30 min at 37 °C and 5 % CO_2.

Imaging was done on the Leica Thunder Imaging System with DMi8 inverted epifluorescence microscope and LED8 illumination source controlled by Las X software (all from Leica Microsystems, Germany) under 40x objective magnification. Time-lapse recordings were 30 min long, with 1 frame captured each 30 s. When monitoring the response to an electric pulse, this pulse was applied at time 1.5 min after the start of time-lapse recording. Additional brightfield and fluorescence snapshots of cells were taken before and after the time-lapse. The FMP dye was excited with green LED (554/24 nm) and its fluorescence was passed through the Leica multiband filter DFT51010 and an additional band-pass filter at 590/50 nm and detected with the Leica DFC9000 Gt camera.

The change in TMV was also measured in response to chemical depolarization by exposing cells to a mixture of 140 mM KCl and 2.5 mM NaCl, prepared by dissolving 1 M KCl (Sigma-Aldrich, #59222) and 5 M NaCl (Sigma-Aldrich, #58221) in sterile distilled water (B.Braun). After staining the cells with FMP dye, the staining solution was replaced by 125 µL of 140 mM NaCl. The imaging chamber was placed on the microscope stage and the cells were imaged at 1 frame per 5 s for 5 min. 30 s after the beginning of the time-lapse imaging, 875 µL of 160 mM KCl was added to the imaging chamber to a final concentration of 140 mM KCl. The NaCl and KCl solutions also contained the FMP dye (0.5 µL/1 ml), which ensured a consistent dye concentration, despite the change of solution.

In some experiments we also used ion channel inhibitors including, tetraethylammonium – TEA (Sigma #T2265) prepared in the sterile distilled water (B.Braun, Germany), Penitrem A (Sigma, # SI-P3053) prepared in DMSO (Sigma, #D2650), and Verapamil (Sigma, #V4629). The final concentration of ion channel inhibitors (TEA – 50 mM, Penitrem A – 2.5 µM, Verapamil – 2.2 µM) in the sample was selected following a previous study [23] and was added to the imaging chamber 5 min before commencing time-lapse imaging. The final concentration of DMSO in the sample did not exceed 1 %.

2.6. Monitoring propidium uptake

To detect changes in membrane permeability due to electroporation we used Propidium Iodide (PI; Molecular Probes, #P1304MP). To keep these experiments similar to those used for measuring the changes in TMV and intracellular calcium, which required ≥ 30 min staining steps (Sections 2.5 and 2.7, respectively), the cells were first incubated in 1 ml LCIS for 30 min at 37 °C and 5 % CO_2. The last 5 min of this incubation, we stained the cells with Hoechst 33342 (Thermo Fisher, #62249) at a

final concentration of 4 μM. Cells were washed with 1 mL LCIS and PI was added to the cells in LCIS at a final concentration of 30 μM. The cells were then handled and imaged in the same way as used for measurements with FMP dye (see Section 2.5), except for the following differences in the imaging settings: PI and Hoechst were respectively excited with green LED (554/24 nm) and violet LED (391/32 nm), and the fluorescence was passed through the DFT51010 filter with additional bandpass filter at 590/50 nm (for PI) and 460/80 nm (for Hoechst).

2.7. Monitoring intracellular calcium transients

To detect changes in intracellular calcium, cells were stained with 2 μM Fluo4-AM (Life Technologies, #F14217) in 1 ml LCIS at 37 °C and 5 % CO_2 for 45 min. For CHO-K1 cells only, we also added 2 μM Pluronic (Molecular Probes, #P3000MP) to facilitate staining. The cells were then handled and imaged in the same way as for measurements with FMP dye (see Section 2.5), except for the following differences in the imaging settings: Fluo4 was excited with blue LED (479/33 nm) and its fluorescence was passed through the DFT51010 filter with additional bandpass filter at 535/70 nm. In addition to 30 min time-lapse imaging at 1 frame per 30 s, we also captured shorter 5 min time-lapse images with faster imaging rate of 1 frame per 3 s.

After the 30 min time-lapse recordings, short-term cell survival was assessed by PI uptake, where Triton X-100 (Fluke, #93420) was used as positive control (see Suppl. Material 1, Section 2 for further details).

2.8. Monitoring changes in mitochondrial transmembrane voltage

U-87 MG cells were stained with 50 nM TMRE (Molecular Probes, #T669) in LCIS at 37 °C and 5 % CO_2 for 20 min. After staining, the cells were washed and imaged in LCIS with the same imaging settings as used with the FMP dye (see Section 2.5).

For a positive control, the proton ionophore uncoupler of oxidative respiration carbonyl cyanide 3-chlorophenylhydrazone (CCCP; Sigma-Aldrich, #C2759) was added to the TMRE-stained cells at 20 mM concentration for 5 min [41].

2.9. Image analysis

Fluorescence images were analyzed in ImageJ Fiji [42]. For FMP, Fluo4 and TMRE, the region of interest (ROI) corresponding to cells was determined based on automatic thresholding of the first image in the time-lapse sequence (Fig. 1c). For PI, the ROI corresponding to the cell nuclear area was determined based on Hoechst images captured before and after PI time-lapse, since the cells exhibited practically no baseline PI fluorescence (Fig. 1d). Further processing was the same for FMP, Fluo4, TMRE and PI. The determined ROI was applied to all images in the time-lapse to determine the mean fluorescence of the cells $F(t)$. Another ROI outside the cell region was manually selected to determine the background intensity $F_B(t)$. The change in fluorescence with time was determined as $\Delta F(t) = (F(t) - F_B(t)) - (F(t=0) - F_B(t=0))$. Further details on the image analysis with representative examples are provided in the Suppl. Material 2.

2.10. Statistical analysis

All results presented in the paper are based on at least three independent experimental repetitions, performed on different days. Statistical analysis was performed using SigmaPlot 11.0 (Systat Software, USA). Analysis was always carried out for each cell line separately. Baseline FMP fluorescence was compared between different temperatures (T_{room} and T_{ctrl}) using t-tests. Results of time-lapse recordings captured at different temperatures were analyzed using Two-way ANOVA (temperature and time as factors) with Holm-Sidak method for pairwise multiple comparison. Three to four time points after the start of the imaging were selected for comparison: for FMP signal at 1 min (before pulse application), 7 min (peak value), 15 min (minimum value) and 30 min (last value); for PI at 1 min and 30 min; and for Fluo4 at 1 min, 1.67 min (peak value), and 30 min (last value) for 30 min time-lapses or at 1 min, 1.65 min (peak value), and 5 min (last value) for 5 min time-lapses. Results from monitoring TMV in response to pulses with different amplitudes were analyzed with One-way ANOVA. Specifically, the minimum value of the FMP fluorescence obtained for each pulse amplitude was compared to the control condition (0 V/cm). Similarly, the maximum value of FMP fluorescence obtained for each pulse amplitude was compared to that observed using chemical depolarization.

A normality test using the Shapiro-Wilk method and equal variance test were carried out prior to conducting any specific statistical analysis. If normality and/or equal variance tests failed, nonparametric tests were performed: Mann-Whitney Rank Sum test (instead of t-test) and ANOVA on ranks (instead of One-way ANOVA and Two-way ANOVA). Statistically significant difference was considered for $p < 0.05$.

2.11. Theoretical modeling

For modeling the change in TMV due to electroporation, we built upon the model of Catacuzzeno et al. [43], which was originally developed to describe the role of calcium-activated potassium channels in intracellular Ca^{2+} oscillations in non-excitable cells in response to hormone stimulation. Full details of the original model and our additions, together with all model equations and parameters, are given in the Suppl. Material 3. Briefly, the model includes four relevant fluxes contributing to the intracellular Ca^{2+} dynamics (all in units of mol·m^{-2}·s^{-1}): J_{in} describes the Ca^{2+} influx through ion channels in the plasma membrane; J_{out} describes the extrusion of Ca^{2+} by plasma membrane Ca^{2+}-ATPases; J_{rel} describes the release of Ca^{2+} from the endoplasmic reticulum (ER); and J_{serca} describes the reuptake of Ca^{2+} into ER by the Ca^{2+}-ATPase SERCA. The model also includes Ca^{2+} binding to Ca^{2+} buffers (B) present in the cytoplasm and ER (Fig. 1b). We added another Ca^{2+} flux across the plasma membrane through N_{pores} with radius r_p (m) formed due to electroporation, derived based on Nernst-Planck description of electro-diffusion [44,45]:

$$J_{ep,Ca} = \frac{N_{pores}\pi {r_p}^2}{A_{pm}} D_{p,Ca} \frac{u_m + \ln(\chi)}{d_m} \frac{\chi - 1}{\ln(\chi)} \frac{[Ca]_e - [Ca]_i \exp(u_m)}{(1 - \chi \exp(u_m))} \quad (1)$$

Parameters A_{pm} (m^2) and d_m (m) are the plasma membrane area and membrane thickness, respectively; $[Ca]_e$, $[Ca]_i$ (mol·m^{-3}) are the extracellular and intracellular Ca^{2+} concentrations, $D_{p,Ca}$ (m^2·s^{-1}) is the diffusion coefficient of Ca^{2+} inside a pore, χ is the ratio between the extracellular and intracellular conductivity, and u_m is the non-dimensionalized TMV. The dynamic changes in TMV, denoted by U_m (V), were described by [43]

$$\frac{dU_m}{dt} = -\frac{1}{C_m}\left(g_{Ca0}(U_m - U_{Ca}) + g_{K,Ca}(U_m - U_K) + g_L(U_m - U_L) + g_{ep}U_m\right) \quad (2)$$

where C_m (F) is the plasma membrane capacitance; g_{Ca0}, $g_{K,Ca}$, and g_L (S) are the maximum conductances of calcium channels, calcium-activated potassium channels, and leak channels, respectively, whereas U_{Ca}, U_K, and U_L (V) are the reversal potentials for the corresponding ions. The last term $g_{ep}U_m$ describes the nonselective current due to electroporation, where g_{ep} (S) is the conductance of N_{pores} that reseal with the resealing function $f_{resealing}(t)$:

$$g_{ep} = N_{pores}\frac{2\sigma_p \pi {r_p}^2}{\pi r_p + 2d_m} f_{resealing}(t) \quad (3)$$

where s_p (S/m) is the effective conductivity inside the pore [46]. The resealing functions considered in the model are given later in Eqs. (4) and (5). The model was implemented and solved in Matlab R2021b

(MathWorks, USA).

3. Results and discussion

The aim of our study was to investigate the mechanisms of long-term changes in TMV after exposing CHO-K1 and U-87 MG cells to a conventional 100-μs-long electroporation pulse using the FMP dye. As we discovered that temperature affected our measurements, we first examined the influence of temperature on the baseline FMP fluorescence (Section 3.1) and on the measured cell response to an electric pulse (Section 3.2). While CHO-K1 cells responded to pulse exposure with an increase in FMP fluorescence, indicating the expected prolonged depolarization [9], U-87 MG cells kept at 33 °C unexpectedly exhibited a decrease in FMP fluorescence below baseline following the initial increase. We hypothesized that this decrease could be an artifact of FMP quencher uptake through the electroporated cell membranes. By conducting additional experiments using pulses of increasing amplitudes (Section 3.3) and employing theoretical modeling combined with experiments using ion channel inhibitors (Section 3.4), we concluded that the observed decrease in fluorescence signal is not an artifact but indicates membrane hyperpolarization due to activation of calcium-activated potassium channels. In Section 3.5, we discuss the challenges of monitoring electroporation-mediated long-term changes in TMV using the FMP dye and other dyes tested in our experiments, and propose further research directions.

3.1. FMP dye baseline fluorescence spontaneously increases at room temperature

In our preliminary experiments at room temperature ($T_{room} = 25.3 \pm 1.4$ °C), we observed that cells stained with the FMP dye often exhibit a spontaneous increase in fluorescence over time. We hypothesized that this might be associated with non-physiological temperature, since the activity of ion channels and pumps that control the TMV decrease their activities at lower (T_{room}) temperatures [47–49]. To test this hypothesis more systematically, we controlled the temperature of the air in the incubator that surrounds the microscope stage, which resulted in sample temperature of $T_{ctrl} = 33.3 \pm 0.2$ °C. At T_{ctrl}, the FMP fluorescence signal was stable for at least 30 min in both CHO-K1 and U-87 MG cells (Fig. 2a, red lines). In contrast, when CHO-K1 cells were imaged at T_{room}, their fluorescence gradually increased over 30 min (Fig. 2a, gray lines). Interestingly, U-87 MG cells not only exhibited a gradual increase in fluorescence at T_{room}, but were also considerably brighter at the start of the imaging. Note that we started the imaging 5 min after placing the sample on the microscope stage, to allow the temperature to equilibrate within the microscope's incubator; thus, the cells were already exposed to T_{room} (or T_{ctrl}) during this time.

To further confirm the observed increased baseline fluorescence in U-87 MG cells at T_{room}, we analyzed a larger number of CHO-K1 and U-87 MG samples. All samples were first stained at 37 °C, positioned on the microscope stage and then imaged 5 min later on the microscope, at either T_{room} or T_{ctrl}. The analysis demonstrated that the temperature significantly affected the baseline fluorescence in both CHO-K1 (*t*-test, $p < 0.001$) and U-87 MG (*t*-test, $p < 0.001$). In U-87 MG cells the baseline fluorescence was also considerably more scattered at T_{room} (Fig. 2b), reflecting greater deviations in T_{room} compared to T_{ctrl}.

3.2. The effects of temperature on the cell response to 100 μs, 1.4 kV/cm pulse: TMV, propidium uptake, and Ca^{2+} transients

The spontaneous increase in FMP fluorescence, shown in Fig. 2a, could be due to the spontaneous depolarization of cells at T_{room} or other effects of temperature on the permeation of the FMP voltage sensor molecule across the cell membrane. We explored this further by studying the effect of temperature on the response of cells to a single 100 μs, 1.4 kV/cm pulse. The chosen pulse amplitude was high enough to result in electroporation of ~40 % of both CHO-K1 and U-87 MG cells in suspension, detected through PI uptake (see Suppl. Material 1, Fig. S1.1). Note that cells attached to surfaces, as used in these experiments, electroporate at even lower electric fields than cells in suspension due to their elongated shape [50].

Changes in TMV were monitored for 30 min at T_{room} and T_{ctrl}. For both cell lines we observed that the pulse exposure triggered prolonged membrane depolarization, lasting minutes after the pulse delivery, both at T_{room} and T_{ctrl}. The maximum increase in FMP fluorescence was observed within 10 min after pulse application and was higher in both cell lines at T_{room}. The latter indicated that the FMP dye differentially stains cells at different temperatures since subsequent experiments with chemical depolarization demonstrated that both cell lines became fully depolarized at T_{ctrl} under these pulsing conditions (see Section 3.3). Furthermore, the temperature greatly influenced the recovery of the FMP signal. At T_{room}, the observed signal did not fully recover to the baseline in either of the cell lines within 30 min. This can be largely attributed to the gradual increase in the baseline FMP fluorescence (Fig. 2a); however, it is also possible that the cells were not able to fully restore their resting TMV at T_{room}. In contrast, at T_{ctrl}, the signal in CHO-K1 cells returned to its baseline ~20 min after the pulse. In U-87 MG cells, the signal even decreased below the baseline, reaching the lowest

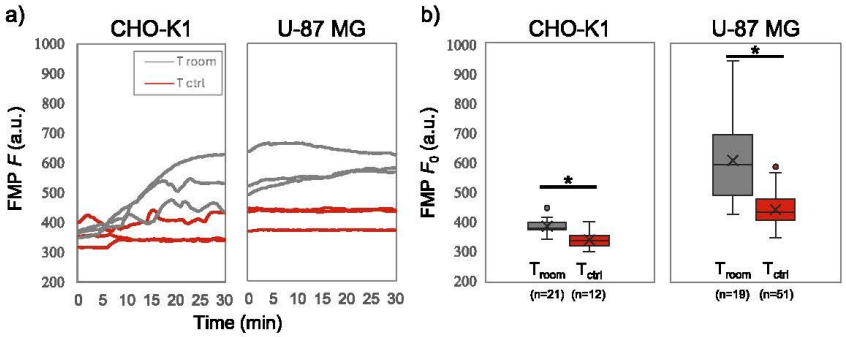

Fig. 2. Temperature-dependent stability of the baseline FMP fluorescence signal. a) Signal in CHO-K1 and U-87 MG cells on a 30-minute time scale at T_{room} (grey lines) and T_{ctrl} (red lines). b) Boxplots showing the fluorescence of CHO-K1 and U-87 MG cells, captured 5 min after placing a sample on the microscope stage at T_{room} or T_{ctrl} (this time corresponds to 0 min in panel a). Note that some of the curves for CHO-K1 in panel a) have small peaks; this was due to small spontaneous activity (small changes in TMV) of CHO-K1 cells that were not observed in U-87 MG (Suppl. Material 1, Section 4).

value 15 min after the pulse, followed by a subsequent increase towards baseline. Faster recovery of TMV at T_{ctrl} compared with T_{room} was expected due to a greater activity of ion channels and pumps that control and restore the resting TMV [47]. Nevertheless, the decrease below baseline in U-87 MG cells indicating transient membrane hyperpolarization was not expected, since previous studies reported only membrane depolarization following electroporation [9,10,10,11,23]. Statistical analysis confirmed significant differences between responses at T_{room} and T_{ctrl} at 1 min ($p = 0.010$), 15 min ($p = 0.001$) and 30 min ($p = 0.04$) in U-87 MG cells. In contrast, in CHO cells we confirmed statistically significant differences only at 1 min ($p = 0.007$) and 30 min ($p = 0.002$).

To shed more light on the difference in TMV responses between T_{room} and T_{ctrl} and between CHO-K1 and U-87 MG cells, we also monitored the time-dependent increase in membrane permeability due to electroporation using PI and keeping other conditions the same as when monitoring the changes in TMV. PI is a nucleic acid stain that can only enter cells with permeabilized membranes. In both cell lines the PI uptake was somewhat higher at T_{room} than at T_{ctrl}, but the difference was not statistically significant. U-87 MG became more brightly stained with PI than CHO-K1 at both temperatures; however, they also exhibited brighter fluorescence when permeabilized with the detergent Triton X-100 (Suppl. Material 1, Fig. S1.2), indicating a greater number of intracellular binding sites for PI (i.e. nucleic acids). To characterize the characteristic time constant of the PI uptake, we fitted the averaged data to an exponential curve, $f = A(1 - \exp(-t/\tau) + kt)$, using the function nlinfit in Matlab. For both cell lines, τ was roughly 50 % longer at T_{room} vs. T_{ctrl} (CHO-K1: $\tau = 78.5$ s vs. 53.0 s; U-87 MG: $\tau = 84.0$ s vs. 54.1 s). In both cell lines the PI curves exhibited a small but persistent increase in PI fluorescence that continued beyond the 30 min observation time. The slope k of this increase was also greater at T_{room} vs. T_{ctrl} (CHO-K1: $k = 1.87{\cdot}10^{-4}$ s^{-1} vs. $0.55{\cdot}10^{-4}$ s^{-1}; U-87 MG: $k = 1.94{\cdot}10^{-4}$ s^{-1} vs. $1.64{\cdot}10^{-4}$ s^{-1}). Both fitted parameters thus indicate slower membrane resealing kinetics at lower temperature, consistent with previous findings [51].

Since Ca^{2+} plays a crucial role in many cellular processes, we additionally monitored the changes in intracellular Ca^{2+} using the fluorescent indicator Fluo4 (Fig. 3c). Following pulse exposure, CHO-K1 cells exhibited a transient peak in intracellular Ca^{2+}, followed by a return to baseline. The peak appeared higher at T_{room} in 30 min time-lapses captured at 1 frame per 30 s. However, additional experiments using a higher imaging frame rate (1 frame per 3 s) demonstrated that the peaks were not significantly different at both T, just that the Ca^{2+} transients were faster at T_{ctrl} (Fig. 3c, inset). The full width at half maximum of the Ca^{2+} transient was ~53 s and ~34 s at T_{room} and T_{ctrl}, respectively. At T_{ctrl}, U-87 MG cells also exhibited a transient peak with full width at half maximum of ~20 s, after which the intracellular Ca^{2+} did not fully return to baseline but remained elevated almost until the end of observation time. In contrast, at T_{room}, the peak change in intracellular Ca^{2+} was much smaller. Additional experiments at higher imaging rate (1 frame per 3 s) confirmed that the Ca^{2+} transients were significantly different (1.65 min; $p = 0.05$) between T_{room} and T_{ctrl} in U-87 MG cells.

At the end of the Ca^{2+} imaging, PI was added to assess the plasma membrane integrity as an indicator of cell viability. There was no significant difference in detected PI fluorescence between T_{room} and T_{ctrl} compared to the negative control (sham-exposed cells). Moreover, the observed increase in PI fluorescence was much lower than the increase obtained after permeabilizing the cells with Triton X-100 as a positive control (Suppl. Material 1, Fig. S2.1). This confirms that most cells were able to restore their membrane integrity 30 min after pulse application.

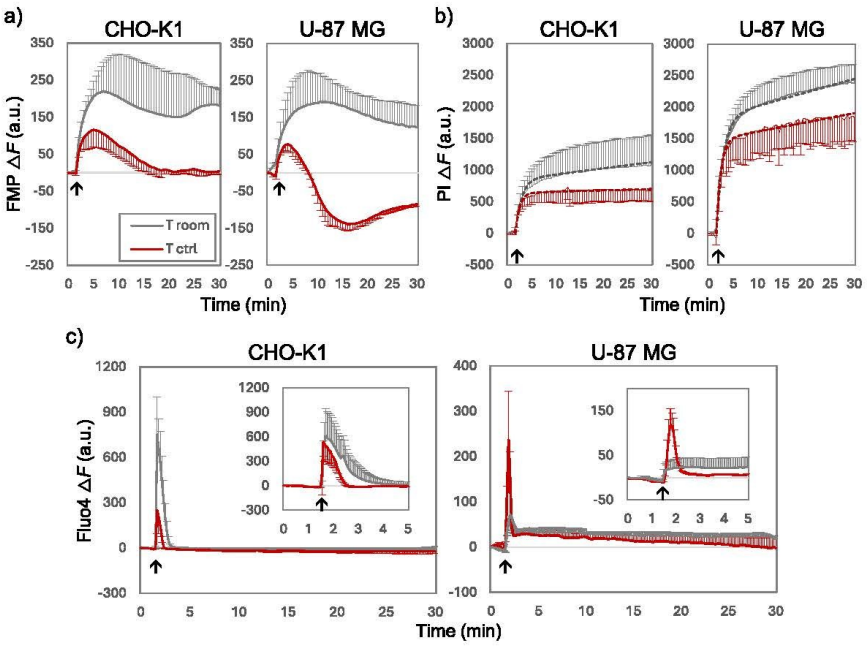

Fig. 3. The impact of temperature on the cell response after electroporation. A single 100 μs, 1.4 kV/cm pulse was delivered at 1.5 min (indicated with arrow), either at T_{room} (grey lines) or T_{ctrl} (red lines). The presented curves show mean ± s.d. from 3 to 5 experiments. Error bars are shown in one direction only for clarity. a) Response in TMV determined with FMP dye. b) Kinetics of PI uptake. The dashed curves show best fit with the function $f = A(1 - \exp(-t/\tau) + kt)$. c) Calcium transients determined with Fluo4 dye. Insets show data from images captured on 5 min time scale using a higher frame rate.

However, we cannot exclude that the cells could have lost their viability later due to delayed cell death mechanisms [52,53].

3.3. Hyperpolarization of U-87 cells is not an artifact of the FMP quencher uptake

The FMP dye contains a quencher molecule that absorbs the fluorescence of the voltage sensor molecule and under physiological conditions remains on the extracellular side. However, when cells become electroporated, the quencher could potentially enter the cells. The decrease in FMP fluorescence below baseline in U-87 MG cells could thus be an artifact of quencher entry instead of membrane hyperpolarization. Furthermore, previous studies have shown that the FMP is able to indicate hyperpolarization [30] but not in all experimental conditions

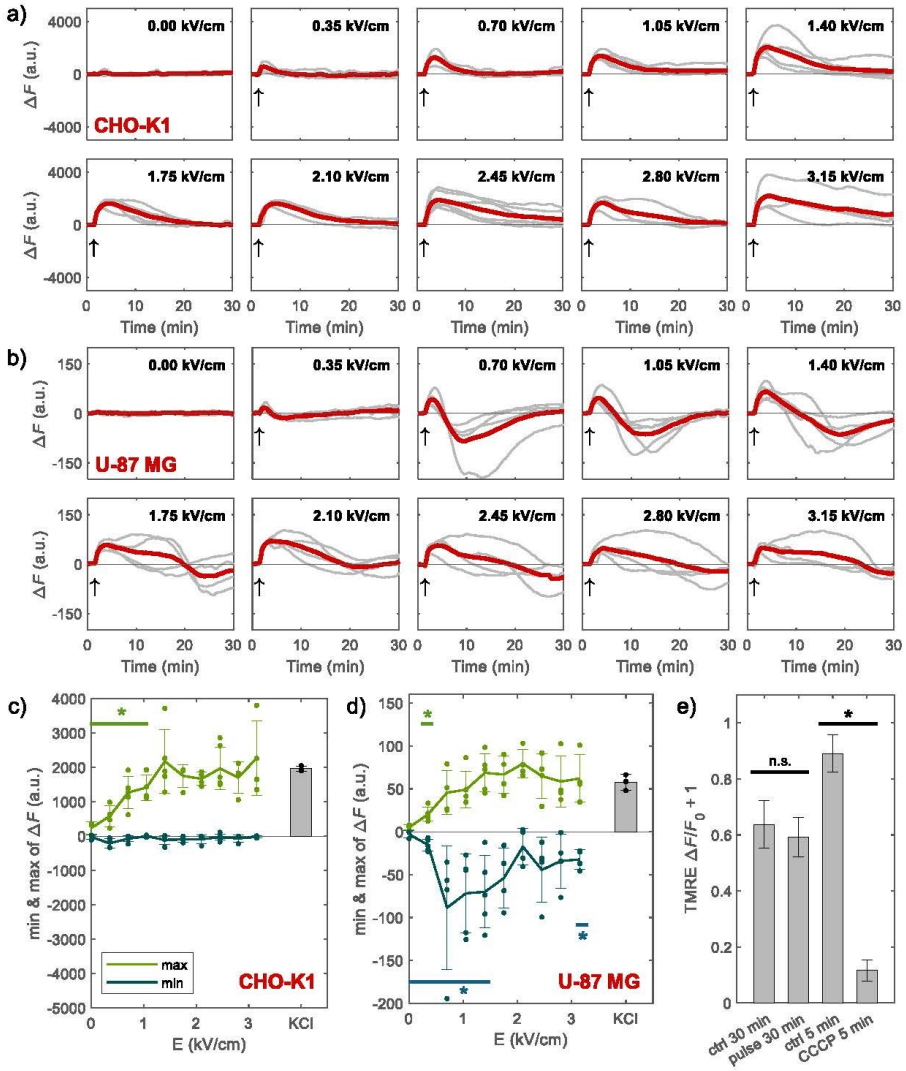

Fig. 4. Response to 100 μs pulse of different amplitudes. a) Time course of the change in FMP fluorescence in CHO-K1 cells after exposure to a pulse of a given amplitude (0 3.15 kV/cm). The time of pulse application is indicated with an arrow. Grey curves show responses from individual samples, obtained from at least three independent experiments; thick red curve shows their mean response. b) Same results as in a) but for U-87 MG cells. c-d) The minimum (blue lines) and maximum (green lines) values, extracted from each curve in panels a-b. Individual data points are presented together with their mean value ± standard deviation. Additionally, the bar presents the response to chemical depolarization (140 mM KCl). e) Relative change in mitochondrial TMV monitored with TMRE dye in U-87 MG cells. As a positive control for depolarization of mitochondria, the cells were exposed to CCCP for 5 min. Statistically significant differences (*: $p < 0.05$) were determined by One-way ANOVA.

[34]. To test this possibility, we exposed CHO-K1 and U-87 MG cells to a single 100 μs pulse of different amplitudes (0–3.15 kV/cm) and monitored the change in TMV over 30 min, similarly as in Fig. 3a. All experiments were performed at T_{ctrl}, since we observed a decrease in FMP fluorescence below baseline in U-87 MG cells only at this temperature.

In CHO-K1 cells, a small increase in fluorescence was already observed at 0.35 kV/cm. Pulses with amplitudes of ≥ 0.70 kV/cm all evoked similar averaged responses; the FMP signal first increased and then returned to baseline, without decreasing below baseline. In U-87 cells a small increase in fluorescence could also be observed at 0.35 kV/cm, in agreement with a previous study [9]. For amplitudes between 0.70 and 1.4 kV/cm we consistently observed an increase in fluorescence followed by a decrease below the baseline. With a further increase in pulse amplitude, this decrease below baseline became less and less profound. This indicates that the decrease below baseline is not a consequence of quencher entry since this entry should become greater with higher pulse amplitude due to a greater increase in membrane permeability.

We further extracted the minimum and maximum values from each curve in Fig. 4a, b and plotted them in Fig. 4c, d. Statistical analysis showed that the minimum values obtained after any of the pulse amplitudes applied to CHO-K1 cells were never significantly different from control. However, for U-87 MG cells, a significant difference was found at pulse amplitudes between 0.7 and 1.4 kV/cm and for 3.15 kV/cm ($p < 0.05$, shown in Fig. 4d). Additionally, we compared the extracted maximum values to chemical depolarization achieved by exposing the cells to 140 mM KCl. In CHO-K1 cells and U-87 MG cells, respectively, a significant difference ($p < 0.05$) was found compared to chemical depolarization for 0.35–1.05 kV/cm and 0.35 kV/cm. This indicates that 1.4 kV/cm pulses used in experiments presented in Fig. 3 completely depolarized the cells.

The FMP dye nonselectively stains both the plasma membrane and the membranes of intracellular organelles. Thus we hypothesized that the decrease in FMP signal below baseline in U-87 MG cells could also be due to hyperpolarization of mitochondrial membranes [54]. To detect changes in mitochondrial TMV, we used tetramethylrhodamine ethyl ester (TMRE). TMRE is a cationic dye that accumulates in active mitochondria because of the large negative TMV that appears across normal mitochondrial membranes. When the mitochondrial TMV becomes less negative (depolarizes), the TMRE concentration in the mitochondria decreases resulting in a decrease in TMRE fluorescence (the opposite of the FMP dye behavior). However, additional experiments monitoring mitochondrial TMV with TMRE dye demonstrated that mitochondria somewhat depolarized during 30 min of imaging, with or without pulse application, and were not responsible for the transient hyperpolarization observed in U-87 MG cells (Fig. 4e). To induce a depolarization of the mitochondrial TMV, CCCP was added to the cells stained with TMRE. A statistically significant difference was detected compared to the control ($p = 0.01$).

Overall, these results support the conclusion that after exposure to 100 μs pulse of intermediate amplitudes (0.7–1.4 kV/cm), the plasma membrane of U-87 MG cells first depolarized and then hyperpolarized.

3.4. Transient hyperpolarization of U-87 cells is likely caused by activation of calcium-activated potassium (K_{Ca}) channels

U-87 MG cells endogenously express calcium-activated potassium (K_{Ca}) channels [55]. These are Ca^{2+} and voltage-gated ion channels whose activation tends to hyperpolarize the membrane through the leak-out of K^+ ions along their electrochemical gradient [43]. To test the hypothesis that activation of K_{Ca} channels could be responsible for hyperpolarization, we first resorted to theoretical modeling. We used a minimal model that was originally developed to describe Ca^{2+} oscillations in hepatocytes [56] and later upgraded to include the contribution of K_{Ca} channels to these oscillations [43]. A recent review paper proposed that K_{Ca} channels play a similar role in modulating Ca^{2+} oscillations during glioblastoma cell migration and invasion [57]. We further upgraded the model to include an increase in nonselective transmembrane ionic current and Ca^{2+} uptake due to electroporation. We considered that at $t_{pulse} = 1.5$ min, when the pulse is applied, there is a certain number of pores N_{pores} created in the membrane due to electroporation. We assumed that, after the pulse exposure, the membrane reseals exponentially with a time constant $\tau = 54$ s, as determined from the fit to PI uptake kinetics in U-87 MG at T_{ctrl}:

$$f_{resealing} = \exp\left(-\frac{t - t_{pulse}}{\tau}\right), t \geq t_{pulse} \quad (4)$$

The model was able to replicate the main experimental observations. Fig. 5a shows the time course of TMV and intracellular Ca^{2+} ($[Ca^{2+}]_i$) depending on the number of pores created in the plasma membrane due to electroporation. If there are no pores created ($N_{pore} = 0$), the TMV stays at its resting value. If enough pores are created, the plasma membrane first depolarizes due to the nonselective leak current, and afterwards transiently hyperpolarizes. The simulated TMV and $[Ca^{2+}]_i$ time courses resemble well our experiments with U-87 MG cells at T_{ctrl} (see Fig. 3a,c). Note that the model shows an immediate depolarization at the time of pulse application ($t_{pulse} = 1.5$ min), whereas experimentally we see a more gradual increase in FMP fluorescence. This is because the FMP dye has a rather slow response time in seconds [29–31]. Studies using potentiometric dyes with fast response indeed demonstrate an immediate step-like depolarization following application of an electroporating pulse [21].

Membrane hyperpolarization in the model is due to activation of K_{Ca} channels, as demonstrated in Fig. 5b, which shows the TMV and $[Ca^{2+}]_i$, depending on the maximum conductance of K_{Ca} channels, when $N_{pore} = 1000$. Without K_{Ca} channels ($g_{Kmax} = 0$ nS), the plasma membrane transiently depolarizes and returns to baseline without any hyperpolarization. This TMV time course resembles that of CHO-K1 cells that express very low levels of endogenous ion channels [58,59] (see Fig. 3a). With increasing levels of expressed K_{Ca} channels, transient hyperpolarization becomes more profound. On the contrary, the time course of $[Ca^{2+}]_i$ is not affected much by K_{Ca} channels, consistent with qualitatively similar Ca^{2+} transients in CHO-K1 and U-87 MG cells observed experimentally at T_{ctrl} (see Fig. 3c).

It is important to emphasize that while the plasma membrane is highly permeable in the first few minutes after the pulse, the nonselective leak current is so high that activation of K_{Ca} channels does not affect the TMV very much. However, as the membrane mostly reseals and the leak current becomes very small, ion channel activation can have a large influence on the restoration of TMV. To illustrate this point, we assumed that a certain fraction δ of pores or permeable defects can persist in the membrane even after completion of the exponential resealing phase characterized by time τ. The presence of such pores can explain the small linear increase in the PI uptake that persisted until the end of observation time (Fig. 3b). The corresponding resealing function is:

$$f_{resealing} = (1 - \delta)\exp\left(-\frac{t - t_{pulse}}{\tau}\right) + \delta, t \geq t_{pulse} \quad (5)$$

The parameter δ is related to the slope k, extracted from the fit to PI uptake curves in Fig. 3b (see Suppl. Material 3 for derivation):

$$\delta = \frac{k\tau}{1 + k\tau} \quad (6)$$

For easier comparison with experiments, we thus varied the value of the slope k. The calculations are presented in Fig. 5c. If k is smaller than a certain value, the TMV response shows both the initial depolarization and the subsequent hyperpolarization. However, with increasing k, the membrane only depolarizes after the pulse. To further explore the conditions in which hyperpolarization can be observed, we made a parametric analysis in which we varied N_{pore} and k, and for each parameter combination we determined the minimum TMV that was

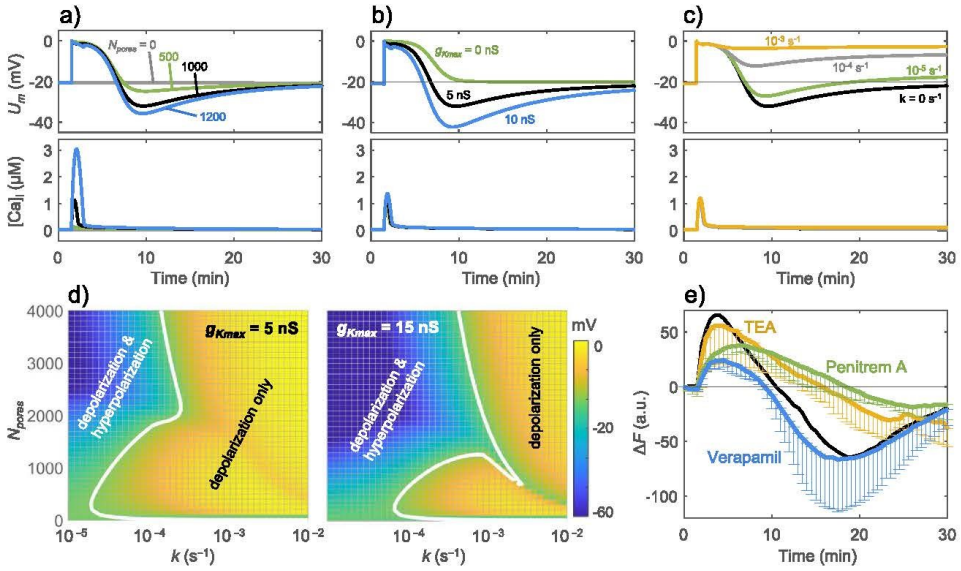

Fig. 5. The influence of K_{Ca} channels on TMV after electroporation. a-c) Time course of TMV and $[Ca^{2+}]_i$ predicted from the theoretical model for different values of model parameters; a) Results for different number of pores N_{pore}, when the maximum conductance of K_{Ca} channels equals g_{Kmax} 5 nS and the parameter k 0 s^{-1}. The pores are created when the pulse is applied at t_{pulse} 1.5 min. b) Similar results as in a), but for different values of g_{Kmax} when N_{pore} 1000 and k 0 s^{-1}. c) Similar results as in a), but for different values of parameter k when g_{Kmax} 5 nS and N_{pore} 1000. d) Parametric analysis showing the minimum TMV value obtained in the model within 30 min after the pulse, depending on parameters k and N_{pore}. Calculations were performed for g_{Kmax} 5 nS (left) and 50 nS (right). e) Experimental measurements of the change in TMV after exposure to 100 ms, 1.4 kV/cm at t_{pulse} 1.5 min in U-87 MG cells with the FMP dye in the presence of ion channel inhibitors TEA, Penitrem A, and Verapamil. Mean ± s.d. from 3 independent experiments. The thin black line shows the average response without ion channel inhibitors, taken from Fig. 4b at 1.4 kV/cm.

achieved within 30 min after the pulse. We performed the parametric analysis for two values of the maximum conductance of K_{Ca} channels (g_{Kmax} = 5 nS and 15 nS), since we did not find an exact value of g_{Kmax} for U-87 MG cells in the literature. The results are presented in Fig. 5d. The white line separates the parameter space in which both depolarization and hyperpolarization can be observed, from the space where only depolarization can be observed after the pulse. The graphs clearly show that hyperpolarization occurs only when k is sufficiently small to be on the left side of the white line. When there are more K_{Ca} expressed in the cells (g_{Kmax} is larger), the white line shifts to larger k.

The parametric analysis additionally elucidates our experimental results. Experimentally, hyperpolarization in U-87 MG cells became less profound with increasing pulse amplitude. The model suggests this is not due to more pores created by a pulse with higher amplitude but to slower or incomplete membrane resealing. Furthermore, we found a greater slope k in PI uptake kinetics at T_{room} compared to T_{ctrl}. Thus, the absence of hyperpolarization in U-87 MG cells at T_{room} could partially be due to a larger k. Even more importantly, at T_{room}, the increase in $[Ca^{2+}]_i$ in U-87 MG cells was significantly lower than at T_{ctrl}. The increase in $[Ca^{2+}]_i$ at T_{room} was likely too low to activate K_{Ca} channels (see the influence of $[Ca^{2+}]_i$ peak amplitude on the extent of hyperpolarization in Fig. 5a). However, the model in the current form was unable to represent the altered $[Ca^{2+}]_i$ profile at T_{room}, thus further research is needed to fully understand the absence of hyperpolarization in U-87 MG cells at T_{room}. Overall, our model confirms that the observed hyperpolarization in U-87 MG cells can be due to the activation of K_{Ca} channels.

The modeling predictions were supported by experiments using ion channel inhibitors. A nonspecific inhibitor of potassium channels TEA, in concentrations high enough to inhibit both large conductance (BK) and intermediate conductance (IK) calcium-activated potassium channels, abrogated hyperpolarization (Fig. 5e). Additional experiments with the BK inhibitor Penitrem A resulted in similar responses as with TEA, suggesting that hyperpolarization is mainly governed by the activation of BK channels. The minimum FMP fluorescence values in the presence of both TEA and Penitrem A were significantly different from control without ion channel inhibitors (Two-way ANOVA, $p \leq 0.03$). On the contrary, the inhibitor of voltage-gated calcium channels Verapamil did not have a significant effect on hyperpolarization. This is to some extent consistent with our assumption in the model that the increase in $[Ca^{2+}]_i$ after the pulse is mainly due to influx of Ca^{2+} through pores in the membrane, rather than activation of Ca^{2+} channels. Nevertheless, while the maximum FMP fluorescence value with TEA and Penitrem A was not significantly different from control, it was significantly lower with Verapamil (Two-way ANOVA, $p = 0.016$). This indicates that calcium channel activation can also contribute to the initial depolarization phase. It should be noted that U-87 MG cells express many different types of ion channels; addition of these channels to the model would likely further improve the agreement with experiment.

Overall, our model and experiments demonstrate that the observed long-term changes in TMV in U-87 MG cells can be explained by the dynamic interplay between the nonselective leak current due to electroporation and ion channel activation. The nonselective leak current acts to depolarize the TMV towards 0 mV, whereas ion channel activation influences the TMV when the nonselective leak current becomes very small and comparable to the currents passing through ion channels. The previous study by Burke et al. on U-87 MG cells exposed cells to a 10 ns, 34 kV/cm pulse demonstrated that immediately after the pulse application, the activation of Ca^{2+}, BK and TRPM8 ion channels contributes to membrane depolarization [23]. The pulse amplitude used in this study was just above the threshold for inducing membrane

depolarization and was thus probably associated with a very small increase in membrane permeability and leak current – small enough to enable the ion channel currents to influence the TMV. Our results indicate that after exposing cells to 100 μs, 1.4 kV/cm pulse, membrane depolarization is mainly associated with the nonselective leak current due to increased membrane permeability. Nevertheless, the lower amplitude of depolarization detected in the presence of Verapamil suggests that activation of calcium channels can to some extent contribute to the initial depolarization phase as well.

3.5. *Challenges associated with monitoring long-term TMV changes after electroporation*

Both our model and experiments with ion channel inhibitors confirm that the decrease in FMP fluorescence below baseline, observed in U-87 MG cells following pulse exposure, can be attributed to plasma membrane hyperpolarization. We nevertheless wanted to additionally confirm this with two alternative voltage-sensitive dyes, ElectroFluor630 and FluoVolt. Both have already been used for monitoring TMV changes in response to high-voltage electric pulses; however, they were previously only used to detect short-term changes, i.e. in the range of seconds [21,22].

Our results, presented in Suppl. Material 1 Section 5, together with a detailed explanation of the dyes, reveal considerable limitations of both dyes. With ElectroFluor630 we observed the well-known gradual internalization of the dye. While this internalization is not necessarily problematic for monitoring rapid TMV changes (such as action potentials) [21,60], it makes it very challenging to monitor long-term and small changes in TMV over a 30 min observation period, since the fluorescence signal continuously drifts. Further limitations of the dye are photobleaching and a rather low sensitivity (~15 % / 100 mV) [61], which for U-87 MG cells with a mean resting voltage of − 16 ± 4 mV [55] requires detection of fluorescence changes below 2.4 %. With FluoVolt, we observed morphological changes and cell rounding over the 30 min period, which we attributed to phototoxicity, as previously reported [62]. Therefore, we found ElectroFluor630 and FluoVolt unsuitable for monitoring long-term changes in TMV after electroporation in our experimental setup. The FMP dye was considered superior for our experimental study.

Nevertheless, FMP dye also has limitations. It was designed for measurements of intact plasma membranes. During electroporation both parts of the dye (the anionic voltage sensor molecule and the quencher molecule) could potentially enter the cell due to increased membrane permeability and influence the fluorescence signal. Our experiments with pulses of different amplitudes (up to 3.15 kV/cm) showed that quencher entry was not critical under our specific pulsing conditions. However, we cannot exclude that other pulse parameters, associated with a greater increase in membrane permeability, would allow the quencher to enter the cells. Another problem impeding the interpretation of results is the unknown chemical structure of both the voltage sensor and quencher molecule, which is considered proprietary information.

It is further interesting to note that our results with the FMP dye became less reproducible for pulses with the highest tested amplitudes (Fig. 4a-b). For pulse amplitudes higher than 1.4 kV/cm, both CHO-K1 and U87-MG cells started to fuse due to electroporation – a phenomenon known as electrofusion [63] – which could be the one of the reasons for lower reproducibility. Moreover, higher pulse amplitude is associated with stronger electroporation and thus greater structural changes of the membrane, which could affect the translocation mechanism of the FMP voltage sensor molecule.

Overall, we find that measuring long-term changes in TMV remains challenging in electroporation research from the methodological point of view and that all the tested dyes (FMP, ElectroFluor630 and FluoVolt) have limitations. A promising alternative could be genetically encoded voltage indicators (GEVIs), which have not yet been experimentally tested when used for observations of the TMV following delivery of high-intensity electric pulses. Nevertheless, one of their limitations is a possible perturbation of the protein voltage sensor domain by a strong electric field, which was already shown in molecular dynamics simulations of voltage-dependent calcium and sodium channels [64,65]. Moreover, all GEVIs require cell transfection, which can perturb the wild-type cell physiology [66].

4. Conclusions and outlook

In our study we investigated the mechanisms of long-term changes in TMV after exposing CHO-K1 and U-87 MG cells to a single 100 μs electroporation pulse. By monitoring changes in TMV over a period of 30 min with the FMP dye, we observed that these changes are cell type and temperature dependent. In CHO-K1 cells, which express low levels of endogenous ion channels, membrane depolarization following pulse exposure could mainly be explained by the nonselective leak current through the permeabilized membrane, which persists until the membrane reseals, enabling the cells to recover their resting TMV. Membrane resealing and TMV recovery was faster at higher (33 °C), more physiological, temperature compared with experiments performed at room temperature (25 °C). U-87 MG cells, which express many endogenous ion channels, exhibited a different response in TMV than CHO-K1. Following the initial depolarization phase, the cells hyperpolarized, but only at 33 °C. Using a theoretical model, supported by experiments with ion channel inhibitors, we found that this hyperpolarization can largely be attributed to the activation of calcium-activated potassium (K_{Ca}) channels. However, since we were unable to completely abrogate hyperpolarization with selected K_{Ca} channel inhibitors, activation of other channels, such as chloride channels could contribute as well [67]. Based on the obtained experimental and theoretical results, we conclude that as long as the membrane is highly permeable, the nonselective leak current is responsible for membrane depolarization. However, when the leak current becomes comparable to the currents through ion channels (towards the end of the membrane resealing phase or when the membrane is only gently electroporated), ion channel activation can significantly contribute to the changes in TMV.

TMV is known to change through the progression of the cell cycle [1]. The TMV controls the activation of voltage-gated ion channels and modulates the function of other membrane proteins exhibiting voltage sensitivity [68]. Since many of these channels conduct calcium ions, changes in TMV affect the intracellular calcium levels and calcium signaling. Ion channels are abundantly expressed in cancer cells including glioblastoma, from which the U-87 MG cell line derives [55]. It was demonstrated that ion channels have an important role in cancer cell proliferation, migration, invasion, and apoptosis, which led to proposition of classifying cancer as one of channelopathies [69,70]. Therefore, ion channels are considered as therapeutic targets for cancer treatment. A recent study in glioblastoma cell lines NG108-15 and U-87 MG confirmed that certain combinations of ion channel modulating drugs significantly reduce proliferation, make the cells senescent, and promote differentiation [71]. Our study demonstrated that electroporation provokes a dynamic change in TMV in U-87 MG cells, which modulates ion channel activation. It would therefore be interesting to study the functional consequences of such changes in TMV and how they affect cell behavior. Such studies would provide new insights into electroporation-based treatments of glioblastoma and other cancers [38,72,73]. Since we found that changes in TMV are temperature-dependent, such studies should ensure controlled temperature conditions, ideally physiological conditions at 37 °C.

To further study long-terms changes in TMV following electroporation, one needs to establish a reliable methodology. While the fast-response voltage-sensitive dyes FluoVolt and ElectroFluor630 were previously used to monitor short-term changes in TMV (time scale of a few seconds) following electroporation [21,22], we found them unsuitable for monitoring long-term TMV changes. The slow-response FMP

dye was better suited for this purpose, although here we also identified several limitations when using the dye in combination with electroporation. Voltage-sensitive dyes are generally designed and calibrated based on experiments made with intact membranes. However, when a cell is electroporated, both the increase in membrane permeability and the perturbations of the membrane structure could potentially interfere with the function of the dye and alter the fluorescence signal. Moreover, for electroporation research, it would be important to test voltage-sensitive dyes in electroporated cells using classical electrophysiological (patch clamp) measurements. Further research should also be focused on developing better methods for monitoring long-term changes in TMV following electroporation. Novel genetically encoded voltage indicators (GEVIs) could present a promising tool [66], provided that the electric field used for electroporation does not damage the GEVI's voltage-sensor domains [65].

CRediT authorship contribution statement

Anja Blažič: Writing – review & editing, Writing – original draft, Visualization, Methodology, Investigation, Formal analysis, Data curation, Conceptualization, Validation. **Manon Guinard:** Writing – review & editing, Methodology, Investigation, Validation. **Tomaž Leskovar:** Writing – review & editing, Methodology, Investigation, Software, Validation. **Rodney P. O'Connor:** Writing – review & editing, Methodology, Conceptualization. **Lea Rems:** Writing – review & editing, Writing – original draft, Supervision, Project administration, Methodology, Funding acquisition, Formal analysis, Conceptualization, Resources, Software, Validation, Visualization.

Declaration of competing interest

The authors declare that they have no known competing financial interests or personal relationships that could have appeared to influence the work reported in this paper.

Data availability

Data will be made available on request.

Acknowledgments

The study was supported by funding from the European Union's Horizon 2020 research and innovation programme under the Marie Skłodowska-Curie grant agreement No. 893077 (to L.R.), Erasmus + programme (to M.G. and A.B.), and by the Slovenian Research and Innovation Agency (ARIS) within research programme P2-0249, research projects J2-2503 and MN-0023, infrastructure programme I0-0022, and funding for Junior Researchers. The work was in part supported by the European Union and ARIS through NextGenerationEU and NOO funding within project MN-0023. The study was also partially supported by ARIS and the University of Ljubljana within the funding for Start-up Research Programme, and by the European Union's Horizon Europe research and innovation programme within the ERC Starting Grant project No. 101115323 – REINCARNATION. Views and opinions expressed are however those of the author(s) only and do not necessarily reflect those of the European Union or the European Research Council. Neither the European Union nor the granting authority can be held responsible for them. The authors thank Tina Cimperman for initial help with analysis of the FMP dye signals, Tina Batista Napotnik for help with experiments with the ElectroFluor630 dye, Simon Žakelj for preparing Verapamil stock solution, and Damijan Miklavčič for useful comments to the manuscript.

Appendix A. Supplementary data

Supplementary data to this article can be found online at https://doi.org/10.1016/j.bioelechem.2024.108802.

References

[1] D.J. Blackiston, K.A. McLaughlin, M. Levin, Bioelectric controls of cell proliferation: ion channels, membrane voltage and the cell cycle, Cell Cycle Georget. Tex 8 (2009) 3527–3536, https://doi.org/10.4161/cc.8.21.9888.
[2] H.G. Sachs, P.J. Stambrook, J.D. Ebert, Changes in membrane potential during the cell cycle, Exp. Cell Res. 83 (1974) 362–366, https://doi.org/10.1016/0014-4827(74)90350-4.
[3] M. Yang, W.J. Brackenbury, Membrane potential and cancer progression, Front. Physiol. 4 (2013) 185, https://doi.org/10.3389/fphys.2013.00185.
[4] S. Sundelacruz, M. Levin, D.L. Kaplan, Role of Membrane Potential in the Regulation of Cell Proliferation and Differentiation, Stem Cell Rev. Rep. 5 (2009) 231–246, https://doi.org/10.1007/s12015-009-9080-2.
[5] L. Vodovnik, D. Miklavčič, G. Serša, Modified cell proliferation due to electrical currents, Med. Biol. Eng. Comput. 30 (1992) CE21–CE28, https://doi.org/10.1007/BF02446174.
[6] G. Thrivikraman, S.K. Boda, B. Basu, Unraveling the mechanistic effects of electric field stimulation towards directing stem cell fate and function: a tissue engineering perspective, Biomaterials 150 (2018) 60–86, https://doi.org/10.1016/j.biomaterials.2017.10.003.
[7] L. Leppik, K.M.C. Oliveira, M.B. Bhavsar, J.H. Barker, Electrical stimulation in bone tissue engineering treatments, Eur. J. Trauma Emerg. Surg. off. Publ. Eur. Trauma Soc. 46 (2020) 231–244, https://doi.org/10.1007/s00068-020-01324-1.
[8] T. Kotnik, L. Rems, M. Tarek, D. Miklavčič, Membrane electroporation and electropermeabilization: mechanisms and models, Annu. Rev. Biophys. 48 (2019) 63–91, https://doi.org/10.1146/annurev-biophys-052118-115451.
[9] J. Dermol-Černe, D. Miklavčič, M. Reberšek, P. Mekuč, S.M. Bardet, R. Burke, D. Arnaud-Cormos, P. Leveque, R. O'Connor, Plasma membrane depolarization and permeabilization due to electric pulses in cell lines of different excitability, Bioelectrochemistry Amst. Neth. 122 (2018) 103–114, https://doi.org/10.1016/j.bioelechem.2018.03.011.
[10] A.G. Pakhomov, R. Shevin, J.A. White, J.F. Kolb, O.N. Pakhomova, R.P. Joshi, K. H. Schoenbach, Membrane permeabilization and cell damage by ultrashort electric field shocks, Arch. Biochem. Biophys. 465 (2007) 109–118, https://doi.org/10.1016/j.abb.2007.05.003.
[11] M. Neunlist, L. Tung, Dose-dependent reduction of cardiac transmembrane potential by high-intensity electrical shocks, Am. J. Physiol. 273 (1997) H2817–H2825, https://doi.org/10.1152/ajpheart.1997.273.6.H2817.
[12] D.L. Atkinson, T.J. Stevenson, E.J. Park, M.D. Riedy, B. Milash, S.J. Odelberg, Cellular electroporation induces dedifferentiation in intact newt limbs, Dev. Biol. 299 (2006) 257–271, https://doi.org/10.1016/j.ydbio.2006.07.027.
[13] R.A. Vadlamani, Y. Nie, D.A. Detwiler, A. Dhanabal, A.M. Kraft, S. Kuang, T. P. Gavin, A.L. Garner, Nanosecond pulsed electric field induced proliferation and differentiation of osteoblasts and myoblasts, J. r. Soc. Interface 16 (2019) 20190079, https://doi.org/10.1098/rsif.2019.0079.
[14] T. Ning, J. Guo, K. Zhang, K. Li, J. Zhang, Z. Yang, Z. Ge, Nanosecond pulsed electric fields enhanced chondrogenic potential of mesenchymal stem cells via JNK/CREB-STAT3 signaling pathway, Stem Cell Res. Ther. 10 (2019) 45, https://doi.org/10.1186/s13287-019-1133-0.
[15] J. Chen, Y. Huang, J. Yang, K. Li, Y. Jiang, B.C. Heng, Q. Cai, J. Zhang, Z. Ge, Multiple nanosecond pulsed electric fields stimulation with conductive poly(l-lactic acid)/carbon nanotubes films maintains the multipotency of mesenchymal stem cells during prolonged in vitro culture, J. Tissue Eng. Regen. Med. 14 (2020) 1136–1148, https://doi.org/10.1002/term.3088.
[16] A. Halim, A.D. Ariyanti, Q. Luo, G. Song, Recent progress in engineering mesenchymal stem cell differentiation, Stem Cell Rev. Rep. 16 (2020) 661–674, https://doi.org/10.1007/s12015-020-09979-4.
[17] P. Liu, E.W. Miller, Electrophysiology, Unplugged: Imaging Membrane Potential with Fluorescent Indicators, Acc. Chem. Res. 53 (2020) 11–19, https://doi.org/10.1021/acs.accounts.9b00514.
[18] A.G. Pakhomov, J.F. Kolb, J.A. White, R.P. Joshi, S. Xiao, K.H. Schoenbach, Long-lasting plasma membrane permeabilization in mammalian cells by nanosecond pulsed electric field (nsPEF), Bioelectromagnetics 28 (2007) 655–663, https://doi.org/10.1002/bem.20354.
[19] L.H. Wegner, W. Frey, A. Silve, Electroporation of DC-3F Cells Is a Dual Process, Biophys. J. 108 (2015) 1660–1671, https://doi.org/10.1016/j.bpj.2015.01.038.
[20] A.G. Pakhomov, A.M. Bowman, B.L. Ibey, F.M. Andre, O.N. Pakhomova, K. H. Schoenbach, Lipid nanopores can form a stable, ion channel-like conduction pathway in cell membrane, Biochem. Biophys. Res. Commun. 385 (2009) 181–186, https://doi.org/10.1016/j.bbrc.2009.05.035.
[21] T. Batista Napotnik, B. Kos, T. Jarm, D. Miklavčič, R.P. O'Connor, L. Rems, Genetically engineered HEK cells as a valuable tool for studying electroporation in excitable cells, Sci. Rep. 14 (2024) 720, https://doi.org/10.1038/s41598-023-51073-5.
[22] A.G. Pakhomov, I. Semenov, M. Casciola, S. Xiao, Neuronal excitation and permeabilization by 200-ns pulsed electric field: an optical membrane potential study with FluoVolt dye, Biochim. Biophys. Acta Biomembr. 2017 (1859) 1273–1281, https://doi.org/10.1016/j.bbamem.2017.04.016.
[23] R.C. Burke, S.M. Bardet, L. Carr, S. Romanenko, D. Arnaud-Cormos, P. Leveque, R. P. O'Connor, Nanosecond pulsed electric fields depolarize transmembrane potential via voltage-gated K+, Ca2+ and TRPM8 channels in U87 glioblastoma cells, Biochim. Biophys. Acta Biomembr. 2017 (1859) 2040–2050, https://doi.org/10.1016/j.bbamem.2017.07.004.

[24] D.V. Vasilyev, Q.J. Shan, Y.T. Lee, V. Soloveva, S.P. Nawoschik, E.J. Kaftan, J. Dunlop, S.C. Mayer, M.R. Bowlby, A novel high-throughput screening assay for HCN channel blocker using membrane potential-sensitive dye and FLIPR, J. Biomol. Screen. 14 (2009) 1119–1128, https://doi.org/10.1177/1087057109345526.
[25] E.R. Benjamin, F. Pruthi, S. Olanrewaju, V.I. Ilyin, G. Crumley, E. Kutlina, K. J. Valenzano, R.M. Woodward, State-dependent compound inhibition of Nav1.2 sodium channels using the FLIPR Vm dye: on-target and off-target effects of diverse pharmacological agents, SLAS Discov. 11 (2006) 29–39, https://doi.org/10.1177/1087057105280918.
[26] S.P. Lee, M.T. Buber, Q. Yang, R. Cerne, R.Y. Cortés, D.G. Sprous, R.W. Bryant, Thymol and related alkyl phenols activate the hTRPA1 channel, Br. J. Pharmacol. 153 (2008) 1739–1749, https://doi.org/10.1038/bjp.2008.85.
[27] M. Finley, J. Cassaday, T. Kreamer, X. Li, K. Solly, G. O'Donnell, M. Clements, A. Converso, S. Cook, C. Daley, R. Kraus, M.-T. Lai, M. Layton, W. Lemaire, D. Staas, J. Wang, Kinetic, analysis of membrane potential dye response to Nav1.7 channel activation identifies antagonists with pharmacological selectivity against NaV1.5, SLAS Discov 21 (2016) 480–489, https://doi.org/10.1177/1087057116629669.
[28] A. Knapman, M. Santiago, Y.P. Du, P.R. Bennallack, M.J. Christie, M. Connor, A continuous, fluorescence-based assay of μ-opioid receptor activation in AtT-20 cells, J. Biomol. Screen. 18 (2013) 269–276, https://doi.org/10.1177/1087057112461376.
[29] R. Fairless, A. Beck, M. Kravchenko, S.K. Williams, U. Wissenbach, R. Diem, A. Cavalié, Membrane potential measurements of isolated neurons using a voltage-sensitive dye, PLOS ONE 8 (2013) e58260, https://doi.org/10.1371/journal.pone.0058260.
[30] K.L. Whiteaker, S.M. Gopalakrishnan, D. Groebe, C.C. Shieh, U. Warrior, D. J. Burns, M.J. Coghlan, V.E. Scott, M. Gopalakrishnan, Validation of FLIPR membrane potential dye for high throughput screening of potassium channel modulators, J. Biomol. Screen. 6 (2001) 305–312, https://doi.org/10.1177/108705710100600504.
[31] A. Yamada, N. Gaja, S. Ohya, K. Muraki, H. Narita, T. Ohwada, Y. Imaizumi, Usefulness and limitation of DiBAC4(3), a voltage-sensitive fluorescent dye, for the measurement of membrane potentials regulated by recombinant large conductance Ca2+-activated K+ channels in HEK293 cells, Jpn. J. Pharmacol. 86 (2001) 342–350, https://doi.org/10.1254/jjp.86.342.
[32] K.R. Konrad, R. Hedrich, The use of voltage-sensitive dyes to monitor signal-induced changes in membrane potential-ABA triggered membrane depolarization in guard cells, Plant J. 55 (2008) 161–173, https://doi.org/10.1111/j.1365-313X.2008.03498.x.
[33] D.F. Baxter, M. Kirk, A.F. Garcia, A. Raimondi, M.H. Holmqvist, K.K. Flint, D. Bojanic, P.S. Distefano, R. Curtis, Y. Xie, A novel membrane potential-sensitive fluorescent dye improves cell-based assays for ion channels, SLAS Discov. 7 (2002) 79–85, https://doi.org/10.1177/108705710200700110.
[34] C. Wolff, B. Fuks, P. Chatelain, Comparative study of membrane potential-sensitive fluorescent probes and their use in ion channel screening assays, J. Biomol. Screen. 8 (2003) 533–543, https://doi.org/10.1177/1087057103257806.
[35] M. Hibino, H. Itoh, K. Kinosita, Time courses of cell electroporation as revealed by submicrosecond imaging of transmembrane potential, Biophys. J. 64 (1993) 1789–1800, https://doi.org/10.1016/S0006-3495(93)81550-9.
[36] K.A. DeBruin, W. Krassowska, Modeling electroporation in a single cell. I. effects Of field strength and rest potential, Biophys. J. 77 (1999) 1213–1224, https://doi.org/10.1016/S0006-3495(99)76973-0.
[37] M. Marty, G. Sersa, J.R. Garbay, J. Gehl, C.G. Collins, M. Snoj, V. Billard, P. F. Geertsen, J.O. Larkin, D. Miklavcic, I. Pavlovic, S.M. Paulin-Kosir, M. Cemazar, N. Morsli, D.M. Soden, Z. Rudolf, C. Robert, G.C. O'Sullivan, L.M. Mir, Electrochemotherapy – an easy, highly effective and safe treatment of cutaneous and subcutaneous metastases: results of ESOPE (European Standard Operating Procedures of Electrochemotherapy) study, Eur. J. Cancer Suppl. 4 (2006) 3–13, https://doi.org/10.1016/j.ejcsup.2006.08.002.
[38] B. Geboers, H.J. Scheffer, P.M. Graybill, A.H. Ruarus, S. Nieuwenhuizen, R.S. Puijk, P.M. van den Tol, R.V. Davalos, B. Rubinsky, T.D. de Gruijl, D. Miklavčič, M. R. Meijerink, High-voltage electrical pulses in oncology: irreversible electroporation, electrochemotherapy, gene electrotransfer, electrofusion, and electroimmunotherapy, Radiology 295 (2020) 254–272, https://doi.org/10.1148/radiol.2020192190.
[39] K.N. Aycock, R.V. Davalos, Irreversible electroporation: background, theory, and review of recent developments in clinical oncology, Bioelectricity 1 (2019) 214–234, https://doi.org/10.1089/bioe.2019.0029.
[40] M. Cemazar, G. Sersa, W. Frey, D. Miklavcic, J. Teissié, Recommendations and requirements for reporting on applications of electric pulse delivery for electroporation of biological samples, Bioelectrochemistry 122 (2018), https://doi.org/10.1016/j.bioelechem.2018.03.005.
[41] T.B. Napotnik, Y.-H. Wu, M.A. Gundersen, D. Miklavčič, P.T. Vernier, Nanosecond electric pulses cause mitochondrial membrane permeabilization in Jurkat cells, Bioelectromagnetics 33 (2012) 257–264, https://doi.org/10.1002/bem.20707.
[42] J. Schindelin, I. Arganda-Carreras, E. Frise, V. Kaynig, M. Longair, T. Pietzsch, S. Preibisch, C. Rueden, S. Saalfeld, B. Schmid, J.-Y. Tinevez, D.J. White, V. Hartenstein, K. Eliceiri, P. Tomancak, A. Cardona, Fiji: an open-source platform for biological-image analysis, Nat. Methods 9 (2012) 676–682, https://doi.org/10.1038/nmeth.2019.
[43] L. Catacuzzeno, B. Fioretti, F. Franciolini, A theoretical study on the role of Ca2+-activated K+ channels in the regulation of hormone-induced Ca2+ oscillations and their synchronization in adjacent cells, J. Theor. Biol. 309 (2012) 103–112, https://doi.org/10.1016/j.jtbi.2012.05.009.
[44] J. Li, H. Lin, Numerical simulation of molecular uptake via electroporation, Bioelectrochemistry 82 (2011) 10–21, https://doi.org/10.1016/j.bioelechem.2011.04.006.
[45] J. Li, W. Tan, M. Yu, H. Lin, The effect of extracellular conductivity on electroporation-mediated molecular delivery, Biochim. Biophys. Acta 2013 (1828) 461–470, https://doi.org/10.1016/j.bbamem.2012.08.014.
[46] J. Li, H. Lin, The current-voltage relation for electropores with conductivity gradients, Biomicrofluidics 4 (2010) 013206, https://doi.org/10.1063/1.3324847.
[47] J.A. Lamas, L. Rueda-Ruzafa, S. Herrera-Pérez, Ion channels and thermosensitivity: TRP, TREK, or both? Int. J. Mol. Sci. 20 (2019) 2371, https://doi.org/10.3390/ijms20102371.
[48] F. Yang, J. Zheng, High temperature sensitivity is intrinsic to voltage-gated potassium channels, eLife 3 (2014) e03255, https://doi.org/10.7554/eLife.03255.
[49] H.G. Glitsch, Electrophysiology of the Sodium-Potassium-ATPase in Cardiac Cells, Physiol. Rev. 81 (2001) 1791–1826, https://doi.org/10.1152/physrev.2001.81.4.1791.
[50] B. Valič, M. Golzio, M. Pavlin, A. Schatz, C. Faurie, B. Gabriel, J. Teissié, M.-P. Rols, D. Miklavčič, Effect of electric field induced transmembrane potential on spheroidal cells: theory and experiment, Eur. Biophys. J. 32 (2003) 519–528, https://doi.org/10.1007/s00249-003-0296-9.
[51] M. Kandušer, M. Šentjurc, D. Miklavčič, Cell membrane fluidity related to electroporation and resealing, Eur. Biophys. J. 35 (2006) 196–204, https://doi.org/10.1007/s00249-005-0021-y.
[52] B. Gabriel, J. Teissié, Control by electrical parameters of short- and long-term cell death resulting from electropermeabilization of Chinese hamster ovary cells, Biochim. Biophys. Acta BBA - Mol. Cell Res. 1266 (1995) 171–178, https://doi.org/10.1016/0167-4889(95)00021-J.
[53] W. Peng, T. Polajžer, C. Yao, D. Miklavčič, Dynamics of cell death due to electroporation using different pulse parameters as revealed by different viability assays, Ann. Biomed. Eng. 52 (2024) 22–35, https://doi.org/10.1007/s10439-023-03309-8.
[54] E.D. Michelakis, G. Sutendra, P. Dromparis, L. Webster, A. Haromy, E. Niven, C. Maguire, T.-L. Gammer, J.R. Mackey, D. Fulton, B. Abdulkarim, M.S. McMurtry, K.C. Petruk, Metabolic modulation of glioblastoma with dichloroacetate, Sci. Transl. Med. 2 (2010), https://doi.org/10.1126/scitranslmed.3000677, 31ra34-31ra34.
[55] T. Ducret, A. Vacher, P. Vacher, Voltage-dependent ionic conductances in the human malignant astrocytoma cell line U87-MG, Mol. Membr. Biol. 20 (2003) 329–343, https://doi.org/10.1080/0968763031000138037.
[56] T. Höfer, Model of intercellular calcium oscillations in hepatocytes: synchronization of heterogeneous cells, Biophys. J. 77 (1999) 1244–1256, https://doi.org/10.1016/S0006-3495(99)76976-6.
[57] L. Catacuzzeno, F. Franciolini, Role of KCa3.1 channels in modulating Ca2+ oscillations during glioblastoma cell migration and invasion, Int. J. Mol. Sci. 19 (2018) 2970, https://doi.org/10.3390/ijms19102970.
[58] N. Gamper, J.D. Stockand, M.S. Shapiro, The use of Chinese hamster ovary (CHO) cells in the study of ion channels, J. Pharmacol. Toxicol. Methods 51 (2005) 177–185, https://doi.org/10.1016/j.vascn.2004.08.008.
[59] A. Varghese, E.M. TenBroek, J. Coles, D.C. Sigg, Endogenous channels in HEK cells and potential roles in HCN ionic current measurements, Prog. Biophys. Mol. Biol. 90 (2006) 26–37, https://doi.org/10.1016/j.pbiomolbio.2005.05.002.
[60] G. Pucihar, T. Kotnik, D. Miklavčič, Measuring the Induced Membrane Voltage with Di-8-ANEPPS, J. vis. Exp. (2009) 1659, https://doi.org/10.3791/1659.
[61] P. Yan, C.D. Acker, W.-L. Zhou, P. Lee, C. Bollensdorff, A. Negrean, J. Lotti, L. Sacconi, S.D. Antic, P. Kohl, H.D. Mansvelder, F.S. Pavone, L.M. Loew, Palette of fluorinated voltage-sensitive hemicyanine dyes, Proc. Natl. Acad. Sci. 109 (2012) 20443–20448, https://doi.org/10.1073/pnas.1214850109.
[62] C.N. Broyles, P. Robinson, M.J. Daniels, Fluorescent, bioluminescent, and optogenetic approaches to study excitable physiology in the single cardiomyocyte, Cells 7 (2018) 51, https://doi.org/10.3390/cells7060051.
[63] K. Trontelj, M. Usaj, D. Miklavčič, Cell electrofusion visualized with fluorescence microscopy, J. vis. Exp. Jove 2010 (1991), https://doi.org/10.3791/1991.
[64] A.R. Ruiz-Fernández, L. Campos, F. Villanelo, S.E. Gutiérrez-Maldonado, T. Perez-Acle, Exploring the conformational changes induced by nanosecond pulsed electric fields on the voltage sensing domain of a Ca2+ channel, Membranes 11 (2021) 473, https://doi.org/10.3390/membranes11070473.
[65] L. Rems, M.A. Kasimova, I. Testa, L. Delemotte, Pulsed electric fields can create pores in the voltage sensors of voltage-gated ion channels, Biophys. J. 119 (2020) 190–205, https://doi.org/10.1016/j.bpj.2020.05.030.
[66] H.H. Yang, F. St-Pierre, Genetically encoded voltage indicators: opportunities and challenges, J. Neurosci. off. J. Soc. Neurosci. 36 (2016) 9977–9989, https://doi.org/10.1523/JNEUROSCI.1095-16.2016.
[67] L. Catacuzzeno, F. Aiello, B. Fioretti, L. Sforna, E. Castigli, P. Ruggieri, A.M. Tata, A. Calogero, F. Franciolini, Serum-activated K and Cl currents underlay U87-MG glioblastoma cell migration, J. Cell. Physiol. 226 (2011) 1926–1933, https://doi.org/10.1002/jcp.22523.
[68] M.A. Kasimova, E. Lindahl, L. Delemotte, Determining the molecular basis of voltage sensitivity in membrane proteins, J. Gen. Physiol. 150 (2018) 1444–1458, https://doi.org/10.1085/jgp.201812086.
[69] A. Litan, S.A. Langhans, Cancer as a channelopathy: ion channels and pumps in tumor development and progression, Front. Cell. Neurosci. 9 (2015) 86, https://doi.org/10.3389/fncel.2015.00086.
[70] H.J. Gould, D. Paul, Cancer as a channelopathy—appreciation of complimentary pathways provides a different perspective for developing treatments, Cancers 14 (2022) 4627, https://doi.org/10.3390/cancers14194627.

[71] J. Mathews, F. Kuehling, D. Baez-Nieto, M. Diberardinis, J.Q. Pan, M. Levin, Ion channel drugs suppress cancer phenotype in NG108-15 and U87 Cells: toward novel electroceuticals for glioblastoma, Cancers 14 (2022) 1499, https://doi.org/10.3390/cancers14061499.

[72] E.P.W. Jenkins, A. Finch, M. Gerigk, I.F. Triantis, C. Watts, G.G. Malliaras, Electrotherapies for glioblastoma, Adv. Sci. 8 (2021) 2100978, https://doi.org/10.1002/advs.202100978.

[73] D. Miklavčič, G. Serša, M. Kryžanowski, S. Novakovič, F. Bobanović, R. Golouh, L. Vodovnik, Tumor treatment by direct electric current-tumor temperature and pH, electrode material and configuration, Bioelectrochem. Bioenerg. 30 (1993) 209–220, https://doi.org/10.1016/0302-4598(93)80080-E.

Supplementary material 1: Additional experimental results

1 Permeabilization and survival in LCIS vs growth medium

Cells *in vitro* are often electroporated in their growth medium [1–5]. However, in our preliminary experiments, we observed that U-87 MG cells showed morphological changes (cell rounding and detachment) after several minutes of keeping them in their growth medium (EMEM) at ambient conditions (Fig. S1.1a), likely due to poor pH buffering capacity of the bicarbonate buffer at ambient CO_2. Such changes were not observed in Live Cell Imaging Solution (LCIS). CHO-K1 were less sensitive and appeared similar in their growth medium (Ham-F12) and LCIS.

We then determined the permeabilization and survival curves for CHO-K1 and U-87 MG cells after exposure to a single 100 µs pulse in their growth medium or LCIS. The permeabilization curve quantifies the cells that become permeabilized, depending on the amplitude of the applied electric pulse. The survival curve quantifies the percentage of cells that are able to survive 24 h after pulse exposure. These experiments were performed on cells in suspension, electroporated in cuvettes, whereby permeabilization was determined by propidium iodide (PI) staining and survival by MTS assay, following out routine protocols [1–6].

To determine cell permeabilization, 150 µl of the cell suspension (1×10^6 cells/ml) in selected medium was transferred to an electroporation cuvette with 2 mm gap distance (VWR, #732-1136), and PI (Molecular Probes, #P1304MP) was added in final concentration of 100 µg/ml. The uptake of PI was detected with a flow cytometer (Attune NxT; Life Technologies, Carlsbad, CA, USA). Samples were excited with a blue laser at 488 nm and emitted fluorescence was detected through a 574/26 nm band-pass filter. 10,000 events were obtained, and data were analyzed using the Attune Nxt software. Fluorescence intensity histograms were used to determine the percentage of cells stained with PI. Gating was set according to sham control (0 V). Measurements for each data point were repeated three times on three different days.

To determine cell survival, cells were electroporated in the same way as for permeabilization experiments. After pulse application, 850 µL of growth medium was added in the electroporation cuvette. 100 µL of the cell suspension (in triplicates) was transferred in a 96-well plate (TPP, Switzerland) and incubated at 37 °C and humidified 5% CO_2 atmosphere. MTS assay (CellTiter 96 AQueous One Solution Cell Proliferation Assay, Promega, USA) was used to assess cell viability 24 hours after electric pulse exposure. According to the manufacturer's instructions, 20 µl of MTS tetrazolium compound was added to the samples, and the 96-well plate was returned to the incubator for 2 hours. The absorbance of formazan (reduced MTS tetrazolium compound) was measured with a spectrofluorometer (Tecan Infinite M200, Tecan, Austria) at 490 nm. The percentage of viable cells was calculated by subtracting the background (absorbance in wells with medium without cells) and normalizing the absorbance of the sample to the absorbance of the sham control.

The results, presented in Fig. S1.1b-c, demonstrate that the electroporation medium did not significantly affect electroporation of CHO-K1 cells (One-way ANOVA). However, U-87 MG cells showed a significant decrease (One-way ANOVA) in cell survival when electroporated in their growth medium compared with LCIS (for 2.8 kV/cm, $p = 0.02$, and for 3.15 kV/cm, $p = 0.008$). In LCIS there was no significant decrease in cell survival compared to control (One-way ANOVA).

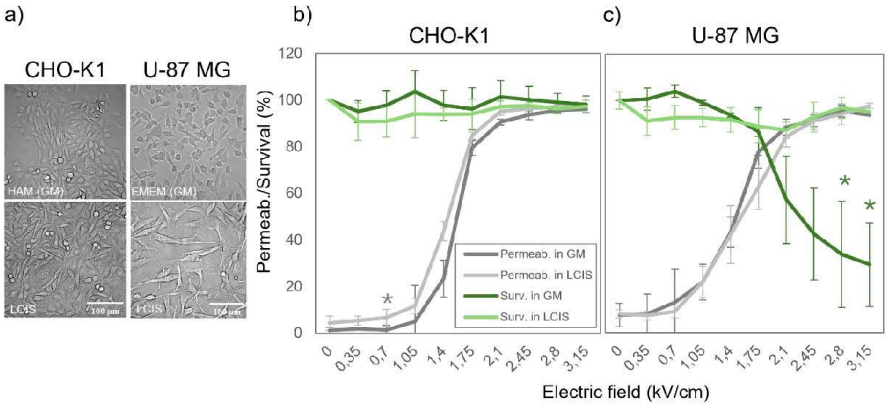

Fig. S1.1: a) The effect of the electroporation medium (growth medium or LCIS) on morphological changes. Cells grown in Lab-Tek imaging chambers were imaged after 20 min in their growth medium or LCIS, both at room temperature. The growth medium affected the morphology of U-87 MG cells, whereas LCIS did not. b-c) The influence of the electroporation medium (growth medium or LCIS) on cell permeabilization and cell survival after exposure to electric pulses of different amplitudes in b) CHO-K1 and c) U-87 MG cells. Statistically significant differences (*: $p<0.05$) were determined by One-way ANOVA.

2 Short-term cell survival after 30 min of time-lapse imaging

Short-term cell survival was assessed after 30 min of Fluo4 time-lapse imaging. Hoechst and PI were added directly to the cells on the microscope in final concentration of 4 µM and 30 µM, respectively. 5 min after addition, the dyes were excited and detected as described in Section 2.6 of the main manuscript.

For positive control we also added 0.2% Triton X and imaged the cells as described in the previous paragraph.

Fig. S1.2 shows no effect on cell survival in CHO-K1 and U-87 MG (Two-way ANOVA; factors: temperature, pulse application) after monitoring calcium transients for 30 min, regardless of whether the experiments were done at T_{room} or T_{ctrl}.

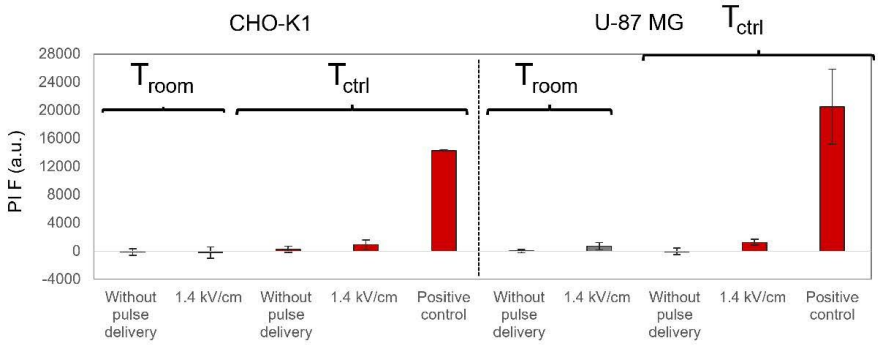

Fig. S1.2: Cell survival in attached cells determined with PI after 30 minutes of monitoring calcium transients with Fluo4 dye for CHO-K1 and U-87 MG cells.

3 Temperature measurements

Measurements of the sample temperature were performed with fiber optic sensor MPK-5 (OpSens Solutions, Quebec, Canada). For measurements at controlled temperature (T_{ctrl}), the incubator surrounding the microscope stage was prewarmed to 37 °C. The sensor was positioned at the bottom of an imaging chamber filled with 1 ml LCIS (Fig. S1.2a), which was prewarmed for 30 min at 37 °C in the same way as during sample staining. Since it took a few minutes to stably position the sensor within the imaging chamber, while keeping the doors of the microscope's incubator open, the sample somewhat cooled down during this time. The microscope's incubator was closed, and the measurements began. Fig. S1.2b shows measurements repeated on three different days. In all repetitions, the sample temperature increased and stabilized within 5 min. We averaged the data from each measurement within the segment 9−10 min, yielding 33.05 °C, 33.26 °C and 33.53 °C for the three measurements. The mean ± standard deviation for these three values is 33.3 °C ± 0.2 °C. Note that the sample temperature was lower than the temperature of the air inside the incubator (~37.5 °C measured with the same sensor), due to evaporation of the liquid from the open chamber.

For measurements at room temperature (T_{room}), we did not control the temperature inside the microscope's incubator, but we did prewarm the imaging chambers to 37 °C. In the first set of measurements, we wanted to see how fast the sample cools down to T_{room}. Immediately after taking the imaging chamber from 37 °C, the chamber was positioned on the microscope stage. The optic fiber was manually held at the bottom of the chamber to avoid the time it took to stability position the sensor like shown in Fig. S1.2a. Three measurements performed using three different imaging chambers on the same day are shown in Fig. S1.2c. The noisiness at the beginning of all measurements is due to movements of the hand that held the sensor. The samples cooled down to steady state temperature within ~15 min. In subsequent measurements, we measured the sample temperature 7-10 min after taking the chamber from 37 °C, which corresponded to the time at which we began imaging a sample in electroporation experiments. The sample temperatures measured on 4 different days were 26.61 °C, 24.40 °C, 26.30 °C, 23.90 °C. The mean ± standard deviation for these four values is 25.3 °C ± 1.4 °C.

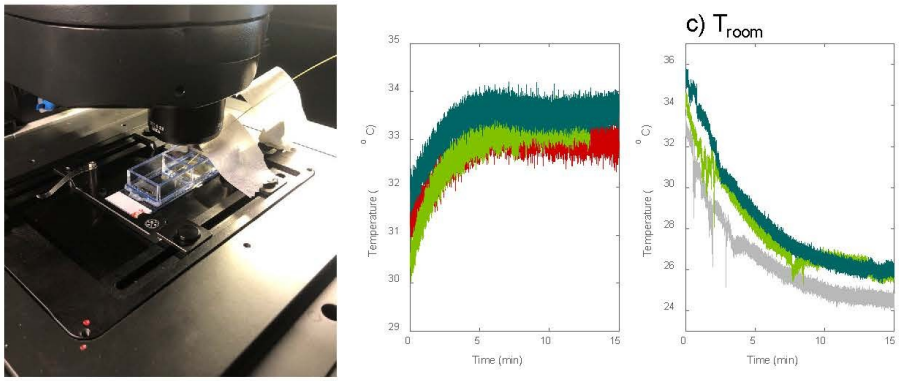

Fig. S1.3: Measurements of the sample temperature. a) Fiber optic sensor positioned within the imaging chamber on the microscope stage. b) Measurements captured when controlling the temperature inside the microscope's incubator at 37 °C. c) Measurements captured at uncontrolled room temperature. See text for further details.

4 Spontaneous changes in TMV in CHO cells

Fig. S1.4 shows spontaneous changes in TMV in (non-excitable) CHO cells. Spontaneous electrical activity was already shown in several non-excitable cells lines [7].

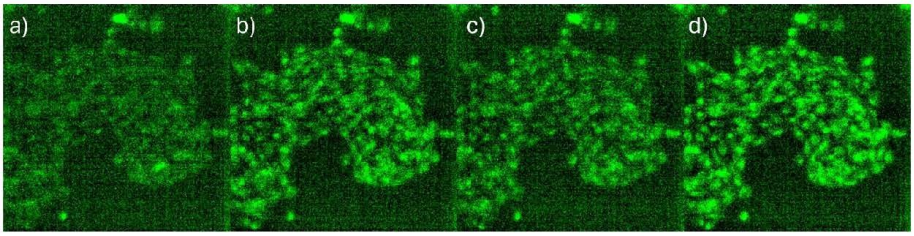

Fig. S1.4: Spontaneous changes in TMV in CHO-K1 cells at different time points without pulse application. a) 0.5 min, b) 10.5 min, c) 15.5 min, d) 18 min.

5 Measuring long-term changes with ElectroFluor630 and FluoVolt

ElectroFluor630 (also known as Di-4-ANEQ(F)PTEA; Potentiometric Probes, USA; #33040) and FluoVolt (Molecular Probes, #F10488) were tested as alternative fluorescent dyes for monitoring long-term changes in TMV in U-87 MG cells. Before cell staining, the growth medium was removed, cells were washed with LCIS, and staining solution was added to the cells grown in the imaging chamber. Following [8], the cells were stained with 12 µM ElectroFluor630 dye in LCIS for 20 min at 4 °C. With FluoVolt dye, the cells were stained following the manufacturer's manual with 5 µL of FluoVolt and 50 µL PowerLoad in LCIS solution for 30 min at 37 °C. Imaging was done on Leica Thunder Imaging System: ElectroFluor630 and FluoVolt were excited with red LED (638/31 nm) and green LED (506/21 nm), and their fluorescence was passed through the DFT51010 filter and CYR71010 filter, respectively.

ElectroFluor630 is classified as a styryl dye, similar to the well-known dye di-4-ANNEPS. These types of dyes spontaneously integrate into the cell membrane and change their fluorescence in response to voltage changes by an electrochromic mechanism [9,10]. The dyes are known to gradually diffuse from the plasma membrane into the cell interior. To inhibit dye internalization, the cells are typically stained at low temperature and then imaged immediately after staining [8,11]. We followed an established protocol for staining the cells at 4°C [8], after which we placed the cells on the microscope at T_{ctrl} (since we observed hyperpolarization only at T_{ctrl}). Representative images in Fig. S1.5b,d demonstrate pronounced internalization of the dye into the cells over time, although dye internalization was detected already at the beginning of observation (0 min). Note, cells were already exposed to T_{ctrl} on the microscope stage during image acquisition. While this internalization is not necessarily problematic for monitoring rapid TMV changes (such as action potentials), it makes it very challenging to monitor long-term and small changes in TMV over 30 min period, since the fluorescence signal continuously drifts. Further limitations of the dye are photobleaching and a rather low sensitivity (~15% / 100 mV) [9], which for U-87 MG cells with a mean resting voltage of -16 ± 4 mV [12] requires detection of fluorescence changes below 2.4%. Due to these limitations, we were unable to perform useful measurements with this dye.

FluoVolt is a photo-induced electron transfer dye comprised of an electron donor complex connected to the fluorophore by a molecular wire. During membrane depolarization, electrons do not move to the fluorophore and the quenching part of the dye is relaxed resulting in fluorescence increase [13].

Similarly to ElectroFluor630, FluoVolt integrates into the plasma membrane and subsequently internalizes into the cell. Compared with ElectroFluor630, FluoVolt has a somewhat higher sensitivity (~25% / 100 mV) but is also prone to photobleaching [14]. When staining U-87 MG cells with FluoVolt, we observed that the cells had undergone some morphological changes even before we imaged them under the microscope. After the time-lapse imaging with pulse delivery, these changes were even more pronounced (Fig. S1.5e-h), likely due to the phototoxic effect of the dye, despite using low illumination intensity (5% LED power, 15 ms exposure time). FluoVolt phototoxicity has been reported previously [15]. Due to observed morphological changes, we did not use the dye further.

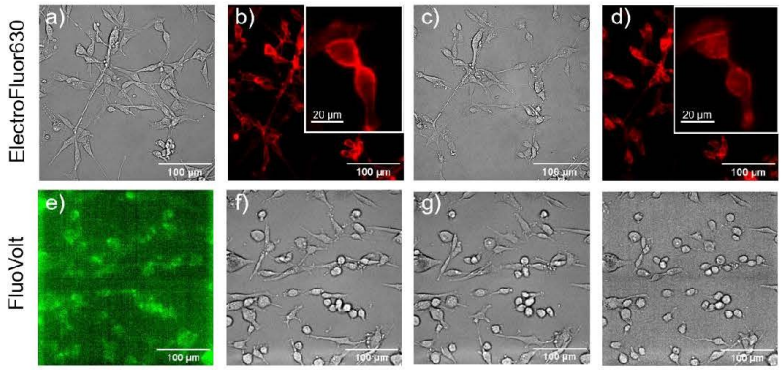

Fig. S1.5: Testing ElectroFluor630 and FluoVolt dyes. a-d) Brightfield and fluorescence images of U-87 MG cells stained with ElectroFluor630 dye were captured 5 min (a, b) and 20 min (c, d) after placing the cells on the microscope stage. e-h) Fluorescence and brightfield images of cells stained with FluoVolt dye were captured 5 min (e, f), 10 min (g), and 35 min (h) after placing the cells on the microscope stage. A pulse (100 µs, 1.4 kV/cm) was delivered 5.5 min after placing the cells on the microscope, i.e., 1.5 min after beginning of 30 min time-lapse imaging.

References

[1] T. Polajžer, D. Miklavčič, Development of adaptive resistance to electric pulsed field treatment in CHO cell line in vitro, Sci. Rep. 10 (2020) 9988. https://doi.org/10.1038/s41598-020-66879-w.

[2] T. Polajzer, T. Jarm, D. Miklavcic, Analysis of damage-associated molecular pattern molecules due to electroporation of cells in vitro, Radiol. Oncol. 54 (2020) 317–328. https://doi.org/10.2478/raon-2020-0047.

[3] T. Polajžer, J. Dermol–Černe, M. Reberšek, R. O'Connor, D. Miklavčič, Cancellation effect is present in high-frequency reversible and irreversible electroporation, Bioelectrochemistry 132 (2020) 107442. https://doi.org/10.1016/j.bioelechem.2019.107442.

[4] T. Potočnik, D. Miklavčič, A. Maček Lebar, Effect of electroporation and recovery medium pH on cell membrane permeabilization, cell survival and gene transfer efficiency in vitro, Bioelectrochemistry 130 (2019) 107342. https://doi.org/10.1016/j.bioelechem.2019.107342.

[5] T. Potočnik, D. Miklavčič, A. Maček Lebar, Gene transfer by electroporation with high frequency bipolar pulses in vitro, Bioelectrochemistry 140 (2021) 107803. https://doi.org/10.1016/j.bioelechem.2021.107803.

[6] T. Batista Napotnik, D. Miklavčič, In vitro electroporation detection methods – An overview, Bioelectrochemistry 120 (2018) 166–182. https://doi.org/10.1016/j.bioelechem.2017.12.005.

[7] P. Rühl, A.G. Nair, N. Gawande, S.N.C.W. Dehiwalage, L. Münster, R. Schönherr, S.H. Heinemann, An Ultrasensitive Genetically Encoded Voltage Indicator Uncovers the Electrical Activity of Non-Excitable Cells, Adv. Sci. (2024) 2307938. https://doi.org/10.1002/advs.202307938.

[8] T. Batista Napotnik, B. Kos, T. Jarm, D. Miklavčič, R.P. O'Connor, L. Rems, Genetically engineered HEK cells as a valuable tool for studying electroporation in excitable cells, Sci. Rep. 14 (2024) 720. https://doi.org/10.1038/s41598-023-51073-5.

[9] P. Yan, C.D. Acker, W.-L. Zhou, P. Lee, C. Bollensdorff, A. Negrean, J. Lotti, L. Sacconi, S.D. Antic, P. Kohl, H.D. Mansvelder, F.S. Pavone, L.M. Loew, Palette of fluorinated voltage-sensitive hemicyanine dyes, Proc. Natl. Acad. Sci. 109 (2012) 20443–20448. https://doi.org/10.1073/pnas.1214850109.

[10] E. Fluhler, V.G. Burnham, L.M. Loew, Spectra, membrane binding, and potentiometric responses of new charge shift probes, Biochemistry 24 (1985) 5749–5755. https://doi.org/10.1021/bi00342a010.

[11] G. Pucihar, T. Kotnik, D. Miklavčič, Measuring the Induced Membrane Voltage with Di-8-ANEPPS, J. Vis. Exp. JoVE (2009) 1659. https://doi.org/10.3791/1659.

[12] T. Ducret, A. Vacher, P. Vacher, Voltage-dependent ionic conductances in the human malignant astrocytoma cell line U87-MG, Mol. Membr. Biol. 20 (2003) 329–343. https://doi.org/10.1080/0968763031000138037.

[13] A.S. Kiester, B.L. Ibey, Z.N. Coker, A.G. Pakhomov, J.N. Bixler, Strobe photography mapping of cell membrane potential with nanosecond resolution, Bioelectrochemistry Amst. Neth. 142 (2021) 107929. https://doi.org/10.1016/j.bioelechem.2021.107929.

[14] A.G. Pakhomov, I. Semenov, M. Casciola, S. Xiao, Neuronal excitation and permeabilization by 200-ns pulsed electric field: An optical membrane potential study with FluoVolt dye, Biochim. Biophys. Acta BBA - Biomembr. 1859 (2017) 1273–1281. https://doi.org/10.1016/j.bbamem.2017.04.016.

[15] C.N. Broyles, P. Robinson, M.J. Daniels, Fluorescent, Bioluminescent, and Optogenetic Approaches to Study Excitable Physiology in the Single Cardiomyocyte, Cells 7 (2018) 51. https://doi.org/10.3390/cells7060051.

Supplementary material 2: Image processing

1 Images of the FMP fluorescence

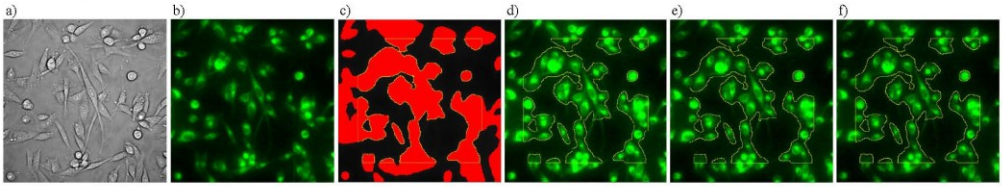

Fig. S2.1: a) Brightfield and b) FMP fluorescence of U87 cells at the beginning of the time-lapse imaging. The first fluorescence image was thresholded in ImageJ Fiji using its embedded automatic thresholding method "Percentile". The resulting mask is shown in c), where the red areas correspond to cell regions. To determine the ROI, the region of the mask was further constrained to the inner ~77% dimensions of the field of view, since the thresholding algorithm did not always select well the cells around the edges of the image (see Fig. S2.3). The final ROI is shown with yellow edges. Application of a pulse 100 µs, 1.4 kV/cm resulted in an increase in fluorescence: shown are the frames at d) maximum fluorescence increase, e) 20 min after the beginning of time-lapse imaging, and f) at the end of the 30 min time-lapse imaging. All fluorescence images were processed with the ImageJ's automatic "Enhance Contrast" function in the same way based on the first captured image. The side length of each image corresponds to 330.15 µm. Images captured at room temperature.

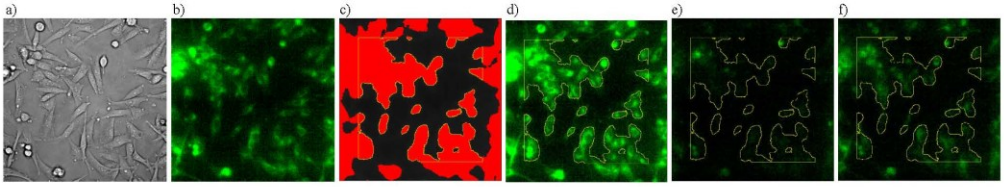

Fig. S2.2: Same representation as in Fig. S2.1, but for U-87 MG cells imaged at controlled temperature. Note the increase in fluorescence in d) followed by decrease in e) and again increase in f).

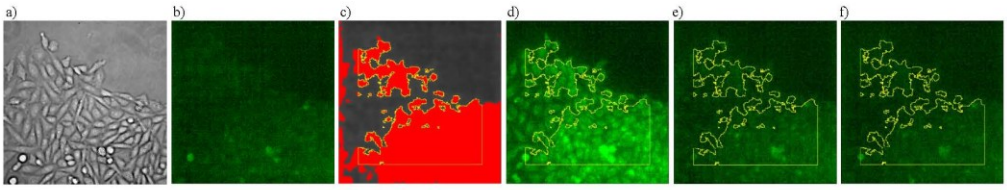

Fig. S2.3: Same representation as in Fig. S2.1, but for CHO-K1 cells imaged at controlled temperature. Images of CHO-K1 cells were processed in the same way as images of U-87 MG cells. Note that the baseline fluorescence in CHO-K1 cells was lower than in U-87 MG cells despite the same illumination settings. For this reason, we increased the illumination for CHO-K1 cells to obtain results in Fig. 5a. The increased illumination did not affect the response of the cells to an electric pulse (cf. Fig. 3a and Fig. 4a).

2 Images of the TMRE fluorescence

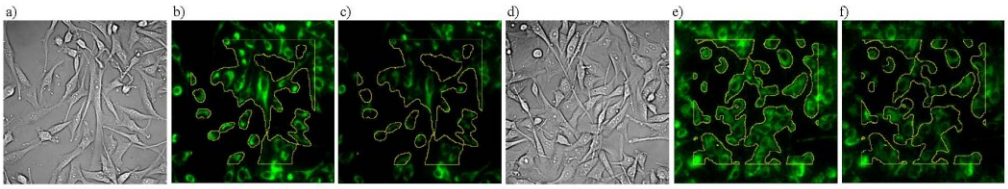

Fig. S2.4: a) Brightfield, b) baseline TMRE fluorescence, and c) TMRE fluorescence at the end of 30 min time-lapse of U-87 MG cells that were exposed to 100 µs, 1.4 kV/cm pulse at 1.5 min after the beginning of the time-lapse, at controlled temperature. d-f) Same as in a-c) but for control cells not exposed to electric pulse. The fluorescence gradually decreased in both pulsed and non-pulsed samples. Images of TMRE were processed in the same way as images of FMP fluorescence: the first image was thresholded in ImageJ Fiji using its embedded automatic thresholding method "Percentile". Also, the imaging settings (% LED power, exposure time) were the same as for the FMP dye.

3 Images of the Fluo4 fluorescence

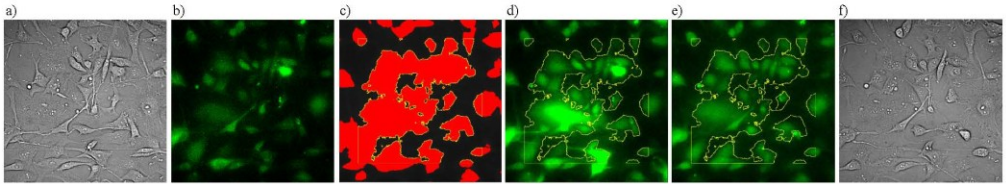

Fig. S2.5: a) Brightfield and b) Fluo4 fluorescence in U87 cells at the beginning of the time-lapse imaging. Images of Fluo4 were processed in the same way as images of FMP fluorescence: the first image was thresholded in ImageJ Fiji using its embedded automatic thresholding method "Percentile". The resulting mask is shown in c). Application of a pulse 100 µs, 1.4 kV/cm resulted in a transient increase in fluorescence followed by decrease: the maximum fluorescence is shown in d) and the fluorescence at the end of the 30 min time-lapse imaging in shown in e). f) The brightfield image, taken after the time-lapse imaging, shows that the cells remained in focus during the entire imaging period. All fluorescence images were processed with the ImageJ's automatic "Enhance Contrast" function in the same way based on the first captured image. The side length of each image corresponds to 330.15 µm. Images captured at room temperature.

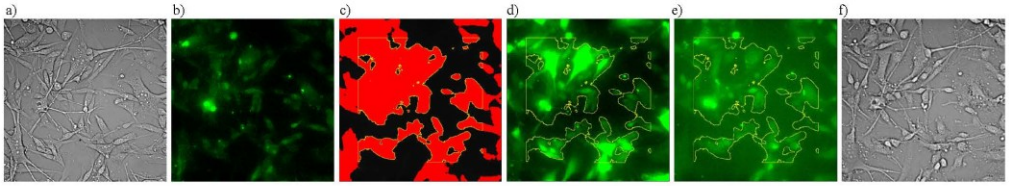

Fig. S2.6: Same representation as in Fig. 2.5, but for images taken at controlled temperature. At controlled temperature the background intensity was approximately linearly increasing with time - note the higher background fluorescence at the end of the time-lapse imaging in panel e) compared with Fig. 2.5e. Similar increase was also observed in control samples that were not exposed to electric pulse; thus, the increase cannot be associated with electroporation. It might be due to gradual leakout of the dye from dead/floating cells in the imaging chamber. To correct for this increase, we determined the average background intensity from each image in the time-lapse and subtracted it from the average intensity within the ROI representing the cells. For consistency, we used the same background subtraction approach also in images captured at room temperature.

4 Images of the Propidium (PI) fluorescence

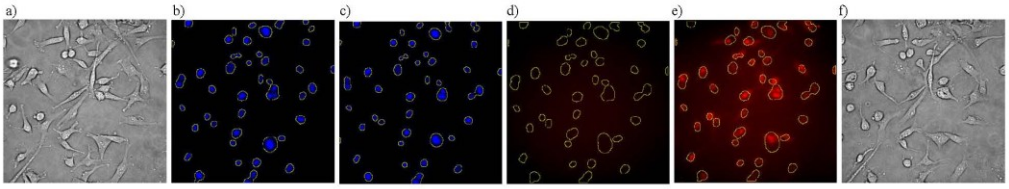

Fig. S2.7: a) Brightfield, b) Hoechst fluorescence at the beginning and c) end of time-lapse imaging of U-87 MG cells. The two Hoechst images were thresholded in ImageJ Fiji using its embedded automatic thresholding method "Huang". The resulting two ROIs were superposed using operator AND to determine the final ROI. Superposition of the two ROIs was used to compensate for small lateral movement of cells during the 30 min observation time. The superposed ROI was then applied to images of the Propidium (PI) fluorescence. d) Defining ROI based on Hoechst images enabled us to locate the cells at the beginning of the time-lapse, when the cells exhibited practically no baseline fluorescence. Application of a pulse 100 µs, 1.4 kV/cm resulted in an increase in PI fluorescence. Panels e) and f) show the PI fluorescence and brightfield image at the end of the 30 min time-lapse, respectively. Note that the background intensity in PI images was approximately linearly increasing with time. We corrected for this background increase in the same way as in Fluo4 images, see the caption of Fig. S2.6. Since the background intensity was not completely homogenous, we manually selected 5 small rectangular regions representing background at different locations in the image and determined the average background intensity from all 5 regions.

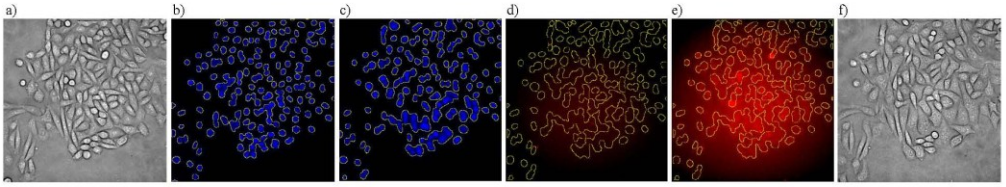

Fig. S2.8: Same representation as in Fig. S2.7, but for CHO-K1 cells.

Supplementary material 3: Model description

1 The model of intracellular calcium dynamics

To describe the intracellular calcium dynamics and changes in transmembrane voltage, we build upon the minimal model proposed by Catacuzzeno et al. [1]. The model includes four relevant fluxes contributing to the intracellular Ca^{2+} dynamics: J_{in}, which describes the uptake of Ca^{2+} from the extracellular medium through ion channels in the plasma membrane; J_{out}, which describes the export of Ca^{2+} to the extracellular medium by plasma membrane Ca^{2+} pumps; J_{rel}, which describes the release of Ca^{2+} from the endoplasmic reticulum (ER); and J_{serca}, which describes the uptake of Ca^{2+} into ER by the SERCA pump. The model also considers the presence of calcium buffers to which Ca^{2+} binds, thereby reducing the concentration of free Ca^{2+} inside the cell. These buffers are found both in the cytoplasm and in the ER. Ca^{2+} binding follows the reaction schemes:

$$Ca^{2+} + B_c \underset{k_{off,c}}{\overset{k_{on,c}}{\rightleftarrows}} CaB_c \tag{S1}$$

$$Ca^{2+} + B_{er} \underset{k_{off,er}}{\overset{k_{on,er}}{\rightleftarrows}} CaB_{er} \tag{S2}$$

where B_c and B_{er} denote the binding sites in the cytoplasm and the ER, respectively, whereas k_{on}, k_{off}, $k_{on,er}$ and $k_{off,er}$ are the reaction rates.

Assuming that Ca^{2+} and Ca^{2+}-binding buffers are homogeneously distributed throughout the cytoplasm and ER, and that the rate of Ca^{2+} binding is much faster than the dynamic changes in intracellular Ca^{2+}, then the changes in Ca^{2+} concentration within the cytoplasm (variable x) and within the ER (variable y) can be described as:

$$\frac{dx}{dt} = \frac{A_{pm}}{C_c}(J_{in} - J_{out}) + \frac{A_{er}}{C_c}(J_{rel} - J_{serca}) \tag{S3}$$

$$\frac{dy}{dt} = -\frac{A_{er}}{C_{er}}(J_{rel} - J_{serca}) \tag{S4}$$

where A_{pm} in A_{er} are, respectively, the surface area of the plasma membrane and the ER membrane. C_c and C_{er} represent the effective volume of the cytoplasm and the ER, respectively:

$$C_c = V_c\left(1 + \frac{B_{T,c}}{K_{D,c}}\right) \tag{S5}$$

$$C_{er} = V_{er}\left(1 + \frac{B_{T,er}}{K_{D,er}}\right) \tag{S6}$$

where V_c and V_{er} are the volume of the cell and the ER, respectively, $B_{T,c}$ and $B_{T,er}$ are the concentrations of calcium buffers in the cytoplasm and ER, respectively, whereas $K_{D,c} = k_{off,c}/k_{on,c}$ and $K_{D,er} = k_{off,er}/k_{on,er}$ are the equilibrium constants for equations (S1) and (S2).

The molar flux density J_{in} is defined as:

$$J_{in} = -\frac{1}{z_{Ca}FA_{pm}}\left(g_{Ca0} + g_{Cac}\frac{p}{p+K_0}\right)(U_m - U_{Ca}) \tag{S7}$$

where g_{Ca0} is the conductivity due to leak inward Ca^{2+} current, g_{Cac} is the maximum Ca^{2+} conductance due to hormonal stimulation, p is the concentration of inositol triphosphate (IP_3), which is released upon hormonal stimulation, K_0 is the reaction constant for the binding of the hormone to the calcium channels in the plasma membrane, U_m is the transmembrane voltage, U_{Ca} is the reversal potential for Ca^{2+} ions, z_{Ca} is the valence of Ca^{2+} ions, F is the Faraday constant and A_{pm} is the surface area of the plasma membrane.

The molar flux density J_{out} is defined as:

$$J_{out} = v_4 \frac{x^2}{x^2 + {K_4}^2} \tag{S8}$$

where K_4 is and the binding constant of Ca^{2+} to calcium pumps in the plasma membrane, whereas v_4 is a corresponding Ca^{2+} flux constant.

The molar flux density J_{serca} is defined as:

$$J_{serca} = v_3 \frac{x^2}{x^2 + {K_3}^2} \tag{S9}$$

where K_3 is and the binding constant of Ca^{2+} to SERCA pump in the ER, whereas v_3 is a corresponding Ca^{2+} flux constant.

The molar flux density J_{rel} is defined as:

$$J_{rel} = (k_1 {m_\infty}^3 {w_\infty}^3 + k_2)(y - x) \tag{S10}$$

where m_∞ describes the Ca^{2+}-mediated fast activation of IP_3 receptors (they release Ca^{2+} from the ER), which is further sensitized by the IP_3 concentration p:

$$m_\infty = \frac{p}{d_p + p} \frac{x}{d_a + x} \tag{S11}$$

where d_p and d_a are model parameters. The variable w_∞ describes the slow inactivation of IP_3 receptors:

$$w_\infty = \frac{Q(p)}{Q(p) + x} \tag{S12}$$

$$Q(p) = d_2 \frac{p + d_1}{p + d_3}$$

where d_1, d_2 are d_3 are model parameters.

The dynamics of the transmembrane voltage U_m due to ionic currents across the plasma membrane are described as:

$$\frac{dU_m}{dt} = -\frac{1}{C_m}\left(\left(g_{Ca0} + g_{Cac}\frac{p}{p + K_0}\right)(U_m - U_{Ca}) + g_K(U_m - U_K) + g_L(U_m - U_L)\right) \tag{S13}$$

where the terms on the right respectively describe the current through calcium channels, calcium-activated potassium channels, and leak channels. U_{Ca}, U_K, and U_L denote the reversal potentials for Ca^{2+}, K^+ and leak ions. The conductance of calcium-activated potassium channels g_K is described by:

$$g_K = g_{Kmax} \frac{x^n}{x^n + {K_{Ca}}^n} \tag{S14}$$

where g_{Kmax} denotes the maximum calcium-activated potassium conductance, whereas K_{Ca} and n are the dissociation constant and Hill coefficient (Fig. S3.1).

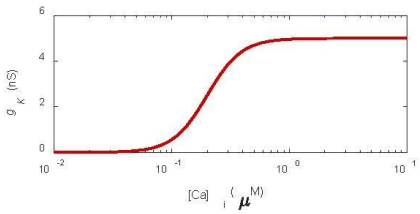

Fig. S3.1: Conductance of calcium-activated potassium channels versus intracellular Ca^{2+} concentration.

We verified that the system of equations (S1)-(S14) correctly reproduces the oscillations of intracellular Ca^{2+} at IP_3 concentration p = 2 μM, as presented in the original paper (Figs. S3.2 and S3.3). Note that while Catacuzzeno et al. [1] also presented a version of the model that includes the current through gap junctions, we neglected this current for simplicity.

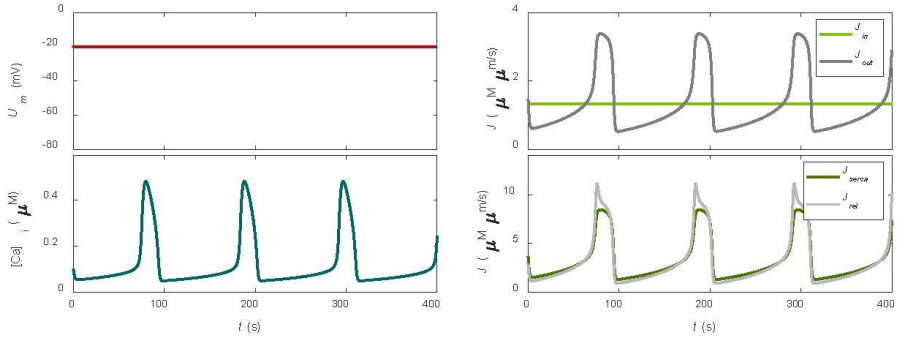

Fig. S3.2: Verification of our implementation of the model by replicating the results presented in Fig. 2 of the original paper [1]. Calculations were performed for IP_3 concentration p = 2 μM and g_{Kmax} = 0 nS.

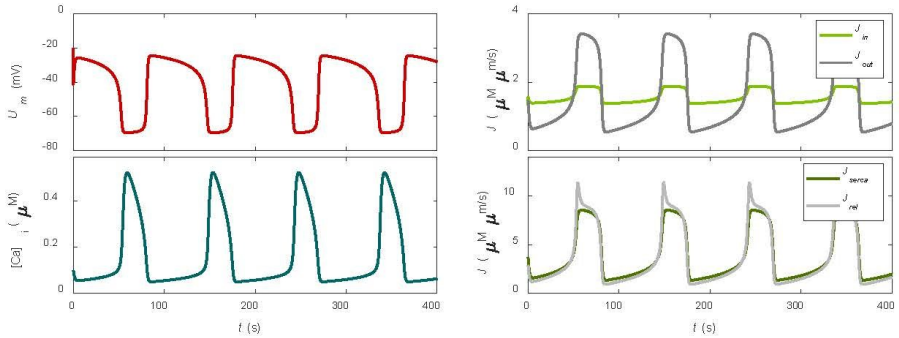

Fig. S3.3: Same calculations as in Fig. S3.2, but for g_{Kmax} = 5 nS.

2 Addition of electroporation to the model

2.1 The nonselective current of Na^+, K^+ and Cl^- ions through pores

Electroporation results in an increase in plasma membrane permeability and thus also an increase in transmembrane ionic currents. Theoretical models were developed mostly under the assumption that these ionic currents are due to the formation of hydrophilic pores, which are formed in the lipid bilayer directly under the influence of an external electric field [2]. However, more recent results suggest that such pores close very rapidly (on submicrosecond time scale) after exposure to electrical pulses [3]. The increase in ionic currents observed on the time scale of minutes after pulse exposure, which contributes to long-lived changes in transmembrane voltage, are more likely related to pores or conductive structures formed as a result of lipid oxidation due to electric field exposure [4] and to pores formed as a result of electric field damage to certain membrane proteins [5]. The ionic current through such pores has not yet been well characterized; therefore, we assume that we can describe the ionic current through any of these types of pores in the same way.

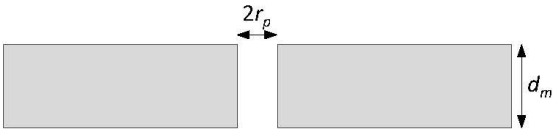

Figure S3.4: Schematic representation of a cylindrical pore with radius r_p within the plasma membrane with thickness d_m.

Let us consider a simplified model of a cylindrical pore with radius r_p within the plasma membrane with thickness d_m, as shown schematically in Fig. S3.4. In electroporation models, it is usually considered that the pore is not selective for any ion type. Rather, the flux of Na^+, K^+ and Cl^- ions, which are most abundant in the extracellular and intracellular media, is represented in terms of the electric conductivity of the extracellular and intracellular aqueous solution [6,7]. The analytical solution for the conductance (unit S) of a cylindrical pore is [7]:

$$G_p = \frac{2\sigma_p \pi {r_p}^2}{\pi r_p + 2d_m} \tag{S15}$$

where σ_p is the effective conductivity (unit S/m) inside the pore, which depends on the conductivities of the extracellular medium σ_e and the intracellular medium σ_i:

$$\sigma_p = \frac{\sigma_e - \sigma_i}{\ln(\sigma_e/\sigma_i)} \tag{S16}$$

The current of Na^+, K^+ and Cl^- ions through a single pore at transmembrane voltage U_m is thus:

$$I_p = G_p U_m \tag{S17}$$

A large number of pores can form in the plasma membrane during the exposure of cells to an electric pulse (some models estimate more than 100,000 pores [6]). However, after the pulse exposure, most pores rapidly close and only a fraction of pores contributes to long-lived membrane permeability that remains increased for minutes [8]. Thus, only these long-lived pores or membrane defects can be responsible for the long-lived changes in the transmembrane voltage that we observed experimentally.

If we assume that the pulse formed N_{pores} long-lived pores, which resealed with function $f_{resealing}(t)$, then we can describe the pore-mediated increase in membrane conductance as:

$$g_{ep} = N_{pores} G_p f_{resealing}(t) \tag{S18}$$

The resealing of these long-lived pores can be discerned from the kinetics of post-pulse transmembrane molecular transport, e.g. propidium (PI) uptake [9]. We thus used our PI uptake measurements to determine the resealing function $f_{resealing}(t)$, as explained later in Section S3.2.3.

In the final model we added the contribution of g_{ep} to eq. (S13):

$$\frac{dU_m}{dt} = -\frac{1}{C_m}\left(g_{Ca0}(U_m - U_{Ca}) + g_{K,Ca}(U_m - U_K) + g_L(U_m - U_L) + g_{ep}U_m\right) \tag{S19}$$

where we assumed a reversal potential of 0 mV due to the nonselective conduction of ions through pores [10]. Equation (S19) is equal to equation (2) of the main manuscript.

2.2 The flux of Ca2+ ions through pores

Ca^{2+} ions are approximately 70× less abundant in the extracellular medium than Na^+ ions, and even 10,000× less abundant in the intracellular medium [11]. Therefore, Ca^{2+} ions do not contribute significantly increase in membrane conductance due to electroporation. However, we need a description of the transport of Ca^{2+} ions through pores to describe the flux that contributes to the increase in intracellular Ca^{2+}. For the molar flux density of a selected solute (in our case Ca^{2+}) through a cylindrical pore, Li and Lin [12] derived the following equation based on the Nernst-Planck description of electro-diffusion:

$$J_p = D_{Ca}\frac{u_m + \ln(\chi)}{d_m}\frac{\chi - 1}{\ln(\chi)}\frac{[Ca]_e - [Ca]_i \exp(u_m)}{(1 - \chi\exp(u_m))} \tag{S20}$$

$[Ca]_i$ and $[Ca]_e$ are the extracellular and intracellular Ca^{2+} concentration, $\chi = \sigma_i/\sigma_e$ is the ratio between the extracellular and intracellular conductivity, and u_m is a nondimensionalized transmembrane voltage (Péclet number):

$$u_m = \frac{z_{Ca}F}{RT}U_m \tag{S21}$$

where z_{Ca} is the valence of Ca^{2+} ions, F is the Faraday constant, R is the universal gas constant, and T is the temperature.

Equation (S20) treats the Ca^{2+} ion as a point charge and ignores the size of the ion. However, for small pores, such as those expected in the plasma membrane after pulse exposure, the size of the ion should be taken into account [13]. When an ion is placed in a pore of comparable size, the ion's movement becomes restricted due to the limited pore space. In addition, the ion needs to overcome an energy barrier, since it is energetically unfavorable to bring a charged particle from an aqueous solution with high dielectric permittivity to a membrane with low permittivity. In other words, the diffusion coefficient of the ion in the pore is reduced by a factor H, which describes the hindered motion of the ion through the pore due to the finite size of the pore, and a factor K, which describes the hindered motion of the ion due to its charge.

Factor H was derived by Bungay in Brenner [14] for a spherical particle with radius r_X, moving through a tube filled with fluid:

$$H = \frac{6\pi}{f_t}(1 - \lambda)^2 \tag{S22}$$

$$\lambda = \frac{r_X}{r_p}$$

$$f_t = \frac{9}{4}\pi^2\sqrt{2}(1-\lambda)^{-\frac{5}{2}}(1 + a_1(1-\lambda) + a_2(1-\lambda)^2) + a_3 + a_4\lambda + a_5\lambda^2 + a_6\lambda^3 + a_7\lambda^4$$

The values of parameters a_i are as follows: a_1 = -1.2167, a_2 = 1.5336, a_3 = -22.5083, a_4 = -5.6117, a_5 = -0.3363, a_6 = -1.216, a_7 = 1.647.

Factor K was derived for a particle with charge z_X under the assumption that the energy barrier has a trapezoidal shape along the central axis of the pore [13,15]:

$$K = (\exp(u_m) - 1)\left(\frac{w_0\exp(w_0 - \nu u_m) - \nu u_m}{w_0 - \nu u_m}\exp(u_m) - \frac{w_0\exp(w_0 + \nu u_m) + \nu u_m}{w_0 + \nu u_m}\right)^{-1} \quad \text{(S23)}$$

$$w_0 = 5.3643\frac{(z_X q_e)^2}{kT} r_p^{-1.803}$$

where ν is the relative length of the pore entrance, and w_0 is the height of the energy barrier.

The molar flux density through the plasma membrane with area A_{pm}, which contains N_{pores} with radius r_p, and considering the membrane resealing function $f_{resealing}$, can then be written as:

$$J_{ep} = \frac{N_{pores}\pi {r_p}^2}{A_{pm}} HKJ_p f_{resealing}(t) \quad \text{(S24)}$$

where J_p is determined by equation (S20), whereas H and K are determined by equations (S22) and (S23) using the radius and valence of Ca^{2+} ions, $r_X = r_{Ca}$ in $z_X = z_{Ca}$. Fig. S3.5 shows the dependence of factors H and K on the pore radius.

In the final model, the flux J_{ep} was added to equation (S3):

$$\frac{dx}{dt} = \frac{A_{pm}}{C_c}\left(J_{in} + J_{ep,Ca} - J_{out}\right) + \frac{A_{er}}{C_c}\left(J_{rel} - J_{serca}\right) \quad \text{(S25)}$$

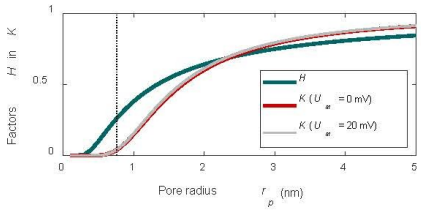

Fig. S3.5: Factors H in K for a Ca^{2+} ion with radius 0.2 nm and valence +2 versus the pore radius. The vertical line marks the pore radius used in the model.

2.3 Derivation of the resealing function

We determined the resealing function through our measurements of the PI uptake. The uptake of PI molecules into a cell after the pulse exposure (when the external electric field is 0 V/cm) is predominantly characterized by diffusion [9]. If we neglect the binding kinetics of PI to nucleic acids within the cell and assume homogenous distribution of PI within the cell, then the time-dependent increase in intracellular PI molar concentration $c(t)$ can be written as:

$$\frac{dc(t)}{dt}\frac{V}{A_{ep}(t)} = -D\frac{c(t)-c_e}{d_m} \tag{S26}$$

where $A_{ep}(t)$ is the total surface area of pores, V is the cell volume, c_e is the extracellular PI concentration, D is the diffusion coefficient of PI within the pores, and d_m in the membrane thickness. If we further assume that $c(t) << c_e$ (this is justified since PI rapidly binds to nucleic acids and there comparably small amount of free PI within the cell), and we consider that $A_{ep}(t) = N\pi r_p^2 f_{resealing}(t)$, then we can rewrite:

$$\frac{dc(t)}{dt} = \frac{D}{V}\frac{c_e}{d_m}N\pi r_p^2 f_{resealing}(t) \tag{S27}$$

We fitted the increase in PI fluorescence to the function $f = A\left(1 - e^{-t/\tau} + kt\right)$. The increase in PI fluorescence is roughly linearly proportional to PI concentration, thus:

$$c(t) = B\left(1 - e^{-t/\tau} + kt\right) \tag{S28}$$

where B is a proportionality constant. The derivative $dc(t)/dt$ is:

$$\frac{dc(t)}{dt} = B\left(\frac{1}{\tau}e^{-t/\tau} + k\right) \tag{S29}$$

Equating (S25) and (S27) gives the resealing function:

$$f_{resealing}(t) = \frac{\tau}{1+k\tau}\left(\frac{1}{\tau}e^{-t/\tau} + k\right) \tag{S30}$$

where we considered $f_{resealing}(0) = 1$, giving $B = Dc_eN\pi r_p^2/(Vd_m)(\tau/(1+k\tau))$. Equation (S30) can be further rewritten to:

$$f_{resealing} = (1-\delta)e^{-t/\tau} + \delta \tag{S31}$$

$$\delta = \frac{k\tau}{1+k\tau} \tag{S32}$$

where δ can be understood as the fraction of pores that do not close on 30 min time scale and is responsible for the small persisted linear increase in PI uptake. If we further consider that the pulse is applied at time $t = t_{pulse}$, then:

$$f_{resealing} = (1-\delta)e^{-(t-t_{pulse})/\tau} + \delta, \qquad t \geq t_{pulse} \tag{S33}$$

Equation (S33) is equal to equation (5) in the main manuscript.

3 Values of the model parameters

The model of intracellular calcium dynamics was developed mainly based on data for rat hepatocytes [1,16]. Since the radius of suspended U-87 MG cells (6.7 μm [17]) as well as CHO-K1 cells (6.1 μm [18]) is very close to the radius of rat hepatocytes (6 μm [1,16]), we kept the values of all parameters the same as in the original publications [1,16].

We assumed that electroporation does not promote formation of IP_3 and set its concentration to p = 0 μM.

For the maximum conductance of calcium-activated potassium channels we used the value of 5 nS from the original publication [1]. In addition, we also performed calculations for a higher value of 15 nS. This value was estimated from electrophysiological measurements of calcium-activated big potassium (BK) channels in U-87 MG cells, where the BK current was 67 ± 9 pA/pF at 140 mV [19]. Considering that the capacitance of U-87 MG cells is ~30 pF [20], we get g_K = 67 pA/pF · 30 pF / 0.14 V ≈ 15 nS.

For the diffusion coefficient of calcium ions, we took the value tabulated for 25°C and converted it to 33°C (measured sample temperature) taking into account a relative temperature coefficient of 2.1%/K [21].

Extracellular conductivity and extracellular calcium ion concentration correspond to the properties of the Live Cell Imaging Solution (LCIS) [22].

Table S3.1: Values of the model parameters.

Parameter	Symbol	Value	Reference
Cell radius	r_{cell}	6 μm	[16]
Cell volume	V_{cell}	$4\pi r_{cell}^3/3$	[16]
Volume of the cytoplasm	V_c	$V_{cell}/3$	[16]
Volume of the ER	V_{er}	$V_{cell}/100$	[16]
Effective volume of the cytoplasm	C_c	$75 \cdot V_c$	[16]
Effective volume of the ER	C_{er}	$225 \cdot V_{er}$	[16]
PM area	A_{pm}	$2 \cdot 10^4 \cdot C_c$	[16]
ER membrane area	A_{er}	$2 \cdot A_{pm}$	[16]
Binding constant of the hormone to PM Ca^{2+} channels	K_0	4.0 μM	[1,16]
Rate constant for Ca^{2+} release through IP_3 receptors	k_1	40 μm/s	[1,16]
Rate constant for leak-mediated Ca^{2+} release from ER	k_2	0.02 μm/s	[1,16]
Binding constant of Ca^{2+} to SERCA	K_3	0.12 μM	[1,16]
Binding constant of Ca^{2+} to PM Ca^{2+}-ATPases	K_4	0.12 μM	[1,16]
Ca^{2+} flux constant through SERCA	v_3	9 μM·μm/s	[1,16]
Ca^{2+} flux constant through PM Ca^{2+}-ATPases	v_4	3.6 μM·μm/s	[1,16]
Equilibrium constants for IP_3 binding to IP_3 receptors	d_p d_a	0.2 μM 0.4 μM	[1,16]
Equilibrium constants for IP_3 receptor inactivation	d_1 d_2 d_3	0.3 μM 0.4 μM 0.2 μM	[1,16]
Binding constant of Ca^{2+} to Ca^{2+}-activated K+ channels	K_{Ca}	0.2 μM	[1]
Ca^{2+} binding sites in Ca^{2+}-activated K+ channels	n	3	[1]
IP_3 concentration	p	0 μM	
Conductance of Ca^{2+} leak current in PM	g_{Ca0}	$g_{Cac}/20$	[1]
IP_3-activated Ca^{2+} conductance in PM	g_{Cac}	2.5 pS	[1]
Maximum conductance of Ca^{2+}-activated K^+ channels	g_{Kmax}	5 nS 15 nS	[1] [19,20]
Conductance of the leak current in PM	g_L	1 nS	[1]
Reversal potential for Ca^{2+} ions	U_{Ca}	100 mV	[1]

Reversal potential for leak current	U_L	−20 mV	[1]
Reversal potential for K^+ ions	U_K	−80 mV	[1]
Extracellular conductivity (LCIS)	σ_e	1.5 S/m	[22]
Intracellular conductivity	σ_i	0.5 S/m	[6]
Extracellular Ca^{2+} concentration (LCIS)	$[Ca]_e$	1.8 mM	[22]
Membrane capacitance	C_m	A_{pm}·0.01 F/m²	[1,16]
Membrane thickness	d_m	5 nm	[6]
Pore radius	r_p	0.76 nm	[6]
Number of pores	N_{pores}	variable	
Parameters of the $f_{reseeling}$ function	τ k	54 s variable	fit to PI uptake
Ca^{2+} radius	r_{Ca}	0.2 nm	[13]
Ca^{2+} valence	z_{Ca}	+2	[1,16]
Ca^{2+} diffusion coefficient	D_{Ca}	$9.3 \cdot 10^{-10}$ m/s²	[21]
Temperature	T	306 K	measured

PM = plasma membrane; ER = endoplasmic reticulum; IP_3 = inositol triphosphate

References

[1] L. Catacuzzeno, B. Fioretti, F. Franciolini, A theoretical study on the role of Ca2+-activated K+ channels in the regulation of hormone-induced Ca2+ oscillations and their synchronization in adjacent cells, Journal of Theoretical Biology 309 (2012) 103–112. https://doi.org/10.1016/j.jtbi.2012.05.009.

[2] T. Kotnik, L. Rems, M. Tarek, D. Miklavčič, Membrane electroporation and electropermeabilization: Mechanisms and models, Annu. Rev. Biophys. 48 (2019) 63–91. https://doi.org/10.1146/annurev-biophys-052118-115451.

[3] E.B. Sözer, S. Haldar, P.S. Blank, F. Castellani, P.T. Vernier, J. Zimmerberg, Dye Transport through Bilayers Agrees with Lipid Electropore Molecular Dynamics, Biophys. J. 119 (2020) 1724–1734. https://doi.org/10.1016/j.bpj.2020.09.028.

[4] M. Breton, L.M. Mir, Investigation of the chemical mechanisms involved in the electropulsation of membranes at the molecular level, Bioelectrochemistry 119 (2018) 76–83. https://doi.org/10.1016/j.bioelechem.2017.09.005.

[5] L. Rems, M.A. Kasimova, I. Testa, L. Delemotte, Pulsed electric fields can create pores in the voltage sensors of voltage-gated ion channels, Biophys. J. 119 (2020) 190–205. https://doi.org/10.1016/j.bpj.2020.05.030.

[6] K.A. DeBruin, W. Krassowska, Modeling electroporation in a single cell. I. Effects of field strength and rest potential, Biophys. J. 77 (1999) 1213–1224. https://doi.org/10.1016/S0006-3495(99)76973-0.

[7] J. Li, H. Lin, The current-voltage relation for electropores with conductivity gradients, Biomicrofluidics 4 (2010) 013206. https://doi.org/10.1063/1.3324847.

[8] M. Pavlin, D. Miklavčič, Theoretical and experimental analysis of conductivity, ion diffusion and molecular transport during cell electroporation — Relation between short-lived and long-lived pores, Bioelectrochemistry 74 (2008) 38–46. https://doi.org/10.1016/j.bioelechem.2008.04.016.

[9] G. Pucihar, T. Kotnik, D. Miklavčič, J. Teissié, Kinetics of Transmembrane Transport of Small Molecules into Electropermeabilized Cells, Biophysical Journal 95 (2008) 2837–2848. https://doi.org/10.1529/biophysj.108.135541.

[10] K.A. DeBruin, W. Krassowska, Modeling Electroporation in a Single Cell. II. Effects of Ionic Concentrations, Biophysical Journal 77 (1999) 1225–1233. https://doi.org/10.1016/S0006-3495(99)76974-2.

[11] Bruce. Alberts, A. Johnson, J. Lewis, M. Raff, K. Roberts, P. Walter, Molecular biology of the cell, Garland Science, New York; Abingdon, UK, 2008.

[12] J. Li, W. Tan, M. Yu, H. Lin, The effect of extracellular conductivity on electroporation-mediated molecular delivery, Biochim. Biophys. Acta 1828 (2013) 461–470. https://doi.org/10.1016/j.bbamem.2012.08.014.

[13] K.C. Smith, A unified model of electroporation and molecular transport, Thesis, Massachusetts Institute of Technology, 2011.
[14] P.M. Bungay, H. Brenner, The motion of a closely-fitting sphere in a fluid-filled tube, International Journal of Multiphase Flow 1 (1973) 25–56. https://doi.org/10.1016/0301-9322(73)90003-7.
[15] A. Barnett, The current-voltage relation of an aqueous pore in a lipid bilayer membrane, Biochimica et Biophysica Acta (BBA) - Biomembranes 1025 (1990) 10–14. https://doi.org/10.1016/0005-2736(90)90184-P.
[16] T. Höfer, Model of Intercellular Calcium Oscillations in Hepatocytes: Synchronization of Heterogeneous Cells, Biophysical Journal 77 (1999) 1244–1256. https://doi.org/10.1016/S0006-3495(99)76976-6.
[17] S. Memmel, V.L. Sukhorukov, M. Höring, K. Westerling, V. Fiedler, A. Katzer, G. Krohne, M. Flentje, C.S. Djuzenova, Cell Surface Area and Membrane Folding in Glioblastoma Cell Lines Differing in PTEN and p53 Status, PLOS ONE 9 (2014) e87052. https://doi.org/10.1371/journal.pone.0087052.
[18] M. Usaj, M. Kanduser, The Systematic Study of the Electroporation and Electrofusion of B16-F1 and CHO Cells in Isotonic and Hypotonic Buffer, J Membrane Biol 245 (2012) 583–590. https://doi.org/10.1007/s00232-012-9470-2.
[19] I.F. Abdullaev, A. Rudkouskaya, A.A. Mongin, Y.-H. Kuo, Calcium-Activated Potassium Channels BK and IK1 Are Functionally Expressed in Human Gliomas but Do Not Regulate Cell Proliferation, PLOS ONE 5 (2010) e12304. https://doi.org/10.1371/journal.pone.0012304.
[20] L. Catacuzzeno, F. Aiello, B. Fioretti, L. Sforna, E. Castigli, P. Ruggieri, A.M. Tata, A. Calogero, F. Franciolini, Serum-activated K and Cl currents underlay U87-MG glioblastoma cell migration, Journal of Cellular Physiology 226 (2011) 1926–1933. https://doi.org/10.1002/jcp.22523.
[21] W.M. Haynes, D.R. Lide, T.J. Bruno, CRC handbook of chemistry and physics: a ready-reference book of chemical and physical data, 2016.
[22] T. Vindiš, A. Blažič, D. Khayyat, T. Potočnik, S. Sachdev, L. Rems, Gene electrotransfer into mammalian cells using commercial cell culture inserts with porous substrate, Pharmaceutics 14 (2022) 1959. https://doi.org/10.3390/pharmaceutics14091959.

2.2 INVASIVE PROPERTIES OF PATIENT-DERIVED GLIOBLASTOMA CELLS AFTER REVERSIBLE ELECTROPORATION

Blažič A., Majc B., Novak M., Breznik B., Rems L. Reversible electroporation enhances invasive properties of patient-derived glioblastoma cells. Radiology and Oncology, accepted for publication

Glioblastoma is a highly invasive brain tumour in which ion channel activity plays a key role in regulating cell migration and infiltration (Abed et al., 2023; Obrador et al., 2024; Younes et al., 2023). Our preceding publication demonstrated that calcium-activated potassium channels are activated following electroporation. Given the established role of these channels in glioblastoma cell invasion (D'Alessandro et al., 2019), we aimed to determine whether sublethal electroporation affects the invasive behaviour of glioblastoma cells. This was addressed using patient-derived cell lines and standardized transwell invasion assays, performed 24 hours after exposure to electric pulses. To explore the potential mechanistic link between electroporation and invasion, we employed mRNA sequencing to evaluate changes in gene expression profiles following treatment. Overall, we sought to determine whether electroporation induces functional and transcriptional adaptations in tumour cells that survive the treatment. We found that reversible electroporation enhanced invasion in a cell line–dependent manner, with a pronounced increase in NIB140 CORE cells and a more modest effect in NIB216 CORE cells, accompanied by transcriptomic signatures associated with extracellular matrix remodelling and ion channel regulation, suggesting that sublethal electroporation can trigger pro-invasive adaptations in surviving glioblastoma cells.

I hereby declare that the version included in this doctoral thesis is identical to the version accepted for publication.

RADIOLOGY AND ONCOLOGY Radiology and Oncology | Ljubljana | Slovenia | www.radioloncol.com 1

research article

Invasive properties of patient-derived glioblastoma cells after reversible electroporation *in vitro*

Anja Blazic[1], Bernarda Majc[2], Metka Novak[2,3], Barbara Breznik[2,4], Lea Rems[1]

[1] Faculty of Electrical Engineering, University of Ljubljana, Ljubljana, Slovenia
[2] Department of Genetic Toxicology and Cancer Biology, National Institute of Biology, Ljubljana, Slovenia
[3] Biotechnical Faculty, University of Ljubljana, Ljubljana, Slovenia
[4] Faculty of Chemistry and Chemical Engineering, University of Ljubljana, Ljubljana, Slovenia

Radiol Oncol 2025

Received 11 August 2025
Accepted 29 September 2025

Correspondence to: Assist. Prof. Lea Rems, Ph.D., Faculty of Electrical Engineering, University of Ljubljana, Tržaška cesta 25, SI-1000 Ljubljana, Slovenia. E-mail: lea.rems@fe.uni-lj.si

Disclosure: No potential conflicts of interest were disclosed.

Background. Electroporation-based therapies are being explored in glioblastoma (GB) treatment, as means of enhancing drug delivery or achieving nonthermal ablation. Yet, little is known about how sublethal exposure affects the invasive behaviour of GB tumour cells.

Materials and methods. Five patient-derived GB cell lines were initially screened for intrinsic invasive potential, and two most invasive (NIB140 CORE and NIB216 CORE) were selected for further experiments with electroporation treatment. Cells in suspension were exposed to bursts of high-frequency biphasic electric pulses resulting in electric field strength of 1 kV/cm, which corresponded to conditions of reversible electroporation. Changes in cell invasion and gene regulation were assessed 24 hours after electroporation using transwell assay and RNA transcriptome analysis, respectively.

Results. Reversible electroporation at 1.0 kV/cm enhanced invasion in a cell line-dependent manner. NIB140 CORE showed a consistent and pronounced increase, with a median of 3.74-fold (274%) higher number of invading cells compared to sham control. In contrast, NIB216 CORE exhibited only a modest increase in invasion (1.30-fold; 30%). Transcriptomic profiling identified modulation of genes linked to extracellular matrix organization and ion channel activity in NIB140 CORE, and cytoskeletal remodelling in NIB216 CORE, indicating the activation of invasion-related pathways.

Conclusions. These findings highlight a potential risk of pro-invasive responses in GB cells. In tumour ablation with irreversible electroporation, this concern relates to cells in the peripheral zone that may experience only sublethal electric fields, while in electrochemotherapy, a similar risk may arise if permeabilized cells are not effectively eliminated due to insufficient local drug delivery. Nevertheless, the two tested cell lines responded differently, underscoring patient-specific heterogeneity and the need for validation in more physiologically relevant models.

Key words: electroporation; high-frequency electric pulses; glioblastoma; patient-derived cells; invasion

Introduction

Electroporation is achieved by brief exposure of cells to high-intensity pulsed electric fields, creating nanoscale defects (i.e., pores) in the cell membrane. Depending on the extent of membrane disruption, cells may either restore homeostasis and survive (reversible electroporation) or fail to recover, leading to cell death (irreversible electroporation, IRE).[1] Clinically, electroporation has gained

recognition as a versatile tool in oncology. IRE can be used as a stand-alone, minimally invasive, non-thermal ablation technique[2,3], whereas reversible electroporation can be used to enhance the uptake and cytotoxicity of chemotherapeutic drugs while allowing for reduced drug dosages (electrochemotherapy; ECT).[4,5] Unlike thermal ablation, electroporation spares major blood vessels and the extracellular matrix, making it especially well-suited for tumours situated near vital or functionally critical structures.[2] Moreover, by enhancing drug delivery and promoting anti-tumour immune activation, electroporation has become recognized as a key component of multimodal cancer therapy.[2]

Glioblastoma (GB), a WHO grade IV astrocytoma, is the most lethal and treatment-resistant primary brain tumour, with a median patient survival of around 15 months and a five-year survival rate below 10%.[6-8] It is characterized by pronounced cellular and molecular heterogeneity, aggressive infiltration into surrounding brain tissue, and the development of a highly immunosuppressive microenvironment. Together, these biological features present significant challenges to developing effective treatments. The blood-brain barrier further limits drug delivery, while therapy-resistant GB stem cells and extensive genomic instability drive inevitable recurrence.[9] Despite the fact that surgery, radiotherapy, and chemotherapy remain the standard treatments for GB, emerging evidence indicates that tumour cells surviving these treatments may acquire an even more invasive phenotype, further complicating disease management.[10] This emphasizes the urgent need for novel, multimodal strategies capable of addressing complex tumour biology and preventing treatment-induced adaptation.

Given these challenges, there is growing interest in exploring alternative strategies for GB treatment. Several animal studies have demonstrated clinical potential of electroporation-based treatments for brain tumours. In canine models, research has primarily focused on IRE as a non-thermal ablation method. First-generation IRE protocols consisted of ninety 50-µs-long monophasic pulses at 4 Hz, producing well-controlled ablation volumes with sharp submillimeter transition zones between treated and healthy tissue.[11-13] A notable prospective study using the NanoKnife system in seven dogs with spontaneous gliomas demonstrated safety and feasibility of IRE for brain tumour treatment.[14] Individualized treatment plans were developed based on magnetic resonance image segmentation and computational optimization to ensure adequate electric field coverage of tumour by a sufficiently high electric field. Procedures involved craniotomy and stereotactic pulse delivery under general anaesthesia. Most adverse effects were mild to moderate and resolved with minimal intervention; however, two dogs experienced severe toxicity – one unrelated to IRE, and the other linked to the highest energy dose. Objective response was observed in four of five dogs with measurable lesions, with one dog remaining tumour-free for over five years.[15] To address limitations such as muscle contractions and neuromuscular stimulation, second-generation high-frequency IRE (H-FIRE) protocols have been developed to minimize these undesired effects.[16] A pilot study in three dogs with spontaneous meningiomas confirmed effective tumour ablation near critical vasculature with no major IRE-related side effects.[17] In addition, the potential of ECT for GB treatment was demonstrated in rodent studies. In rats with induced gliomas, ECT with intravenous bleomycin improved their survival[18], while intratumoral bleomycin combined with a newly designed electrode achieved complete tumour elimination in 69% of treated animals.[19] Another study combining IRE and ECT with intravenous cisplatin via monopolar electrode showed delayed tumour growth and improved survival in glioma-bearing rats.[20] These results led to a phase I clinical trial (NCT01322100) investigating ECT for brain metastases, which was however discontinued due to low patient enrolment.[21]

Despite these encouraging findings, electroporation has not yet been clinically established for brain tumours. Treatment responses in preclinical studies were variable, and complete tumour control was not achieved in all animals. The underlying causes of this heterogeneity remain unclear. One contributing factor may be the inhomogeneous electric field distribution during treatment, which creates a central region of IRE surrounded by a narrow peripheral zone of reversibly electroporated cells.[22-24] In highly infiltrative tumours like GB, some tumour cells are likely to be exposed only to sublethal electric field strengths, i.e. reversible electroporation, and survive the treatment. If electroporation alters the behaviour of surviving tumour cells, making them more invasive or aggressive, this might pose a potential risk for recurrence. A similar concern may arise in ECT, if insufficient drug delivery allows electroporated cells to survive the treatment. Thus, there is need for a deeper understanding of how reversible electroporation affects GB cells behaviour. Additionally,

further preclinical studies are warranted, as even the most relevant animal models, such as spontaneous canine gliomas, still show important discrepancies compared to human GB. While animal gliomas can mimic human GB tumour heterogeneity and histological features, they include a lower number of mutated genes and a different immune cell response.[25-27] Moreover, investigating the invasive behaviour of cells within sublethal regions is ethically and experimentally challenging *in vivo*, which further highlights the importance of clinically relevant *in vitro* models before progressing towards clinical application.

To investigate electroporation-induced changes in GB cell behaviour under clinically relevant conditions, we employed patient-derived primary cultures that more accurately reflect the genetic background, heterogeneity and invasive properties of human tumours compared to commercially available cell lines.[28] This study was motivated by increasing evidence that sublethal therapies may promote a more aggressive phenotype in surviving tumour cells.[10,29] Furthermore, our previous study[30] revealed that reversible electroporation activates Ca^{2+}-activated potassium channels in U-87 MG GB cell line, which are known to play a key role in regulating GB invasion.[31,32] Therefore, we focused specifically on evaluating how electroporation affects the invasion of GB cells. We began by characterizing the invasive potential of five patient-derived GB cell lines and selected two cultures with the highest invasive capacities for further investigation. We then evaluated changes in tumour cell invasion induced by reversible electroporation. To ensure that we specifically examined the response of reversibly electroporated cells only, we employed a suspension-based approach, which provides a controlled system without the confounding effects of mixed reversible and irreversible populations. To gain deeper insight into how electroporation affects gene expression in surviving tumour cells, we additionally performed RNA sequencing in treated and non-treated samples. The findings presented here provide important insights that may contribute to the development of effective electroporation-based strategies for GB therapy.

Materials and methods

Cells

Experiments were performed using five different cell lines obtained from Slovenian GlioBank managed by the National Institute of Biology (NIB).[33] Patients or their authorized representatives signed an informed consent in accordance with the Declaration of Helsinki. Collection and processing of tumour tissue material was approved by the National Medical Ethics Committee of the Republic of Slovenia (numbers 92/06/12, 0120-190/2018-4, 0120-190/2018-26, 0120-190/2018-32, and 0120-190/2018-35). Cell lines established from tumours were labelled with internal code numbers: NIB140 CORE, NIB216 CORE, NIB220 RIM, NIB237 CORE and NIB261 REC. CORE and RIM indicate the anatomical tumour regions from which the tumour cells were derived (the tumour core and infiltrative rim, respectively), while REC refers to cells isolated from a recurrent GB lesion. All cell lines were grown in Dulbecco's Modified Eagle Medium (DMEM; Gibco, #41965039), supplemented with 10% foetal bovine serum (Gibco, #10500064) and antibiotics Penicillin-Streptomycin (Sigma-Aldrich, Germany, #P0781), hereafter referred to as DMEM10.

Cells were routinely passaged every 3 to 4 days and were maintained in a humidified environment at 37°C with 5% CO_2. For determining the cell doubling time, $2x10^5$ cells were seeded per well of a 6-well plate (TPP, Switzerland), incubated at 37°C, 5% CO_2, and then trypsinized and counted at selected times 20–100 hours after seeding. For electroporation, cells were trypsinized, counted, and centrifuged at 300 × g for 3 minutes. The resulting pellet was resuspended in DMEM10 with 10 mM HEPES, Sigma-Aldrich, #H0887 (hereafter referred to as DMEM10+) to achieve a final cell density of 1×10^6 cells/ml.

Electric pulse exposure

Cells were exposed to H-FIRE pulses, which were previously used in GB investigations *in vitro*,[34] as well as *in vivo* for the treatment of spontaneous canine meningiomas[17] and in a study examining blood-brain barrier disruption mechanisms.[35] Specifically, we applied 100 bursts of biphasic pulses, with 2 µs negative and 2 µs positive phase, 5 µs interphase and 5 µs interpulse delay, 25 pulses/burst, at 1 Hz burst repetition frequency (Supplementary Figure S1). The pulse amplitude was varied between 100–400 V, corresponding to 0.5–2 kV/cm. Pulses were delivered by a high-frequency pulse generator L-POR (mPOR, Slovenia), through 2 mm electroporation cuvettes (VWR, #732-1136). The current and voltage were routinely monitored on an oscilloscope Wavesurfer

422, 200 MHz, using high-voltage differential probe ADP305 and current probe CP030 (all from Teledyne LeCroy, USA). The electric field to which the cells were exposed was estimated as the ratio between the applied voltage and the interelectrode distance.

We aimed to perform experiments at close-to-physiological temperature, which is relevant to *in vivo* tumour treatment. Thus, each cuvette was first preheated in an incubator at 33°C for at least 15 minutes. Subsequently, the cell suspension was added to the preheated cuvette, and placed back into the incubator at 33°C. Following an additional 10-minute incubation period, electric pulses were delivered to the cuvette inside the incubator. The temperature of 33°C was chosen based on our previous findings in U-87 MG GB cells, where electroporation at this temperature, but not at room temperature (~25°C), triggered activation of Ca^{2+}-activated potassium channels that are associated with membrane hyperpolarization and increased invasive potential.[30] In addition, responses at 33°C are expected to more closely approximate those at physiological temperature (37°C) than at room temperature, while maintaining a margin of safety against heating, as the sample temperature increased by > 8°C when the strongest electric pulses were delivered.

Joule heating of the sample due to pulse delivery was measured using a fibre optic sensor MPK-5 (OpSens Solutions, Canada). The sample temperature increased by 1.3°C ± 0.3°C at 200 V (1 kV/cm) and 8.3°C ± 0.7°C at 400 V (2 kV/cm), recordings shown in Supplementary Figure S2. This temperature increase was measured at room temperature (24–26°C); the increase during pulse delivery at 33°C is expected to be somewhat higher due to lower heat dissipation in warmer atmosphere.

Permeabilization assay

Cell suspension (150 µl, 1 × 10^6 cells/ml) prepared in DMEM10+ was mixed with propidium iodide (PI, Molecular probes, #P1304MP) in a final concentration of 100 µg/ml. PI is a nucleic acid stain that selectively penetrates cells with compromised membranes, where it binds to DNA and emits fluorescence. When added to cell suspension before pulse delivery, it enables identification of electroporated cells.[36] 3 minutes after pulse application, 350 µl of electroporation solution was added to the cell suspension and the sample was removed from the electroporation cuvette. The percentage of PI-stained cells was quantified by flow cytometer (Attune NxT, Carlsbad, CA, USA) using blue laser excitation at 488 nm and detecting the emitted fluorescence through a 574/26 nm band-pass filter. 10,000 events representing individual cells were obtained, and data were analysed using the Attune Nxt software. Cells with fluorescence intensity above a certain gate value, defined based on fluorescence intensity histogram, were considered electroporated. Gating was set according to sham control (0 V). Measurements for each data point were repeated at least three times on three different days.

PI-based viability assay

Cell suspension (150 µL, 1 × 10^6 cells/mL) was prepared in DMEM10+ and transferred to an electroporation cuvette. After pulse application and additional 10-minute incubation at 33 °C, 850 µL of DMEM10+ was added to the cuvette. Afterwards, 100 µL of the treated cell suspension was plated into 24-well plate (TPP, Switzerland) containing 1 mL of DMEM10, and the plate was incubated at 37°C in a humidified atmosphere with 5% CO_2 for 24 hours. PI was used to assess cell viability 24 hours after the electric pulse exposure. First, cells were harvested (attached and unattached) and centrifuged at 300 × g for 3 minutes. The cell pellet was then resuspended in 150 µL of growth medium together with PI in a final concentration of 100 µg/ml, and cells were incubated at room temperature for 5 minutes. The number of all cells (N_{total}) and the number of PI-stained cells (N_{PI+}) in a fixed sample volume was quantified by flow cytometer (Attune NxT; Life Technologies, USA), using a 488 nm blue laser and 574/26 nm band-pass filter. The percentage of viable cells was determined from $(N_{total}-N_{PI+})/N_{total,ctrl}$, as described in our previously published protocol[37], where $N_{total,ctrl}$ represents the total number of cells in sham control.

MTS-based viability assay

Cells were prepared and exposed to electric pulses in the same way as for the PI–based viability assay. 50 µL of the treated cell suspension was then plated into 96-well plate (TPP) containing 50 µL of DMEM10 and the plate was incubated at 37°C and 5% CO_2. MTS metabolic assay (CellTiter 96 AQueous One Solution Cell Proliferation Assay, Promega, USA) was used to assess cell viability 24 hours after pulse exposure. Viable cells reduce the MTS tetrazolium compound into a soluble formazan product, the concentration of which cor-

relates with the number of metabolically active cells and is determined by absorbance measurement. According to the manufacturer's instructions, 20 µL of MTS tetrazolium compound was added to the samples, and the 96-well plate was returned to the incubator for 2 hours. The absorbance of formazan was measured with a plate reader (Tecan Infinite M200, Tecan, Austria) at 490 nm. The percentage of viable cells was calculated by subtracting the background (absorbance in wells with medium only) and normalizing the sample absorbance to the absorbance of the sham control.

Transwell invasion assay

Transwell invasion assay was performed following a previously published protocol[38], as shown in Figure 1. Transwell inserts containing membranes with 8.0-µm pores (Corning Life Sciences, #353097), pre-coated with Matrigel (Corning, #354234), were used to assess the invasive potential of the cell lines. A total of 25 µL of Matrigel solution, diluted 1:3 in DMEM supplemented with 2% FBS, was added to each insert and incubated at 37°C for 30 minutes to allow gelling. The lower chambers of 24-well plates were filled with 500 µL of DMEM10. To prevent premature polymerization, Matrigel was handled on ice using pre-cooled pipette tips throughout the procedure. For each insert, 80 000 cells (pre-treated with pulse exposure or not) were suspended in 100 µL of DMEM with 2% FBS and mixed with 50 µL of Matrigel diluted in DMEM to achieve a final Matrigel concentration of 0.5 mg/mL. After a 10-minute incubation at 37°C in a humidified 5% CO_2 atmosphere, an additional 50 µL of DMEM with 2% FBS was added to each insert, resulting in a final volume of 200 µL. The inserts were then incubated for 24 hours.

Following incubation, non-invading cells and remaining Matrigel were removed from the upper surface of the membrane using a cotton swab. The inserts were transferred to fresh wells containing 500 µL of DPBS (Gibco, #14190) and washed twice. Cells on the underside of the membrane were fixed with 4% paraformaldehyde (Sigma-Aldrich, # 158127) for 15 minutes at room temperature, followed by two DPBS washes. Membranes were then incubated in DPBS containing 1% bovine serum albumin (BSA; Sigma-Aldrich, #A2153 or Fisher BioReagents, #BP9702) and 0.1% Triton X-100 (Sigma-Aldrich, #T8787) for 30 minutes at room temperature to block non-specific binding. For proliferation assessment, Ki-67 FITC-conjugated antibody (Miltenyi Biotec, #130-117-691) was added at a 1:50 dilution in DPBS, and membranes were incubated for 1 hour at room temperature. After one PBS wash, cell nuclei were counterstained with Hoechst 33342 (Thermo Fisher Scientific, #62249) diluted 1:1000 in PBS and incubated for at least 5 minutes.

Transwell invasion and proliferation assays were performed in five GB cell lines (NIB 140 CORE, NIB216 CORE, NIB220 RIM, NIB237 CORE and NIB261 REC) and selected electroporated samples (NIB 140 CORE and NIB216 CORE) to evaluate treatment-induced changes in GB cell behaviour. Tile-scan imaging of the entire membrane undersurface with invading cells was carried out using two fluorescence microscopy systems. For characterizing baseline invasion in all five GB cell lines, cells were imaged using the EVOS FL Auto 7000 system (Thermo Fisher Scientific, USA), which employed both brightfield and fluorescence channels to visualize nuclei stained with Hoechst and proliferating cells labelled with Ki-67 under 10× objective magnification. Imaging was performed using excitation wavelengths of 395 nm for Hoechst and 475 nm for Ki-67. For characterizing invasion in electroporated cells and corresponding sham control groups, the same fluorescence channels were used to image the samples on the Leica Thunder Imaging System with DMi8 inverted epifluorescence microscope and LED8 illumination source controlled by Las X software (all from Leica Microsystems, Germany) under 10× objective magnification.

Image analysis was performed using ImageJ Fiji.[39] Nuclei were first segmented based on Hoechst staining (as presented in Figure 1), and the resulting regions of interest (ROIs) were applied to the Ki-67 channel to extract signal intensity and determine proliferation status. Quantification of invading and proliferating cells was performed across at least three independent experiments.

Statistical analysis

All results are presented as mean ± standard deviation (SD), based on a least of three independent experiments performed on separate days. Statistical analyses were conducted using SigmaPlot version 11.0 (Systat Software Inc., San Jose, CA, USA), with analyses performed separately for each cell line. Normality was assessed using the Shapiro–Wilk test, and homogeneity of variance was evaluated using Levene's test. For datasets meeting assumptions of normality and equal variance, one-way ANOVA was applied, followed by Holm–Sidak's

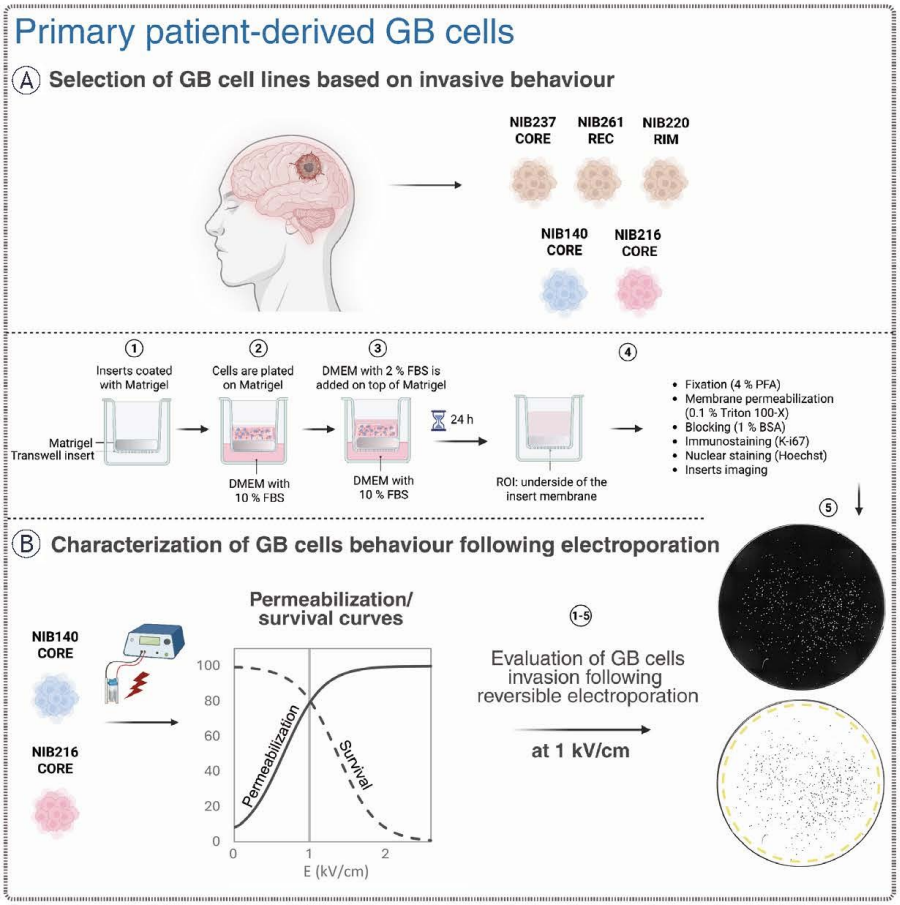

FIGURE 1. Overview of the experimental workflow for evaluating patient-derived glioblastoma (GB) cell behaviour before and after electroporation. Created with BioRender.com. **(A)** Five patient-derived glioblastoma cell lines, including cells from the tumour core (CORE), infiltrative rim (RIM), and a recurrent lesion (REC), were initially screened using a transwell invasion assay. Cells were plated on Matrigel-coated inserts and incubated for 24 hours. Invading cells migrating to the lower surface of the insert membrane were fixed, permeabilized, and stained with Hoechst (nuclei) and then immunostained for Ki-67 (a proliferation marker). The cells were subsequently imaged to quantify the number of invading and proliferating cells. **(B)** NIB140 CORE and NIB216 CORE were selected for further experiments with electroporation based on their invasive behaviour. Electric pulses of increasing electric field strength were applied to cells in electroporation cuvettes and the resulting membrane permeabilization and survival were quantified to generate characteristic response curves. Additionally, we assessed the metabolic activity of cells using MTS. Post-treatment invasion assay and fluorescence imaging was used to assess changes in invasive potential, with image analysis performed in ImageJ Fiji to quantify total and proliferating cell numbers based on nuclear segmentation and Ki-67 expression.

post hoc test for multiple comparisons. When assumptions were not met, nonparametric ANOVA on ranks was used, followed by Dunn's post hoc test. For comparisons involving two groups only, a Student's t-test was used when normality and variance assumptions were satisfied; otherwise, a Mann–Whitney U test was applied. A p-value < 0.05 was considered statistically significant.

RNA transcriptome analysis

Total RNA was extracted from GB cells (NIB140 CORE and NIB216 CORE) using the E.Z.N.A.® Total RNA Kit I (Omega Bio-Tek, Norcross, GA, USA; Cat. No. R6834). To replicate the conditions used in the Transwell invasion assay, cells were first exposed to an external electric field as described in the section above. Ten minutes following pulse exposure, 850 µL of DMEM10+ was added directly to the electroporation cuvette. The full volume was then transferred to a single well in 6-well plate, and an additional 2 mL of DMEM10 was added, bringing the total volume per well to 3 mL. Sham-treated control cells were handled identically but were not subjected to pulse exposure. The total RNA was extracted 24 hours after the pulse exposure.

Transcriptome analysis was performed by NovoGene (Munich, Germany). Total RNA was extracted from electroporated and sham control samples and subjected to quality control using the RNA Nano 6000 Assay Kit of the Bioanalyzer 2100 system (Agilent Technologies, CA, USA). mRNA was purified from total RNA using poly-T oligo-attached magnetic beads, fragmented, and reverse transcribed into cDNA. After second-strand synthesis and adaptor ligation, libraries containing 370–420 bp fragments were purified using the AMPure XP system and subsequently amplified by PCR. Following amplification, PCR products were purified again. Library quality was assessed using the Agilent Bioanalyzer 2100, and clustering was performed on a cBot Cluster Generation System using the TruSeq PE Cluster Kit v3-cBot-HS (CA, USA). The libraries were then sequenced on an Illumina NovaSeq platform, generating 150 bp paired-end reads. Raw reads were processed using fastp for adapter trimming and quality filtering. Clean reads were aligned to the reference genome using HISAT2 (v2.0.5), and transcript assembly was performed with StringTie (v1.3.3b). Gene-level read counts were generated with featureCounts (v1.5.0-p3), and gene expression was quantified as fragments per kilobase of transcript per million mapped reads (FPKM), which accounts for both transcript length and sequencing depth.

Differential gene expression analysis was performed in NovoMagic (https://eu-magic.novogene.com/) using DESeq2 (v1.20.0), based on a negative binomial model. Gene ontology (GO) enrichment analysis was conducted using the clusterProfiler R package, correcting for gene length bias. GO terms with adjusted $p < 0.05$ were considered significantly enriched. For visualization, unadjusted p-values ($p \leq 0.05$) were used in volcano plots to highlight global transcriptional changes, whereas adjusted p-values (Benjamini-Hochberg correction) were used in GO enrichment plots to account for multiple testing and reduce false discovery.

The raw RNA-seq data are publicly available in the Gene Expression Omnibus (GEO) repository under accession number GSE305017.

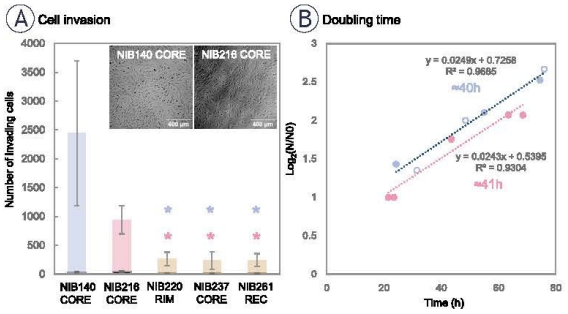

FIGURE 2. Patient-derived glioblastoma (GB) cell lines display variable intrinsic invasive potential. **(A)** Transwell invasion assay was performed with non-treated cell lines to assess the intrinsic invasive potential of five GB cell lines derived from different tumour regions. NIB140 CORE showed the highest number of invading cells, followed by NIB216 CORE, whereas NIB220 RIM, NIB237 CORE, and NIB261 REC displayed significantly lower invasion. Statistical analysis was performed using ANOVA on ranks. Significant differences are indicated with asterisks (*); $p < 0.05$. The number of Ki-67 positive (proliferating) cells, shown in black at the base of each bar, was low in all tested cell lines (< 10 %). Data are presented as mean ± SD from at least 4-5 independent experiments. **(B)** Doubling times were determined based on cell growth curves plotted as $\log_2(N/N_0)$ versus time, where N_0 is the number of seeded cells at time 0 h, and N is the number of cells at selected time points (hours). Linear regression was applied to each cell line (R^2 values shown), and doubling time was calculated from the slope of the fitted line. NIB140 CORE and NIB216 CORE showed similar doubling time (40–41 h).

Results

Selection of patient-derived GB cell lines based on their invasive properties

To characterize heterogeneity in invasive behaviour among patient-derived GB cell lines, we performed a standardized transwell invasion assay (Figure 1) using five lines representing distinct tumour regions. As shown in Figure 2, invasive potential varied markedly across the cell lines. NIB140 CORE and NIB216 CORE exhibited the highest levels of invasion, while NIB220 RIM, NIB237 CORE, and NIB261 REC displayed significantly lower invasive activity compared to NIB140 CORE and NIB216 CORE (ANOVA on ranks, p <

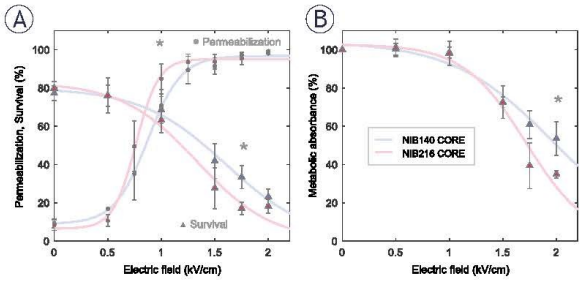

FIGURE 3. Permeabilization and survival of NIB140 CORE and NIB216 CORE glioblastoma (GB) cell lines in response to H-FIRE pulses resulting in different electric field strengths. **(A)** The percentage of permeabilized cells was assessed by propidium iodide (PI) uptake 3 minutes after pulse delivery (presented as •). The percentage of viable cells was assessed by PI assay 24 hours after pulse delivery (presented as ▲). **(B)** Cell survival was assessed by metabolic MTS assay 24 hours after pulse delivery. Data are presented as mean ± SD from at least three independent experiments. Solid lines are least-square fits to sigmoid curves. Statistically significant differences ($p < 0.05$) between cell lines at specific electric field strengths were tested using Student's t-test and are indicated by asterisks (*). Data for NIB140 CORE and NIB216 CORE are shown in blue and pink, respectively.

0.05). Based on their invasion profiles, NIB140 CORE and NIB216 CORE were selected for subsequent experiments to investigate electroporation responses across the two GB subtypes representing the highest levels of invasion. After 24 hours, the expression of the proliferation marker Ki-67 was low in all tested cell lines (< 10%), confirming that the observed invasion was not driven by cell proliferation, as shown in Figure 2A. The number of proliferating cells is represented at the base of each bar, illustrating that proliferation does not account for the observed invasive behaviour.

To further confirm that the observed invasion was not driven by proliferation, we measured the doubling time of each cell line. NIB140 CORE and NIB216 CORE displayed doubling times of ~40 and ~41 hours, respectively. Representative growth curves used for this estimation are shown in Figure 2B, illustrating that the 24-hour post-treatment time point falls well before either population is expected to divide. This supports the interpretation that the observed behaviour reflects actual invasion properties rather than proliferative expansion.

Permeabilization and survival at different electric field strengths

We next investigated how the selected NIB140 CORE and NIB216 CORE cell lines respond to pulses of increasing electric field intensities. Membrane permeabilization was assessed 3 minutes after electroporation using propidium iodide (PI) staining, while cell survival was evaluated 24 hours post-treatment using both PI staining and the metabolic MTS assay. Both NIB140 CORE and NIB216 CORE exhibited a characteristic sigmoidal increase in the percentage of permeabilized cells with increasing electric field strength, reaching maximal values above 1.25 kV/cm (Figure 3A). Survival determined by PI assay declined above 1 kV/cm (Figure 3A). These results align with previous H-FIRE studies demonstrating that glioma cells can recover metabolic activity and proliferative capacity when exposed to sublethal electric fields, whereas higher intensities induce irreversible membrane damage.[34]

NIB216 CORE displayed somewhat greater permeabilization at intermediate electric field strength and a more pronounced decrease in viability at higher field strengths compared to NIB140 CORE, indicating greater sensitivity to electroporation-induced stress. This was further supported by MTS assay results (Figure 3B), which showed a greater reduction in metabolic activity in NIB216 CORE. Statistically significant differences (Student's t-test) between the two cell lines were observed at 1 kV/cm for membrane permeabilization ($p=0.037$), 1.75 kV/cm for survival ($p=0.001$), and 2 kV/cm for metabolic activity ($p=0.024$), with significant differences indicated by asterisks (Figure 3). Nevertheless, the differences between the tested cell lines were relatively small, suggesting that similar electric field strengths can be used to treat different GB cell lines.

Reversible electroporation enhances invasion of GB cells in a cell type-dependent manner

Based on permeabilization and survival curves (Figure 3), we chose an electric field strength of 1.0 kV/cm to further assess whether sublethal electroporation alters GB cell invasion. At this electric field strength, both NIB140 CORE and NIB216 CORE cell lines reached > 80% permeabilization while maintaining viability above 80% relative to sham-treated control (0 kV/cm). The chosen electric field strength mimics the conditions in reversibly electroporated border zone surrounding the ablated area, when using IRE for tumour treatment. Also, these conditions of reversible electroporation are in line with clinically relevant protocols used for ECT.[40]

Electroporation enhanced the invasion potential of GB cells in a cell type-dependent manner, as quantified 24 hours following exposure to 1.0 kV/cm. Since the number of invading cells varied from day to day, already in control samples, we present results for each of the three biological replicates separately, with 2–3 technical replicates (transwell inserts) per one biological replicate. In NIB140 CORE, the number of invading cells was consistently and significantly higher in electroporated samples compared to sham-treated controls across all three biological replicates (Figure 4A; Student's t-test, $p < 0.05$; 2–3 technical replicates per one biological replicate). In contrast, NIB216 CORE showed a more variable response, with significance reached in one biological replicate only (Figure 4B), indicating a modest and less consistent effect. We then averaged the technical replicates and normalized this averaged number of invading cells in electroporated samples to the corresponding number in sham-treated controls for each biological replicate. The obtained fold-increase in invading cells across biological replicates is presented in the box plot in Figure 4C. This analysis confirmed a consistent increase in invasion in NIB140 CORE and only modest trend in NIB216 CORE. Notably, NIB140 CORE exhibited a significantly greater 3.74-fold increase compared to just 1.30-fold in NIB216 CORE (Student's t-test, $p < 0.05$), potentially reflecting intrinsic differences in these cell lines.

Enhanced cell invasion following sublethal electroporation was further supported by analysis of the proliferation marker Ki-67. The proportion of Ki-67–positive cells remained below 10% across all conditions (Figure 4D), with no significant differences between electroporated and sham-treated controls (Student's t-test). These findings reinforce the conclusion that proliferation did not contribute considerably to the increased number of invading cells following electroporation. An example of this electroporation-induced increase in invasion potential in NIB140 CORE cell line is illustrated in Figure 4E, where representative images demonstrate a higher number of invading cells after electroporation at 1 kV/cm.

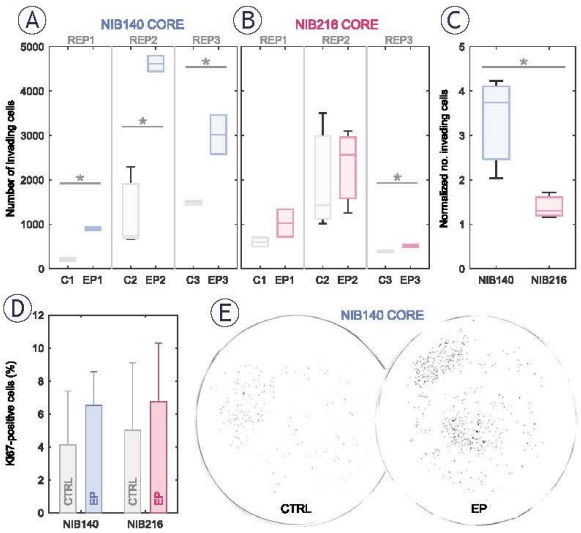

FIGURE 4. Electroporation enhances the invasion potential of patient-derived glioblastoma (GB) cell lines in a cell type-dependent manner. Invasion was assessed 24 hours after electroporation using H-FIRE pulses resulting in electric field strength of 1 kV/cm. **(A-B)** Box-and-whisker plots showing the number of invading cells in NIB140 CORE **(A)** and NIB216 CORE **(B)** in sham-treated (grey) and electroporated samples (blue or pink). Each group represents a separate biological replicate (REP1–REP3), with 2–3 technical replicates per biological replicate. The horizontal line within each box represents the median, and whiskers indicate the full range of values. **(C)** Relative increase in the number of invading cells in electroporated samples compared to sham controls. Data are presented as mean ± SD from three biological replicates. **(D)** Percentage of Ki-67–positive (proliferating) cells in sham-treated and electroporated samples. Values remained below 10 % across all conditions, demonstrating that the observed increase in invasion was not due to increased proliferation. **(E)** Representative masks obtained after thresholding images of Hoechst-stained NIB140 CORE invading cells, showing increased invasion following electroporation.

RNA transcriptome analysis corroborates enhanced invasion of reversibly electroporated GB cells

To gain insight into the molecular changes associated with electroporation, we performed RNA sequencing on NIB140 CORE and NIB216 CORE cells harvested 24 hours after exposure to 1.0 kV/cm. Gene expression level analysis in electroporated (EP) and sham-treated (CTRL) samples, presented through co-expression Venn diagrams (Figure 5A), revealed 222 and 239 genes that were uniquely expressed in the electroporated NIB140 CORE and NIB216 CORE samples, respectively. Differential gene expression analysis, presented through volcano plots (Figure 5B) further confirmed electroporation-induced transcriptomic changes in the two cell lines, with both significantly downregulated and upregulated genes.

Additionally, comparison between the sham-treated NIB140 CORE and NIB216 CORE revealed that these cell lines considerably differ in their baseline transcriptomic profiles. Co-expression

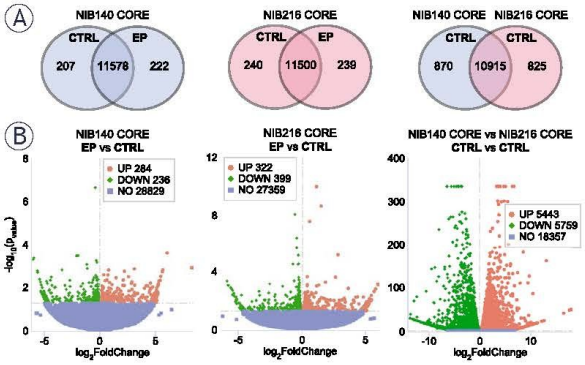

FIGURE 5. Transcriptomic differences between electroporated and sham-treated NIB140 CORE and NIB216 CORE cell lines. RNA transcriptome analysis was performed in cells harvested 24 hours after electroporation. **(A)** The gene expression levels analysis is presented through co-expression Venn diagrams showing the overlap in expressed genes between sham-treated (CTRL, 0 V) and electroporated (EP, 1 kV/cm) samples of each cell line, and between sham-treated NIB140 CORE and NIB216 CORE. **(B)** The differential gene expression analysis is presented through volcano plots. Red and green points represent significantly upregulated and downregulated genes, respectively ($p < 0.05$), while blue points indicate non-significant changes. Genes were classified as differentially expressed, if they met the threshold of $|\log_2 FoldChange| > 0.0$.

Venn diagram (Figure 5A) showed 10,915 genes co-expressed in both cell lines, with 870 and 825 genes uniquely expressed in NIB140 CORE and NIB216 CORE, respectively. Volcano plot (Figure 5B) further confirmed the large transcriptomic divergence between the two cell lines. This divergence indicates that the intrinsic transcriptomic differences between NIB140 CORE and NIB216 CORE exceed the shifts induced by electroporation, which may explain the different extents to which electroporation changed the invasion of these two cells lines (Figure 4).

To better understand the biological relevance of the observed transcriptomic changes, we performed gene ontology (GO) enrichment analysis on significantly upregulated and downregulated genes in NIB140 CORE and NIB216 CORE cells following electroporation (Figure 6). In NIB140 CORE, differentially expressed genes were enriched in invasion-associated pathways, including channel activity and extracellular matrix organization (Figure 6A), which aligned with the observed increase in invasion (Figures 4A, C). In contrast, the transcriptional response in NIB216 CORE lacked strong enrichment of motility-related pathways, consistent with the modest increase in invasion (Figures 4B, C). However, several downregulated categories in NIB216 CORE—including actin filament binding, actin cytoskeleton, extracellular matrix, and focal adhesion—suggest cytoskeletal remodelling and/or disruption. In addition, genes associated with leading-edge membrane, cell projection membrane, and synaptic membrane were upregulated. These differences underscore the intertumoral variability in molecular responses to electroporation and support a potential mechanistic link between transcriptomic changes and the significantly enhanced invasion observed in the NIB140 CORE cell line, which would, however, need to be further supported at the functional level.

Discussion

Our study investigated how sublethal exposure to electroporation pulses affects the invasion of GB tumour cells. After initial screening of five patient-derived GB cells lines for their intrinsic invasive potential, we selected the two most invasive cell lines (NIB140 CORE and NIB216 CORE) for further electroporation experiments. We characterized cell permeabilization and survival after exposure to H-FIRE pulses resulting in different electric field strengths and found that 1 kV/cm corresponds to conditions of reversible electroporation in both cell lines. At 1 kV/cm, the majority of cells became permeabilized due to electroporation while still retaining their viability 24 hours later. We then assessed changes in their invasion behaviour 24 hours after electroporation. Electroporation enhanced invasion in a cell line–dependent manner: NIB140 CORE consistently showed a pronounced response with a median 3.74-fold higher number of invading cells compared to sham-treated controls. While the number of invading cells was consistently higher in electroporated samples, we observed a rather high variability across biological replicates. This variability can be explained by the use of patient-derived cells, which are expected to respond more heterogeneously than established cell lines that often fail to replicate key tumour characteristics.[28,33,41] Unlike in NIB140 CORE, electroporation induced only a modest increase in the number of invading cells in NIB216 CORE (1.30-fold). Moreover, NGS-based profiling included in the clinical pathology report identified the *EGFRvIII* variant in NIB140 CORE cell line (but not in NIB216 CORE), a mutation known to enhance invasion and contribute to treatment resistance in GB.[42]

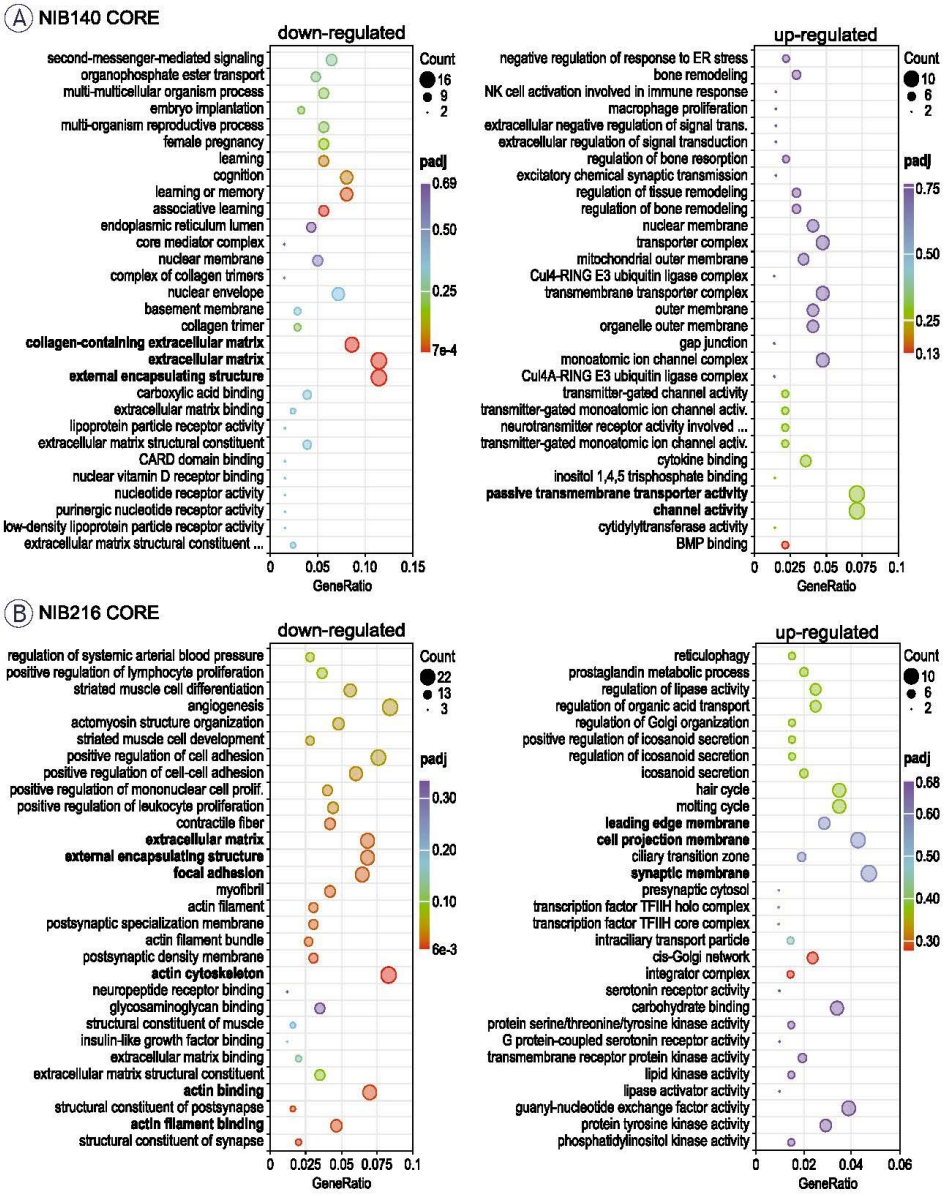

FIGURE 6. Functional enrichment analysis of differentially expressed genes following electroporation. **(A)** Gene ontology (GO) enrichment analysis of significantly upregulated (right) and downregulated (left) genes in NIB140 CORE cells 24 hours after electroporation. **(B)** GO enrichment analysis for NIB216 CORE. Dot size reflects the number of genes contributing to each GO term, while colour intensity indicates statistical significance (adjusted p-value, padj). The GeneRatio represents the proportion of differentially expressed genes associated with each GO term relative to the total number of input genes. Selected invasion-relevant categories are highlighted in bold. GO terms include biological processes, molecular functions, and cellular components.

To better understand the molecular basis of increased invasion after electroporation and the associated differences between the two tested cell lines, we performed transcriptomic analysis. In NIB140 CORE cells, we observed upregulation of genes associated with the channel activity and passive transmembrane transport activity – *CHRNE, KCNMA1, KCNAB1, TRPC4, GJC3, GPR89A, TTYH2, GRIN2A, RHCE*, and *GLRA3*.[43] Notably, ion channel–related genes such as *KCNMA1* and *KCNAB1*, i.e. the alpha and beta subunits of the big potassium K_{Ca} channel, were detected, supporting their potential role in enhanced invasive behaviour in GB observed in previous studies.[29,32] Genes related to extracellular matrix (ECM) organization (collagen containing ECM, ECM and external encapsulating structure) were downregulated (*COL14A1, EFEMP1, ITGB4, COL8A1, P3H2, THBS2, INHBE, MATN4, PTPRZ1, MMP9, ANGPTL5* and *COL5A2)* indicating ECM remodelling.[44,45] In this context, it is notable that MMP9, a metalloproteinase classically associated with invasion, was downregulated in NIB140 CORE. This may appear counterintuitive given the observed increase in invasion, but it is consistent with reports that GB cells can compensate protease activity by other protease families or proteases of the same family, adopt protease-independent, ion channel- and adhesion-driven or even adhesion-independent migration strategies.[46] Thus, while MMP9 itself was not upregulated, ECM- and ion channel–related pathways were altered, supporting the idea that alternative mechanisms may drive invasion in this context.[46] In contrast, NIB216 CORE showed downregulation of genes involved in cytoskeleton remodelling and focal adhesion (*COL11A1, CNN1, ALPL, HAPLN1, TGFB1I1, F3, IGFBP7, ADAM19, COL4A1, POSTN, LOXL4, MXRA7, CCN2, LGALS1, COL4A2, GPC4, TFPI2, CD248, VASP, TAGLN, TPM2, PDLIM7, PPP1R18, ARPC4, CORO1A, ACTN1, FHDC1, PICK1, SPTBN2, ADSS1, MYOZ1, TMEM201, MARCKSL1* and *MYH9*) suggesting cytoskeletal disruption.[47] Meanwhile, upregulated response was linked to membrane dynamics – leading edge membrane, cell projection membrane and synaptic membrane (*ANK1, DPP4, LAMP5, EGFR, C2CD5* and *PSD3*) indicating changes in membrane plasticity and intracellular communication.[48] It should be noted that, based on our data, we cannot determine whether the observed effects arise directly from pulse-induced biophysical changes or indirectly through stress-mediated signalling. Furthermore, this data should be interpreted with caution, as validation at the protein level (e.g., Western blot or ELISA) will be required to confirm whether the observed gene expression changes translate into functional effects.

A recent study by Wang *et al.*[49] reported that electroporation suppresses invasion of U-87 MG GB cells. Similar to our study, cells in suspension were electroporated and changes in invasion were assessed 24 hours later using a transwell invasion assay. The pulse parameters used for electroporation was somewhat different from ours and consisted of 4–8 bursts of 50 biphasic 2 µs pulses with 0.2 µs interphase and 100 µs interpulse delay, 15 Hz burst repetition frequency, and 4 kV/cm electric field strength. With 6 and 8 bursts, cell survival dropped to ~73% and 42%, respectively, and this decrease in the number of viable cells was expectedly reflected in lower number of invading cells. Nevertheless, the number of invading cells decreased to ~56% of control also with 4 bursts, where ~90% cells survived the treatment. Decreased invasion was associated with downregulation of *SIRT1* gene and *SIRT2* genes and impaired mitochondrial function. In contrast, we observed increased invasion and no significant changes in any of *SIRT1–7* genes (p=0.1; Benjamini-Hochberg correction) in our study. Furthermore, we observed a trend of increased invasion even at higher electric field strength of 2 kV/cm, after compensating for the reduced number of surviving cells, although this increase in invasion was not statistically significantly different from control, results presented in Supplementary Figure S3. The different results obtained by us compared to Wang *et al.*[49] could stem from multiple reasons. Aside from differences in pulse parameters and sample temperature during electroporation, we used patient-derived GB cells lines. As shown by our transcriptomic analysis, different GB cells lines have considerably different gene expression profiles, which affects their response to electroporation. This highlights the value of patient-derived models in capturing clinically relevant transcriptional responses and treatment dynamics compared to immortalized cell lines. The importance of using patient-derived cells to better capture the biological complexity and treatment responses of GB is further illustrated by comparing our results to the study by Casciati *et al.*[50] In this study, adherent U-87 MG cells were exposed to five electric pulses, each lasting 40 µs at 1 Hz and 30 kV/cm (0.3 MV/m). While they also cultured neurospheres under serum-free conditions to enrich for GB stem-like cells, these were still derived from the U-87 MG line, which lacks key features of primary tumours,

including heterogeneity and true invasive behaviour.[51] Notably, Casciati *et al.* reported that pulse exposure substantially influenced the fate of GB neurospheres by differentially regulating genes involved in hypoxia, inflammation, and p53/cell cycle checkpoints, ultimately reducing their capacity for neurosphere formation and transmigration *in vitro*. Furthermore, pulse exposure also reduced the ability to form new neurospheres and inhibited invasion. Importantly, exclusively in U-87 neurospheres, pulse exposure altered the expression of stemness- and differentiation-related genes. While these findings are promising, the observed inconsistency with our results—despite differences in pulse parameters—might reflect cell model-specific differences in electroporation responses. This highlights the need to validate such effects in more physiologically relevant models. Given the aggressive, therapy-resistant nature of GB stem-like cells and their contribution to tumour progression and recurrence[52,53], future electroporation studies should consider the use of patient-derived stem-like populations to more accurately reflect clinically relevant outcomes.

While most preclinical studies of electroporation-based brain tumour therapy have focused on IRE as a non-thermal ablation method, particularly in canine glioma models[11,12,14,17,54], our findings highlight the less-explored effects on tumour cells located in the periphery of IRE-treated zones. This raises an important consideration regarding unintended effects in tumour margins that remain viable after treatment—regions likely exposed to sublethal electric fields due to the highly infiltrative nature of GB. Our results demonstrate that tumour cells surviving electroporation may acquire enhanced invasive potential, a concern that arises specifically when no cytotoxic agents are present. However, a similar concern applies to ECT if insufficient local drug concentrations are achieved, since permeabilized cells might survive the treatment. When adequate concentrations are ensured, ECT directly addresses this risk by eliminating reversibly permeabilized cells through enhanced intracellular accumulation of cytotoxic agents, such as bleomycin and cisplatin.[18,19] Bleomycin induces DNA strand breaks, while cisplatin causes DNA crosslinking and apoptosis—mechanisms that require cytosolic access and are otherwise ineffective across intact membranes.[55–56] Since the primary effect of electroporation is to increase membrane permeability, it provides a unique opportunity to deliver these otherwise impermeable drugs efficiently. In addition, electroporation has been shown in *in vivo* models to transiently disrupt the blood–brain barrier, further highlighting its potential for enhancing drug delivery to tumour tissue within the central nervous system.[35,57,58] Moreover, studies in melanoma cells showed that ECT does not affect the cells' metastatic potential.[59,60] Taken together, our findings suggest that ECT, by combining reversible electroporation with sufficient concentrations of cytotoxic agents, may offer a more effective and safer therapeutic strategy for glioblastoma than IRE as a standalone treatment. Furthermore, this approach may help overcome some limitations of current chemotherapy regimens, such as temozolomide, which has been shown to expand the GB stem cell population through conversion of differentiated tumour cells both *in vitro* and *in vivo*.[61]

While our results offer new insights into GB cell responses to electroporation, this study has several limitations. First, the use of suspension cultures does not fully recapitulate the structural complexity, cell–cell interactions, and diffusion gradients present *in vivo*. These factors may influence electroporation-induced processes such as membrane repair, intracellular signalling, and invasion. Although patient-derived GB cells were used, future studies should also examine cells from spatially distinct tumour regions (e.g., core vs. rim), which may exhibit different responses due to intratumoral heterogeneity. In addition, GB stem-like cells, known for their high invasion potential and therapy resistance[52,63], were not specifically addressed here and represent a critical subpopulation for further investigation. To better approximate the tumour microenvironment, future experiments should employ advanced *in vitro* models such as multicellular spheroids or organoids, which incorporate three-dimensional architecture and preserve key features of GB biology, including heterogeneity, invasion, and treatment resistance. Arroyo *et al.*[63] have recently advanced this field by developing a multicellular spheroid–hydrogel platform, demonstrating that higher electric field strengths and longer pulse widths constrained migration and proliferation over several days, underscoring the importance of 3D models for validating electroporation responses. Finally, this study focused on short-term transcriptional and behavioural changes, with analysis limited to the 24-hours timepoint following electroporation. Long-term effects were not addressed here and remain to be explored, particularly in the context of combination therapies. Experiments were performed at 33°C to build on prior findings of ion

channel activation in GB cells[30], while also minimizing the risk of thermal damage. Future studies could further examine temperature dependence alongside 3D models to better approximate physiological conditions. Moreover, future work should investigate how electroporation interacts with established treatments, including radiation and chemotherapeutic agents such as temozolomide, cisplatin, or bleomycin, to better understand the impact on cell viability and invasion.

Overall, our findings suggest that sublethal electroporation can enhance GB cell invasion potential in a cell line-dependent manner. A more pronounced and consistent effect was observed in NIB140 CORE cells (3.74-fold increase), while NIB216 CORE showed only a modest increase (1.30-fold) in the number of invading cells following reversible electroporation. While our findings suggest that combining reversible electroporation with sufficient concentrations of cytotoxic agents (ECT) may offer advantages over IRE alone, this requires further validation in more physiologically relevant models.

Acknowledgments

This research was supported by Slovenian Research and Innovation Agency (ARIS) through research programmes P2-0249 and P1-0245, infrastructure programme I0-0022, and funding for Young Researchers. This work was supported by the Slovenian Research and Innovation Agency through research projects J3-4504, N3-0394 and NC-25002 and NIB Development pillar funds RSF projects 842/2024 and 946/2025. The research was also supported by the European Union and ARIS through NextGenerationEU and NOO funding within project MN-0023 and European Union's Horizon project Twinning for excellence to strategically advance research in carcinogenesis and cancer (CutCancer; 101079113).

Use of AI-assisted technologies in the writing process

During the preparation of this paper, the authors used Claude (Anthropic, CA, USA) and ChatGPT (OpenAI, CA, USA) to improve the style and readability in some parts of the text. After using this tool/service, the authors have reviewed and edited the content as required and take full responsibility for the content of the publication.

References

1. Kotnik T, Rems L, Tarek M, Miklavčič D. Membrane electroporation and electropermeabilization: mechanisms and models. *Annu Rev Biophys* 2019; **48:** 63-91. doi: 10.1146/annurev-biophys-052118-115451
2. Aycock KN, Davalos RV. Irreversible electroporation: background, theory, and review of recent developments in clinical oncology. *Bioelectr* 2019; **1:** 214-234. doi: 10.1089/bioe.2019.0029
3. Jacobs EJ, Rubinsky B, Davalos RV. Pulsed field ablation in medicine: irreversible electroporation and electropermeabilization theory and applications. *Radiol Oncol* 2025; **59:** 1-22. doi: 10.2478/raon-2025-0011
4. Mir LM, Gehl J, Serša G, Collins CG, Garbay JR, Billard V, et al. Standard operating procedures of the electrochemotherapy: instructions for the use of bleomycin or cisplatin administered either systemically or locally and electric pulses delivered by the CliniporatorTM by means of invasive or non-invasive electrodes. *EJC Suppl* 2006; **4:** 14-25. doi: 10.1016/j.ejcsup.2006.08.003
5. Miklavčič D, Mali B, Kos B, Heller R, Serša G. Electrochemotherapy: from the drawing board into medical practice. *BioMed Eng Online* 2014; **13:** 29. doi: 10.1186/1475-925X-13-29
6. Grochans S, Cybulska AM, Siminska D, Korbecki J, Kojder K, Chlubek D, et al. Epidemiology of glioblastoma multiforme-literature review. *Cancers* 2022; **14:** 2412. doi: 10.3390/cancers14102412
7. Ostrom QT, Price M, Neff C, Cioffi G, Waite KA, Kruchko C, et al. CBTRUS statistical report: primary brain and other central nervous system tumors diagnosed in the United States in 2015-2019. *Neuro Oncol* 2022; **24(Suppl 5):** v1-95. doi: 10.1093/neuonc/noac202
8. Obrador E, Moreno-Murciano P, Oriol-Caballo M, Lopez-Blanch R, Pineda B, Gutierrez-Arroyo JL, et al. Glioblastoma therapy: past, present and future. *Int J Mol Sci* 2024; **25:** 2529. doi: 10.3390/ijms25052529
9. Liu Y, Zhou F, Ali H, Lathia JD, Chen P. Immunotherapy for glioblastoma: current state, challenges, and future perspectives. *Cell Mol Immunol* 2024; **21:** 1354-75. doi: 10.1038/s41423-024-01226-x
10. Pichol-Thievend C, Anezo O, Pettiwala AM, Bourmeau G, Montagne R, Lyne AM, et al. VC-resist glioblastoma cell state: vessel co-option as a key driver of chemoradiation resistance. *Nat Commun* 2024; **15:** 3602. doi: 10.1038/s41467-024-47985-z
11. Garcia P, Rossmeisl JH, Neal R, Ellis TL, Olson JD, Henao-Guerrero N, et al. Intracranial nonthermal irreversible electroporation: in vivo analysis. *J Membr Biol* 2010; **236:** 127-36. doi: 10.1007/s00232-010-9284-z
12. Ellis TL, Garcia PA, Rossmeisl JH, Henao-Guerrero N, Robertson J, Davalos RV. Nonthermal irreversible electroporation for intracranial surgical applications. *J Neurosurg* 2011; **114:** 681-8. doi: 10.3171/2010.5.JNS091448
13. Rossmeisl JH, Garcia PA, Roberston JL, Ellis TL, Davalos RV. Pathology of nonthermal irreversible electroporation (N-TIRE)-induced ablation of the canine brain. *J Vet Sci* 2013; **14:** 433-40. doi: 10.4142/jvs.2013.14.4.433
14. Rossmeisl JH, Garcia PA, Pancotto TE, et al. Safety and feasibility of the NanoKnife system for irreversible electroporation ablative treatment of canine spontaneous intracranial gliomas. *J Neurosurg* 2015; **123:** 1008-25. doi: 10.3171/2014.12.JNS141768
15. Garcia PA, Kos B, Rossmeisl JH, Pavliha D, Miklavčič D, Davalos RV. Predictive therapeutic planning for irreversible electroporation treatment of spontaneous malignant glioma. *Med Phys* 2017; **44:** 4968-80. doi: 10.1002/mp.12401
16. Arena CB, Sano MB, Rossmeisl JH, Caldwell JL, Garcia PA, Rylander MN, et al. High-frequency irreversible electroporation (H-FIRE) for non-thermal ablation without muscle contraction. *Biomed Eng Online* 2011; **10:** 102. doi: 10.1186/1475-925X-10-102
17. Latouche EL, Arena CB, Ivey JW, Garcia PA, Pancotto TE, Pavlisko N, et al. High-frequency irreversible electroporation for intracranial meningioma: a feasibility study in a spontaneous canine tumor model. *Technol Cancer Res Treat* 2018; **17:** 1533033818785285. doi: 10.1177/1533033818785285
18. Salford LG, Persson BR, Brun A, Ceberg CP, Kongstad PC, Mir LM. A new brain tumour therapy combining bleomycin with in vivo electropermeabilization. *Biochem Biophys Res Commun* 1993; **194:** 938-43. doi: 10.1006/bbrc.1993.1911

19. Agerholm-Larsen B, Iversen HK, Ibsen P, Moller JM, Mahmood F, Jensen KS, et al. Preclinical validation of electrochemotherapy as an effective treatment for brain tumors. *Cancer Res* 2011; **71:** 3753-62. doi: 10.1158/0008-5472.CAN-11-0451

20. Sharabi S, Guez D, Daniels D, Cooper I, Atrakchi D, Liraz-Zaltsman S, et al. The application of point source electroporation and chemotherapy for the treatment of glioma: a randomized controlled rat study. *Sci Rep* 2020; **10:** 2178. doi: 10.1038/s41598-020-59152-7

21. Linnert M, Iversen HK, Gehl J. Multiple brain metastases – current management and perspectives for treatment with electrochemotherapy. *Radiol Oncol* 2012; **46:** 271-8. doi: 10.2478/v10019-012-0042-y

22. Jacobs Iv EJ, Campelo SN, Charlton A, Altreuter S, Davalos RV. Characterizing reversible, irreversible, and calcium electroporation to generate a burst-dependent dynamic conductivity curve. *Bioelectrochemistry* 2024; **155:** 108580. doi: 10.1016/j.bioelechem.2023.108580

23. Nakagawa H, Farshchi-Heydari S, Maffre J, Sharma T, Govari A, Beeckler C, et al. Evaluation of ablation parameters to predict irreversible lesion size during pulsed field ablation. *Circ Arrhythm Electrophysiol* 2024; **17:** e012814. doi: 10.1161/CIRCEP.124.012814

24. Miklavčič D, Šemrov D, Mekid H, Mir LM. A validated model of in vivo electric field distribution in tissues for electrochemotherapy and for DNA electrotransfer for gene therapy. *Biochim Biophys Acta Gen Subj* 2000; **1523:** 73-83. doi: 10.1016/S0304-4165(00)00101-X

25. Amin SB, Anderson KJ, Boudreau CE, Martinez-Ledesma E, Kocakavuk E, Johnson KC, et al. Comparative molecular life history of spontaneous canine and human gliomas. *Cancer Cell* 2020; **37:** 243-57.e7. doi: 10.1016/j.ccell.2020.01.004

26. Sahu U, Barth RF, Otani Y, McCormack R, Kaur B. Rat and mouse brain tumor models for experimental neuro-oncology research. *J Neuropathol Exp Neurol* 2022; **81:** 312-29. doi: 10.1093/jnen/nlac021

27. Chow L, Wheat W, Ramirez D, Impastato R, Dow S. Direct comparison of canine and human immune responses using transcriptomic and functional analyses. *Sci Rep* 2024; **14:** 2207. doi: 10.1038/s41598-023-50340-9

28. Xie Y, Bergström T, Jiang Y, Johnson P, Marinescu VD, Lindberg N, et al. The human glioblastoma cell culture resource: validated cell models representing all molecular subtypes. *EBioMedicine* 2015; **2:** 1351-1363 doi: 10.1016/j.ebiom.2015.08.026

29. Steinle M, Palme D, Misovic M, Rudner J, Dittmann K, Lukowski R, et al. Ionizing radiation induces migration of glioblastoma cells by activating BK K(+) channels. *Radiother Oncol* 2011; **101**: 122-126. doi: 10.1016/j.radonc.2011.05.069

30. Blažič A, Guinard M, Leskovar T, O'Connor RP, Rems L. Long-term changes in transmembrane voltage after electroporation are governed by the interplay between nonselective leak current and ion channel activation. *Bioelectrochemistry* 2025; **161:** 108802. doi: 10.1016/j.bioelechem.2024.108802

31. Younes S, Mourad N, Salla M, Rahal M, Hammoudi Halat D. Potassium ion channels in glioma: from basic knowledge into therapeutic applications. *Membranes* 2023; **13:** 434. doi: 10.3390/membranes13040434

32. D'Alessandro G, Monaco L, Catacuzzeno L, Antonangeli F, Santoro A, Esposito V, et al. Radiation increases functional KCa3.1 expression and invasiveness in glioblastoma. *Cancers* 2019; **11:** 279. doi: 10.3390/cancers11030279

33. Novak M, Majc B, Malavolta M, Porčnik A, Mlakar J, Hren M, et al. The Slovenian translational platform GlioBank for brain tumor research: identification of molecular signatures of glioblastoma progression. *Neurooncol Adv* 2025; **7:** vdaf015. doi: 10.1093/noajnl/vdaf015

34. Murphy KR, Aycock KN, Hay AN, Rossmeisl JH, Davalos RV, Dervisis NG. High-frequency irreversible electroporation brain tumor ablation: exploring the dynamics of cell death and recovery. *Bioelectrochemistry* 2022; **144:** 108001. doi: 10.1016/j.bioelechem.2021.108001

35. Partridge BR, Kani Y, Lorenzo MF, Campelo SN, Allen IC, Hinckley J, et al. High-frequency irreversible electroporation (H-FIRE) induced blood-brain barrier disruption is mediated by cytoskeletal remodeling and changes in tight junction protein regulation. *Biomedicines* 2022; **10:** 1384. doi: 10.3390/biomedicines10061384

36. Batista Napotnik T, Miklavčič D. In vitro electroporation detection methods – An overview. *Bioelectrochemistry* 2018; **120:** 166-182. doi: 10.1016/j.bioelechem.2017.12.005

37. Blažič A, Šmerc R, Polajžer T, Miklavčič D, Rems L. Reassessing lidocaine as an electroporation sensitizer in vitro. *Sci Rep* 2025; **15:** 25593. doi: 10.1038/s41598-025-11695-3

38. Hira VV, Breznik B, Van Noorden CJ, Lah T, Molenaar RJ. 2D and 3D in vitro assays to quantify the invasive behavior of glioblastoma stem cells in response to SDF-1α. *Biotechniques* 2020; **69:** 339-46. doi: 10.2144/btn-2020-0046

39. Schindelin J, Arganda-Carreras I, Frise E, Kaynig V, Longair M, Pietzsch T, et al. Fiji: an open-source platform for biological-image analysis. *Nat Methods* 2012; **9:** 676-82. doi: 10.1038/nmeth.2019

40. Morozas A, Malyško-Ptašinskė V, Kulbacka J, Ivaška J, Ivaškienė T, Novickij V. Electrochemotherapy for head and neck cancers: possibilities and limitations. *Front Oncol* 2024; **14:** 1353800. doi: 10.3389/fonc.2024.1353800

41. Li A, Walling J, Kotliarov Y, Center A, Steed MA, Ahn SJ, et al. Genomic changes and gene expression profiles reveal that established glioma cell lines are poorly representative of primary human gliomas. *Mol Cancer Res* 2008; **6:** 21-30. doi: 10.1158/1541-7786.MCR-07-0280

42. Keller S, Schmidt MHH. EGFR and EGFRvIII promote angiogenesis and cell invasion in glioblastoma: combination therapies for an effective treatment. *Int J Mol Sci* 2017; **18:** 1295. doi: 10.3390/ijms18061295

43. Abed T, Ganser K, Eckert F, Stransky N, Huber SM. Ion channels as molecular targets of glioblastoma electrotherapy. *Front Cell Neurosci* 2023; **17:** 1133984. doi: 10.3389/fncel.2023.1133984

44. Wei R, Zhou J, Bui B, Liu X. Glioma actively orchestrate a self-advantageous extracellular matrix to promote recurrence and progression. *BMC Cancer* 2024; **24:** 974. doi: 10.1186/s12885-024-12751-3

45. Aitchison EE, Dimesa AM, Shoari A. Matrix metalloproteinases in glioma: drivers of invasion and therapeutic targets. *BioTech* 2025; **14:** 28. doi: 10.3390/biotech14020028

46. Lehmann S, Boekhorst VT, Odenthal J, Bianchi R, Helvert S, Ikenberg K, et al. Hypoxia induces a HIF-1-dependent transition from collective-to-amoeboid dissemination in epithelial cancer cells. *Curr Biol* 2017; **27:** 392-400. doi: 10.1016/j.cub.2016.11.057

47. Graybill PM, Davalos RV. Cytoskeletal disruption after electroporation and its significance to pulsed electric field therapies. *Cancers* 2020; **12:** 1132. doi: 10.3390/cancers12051132

48. Azuaje F, Tiemann K, Niclou SP. Therapeutic control and resistance of the EGFR-driven signaling network in glioblastoma. *Cell Commun Signal* 2015; **13:** 23. doi: 10.1186/s12964-015-0098-6

49. Wang X, Hong T, Liu G, Rao J, Shi F, Wang H, et al. High-frequency irreversible electroporation suppresses invasion and metastasis by targeting SIRT1/2 in highly invasive tumor cells: an in vitro study. *Bioelectrochemistry* 2025; **166:** 109036. doi: 10.1016/j.bioelechem.2025.109036

50. Casciati A, Tanori M, Gianlorenzi I, Rampazzo E, Persano L, Viola G, et al. Effects of ultra-short pulsed electric field exposure on glioblastoma cells. *Int J Mol Sci* 2022; **23:** 3001. doi: 10.3390/ijms23063001

51. Allen M, Bjerke M, Edlund H, Nelander S, Westermark B. Origin of the U87MG glioma cell line: good news and bad news. *Sci Transl Med* 2016; **8:** 354re3. doi: 10.1126/scitranslmed.aaf6853

52. Cheng L, Wu Q, Guryanova OA, Huang Q, Rich JN, Bao S, et al. Elevated invasive potential of glioblastoma stem cells. *Biochem Biophys Res Commun* 2011; **406:** 643-8. doi: 10.1016/j.bbrc.2011.02.123

53. Prager BC, Bhargava S, Mahadev V, Hubert CG, Rich JN. Glioblastoma stem cells: driving resilience through chaos. *Trends Cancer* 2020; **6:** 223-235. doi: 10.1016/j.trecan.2020.01.009

54. Garcia PA, Pancotto T, Rossmeisl JH, Henao-Guerrero N, Gustafson NR, Daniel GB, et al. Non-thermal irreversible electroporation (N-TIRE) and adjuvant fractionated radiotherapeutic multimodal therapy for intracranial malignant glioma in a canine patient. *Technol Cancer Res Treat* 2011; **10:** 73-83. doi: 10.7785/tcrt.2012.500181

55. Dasari S, Bernard Tchounwou P. Cisplatin in cancer therapy: molecular mechanisms of action. *Eur J Pharmacol* 2014; **740:** 364-378. doi: 10.1016/j.ejphar.2014.07.025

56. Serša G, Čemažar M, Miklavčič D, Rudolf Z. Electrochemotherapy of tumours. *Radiol Oncol* 2006; **40:** 163-74. [internet]. [cited 2025 Jul 15]. Available at https://www.radioloncol.com/index.php/ro/article/view/1258

57. Lorenzo MF, Thomas SC, Kani Y, Hinckley J, Lee M, Adler J, et al. Temporal characterization of blood–brain barrier disruption with high-frequency electroporation. *Cancers* 2019; **11:** 1850. doi: 10.3390/cancers11121850

58. Sharabi S, Bresler Y, Ravid O, Shemesh C, Atrakchi D, Schnaider-Beeri M, et al. Transient blood-brain barrier disruption is induced by low pulsed electrical fields in vitro: an analysis of permeability and trans-endothelial electric resistivity. *Drug Deliv* 2019; **26:** 459-69. doi: 10.1080/10717544.2019.1571123

59. Todorovic V, Sersa G, Mlakar V, Glavac D, Flisar K, Cemazar M. Metastatic potential of melanoma cells is not affected by electrochemotherapy. *Melanoma Res* 2011; **21:** 196-205. doi: 10.1097/CMR.0b013e328337abd7

60. Todorovic V, Sersa G, Mlakar V, Glavac D, Cemazar M. Assessment of the tumourigenic and metastatic properties of SK-MEL28 melanoma cells surviving electrochemotherapy with bleomycin. *Radiol Oncol* 2012; **46:** 32-45. doi: 10.2478/v10019-012-0010-6

61. Auffinger B, Tobias AL, Han Y, Lee G, Guo D, Dey M, et al. Conversion of differentiated cancer cells into cancer stem-like cells in a glioblastoma model after primary chemotherapy. *Cell Death Differ* 2014; **21:** 1119-1131. doi: 10.1038/cdd.2014.31

62. Wang Z, Zhang H, Xu S, Liu Z, Cheng Q. The adaptive transition of glioblastoma stem cells and its implications on treatments. *Sig Transduct Target Ther* 2021; **6:** 1-13. doi: 10.1038/s41392-021-00491-w

63. Arroyo JP, Jacobs EJ, Ahmad RN, Amin AJ, Verbridge SS, Davalos RV. Characterization of glioma spheroid viability and metastatic potential following monophasic and biphasic pulsed electric fields. *Bioelectrochemistry* 2025; **165:** 109005. doi: 10.1016/j.bioelechem.2025.109005

RADIOLOGY AND ONCOLOGY Radiology and Oncology | Ljubljana | Slovenia | www.radioloncol.com 1

Invasive properties of patient-derived glioblastoma cells after reversible electroporation *in vitro*

Anja Blazic, Bernarda Majc, Metka Novak, Barbara Breznik, Lea Rems

doi: 10.2478/raon-2025-0058

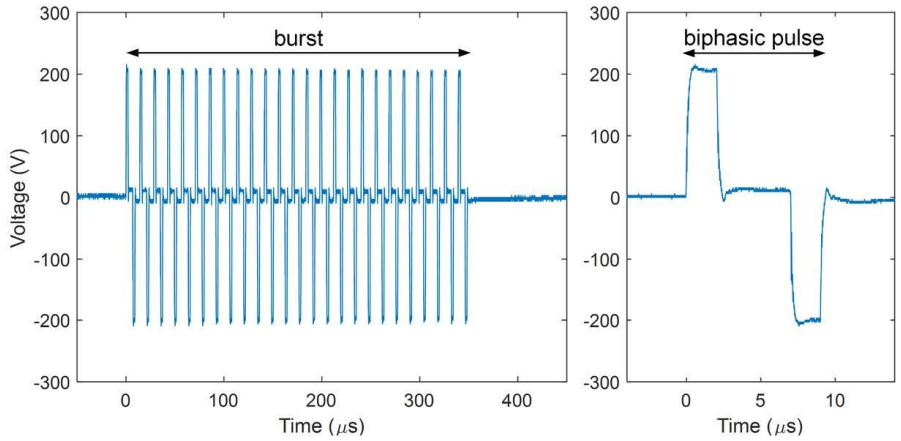

SUPPLEMENTARY FIGURE S1. H-FIRE waveform used in experiments. Each sample was exposed to 100 bursts of biphasic pulses, 2 μs negative and positive phase, with 5 μs interphase and 5 μs interpulse delay, with 25 pulses/burst, and 1 Hz burst repetition frequency. The graphs show one burst of biphasic pulses (left) and one biphasic pulse within the burst (right). The voltage set on the pulse generator was 200 V.

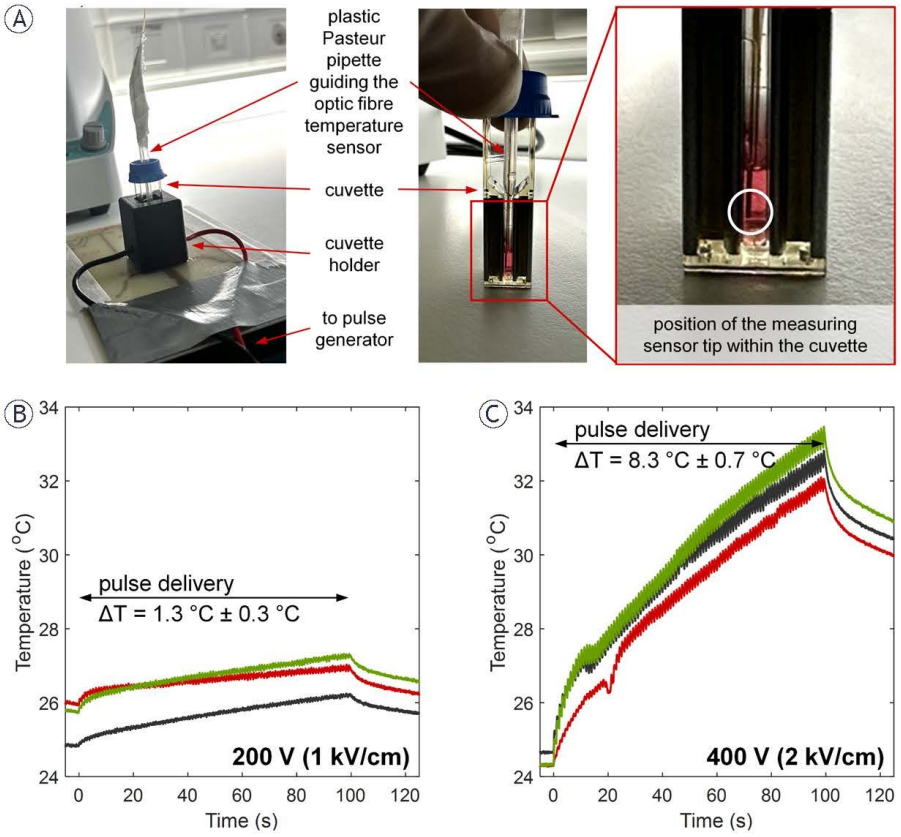

SUPPLEMENTARY FIGURE S2. Increase in sample temperature during delivery of the H-FIRE waveform. **(A)** Temperature measurements were performed using fibre optic sensor MPK-5 (OpSens Solutions, Quebec, Canada) during delivery of electric pulses at ambient temperature. The sensor was inserted into electroporation medium between the electrodes inside the cuvette. A plastic Pasteur pipette, cut at the top and bottom side, was used to guide the optic fibre and keep it in place during measurements. **(B)** Temperature recordings from 3 samples exposed to H-FIRE waveform with amplitude of 200 V **(C)** and 400 V. The ΔT shows the difference in temperature at the end and the beginning of pulse delivery (mean ± standard deviation of the three measurements).

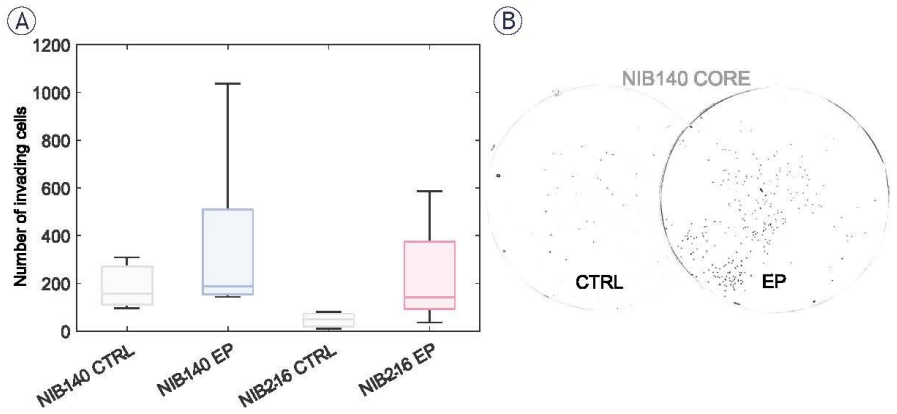

SUPPLEMENTARY FIGURE S3. Increased invasion of patient-derived GB cells following exposure to H-FIRE waveform resulting in electric field strength of 2 kV/cm. **(A)** Quantification of the number of invading cells in NIB140 and NIB216 CORE cell lines. Electroporated (EP) samples showed a trend toward increased invasion compared to untreated controls (CTRL); however, the differences were not statistically significant for neither NIB140 CORE (Mank-Whitney Rank test, $p = 0.517$) nor NIB216 CORE (Student's t-test; $p = 0.159$). Data are presented as box plots showing median, interquartile range, and full data range from three biological replicates (1–3 technical replicates per biological replicate). **(B)** Representative image of transwell inserts highlighting increased invasion following electroporation for NIB140 cell line.

2.3 REASSESSING LIDOCAINE AS AN ELECTROPORATION SENSITIZER *IN VITRO*

Blažič A., Šmerc R., Polajžer T., Miklavčič D., Rems L. 2025b. Reassessing lidocaine as an electroporation sensitizer in vitro. Scientific Reports, 15, 1: 25593, https://doi.org/10.1038/s41598-025-11695-3

Lidocaine, an inhibitor of voltage-gated sodium channels, is commonly administered before performing electrochemotherapy to minimize patient discomfort (Gehl et al., 2018; Mir et al., 2006). In addition to its anaesthetic properties, lidocaine has also been proposed as a potential electroporation sensitizer, possibly through its effects on cell membrane charge and the function of the ATPases (Grys et al., 2014; Pan F. et al., 2020; Sherba et al., 2020). However, these effects have not been systematically studied, particularly under physiologically relevant conditions; i.e., at relevant/therapeutic concentrations. Therefore, our aim was to investigate whether lidocaine applied at clinically relevant concentrations alters electroporation outcomes, i.e., cell membrane permeabilization and decrease in cell viability. We found that 10 mM lidocaine had only minor effects on membrane permeabilization and cell survival, whereas 35 mM significantly enhanced electroporation efficiency and reduced the threshold for irreversible electroporation by up to 40 %, but such concentrations exceed those reached in tissues following local administration, indicating that lidocaine's sensitizing effect is unlikely to be clinically relevant under standard therapeutic conditions.

www.nature.com/scientificreports

scientific reports

Check for updates

OPEN

Reassessing lidocaine as an electroporation sensitizer in vitro

Anja Blažič, Rok Šmerc, Tamara Polajžer, Damijan Miklavčič & Lea Rems✉

High-intensity pulsed electric fields induce transient increase in membrane permeability, a phenomenon known as electroporation, with broad applications in medicine, including electrochemotherapy (ECT), gene electrotransfer and tissue ablation. As electroporation technologies become increasingly established in clinical practice, understanding how commonly used pharmacological agents influence treatment outcomes is gaining importance. Lidocaine, a widely used local anesthetic and ion channel modulator, has recently been investigated as a potential sensitizer to enhance the efficacy of electroporation. Here, we examined the effects of lidocaine on membrane permeabilization and cell viability using standard 8 × 100 µs ECT pulses across four cell lines: melanoma B16-F1, myoblast C2C12, CHO-K1 cells with low ion channel expression, and NS-HEK cells with stable $Na_v1.5$ expression. We show that 10 mM lidocaine has only modest effects on electroporation outcomes, while 35 mM considerably lowers the electric field threshold for irreversible electroporation by 25–40% in melanoma cells. However, concentrations of even 10 mM exceed those reported in tissues following local administration of lidocaine. This questions the clinical relevance of lidocaine's sensitization effect and warrants further investigation. Our study also highlights the importance of evaluating drug–electroporation interactions under rigorously controlled experimental conditions to ensure meaningful translation into clinical applications.

Keywords Electroporation, Sensitization, Electropermeabilization, Cell survival, Lidocaine, Melanoma cells

High-intensity pulsed electric fields are widely used in medicine[1] as well as in biotechnology[2] and food technology[3] to achieve a transient increase in cell membrane permeability, a phenomenon known as electroporation. Among the most developed clinical applications are electrochemotherapy, irreversible electroporation for tissue ablation (tumor, cardiac), and gene electrotransfer[4–6]. The extent of electroporation depends primarily on the pulse parameters—including duration, amplitude, and repetition rate—which determine whether the process is reversible, allowing cell survival, or irreversible, leading to cell death[7]. Sensitization methods can be used to increase the extent of membrane permeabilization or cell death under fixed pulse parameters. These methods include the addition of surfactants and the application of hypotonic shock[8,9]. Additionally, they can involve modifications to pulse delivery, such as dividing a train of pulses into two shorter sequences administered several minutes apart, although this approach is not applicable to all conditions[10,11].

Pharmacological agents like lidocaine have also been explored as sensitizers[12–14]. Lidocaine is an ion channel modulator that primarily inhibits voltage-gated sodium channels but also interacts with other membrane proteins and influences the biophysical properties of the membrane[15,16]. It is used as a local anesthetic and, at lower concentrations, as class 1b antiarrhythmic drug[17]. Recent studies have demonstrated that lidocaine can considerably modulate electroporation outcomes. Specifically, Grys et al.[12] showed that 10 mM lidocaine reduced the electric field thresholds for reversible and irreversible electroporation in cancer cells and human fibroblasts. Similarly, Sherba et al.[13] observed that 10 mM lidocaine enhanced irreversible electroporation in mouse fibroblasts. An in vivo study by Pan et al.[14] further indicated that intra-arterial (directly into the hepatic artery) administration of 5 mg/ml (18.5 mM, 0.5%) before and 5 mg/ml during pulse application could expand irreversibly electroporated zones in porcine liver.

The intriguing effect of lidocaine in lowering electroporation thresholds (i.e., increasing the electroporation zone) has potentially important implications for electrochemotherapy (ECT). According to standard operating procedures for ECT, lidocaine is used as a local anesthetic to provide pain relief during the treatment of cutaneous tumors and skin metastases[18,19]. Similarly, lidocaine is used as anesthetic before gene electrotransfer (GET) for gene therapy applications[20,21]. However, previous studies employed experimental conditions that were not directly relevant to typical ECT and GET conditions. The in vitro experiments used a low conductivity electroporation solution (<1 mS/cm); while such solution may approximate the conductivity of certain low-conductive tissues (e.g. bone and fat), it does not represent the ionic environment relevant to tumor or muscle tissues, which are typical targets of ECT and GET, respectively[22]. The pulse parameters also differed from the

Faculty of Electrical Engineering, University of Ljubljana, Ljubljana 1000, Slovenia. ✉email: lea.rems@fe.uni-lj.si

clinical ECT protocol (8×100 µs pulses applied at a repetition rate of 1 Hz)[18,19]. In vitro studies by Grys et al.[12] and Sherba et al.[13] used single pulses with duration of 80–620 ms and 0.06–1.00 ms, respectively. The in vivo study by Pan et al.[14] used conventional irreversible electroporation pulse protocol applying 90 pulses of 90 µs. Additionally, as lidocaine is primarily metabolized in the liver[23], this could potentially influence the in vivo results.

Building on previous studies, we investigated how the presence of lidocaine affects membrane permeability and cell survival when cells are exposed to conventional ECT pulses in vitro. We selected four different cell lines: B16-F1 mouse melanoma cells to reflect the clinical application of ECT in cutaneous tumors and skin metastases[18,19]; C2C12 mouse myoblasts as a model for GET[24]; CHO-K1 cells as a model of cells with low endogenous ion channel expression[25]; and NS-HEK cells with stable expression of $Na_V1.5$ channels[26,27] to explore the potential role of sodium channels in the observed outcomes. We performed experiments using both a low conductivity solution and a Tyrode solution that mimics the typical conductivity and ionic composition of extracellular fluids[28]. Using a 10 min lidocaine incubation period[12], we tested two concentrations: 10 mM (0.3%), aligned with previous in vitro research[12,13], and 35 mM (1%), corresponding to standard anesthetic injection dosage. Overall, our findings indicate that lidocaine has modest effects on membrane permeabilization and cell survival at 10 mM, while a pronounced reduction in survival was observed only at a higher concentration of 35 mM.

Results

Our experiments were designed to evaluate the effect of lidocaine (in hydrocholoride salt form) on membrane permeabilization and cell survival following electroporation. The experimental protocol consisted of four parts, as shown in Fig. 1: (1) B16-F1, C2C12, CHO-K1, or NS-HEK cells were first suspended in the chosen electroporation solution with or without lidocaine and incubated for 10 min. (2) Cells were then exposed to 8× 100 µs pulses of chosen amplitude delivered at 1 Hz in standard electroporation cuvettes, either in the presence of propidium iodide (PI; for permeabilization analysis) or its absence (for cell survival assessment); (3) Membrane permeabilization was assessed based on PI uptake using flow cytometer, 3 min after electroporation. PI is a nucleic acid stain that selectively enters cells with compromised membranes. It is typically used for assessing cell survival but is commonly applied in electroporation experiments to evaluate membrane permeabilization[29,30]; (4) For cell survival assessment, cells were centrifuged following pulse delivery, resuspended in growth medium, plated and incubated for 24 h. Afterwards, dead cells were stained with PI, and non-stained live cells were counted using flow cytometry to determine cell survival. Note that permeabilization and survival were assessed on separate samples.

Effect of 10 mM lidocaine on membrane permeabilization in low conductivity electroporation solution

We first evaluated how 10 mM lidocaine (0.3%) affects membrane permeabilization in a low conductivity (LC) solution, which was used in a previous in vitro study investigating the effect of lidocaine on the electroporation outcome[12]. We observed that adding 10 mM lidocaine to this LC solution caused two changes: a decrease in pH

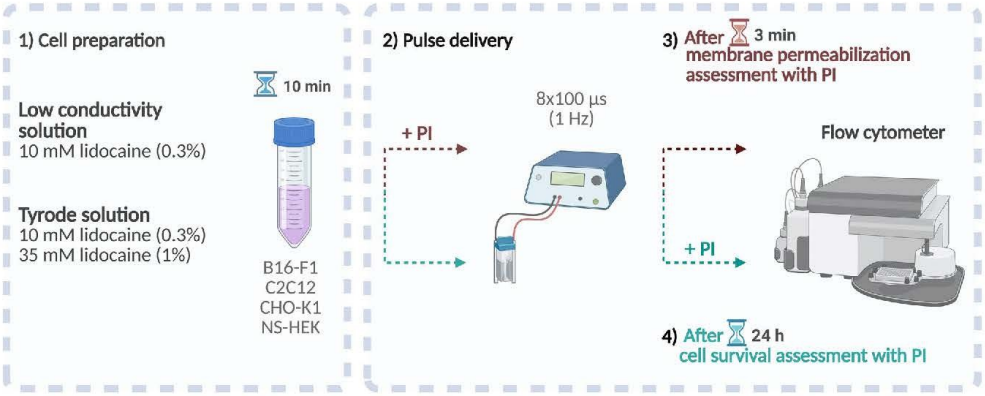

Fig. 1. Schematic representation of the experimental design. The workflow consisted of four parts: (1) Incubation of cells (B16-F1, C2C12, CHO-K1, or NS-HEK) with or without lidocaine in the chosen electroporation solution for 10 min; (2) Application of eight 100 µs electric pulses at 1 Hz, in the presence of propidium iodide (PI) for membrane permeabilization analysis or in its absence for cell survival analysis; (3) Measurement of membrane permeabilization by PI uptake 3 min after electroporation using flow cytometry; and (4) Assessment of cell survival 24 h after electroporation by staining with PI and counting unstained live cells with flow cytometry. Permeabilization and survival were assessed on separate samples. Created with BioRender.com.

from 7.0 to 6.6 and an increase in conductivity from 0.87 mS/cm to 2.41 mS/cm, while the osmolality remained practically unchanged. To better understand the impact of pH reduction and conductivity increase, we prepared two additional LC solutions: one in which pH was decreased using 1 M HCl solution, and another in which conductivity was increased with physiological saline (0.9% NaCl), hereafter referred to as saline. All media's pH, conductivity, and osmolality values are presented in Fig. 2a. For each of the four tested cell lines (B16-F1, C2C12, CHO-K1, and NS-HEK) we thus had three control and one experimental group based on the electroporation solution: LC pH 7 (Control 1), LC pH 6.5 (Control 2), LC + saline (Control 3), and LC + 10 mM lidocaine.

a) Color legend and electroporation solution properties

Legend	Low conductivity solution (LC)	pH value	Conductivity (mS/cm)	Osmolality (mOsm/kg)
	LC pH 7 (Control 1)	7.0	0.87; 22.0°C	308
	LC pH 6.6 (Control 2)	6.6	0.87; 22.0°C	316
	LC + saline (Control 3)	7.0	2.67; 22.4°C	311
	LC + 10 mM lidocaine (0.3%)	6.5	2.41; 21.5°C	308

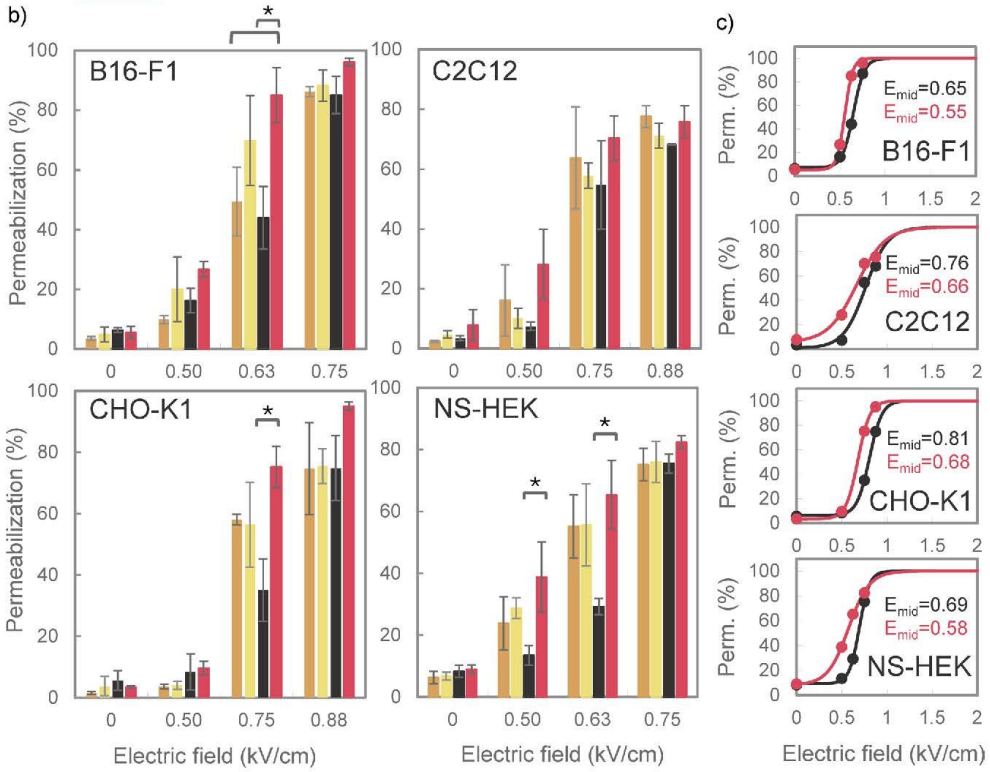

Fig. 2. The effect of 10 mM lidocaine on membrane permeabilization in low conductivity (LC) electroporation solution. (a) Table listing all tested electroporation solutions with their pH, conductivity and osmolality values, and the corresponding color legend for panels b and c. (b) The percentage of permeabilized cells was assessed using four different cell lines (B16-F1, C2C12, CHO-K1 and NS-HEK) after exposure to 8 × 100 µs pulses (1 Hz). Results are presented as mean ± SD ($N = 3$), with statistically significant differences indicated by * ($p < 0.05$, One-way ANOVA or ANOVA on ranks). Note that the electric field strength on the x-axis does not scale linearly. (c) Sigmoidal curves, fitted to data for LC + saline (black line) and LC + 10 mM lidocaine (red line) from panel b, showing the relationship between electric field strength and membrane permeabilization. Dots indicate the mean values from panel b. Fits were obtained using the least-square method in Matlab 2021b (MathWorks, USA). E_{mid} represents the electric field strength (in kV/cm) at the inflection point, where approximately 50% of the cells became permeabilized.

Results presented in Fig. 2b indicate that pH variations had no effect on membrane permeabilization, as no significant differences were observed between LC pH 7 (Control 1) and LC pH 6.5 (Control 2) in none of the cell lines. Similarly, no significant differences were found between LC pH 7 (Control 1) and LC + saline (Control 3), though we observed somewhat reduced permeabilization in solution with higher conductivity (Control 3) under some conditions (in CHO-K1 cells at 0.75 kV/cm, and in NS-HEK cells at 0.50 and 0.63 kV/cm). This aligns with previous studies showing that electroporation is enhanced in solutions with lower conductivity[31,32]. Adding 10 mM lidocaine significantly increased membrane permeabilization compared to LC pH 7 (Control 1), but only in B16-F1 cells at 0.63 kV/cm. Nevertheless, lidocaine-mediated increase in permeabilization became more evident when compared to the control with similar conductivity, i.e., LC + saline (Control 3). This increase was observed across all cell lines and reached statistical significance in B16-F1 at 0.63 kV/cm, CHO-K1 at 0.75 kV/cm, and NS-HEK at 0.50 kV/cm and 0.63 kV/cm. At these specific electric field strengths, lidocaine increased the percentage of permeabilized cells by up to ~ 40% compared to control.

The greatest differences in permeabilization between lidocaine-treated and control groups were observed at intermediate electric fields, where the percentage of permeabilized cells was rapidly increasing with electric field strength. To better illustrate how lidocaine affected the functional relationship between the electric field strength and the percentage of permeabilized cells, we fitted data from LC + 10 mM lidocaine and LC + saline to sigmoidal curves, presented in Fig. 2c. Across all cell lines, lidocaine shifted the curves towards lower electric field strengths, but only to a modest extent. The electric field strength at the inflection point (E_{mid}, where approximately half of the cells became permeabilized) decreased by 15%, 13%, 16%, and 16% in B16-F1, C2C12, CHO-K1, and NS-HEK, respectively.

These initial experiments demonstrated the importance of designing an appropriate control for assessing drug-specific effects. Saline is commonly used as a placebo or solvent in clinical and in vivo studies[14,33]. It has similar conductivity as the stock lidocaine hydrochloride solution (69.3 mM, 2%) that was added to the samples in our experiments and its main anion is chloride (same as in lidocaine hydrochloride solution). Furthermore, addition of equal volume of saline or lidocaine solution dilutes the other components of the electroporation solution in the same proportion. Thus, we performed all subsequent experiments using saline as "placebo" to assess the effect of lidocaine on electroporation outcome.

Effect of 10 mM lidocaine on membrane permeabilization in Tyrode solution

Further experiments were conducted in a Tyrode solution that has approximately the same conductivity as saline and is ~ 15× more conductive than the LC solution. We compared two groups: Tyrode solution with saline and Tyrode solution with 10 mM lidocaine. In both groups the electroporation solution had very similar pH, conductivity, and osmolality values (Fig. 3a). 10 mM lidocaine significantly increased cell membrane permeabilization compared to control in B16-F1 at 0.63 kV/cm and 0.75 kV/cm, in C2C12 at 0.88 kV/cm, and in NS-HEK cells at 0.63 kV/cm, but not in CHO-K1 cells (Fig. 3b). Sigmoidal curves fitted to the data are presented in Fig. 3c. The electric field strength at the inflection point (E_{mid}) decreased in the presence of lidocaine by 15%, 9%, 8%, and 1% in B16-F1, C2C12, NS-HEK, and CHO-K1, respectively.

Effect of 10 mM lidocaine on cell survival in Tyrode solution

The effect of 10 mM lidocaine on cell survival was assessed using PI, as explained in Fig. 1. We used a wider range of pulse amplitudes, compared to permeabilization experiments, to achieve cell survival close to 0%. Our results (Fig. 4b) demonstrated that 10 mM lidocaine significantly reduced survival in B16-F1 cells at 1 kV/cm and CHO-K1 cells at 1.5 kV/cm, but not in C2C12 and NS-HEK cells. Fits to sigmoidal curves (Fig. 4c) showed that lidocaine decreased the E_{mid} for survival by 18%, 11%, 6%, and 5% in B16-F1, C2C12, CHO-K1, and NS-HEK, respectively.

Effect of 35 mM lidocaine on permeabilization and survival in melanoma cells

B16-F1 cells were selected for further investigation because they showed the most pronounced sensitization effect with 10 mM lidocaine. To assess whether this effect could be enhanced, we tested a higher lidocaine concentration of 35 mM (1%). While the addition of 35 mM lidocaine did not affect the conductivity or osmolality of the Tyrode solution, it lowered its pH to 6.9 (Fig. 5a). To account for this pH change, we added another experimental group with 35 mM lidocaine, where the pH was adjusted to 7.3 using NaOH. As shown in Fig. 5b, the presence of 35 mM lidocaine significantly increased membrane permeabilization in both 35 mM lidocaine groups, regardless of pH adjustment, at 0.5 kV/cm, 0.63 kV/cm, and 0.75 kV/cm. However, E_{mid} obtained by sigmoidal fitting (Fig. 5c) decreased by only 8–9% compared to saline control. For cell survival (Fig. 5b), 35 mM lidocaine had a much more pronounced effect, significantly reducing survival at 1 and 1.5 kV/cm compared to control. Moreover, the effect was pH-dependent: the group with pH adjusted to 7.3 showed a 40% decrease in E_{mid} for survival, while the group without pH adjustment (pH 6.9) showed a 25% decrease in E_{mid} compared to control.

Illustrating the impact of lidocaine on reversible and irreversible electroporation volumes using a simplified numerical model

Our experimental results indicated that lidocaine decreased the E_{mid} field strength for membrane permeabilization to a modest extent (by 1–16% compared to control) at both tested concentrations. In contrast, lidocaine decreased the E_{mid} for cell survival in a markedly concentration-dependent manner: 10 mM lidocaine decreased E_{mid} by 5–18%, while 35 mM lidocaine decreased E_{mid} by 25–40%. To gain a better understanding of how this decrease in E_{mid} would translate into an increase in volume corresponding to reversible (RE) and irreversible (IRE) electroporation at a tissue level, we used a simplified numerical model (Fig. 6a). We calculated the electric field distribution around two needle electrodes (Fig. 6b) and determined the volume, where electric field was

a) Color legend and electroporation solution properties

Legend	Tyrode solution	pH value	Conductivity (mS/cm)	Osmolality (mOsm/kg)
	Tyrode buffer + saline	7.3	13.11; 21.5˚C	283
	Tyrode buffer + 10 mM lidocaine (0.3%)	7.2	12.76; 21.5˚C	282

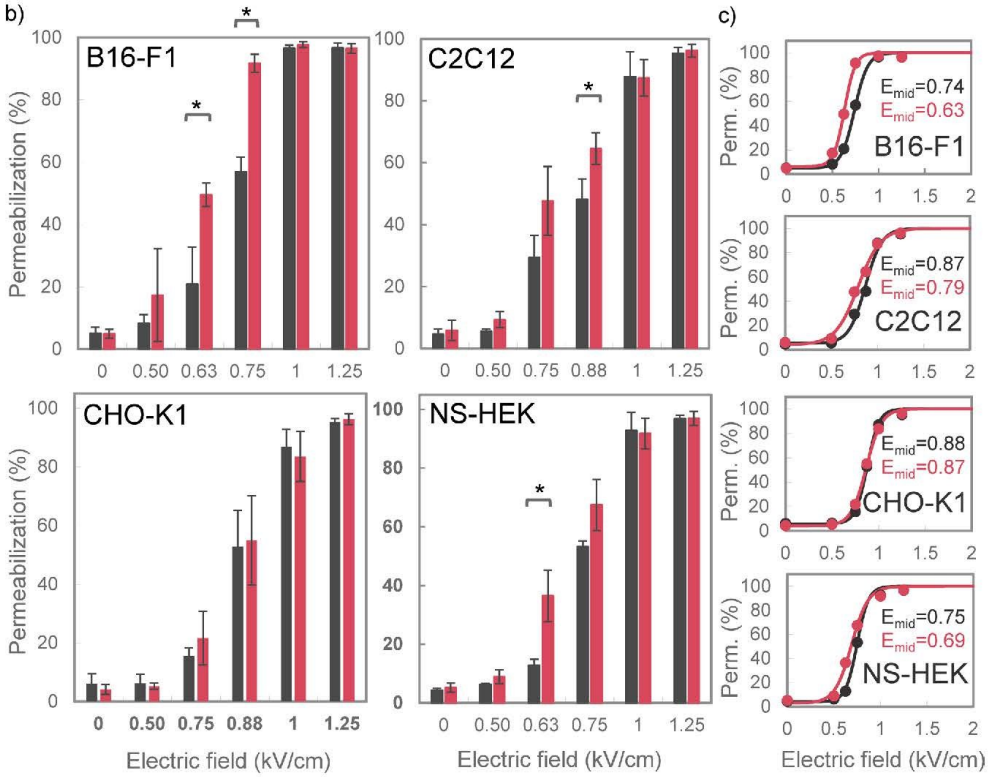

Fig. 3. The effect of 10 mM lidocaine on membrane permeabilization in Tyrode solution. (a) Table listing all tested electroporation solutions with their pH, conductivity and osmolality values, and the corresponding color legend for panels b and c. (b) The percentage of permeabilized cells was assessed using four different cell lines (B16-F1, C2C12, CHO-K1 and NS-HEK) after exposure to 8 × 100 µs pulses (1 Hz). Results are presented as mean ± SD ($N = 3$), with statistically significant differences indicated by * ($p < 0.05$, One-way ANOVA or ANOVA on ranks). Note that the electric field strength on the x-axis does not scale linearly. (c) Sigmoidal curves, fitted to the data in panel b, showing the relationship between electric field strength and membrane permeabilization. Dots indicate the mean values from panel b. E_{mid} represents the electric field strength (in kV/cm) at the inflection point.

higher than E_{mid} for permeabilization (for RE) and E_{mid} for survival (for IRE). We considered only E_{mid} values obtained in experiments with Tyrode buffer. The model was designed as a simplified representation of the tissue and was not intended to capture the full complexity of the biological structure or conductivity changes due to electroporation. As such, the calculated RE and IRE volumes should be interpreted as approximate estimates that illustrate the expected trends, rather than as clinically predictive values.

The calculated values of the increase in RE and IRE tissue volumes due to lidocaine are listed in Fig. 6c. At 10 mM lidocaine concentration, the largest increase in RE volume was observed with B16-F1 cells (22.2%), followed by C2C12 cells (14.5%) and NS-HEK cells (11.3%), with CHO-K1 cells showing the smallest increase (1.7%). For IRE volumes at the same lidocaine concentration, B16-F1 cells again showed the largest increase (43.7%), while the effects were progressively smaller for C2C12 (28.8%), CHO-K1 (14.6%), and NS-HEK cells (9.5%). In experiments with B16-F1cells, increasing the lidocaine concentration to 35 mM somewhat increased

a) Color legend and electroporation solution properties

Legend	Tyrode solution	pH value	Conductivity (mS/cm)	Osmolality (mOsm/kg)
	Tyrode buffer + saline	7.3	13.11; 21.5°C	283
	Tyrode buffer + 10 mM lidocaine (0.3%)	7.2	12.76; 21.5°C	282

b)

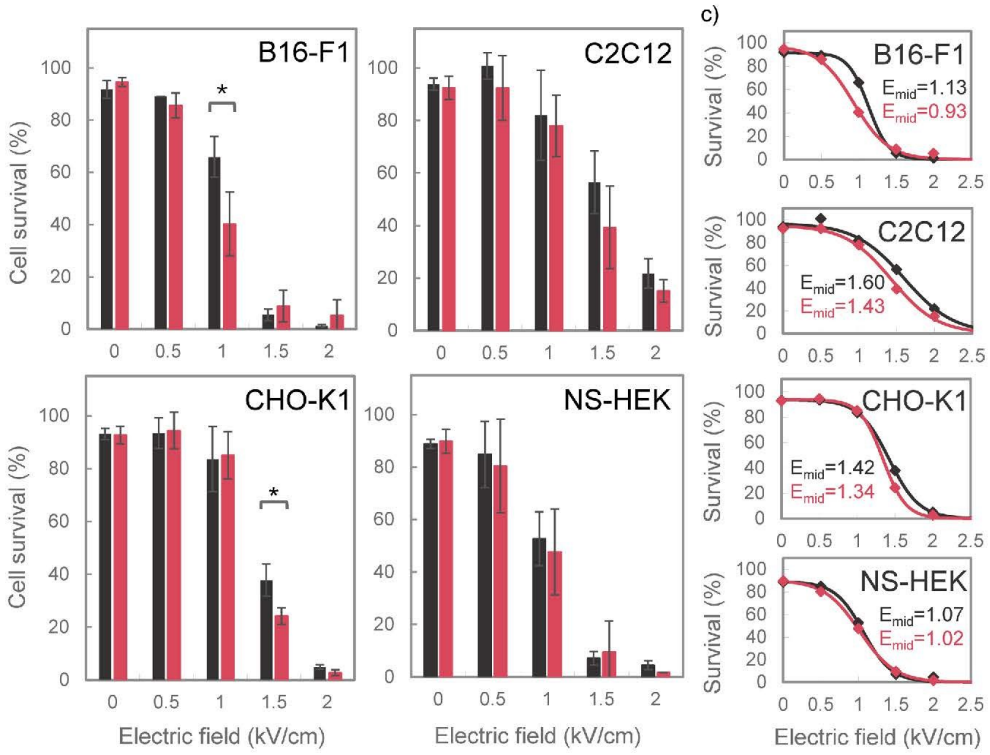

Fig. 4. The effect of 10 mM lidocaine on cell survival in Tyrode solution. (a) Table listing all tested electroporation solutions with their pH, conductivity and osmolality values, and the corresponding color legend for panels b and c. (b) The percentage of survived cells was assessed using four different cell lines (B16-F1, C2C12, CHO-K1 and NS-HEK) after exposure to 8 × 100 µs pulses (1 Hz). Results are presented as mean ± SD ($N = 3$), with statistically significant differences indicated by * ($p < 0.05$, One-way ANOVA or ANOVA on ranks). (c) Sigmoidal curves, fitted to the data in panel b, showing the relationship between electric field strength and cell survival. Dots indicate the mean values from panel b. E_{mid} represents the electric field strength (in kV/cm) at the inflection point.

the RE volume (13.2%, and 11.1% for the groups without and with adjusted pH, respectively). In contrast, this increased concentration profoundly increased the IRE volume by 99.4% and 184.9% compared to saline control, for the groups without and with adjusted pH, respectively.

Discussion

Revisiting the effect of lidocaine on electroporation outcome: challenging previous in vitro studies

Previous in vitro studies showed a profound effect of lidocaine on electroporation outcomes[12,13]. Specifically, Grys et al.[12] demonstrated that 10 mM lidocaine reduced the electric field required to achieve 50% membrane permeabilization (detected by calcein uptake) and 50% cell survival (detected by fluorescein diacetate and ethidium bromide) in AT-2 rat prostate carcinoma cells by 62% and 39%, respectively. These findings indicated that lidocaine facilitates electroporation by significantly lowering the required electric field, with a more pronounced effect on membrane permeabilization than cell survival. The authors attributed this effect to the

a) Color legend and electroporation solution properties

Legend	Tyrode solution	pH value	Conductivity (mS/cm)	Osmolality (mOsm/kg)
	Tyrode buffer + saline	7.2	13.0; 21.5°C	284
	Tyrode buffer + 35 mM lidocaine (1%) pH 6.9	6.9	12.8; 22.0°C	284
	Tyrode buffer + 35 mM lidocaine (1%) adjusted pH 7.3	7.3	12.9; 22.0°C	284

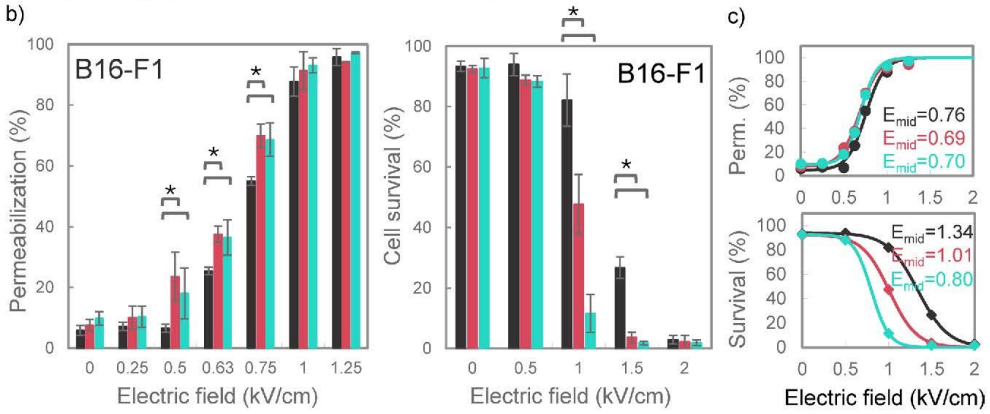

Fig. 5. The effect of 35 mM lidocaine on membrane permeabilization and cell survival in Tyrode solution. (a) Table listing all tested electroporation solutions with their pH, conductivity and osmolality values, and the corresponding color legend for panels b and c. (b) Percentage of permeabilized and percentage of live B16-F1 cells assessed after pulse exposure to 8 × 100 µs pulses in the presence of 35 mM (1%) lidocaine. Results are presented as mean ± SD ($N = 3$), with statistically significant differences indicated by * ($p < 0.05$, One-way ANOVA). (c) Sigmoidal curves, fitted to data in panel b, showing the relationship between electric field strength and membrane permeabilization or cell survival. Dots indicate the mean values from panel b. E_{mid} represents the electric field strength (in kV/cm) at the inflection point.

ability of lidocaine to alter the surface charge of the cell membrane, as similar reductions in electroporation thresholds were observed with cationic dyes, such as 9-aminoacridine (9-AAA) and toluidine blue. Note that different effects were observed among various local anesthetics, with procaine exhibiting a more pronounced effect than lidocaine. Similarly, Sherba et al.[13] reported that 10 mM lidocaine significantly enhanced irreversible electroporation in NIH-3T3 mouse fibroblasts (at a specific electric field strength the percentage of cells killed increased by up to ~ 60% in lidocaine-treated group), as measured by counting the number of adherent cells. This enhancement was attributed to the lidocaine's inhibition of ion-transporting ATPases, impairing the recovery of intracellular ionic homeostasis after electroporation. This interpretation was supported by the observation that lidocaine eliminated the protective effect of Mg^{2+} ions on cell survival, since these ions are required for Na^+/K^+ ATPase activation[13].

In contrast, our findings suggest a less pronounced effect of 10 mM lidocaine on electroporation outcomes compared to previous reports. This was consistently observed across all cell lines, both in terms of membrane permeabilization (Figs. 2 and 3) and cell survival (Fig. 4), and regardless of whether cells were electroporated in low conductivity or Tyrode solution. The decrease in electric field strength required for ~ 50% cell permeabilization and ~ 50% survival (represented by E_{mid} values) did not exceed 16% and 18%, respectively, in our study (Figs. 2–4). At specific electric field strengths, 10 mM lidocaine increased the percentage of permeabilized cells and the percentage of cells killed, but merely up to ~ 40% and ~ 30%, respectively, compared to control. Reduction in electric field threshold comparable to previous in vitro studies was observed only at the much higher concentration of 35 mM lidocaine, which resulted in 25–40% lower E_{mid} for survival in B16-F1 cells. Notably, at this higher concentration, lidocaine affected cell survival to a much greater extent than membrane permeabilization, indicating that lidocaine's cytotoxic effect is not simply due to excessive membrane damage.

Revisiting the effect of lidocaine on electroporation outcome: the role of experimental conditions

Our study showed a less pronounced effect of lidocaine on electroporation outcomes compared to previous in vitro studies, possibly due to more rigorous controls. In previous studies, Grys et al.[12] used a low conductivity sucrose-based solution buffered with PBS (without reporting its pH, conductivity or osmolality). Similarly, Sherba et al.[13] used a low conductivity sucrose-based solution buffered with HEPES (0.5 mS/cm; pH 7.4; ~300 mOsm). We showed that the addition of lidocaine to such solution considerably increases its conductivity and

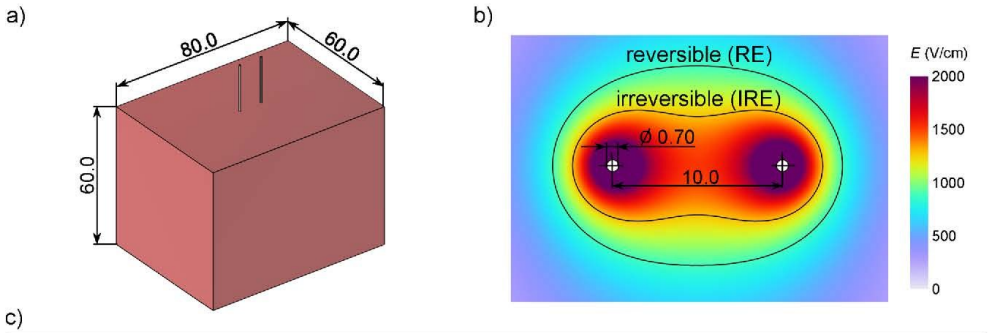

c)

Cell line	B16-F1 + 10 mM lido.	C2C12 + 10 mM lido.	CHO-K1 + 10 mM lido.	NS-HEK + 10 mM lido.	B16-F1 + 35 mM lido.	B16-F1 + 35 mM lido. adjusted pH
RE vol. w/o lido. (cm³)	3.40	2.72	2.67	3.34	3.28	3.28
IRE vol. w/o lido. (cm³)	1.71	0.72	0.94	1.92	1.07	1.07
RE vol. w/ lido. (cm³)	4.15	3.11	2.72	3.71	3.71	3.65
IRE vol. w/ lido. (cm³)	2.46	0.92	1.07	2.11	2.14	3.06
RE vol. increase (%)	22.2	14.5	1.7	11.3	13.2	11.1
IRE vol. increase (%)	43.7	28.8	14.6	9.5	99.4	184.9
Calculated contours						

Fig. 6. Calculations of the increase in the reversible (RE) and irreversible (IRE) electroporation tissue volumes due to lidocaine. (a) Geometry of the numerical model of tissue with two needle electrodes and indicated dimensions (in mm). The electrodes are inserted 30 mm into the tissue. (b) Cross-sectional view of an example calculation illustrating the electric field distribution and highlighting the regions of RE and IRE. (c) Calculated values of the increase in RE and IRE tissue volumes due to lidocaine. Rows 1 and 2 show the absolute volumes of RE and IRE without lidocaine (saline control). Rows 3 and 4 show the absolute volumes of RE and IRE with added lidocaine. Rows 5 and 6 show the relative increase in RE and IRE volumes with the addition of lidocaine. Row 7 shows representative cross-sections, with green indicating the calculated increase in RE volume and red indicating the increase in IRE volume due to lidocaine.

lowers its pH value, despite buffer presence (Fig. 2a). Since lidocaine has a pKa value of 7.6–8[34], small changes in pH from physiological can have a considerable effect of the charge state of lidocaine[35] and consequently its interactions with the cell membrane[16]. Furthermore, if the lidocaine stock solution is prepared without osmolality adjustments, it can result in hypotonic conditions. For these reasons, we used an isotonic lidocaine hydrochloride injection solution, added the same volume of physiological saline (0.9% NaCl) to control samples, and adjusted pH when necessary. This successfully maintained comparable pH, conductivity, and osmolality across lidocaine-treated and control groups.

While our results showed that 10 mM lidocaine's effect on membrane permeabilization is similar regardless of the pH and conductivity variations in low conductivity solution (Fig. 2), the combined alterations in pH, conductivity, and osmolality compared to controls could have amplified lidocaine's apparent effects in previous studies. Moreover, Grys et al.[12] employed a microfluidic system with localized electric fields applied for 80 ms or 620 ms, significantly longer than the 100 µs pulses used in our study, resulting in greater membrane destabilization and potential temperature increases and/or electrochemical reactions. These methodological differences could explain the reduced effect of lidocaine observed in our study, highlighting the importance of consistent experimental conditions when evaluating pharmacological agents in electroporation.

In contrast to low conductivity media, adding lidocaine to Tyrode solution did not appreciably alter pH or conductivity because both the lidocaine stock and Tyrode solutions had similar conductivity, and Tyrode's high HEPES concentration (10 mM) effectively buffered the slightly acidic lidocaine solution. Nevertheless, adding saline to control samples remained important to account for the dilution of other components within the electroporation solution upon lidocaine addition. This ensured that observed effects were attributed to lidocaine rather than changes in ionic composition. Specifically, Ca^{2+} concentration has a known impact on survival of electroporated cells[36], with lower Ca^{2+} concentrations typically improving survival. Thus, maintaining equal

dilution of Tyrode solution (containing 2 mM Ca^{2+}) in both lidocaine-treated and control samples was important, as reduced Ca^{2+} concentration in lidocaine-treated samples alone could mask lidocaine's lethal effects.

Possible mechanisms of lidocaine's effect on permeabilization and survival

Lidocaine may influence membrane permeabilization and cell survival following electroporation through multiple mechanisms, although it remains uncertain which are predominantly responsible for the observed effects. One proposed mechanism involves the modulation of membrane surface charge, as lidocaine is a cationic molecule that can reduce the negative surface potential, thereby enhancing membrane permeabilization. Grys et al.[12] proposed this mechanism after observing similar effects with other cationic dyes. If surface charge was the primary mechanism, lidocaine should be considerably more effective in low conductivity solution, where fewer ions are available to screen membrane surface charge, compared to high-conductivity Tyrode solution with abundant screening ions. Our results provide mixed support for this hypothesis: we observed somewhat greater permeabilization enhancement (i.e., greater shifts in E_{mid}) in low conductivity solution for CHO-K1 and NS-HEK cells, but similar effects in both solutions for B16-F1 and C2C12 cells. This suggests that while surface charge modulation may contribute to lidocaine's effects, it is not the sole mechanism and additional cell-type-specific factors must be involved.

Experimental studies in model lipid membranes and molecular dynamics simulations further demonstrated that lidocaine interacts directly with phospholipids[16], increasing membrane fluidity[37,38] and bending elasticity[39] while reducing the lipid phase transition temperature[39]. Lidocaine can also induce membrane protein clustering[37]. The nature of these interactions depends on lidocaine's protonation state: the charged form preferentially localizes to the lipid headgroup region, while the uncharged form can penetrate into the hydrophobic lipid core and traverse the bilayer[16,40,41]. These lidocaine-membrane interactions likely make the cell membrane more susceptible to electroporation and thus contribute to increased membrane permeabilization. Additionally, since different cell types vary in their membrane lipid and protein compositions, these compositional differences could influence how lidocaine alters membrane properties and may partially explain the cell-type-specific variations in lidocaine's effects.

Another possible mechanism involves lidocaine's well-known interaction with voltage-gated sodium (Na_V) channels[34]. Our study included three cell lines that express Na_V channels; NS-HEK are genetically engineered to express $Na_V1.5$, while Na_V expression has also been documented in C2C12 cell line[42] and in melanoma cells[43], from which the B16-F1 cell line derives. Additionally, we used CHO-K1 cells, known for their low expression of voltage-gated ion channels[25], although a subpopulation of these cells may express some Na_V channels[44]. In Tyrode solution, lidocaine indeed had no effect on CHO-K1 permeabilization while significantly increasing permeabilization in all three Na_V-expressing cell lines at least at one electric field strength. However, we observed a significant increase in CHO-K1 membrane permeabilization in low conductivity solution (Fig. 2) and decreased survival in Tyrode solution (Fig. 4). This suggests that lidocaine-Na_V interaction may contribute to the observed effects of lidocaine, but cannot fully explain them.

Cell survival following electroporation depends on multiple biological processes, including membrane repair mechanisms, intracellular signaling, and metabolic responses[45]. Lidocaine has been reported to inhibit membrane-associated ATPases, impairing membrane recovery and restoration of intracellular ionic homeostasis after electroporation[13]. While this mechanism could contribute to the variability in lidocaine's effects on cell survival across different cell lines, it does not align fully with our cell-type-specific findings; B16-F1 cells showed the most pronounced survival effects despite having downregulated ATPase activity[46]. Moreover, in B16-F1 cells, we observed that increasing the pH from 6.9 to 7.3 led to a pronounced reduction in the lethal electric field at 35 mM lidocaine, while membrane permeabilization was much less affected. This suggests that survival mechanisms are more sensitive to pH alterations than membrane integrity, consistent with trends observed in other cell lines[47]. This effect might also reflect the enhanced survival and function of cancer cells in a more acidic microenvironment commonly found in hypoxic tumors (pH: 6.2–6.9)[48].

Finally, electroporation-enhanced cellular uptake of lidocaine likely potentiates its intrinsic cytotoxicity, similarly as observed with chemotherapeutic drugs in electrochemotherapy. In our previous publication we observed that lidocaine is more toxic to B16-F1 melanoma cells than to C2C12, CHO-K1 and NS-HEK[49]. This aligns with existing literature that recognizes lidocaine as a potential anticancer agent. Lidocaine's anticancer properties have been documented across various cancer types, including lung, breast, liver, gastric, colorectal, melanoma, glioma, and tongue cancer[50]. It can act as a chemosensitizer, enhancing the efficacy of chemotherapeutic agents, including cisplatin that is commonly used in electrochemotherapy[51]. The proposed mechanisms underlying its anticancer activity are multifaceted, involving the suppression of cancer cell growth, activation of pro-apoptotic pathways, regulation of epigenetic modifications, increased generation of reactive oxygen species (ROS), modulation of key signaling pathways, inhibition of ABC transporters, and prevention of metastasis and angiogenesis. Moreover, lidocaine has been shown to regulate heat shock proteins (HSPs), matrix metalloproteinase-9 (MMP-9), GOLTI1A, p53, p38, TRPM7, and TRPV1/6, further contributing to apoptosis induction, cell cycle arrest, and ion channel regulation[50]. Notably, according to https://clinicaltrials.gov/, the anticancer potential of lidocaine is being investigated in clinical trials, including early-phase trials for pancreatic cancer (NCT04048278, recruiting) and the efficacy and prognosis of colorectal cancer (NCT04162535, unknown status)[50].

Clinical relevance

The practical implications of lidocaine-mediated changes in electroporation thresholds were evaluated by computing the resulting reversible (RE) and irreversible (IRE) electroporation volumes. When taking results from B16-F1 cells, 10 mM lidocaine expanded both RE and IRE volumes by 22.2% and 43.7%, respectively. At 35 mM (1%) lidocaine, the effect on RE was comparable to 10 mM lidocaine, while the effect on IRE was

much more pronounced: the IRE volume nearly doubled (99.4%) in the non-pH-adjusted condition, while pH adjustment to 7.3 led to an even greater IRE expansion of 184.9% (Fig. 6c). Comparable IRE enhancement was observed by Pan et al.[14], who used intra-arterial administration of 0.5% lidocaine before and during pulse delivery in a porcine liver model. Two protocols were tested, both applying 90 pulses of 90 µs. In Protocol 1, which employed a 2.0 cm electrode spacing, the IRE lesion volume increased by approximately 59% (from 19.9 ± 3.9 cm^3 to 31.6 ± 13.0 cm^3). In Protocol 2, with a wider 2.5 cm spacing, the IRE volume more than doubled (from 22.6 ± 6.4 cm^3 to 46.0 ± 5.4 cm^3). Importantly, administration of lidocaine during the pulse delivery ensured high local tissue concentrations during electroporation—a key difference from standard local anesthetic use where lidocaine is only administered several minutes before electroporation.

When lidocaine is used as a local anesthetic, the clinical relevance of its effects on RE and IRE volumes remains uncertain. Lidocaine tissue concentrations, several minutes after anesthetic injection, typically reach only a few mM[52,53], well below our tested concentrations. Yet, it is important to note that these studies report total tissue concentrations of lidocaine, averaging both intracellular and extracellular compartments. Since the extracellular volume fraction is smaller, actual extracellular concentration may be higher than reported whole-tissue values, possibly approaching or even exceeding the concentrations tested in our experiments. Moreover, in fibrotic or previously irradiated tissues, where drug diffusion is often impaired, higher doses of lidocaine are injected and consequently higher local concentrations are expected[19].

We further recognize that our experiments were conducted without chemotherapeutic agents like bleomycin and cisplatin, which are co-administered in ECT treatments. In the clinical context, even modest lidocaine-mediated increases in membrane permeability could substantially enhance the uptake and cytotoxicity of these agents, thereby improving therapeutic efficacy. Although our data showed that 10 mM lidocaine alone had only modest effects on membrane permeabilization and survival, these effects might still be clinically relevant when combined with chemotherapeutics. Furthermore, lidocaine's anticancer and chemosensitizing properties, discussed in the preceding subsection, could act synergistically with cytotoxic drugs. Overall, the potential sensitizing effect of lidocaine in ECT warrants further investigation.

Beyond electrochemotherapy and irreversible electroporation for tumor treatment, lidocaine is clinically relevant in cardiac therapy as a class 1b antiarrhythmic agent for treating ventricular arrhythmias[17]. The FDA recently approved pulsed field ablation (PFA) for treating atrial fibrillation, and this electroporation-based technology is now being extended to ventricular applications[5]. However, plasma lidocaine concentrations in patients receiving antiarrhythmic therapy remain in the micromolar range[15], far below our tested concentrations, making it unlikely that clinically relevant doses would significantly impact electroporation outcomes. This conclusions is supported by our findings in C2C12 cells, a model for both skeletal and cardiac muscle[54], where 10 mM lidocaine produced only minor effects on membrane permeabilization (Fig. 3) and no significant impact on cell survival (Fig. 4).

Conclusions

Lidocaine is widely used as a local anesthetic in clinical setting in electroporation-based medical treatments, such as electrochemotherapy and gene electrotransfer, and has been proposed as a potential electroporation sensitizer. Our study demonstrated that 10 mM lidocaine has only modest effects on electroporation outcomes, reducing electric field thresholds for reversible and irreversible electroporation by less than 16–18%, which is considerably smaller than reported in previous in vitro studies. We attribute this discrepancy to more carefully controlled experimental conditions in our study, which ensured that the pH, conductivity, osmolality, and dilution of the electroporation solution were comparable in both lidocaine-treated and control groups.

We found that the effect of lidocaine is to some extent cell type-dependent, with the most pronounced impact observed in B16-F1 melanoma cells. Variations in lidocaine's effect on membrane permeabilization across different cell types could be influenced by membrane-level properties such as lipid composition, fluidity, and membrane protein expression profile. Further research is needed to elucidate the underlying mechanisms, for instance through molecular dynamics simulations exploring direct interactions between lidocaine and the lipid bilayer during electroporation.

Testing a higher concentration of 35 mM (1%) lidocaine in B16-F1 cells resulted in profound decrease in cell survival, reducing the threshold for irreversible electroporation by 25-40%. Importantly, lidocaine's impact on cell survival was disproportionately greater than its effect on membrane permeabilization, suggesting that enhanced cellular uptake across electroporated membranes potentiates lidocaine's intrinsic cytotoxicity rather than simply causing excessive membrane damage. This mechanism aligns with lidocaine's recognized anticancer properties in melanoma and other cancer types.

While lidocaine can considerably modulate electroporation outcomes at higher concentrations (e.g. 35 mM), the local concentration that establishes in the tissue after anesthetic injection is typically at least 10× lower, questioning the clinical relevance of this effect. Nevertheless, this effect might be important when considering combination with cytotoxic drugs, where even small enhancements in membrane permeability could considerably potentiate drug cytotoxicity. It would thus be interesting to further study potential synergistic effects between lidocaine and chemotherapeutic drugs, both in vitro and in vivo.

Materials and methods

Cell culture

Experiments were performed using four different cell lines: Chinese hamster ovary cells (CHO-K1, #85051005), mouse C3H muscle myoblast (C2C12, #91031101) and mouse melanoma cells (B16-F1, #92101203), all from the European Collection of Authenticated Cell Cultures. Additionally, we performed experiments on genetically engineered human embryonic kidney cells (tet-on spiking HEK, now available from ATCC, cat. no. crl-3479),

which we received from the group of Adam E. Cohen, Harvard University[26,27]. Tet-on spiking HEK cells have stable expression of $Na_V1.5$ channels and conditional (doxycycline-induced) expression of $K_{ir}2.1$ channels. When grown in the presence of doxycycline, cells are able to generate action potentials and thus become spiking (S-HEK), otherwise they are nonspiking (NS-HEK).

All cell lines were grown in their corresponding growth medium with additional supplements. CHO-K1 cells were grown in Ham-F12 (#N6658). C2C12 and B16-F1 cells were grown in DMEM (#D6546 and #D5671, respectively). The growth media for CHO-K1, C2C12 and B16-F1 were supplemented with 10% fetal bovine serum (#F9665), L-glutamine (#G7513), and antibiotics Penicillin-Streptomycin (#P0781) and Gentamicin (#G1397). NS-HEK cells were grown in DMEM (#D5671) supplemented with 10% fetal bovine serum (#F2442), L-glutamine (#G7513) and antibiotics Penicillin-Streptomycin (#P0781), Puromycin Dihydrochloride (#A1113803), Blasticidin (#A1113903) and Geneticin (#10131035). The last three antibiotics were from Thermo Fischer Scientific, all other listed media were from Sigma-Aldrich.

Cells were routinely passaged every 3 to 4 days, and passages between 5 and 30 (and 3–15 for NS-HEK cells) were used for experiments. Cells were grown in a humidified environment at 37 °C and 5% CO_2. For experiments, cells were first trypsinized and counted. Afterwards, cells were centrifuged for 5 min/200 g and the pellet was then resuspended in the chosen electroporation solution (compositions described in section "Electroporation solutions") to obtain a final cell density of 1×10^6 cells/ml.

Electroporation solutions

Tyrode solution was prepared in our laboratory in final composition of 125 mM NaCl (Sigma-Aldrich, #SI-71382), 2 mM KCl (Merck, #1049360550), 2 mM $CaCl_2$ (Sigma-Aldrich, #SL-C4901), 1 mM $MgCl_2$ (Sigma-Aldrich, #M8266), 10 mM HEPES (Merck, #1101100250), and 30 mM glucose (Merck, #MC-1083351000). Tyrode solution pH was titrated using NaOH (Merck, #1.06498.1000) or 1 M HCl (Sigma-Aldrich, #30721-M) to 7.3, which reflects the typical pH of healthy blood and extracellular fluid (commonly referred as "physiological pH")[28] used in in vitro experiments.

Low conductivity (LC) electroporation solution was prepared following the composition reported in a previous in vitro study[12]. LC solution consisted of 9.5% sucrose, mixed in ratio 19:1 with PBS (Gibco, #14190-094) that had been supplemented with 9 µM $CaCl_2$ and 1 mM $MgCl_2$.

Lidocaine HCl stock solution (20 mg/ml; 2%; 69.3 mM) was prepared by the Pharmacy of the University Medical Centre Ljubljana, Slovenia (Suppl. Fig. S1). This solution is isotonic, formulated with NaCl to adjust osmolality, and NaOH to adjust pH, and is routinely used for injections in clinical practice. The pharmacy-provided final particle concentrations are: lidocaine 0.074 mmol/ml (17.3 mg/ml), Na^+ 0.084 mmol/ml (1.93 mg/ml), and Cl^- 0.156 mmol/ml (5.53 mg/ml). To achieve the desired final concentration of 10 mM (0.3%) or 35 mM (1%), 144.5–500 µl of lidocaine stock solution (or equal volume of physiological saline, 0.9% NaCl, B.Braun) was added to 855.5 µl–500 µl of the chosen electroporation solution, respectively. The pharmacological activity and stability of lidocaine in Tyrode solution was confirmed by monitoring inhibition of action potentials in S-HEK cells (Suppl. Fig. S2).

All solutions' pH, conductivity, and osmolality values were measured using a pH meter (Metler Toledo), conductometer SevenCompact (Metler Toledo), and osmometer (Osmomat 3000, Gonotec), respectively.

Electric pulses

Cells were exposed to 8×100 µs electric pulses of chosen amplitude (50–400 V), delivered by a high-frequency pulse generator L-POR (mPOR, Slovenia), through 2 mm electroporation cuvettes (VWR, #732–1136). The current and voltage were measured by the oscilloscope Wavesurfer 422, 200 MHz, the current probe CP030, and the differential probe ADP305, all from Teledyne LeCroy, USA (recording shown in Suppl. Fig. S3). The electric field to which the cells were exposed was estimated as the ratio between the applied voltage and the interelectrode distance.

Permeabilization assay

The permeabilization assay followed our earlier work[47,55–58]. Cell suspension (150 µl, 1×10^6 cells/ml) in the chosen electroporation solution was mixed with propidium iodide (PI, Molecular probes, #P1304MP) in a final concentration of 100 µg/ml. 3 min after pulse application, 350 µl of electroporation solution was added to the cell suspension and the sample was transferred from the electroporation cuvette to a 1.5 ml tube. The sample was analyzed within 4 min after pulse exposure by flow cytometer (Attune NxT, Carlsbad, CA, USA) using blue laser excitation at 488 nm and detecting the emitted fluorescence through a 574/26 nm band-pass filter. 10,000 events were obtained, and data were analyzed using the Attune Nxt software. Fluorescence intensity histograms were used to determine the percentage of PI-stained cells. Gating was set according to sham control (0 V; with saline), presented in grey color in Fig. 7a–c. Measurements for each data point were repeated three times on three different days.

Viability assay

Cell suspension (150 µl, 1×10^6 cells/ml) in the chosen electroporation solution was pulsed in a cuvette. After a 10-minute waiting period, 850 µL of growth medium supplemented with 10 mM HEPES solution (Sigma-Aldrich, #SI-H0887) was added. For experiments with 10 mM lidocaine, 900 µL of suspension with 1.5×10^5 cells/mL was transferred from the cuvette to a tube, and an additional centrifugation step was applied to avoid the inherent cytotoxicity of lidocaine (for B16-F1 performed twice), observed in our previous publication[49]. Both lidocaine-treated and control samples underwent the same centrifugation procedure to ensure consistent handling across all experimental conditions. Afterwards, cells were resuspended in 850 µL of growth medium supplemented with 10 mM HEPES, and 100 µL of cells was plated in a 24-well plate (TPP Techno Plastic Products AG, Switzerland)

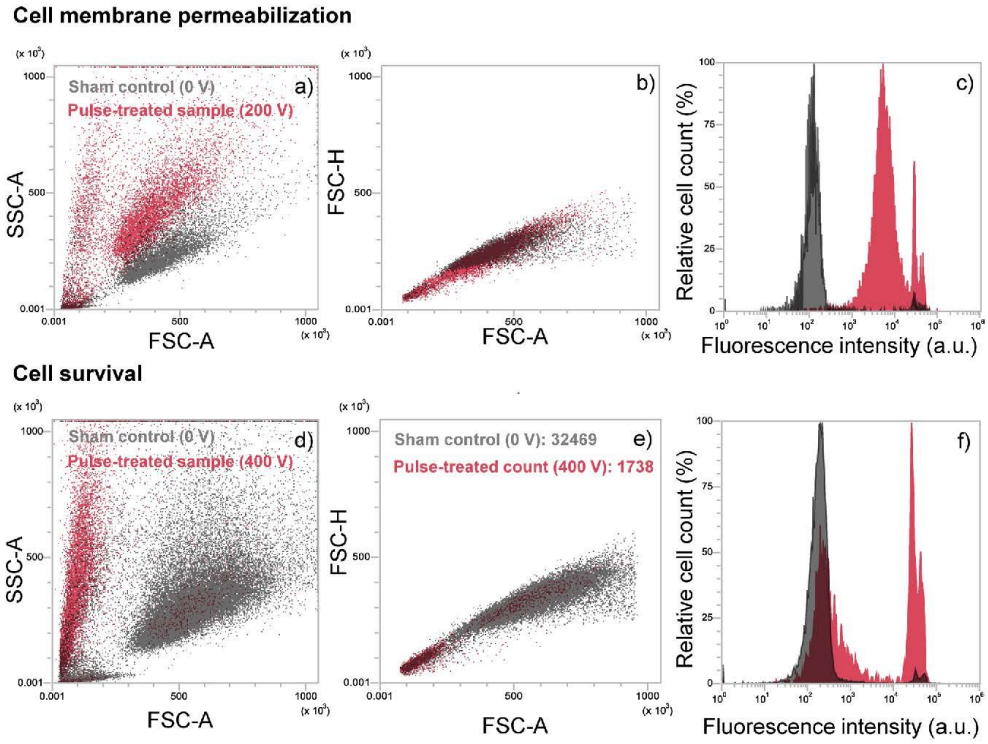

Fig. 7. Assessment of membrane permeabilization and cell survival on a flow cytometer in the absence of lidocaine. a, d) SSC/FSC plot of untreated (sham control, 0 V) and pulse-treated cells (200–400 V). b, e) FSC area vs. height plot of cell count of untreated (sham control, 0 V) and treated cells (200–400 V). c, f) Fluorescence histogram of untreated (sham control, 0 V) and treated cells (200–400 V).

in 1 mL growth medium. Cells were incubated at 37 °C and humidified 5% CO_2 atmosphere. For experiments with 35 mM lidocaine, the procedure was the same, except that cells were suspended in a higher volume (5 mL) in the centrifugation step.

Propidium iodide (PI) was used to assess cell viability 24 h after pulse application. This approach was chosen over the metabolic MTS assay, used in our previous publication[49], due to two potential limitations: (i) lidocaine may affect cellular metabolic activity and mitochondrial function, which could interfere with metabolic assay results[59], and (ii) melanin produced by B16-F1 melanoma cells has an absorbance spectrum overlapping with MTS measurements at 490 nm, potentially overestimating cell survival[60]. Therefore, PI provided a more accurate assessment of cell survival. The protocol was similar to a previous study[60]. After 24 h, cells were harvested (attached and unattached) and centrifuged at 500 g for 5 min. The cell pellet was then resuspended in 130 µL of growth medium together with PI in a final concentration of 100 µg/ml, and cells were incubated at room temperature for 5 min. Samples were then analyzed by flow cytometer similarly as in the permeabilization assay (section "Permeabilization assay"), with one crucial difference. Instead of counting the percentage of PI-stained cells in a fixed number of detected events, we counted the number of PI-stained cells as well as the number of all cells in a fixed sample volume and determined the survival according to equation:

$$Cell\ survival = \frac{N_{total} - N_{PI+}}{N_{total,ctrl}} \quad (1)$$

where N_{total} and N_{PI+} represent, respectively, the number of all cells and the number of PI-stained cells in an experimental group, whereas $N_{total,ctrl}$ represents the total number of cells in sham control (0 V; with saline). This normalization was important because electroporation reduced the number of viable cells (as seen in Fig. 7d, e), so measuring PI-stained cells alone would be unreliable and would lead to considerably overestimated survival rates.

Statistical analysis

All results are presented as mean values ± standard deviation (SD), based on at least three independent experimental repetitions performed on different days. Statistical analyses were performed using SigmaPlot 11.0 (Systat Software Inc., San Jose, CA, USA). Analysis was always carried out for each cell line separately. Data was first tested for normality using the Shapiro-Wilk test and for homogeneity of variance using Levene's test. For datasets meeting these assumptions, One-way ANOVA was conducted, followed by Holm-Sidak's post-hoc test for multiple comparisons (in LC solution, Fig. 2, and in experiments with 35 mM lidocaine, Fig. 5), and Holm-Sidak's post-hoc test for comparison versus control (in Tyrode buffer, comparing 10 mM lidocaine vs. control with physiological saline, Figs. 3 and 4). If normality and/or equal variance tests failed, nonparametric ANOVA on ranks was performed, followed by Dunn's post-hoc test. The p-value of <0.05 was considered statistically significant.

Numerical calculations of reversible and irreversible electroporation volumes

The distribution of the electric field within the tissue was calculated with the COMSOL Multiphysics software (version 6.3, COMSOL AB, Stockholm, Sweden) using the finite element method. A three-dimensional model was built with the dimensions shown in Fig. 6a and b. The electrodes were inserted 30 mm into the tissue. The Electric Currents physics interface was used with a Stationary study. A voltage of 2000 V was applied to the electrodes. First, the reversible (RE) and irreversible (IRE) electroporation volumes for saline control were determined. Experimentally determined electric field values corresponding to 50% permeabilization and 50% survival were used as threshold values for RE and IRE, respectively. The tissue was modelled as an isotropic and homogeneous domain, and we neglected any changes in tissue conductivity due to electroporation. Since the distribution of the electric field under such conditions is determined by Laplace's equation for the electric potential, $\Delta V = 0$, the solution is independent of specific tissue electrical properties. Thus, we used arbitrary values for tissue conductivity and permittivity, and the results can be considered representative of any isotropic homogenous tissue. The electroporated volumes with the addition of lidocaine were then calculated and the relative increase in RE and IRE volumes compared to saline control was determined.

Data availability

The data presented in this study is available on request from the corresponding author.

Received: 18 April 2025; Accepted: 11 July 2025
Published online: 15 July 2025

References

1. Yarmush, M. L., Golberg, A., Serša, G., Kotnik, T. & Miklavčič, D. Electroporation-based technologies for medicine: principles, applications, and challenges. *Annu. Rev. Biomed. Eng.* **16**, 295–320 (2014).
2. Kotnik, T. et al. Electroporation-based applications in biotechnology. *Trends Biotechnol.* **33**, 480–488 (2015).
3. Mahnič-Kalamiza, S., Vorobiev, E. & Miklavčič, D. Electroporation in food processing and biorefinery. *J. Membr. Biol.* **247**, 1279–1304 (2014).
4. Geboers, B. et al. High-Voltage electrical pulses in oncology: irreversible electroporation, electrochemotherapy, gene electrotransfer, electrofusion, and electroimmunotherapy. *Radiology* **295**, 254–272 (2020).
5. Chun, K. R. J. et al. State-of-the-art pulsed field ablation for cardiac arrhythmias: ongoing evolution and future perspective. *EP Eur* **26**, 745 (2024).
6. Lambricht, L. et al. Clinical potential of electroporation for gene therapy and DNA vaccine delivery. *Expert Opin. Drug Deliv.* **13**, 295–310 (2016).
7. Kotnik, T., Rems, L., Tarek, M. & Miklavčič, D. Membrane electroporation and electropermeabilization: mechanisms and models. *Annu. Rev. Biophys.* **48**, 63–91 (2019).
8. Hood, M. T. & Stachow, C. Influence of polyethylene glycol on the size of Schizosaccharomyces Pombe electropores. *Appl. Environ. Microbiol.* **58**, 1201–1206 (1992).
9. Melkonyan, H., Sorg, C. & Klempt, M. Electroporation efficiency in mammalian cells is increased by dimethyl sulfoxide (DMSO). *Nucleic Acids Res.* **24**, 4356–4357 (1996).
10. Pakhomova, O. N., Gregory, B. W. & Pakhomov, A. G. Facilitation of electroporative drug uptake and cell killing by electrosensitization. *J. Cell. Mol. Med.* **17**, 154–159 (2013).
11. Dermol, J., Pakhomova, O. N., Pakhomov, A. G. & Miklavčič, D. Cell electrosensitization exists only in certain electroporation buffers. *PloS One.* **11**, e0159434 (2016).
12. Grys, M., Madeja, Z. & Korohoda, W. Decreasing the thresholds for electroporation by sensitizing cells with local cationic anesthetics and substances that decrease the surface negative electric charge. *Cell Mol. Biol. Lett* **19**, 412 (2014).
13. Sherba, J. J. et al. The effects of electroporation buffer composition on cell viability and electro-transfection efficiency. *Sci. Rep.* **10**, 3053 (2020).
14. Pan, F. et al. Intra-arterial injection of Lidocaine as a cell sensitizer during irreversible electroporation. *J. Vasc Interv Radiol.* **31**, 831–839e2 (2020).
15. Hermanns, H. et al. Molecular mechanisms of action of systemic Lidocaine in acute and chronic pain: a narrative review. *Br. J. Anaesth.* **123**, 335–349 (2019).
16. Bernardi, R. C. et al. Molecular dynamics study of biomembrane/local anesthetics interactions. *Mol. Phys.* **107**, 1437–1443 (2009).
17. Chaudhry, G. M. & Haffajee, C. I. Antiarrhythmic agents and proarrhythmia. *Crit. Care Med.* **28**, N158–164 (2000).
18. Mir, L. M. et al. Standard operating procedures of the electrochemotherapy: instructions for the use of bleomycin or cisplatin administered either systemically or locally and electric pulses delivered by the cliniporatortm by means of invasive or non-invasive electrodes. *EJC Suppl.* **4**, 14–25 (2006).
19. Gehl, J. et al. Updated standard operating procedures for electrochemotherapy of cutaneous tumours and skin metastases. *Acta Oncol.* **57**, 874–882 (2018).
20. Daud, A. I. et al. Phase I trial of Interleukin-12 plasmid electroporation in patients with metastatic melanoma. *J. Clin. Oncol.* **26**, 5896–5903 (2008).
21. Bhatia, S. et al. Intratumoral delivery of plasmid IL12 via electroporation leads to regression of injected and noninjected tumors in Merkel cell carcinoma. *Clin. Cancer Res.* **26**, 598–607 (2020).

22. Gabriel, S., Lau, R. W. & Gabriel, C. The dielectric properties of biological tissues: II. Measurements in the frequency range 10 hz to 20 ghz. *Phys. Med. Biol.* **41**, 2251 (1996).
23. Oellerich, M. & Armstrong, V. W. The MEGX test: a tool for the real-time assessment of hepatic function. *Ther. Drug Monit.* **23**, 81–92 (2001).
24. Markelc, B. et al. Muscle gene electrotransfer is increased by the antioxidant tempol in mice. *Gene Ther.* **19**, 312–320 (2012).
25. Gamper, N., Stockand, J. D. & Shapiro, M. S. The use of Chinese hamster ovary (CHO) cells in the study of ion channels. *J. Pharmacol. Toxicol. Methods.* **51**, 177–185 (2005).
26. Tian, H. et al. Video-based pooled screening yields improved far-red genetically encoded voltage indicators. *Nat. Methods*. https://doi.org/10.1038/s41592-022-01743-5 (2023).
27. McNamara, H. M., Zhang, H., Werley, C. A. & Cohen, A. E. Optically controlled oscillators in an engineered bioelectric tissue. *Phys. Rev. X.* **6**, 031001 (2016).
28. Alberts, B. *Molecular Biology of the Cell* (Garland Science, 2015).
29. Batista Napotnik, T. & Miklavčič, D. In vitro electroporation detection methods – an overview. *Bioelectrochemistry* **120**, 166–182 (2018).
30. Crowley, L. C. et al. Measuring cell death by propidium iodide uptake and flow cytometry. *Cold Spring Harb. Protoc.* (2016).
31. Djuzenova, C. S. et al. Effect of medium conductivity and composition on the uptake of Propidium iodide into electropermeabilized myeloma cells. *Biochim. Biophys. Acta BBA - Biomembr.* **1284**, 143–152 (1996).
32. Müller, K. J., Sukhorukov, V. L. & Zimmermann, U. Reversible electropermeabilization of mammalian cells by high-intensity, ultra-short pulses of submicrosecond duration. *J. Membr. Biol.* **184**, 161–170 (2001).
33. Coudert, A. E. et al. Phase III, randomized, double-blind, placebo-controlled trial of topical 2% Lidocaine for the prevention and treatment of oral mucosal pain in children. *Clin. Oral Investig.* **18**, 1189–1194 (2014).
34. Liu, H., Atkins, J. & Kass, R. S. Common molecular determinants of flecainide and Lidocaine block of heart Na + channels: evidence from experiments with neutral and quaternary flecainide analogues. *J. Gen. Physiol.* **121**, 199–214 (2003).
35. Becker, D. E. & Reed, K. L. Local anesthetics: review of Pharmacological considerations. *Anesth. Prog.* **59**, 90–102 (2012).
36. Frandsen, S. K., Vissing, M. & Gehl, J. A. Comprehensive review of calcium electroporation—a novel cancer treatment modality. *Cancers* **12**, 290 (2020).
37. Park, J. S. et al. The effect of Lidocaine · HCl on the fluidity of native and model membrane lipid bilayers. *Korean J. Physiol. Pharmacol.* **16**, 413 (2012).
38. Zapata-Morin, P. A., Sierra-Valdez, F. J. & Ruiz-Suárez, J. C. The interaction of local anesthetics with lipid membranes. *J. Mol. Graph Model.* **53**, 200–205 (2014).
39. Yi, Z., Nagao, M. & Bossev, D. P. Effect of charged Lidocaine on static and dynamic properties of model bio-membranes. *Biophys. Chem.* **160**, 20–27 (2012).
40. Högberg, C. J., Maliniak, A. & Lyubartsev, A. P. Dynamical and structural properties of charged and uncharged Lidocaine in a lipid bilayer. *Biophys. Chem.* **125**, 416–424 (2007).
41. Saeedi, M., Lyubartsev, A. P. & Jalili, S. Anesthetics mechanism on a DMPC lipid membrane model: insights from molecular dynamics simulations. *Biophys. Chem.* **226**, 1–13 (2017).
42. Ding, K. et al. Expression and electrophysiological characteristics of VGSC during mouse myoblasts differentiation. *Cell. Signal.* **113**, 110970 (2024).
43. Koltai, T. Voltage-gated sodium channel as a target for metastatic risk reduction with re-purposed drugs. *F1000Research* **4**, 297 (2015).
44. Skryma, R., Prevarskaya, N., Vacher, P. & Dufy, B. Voltage-dependent ionic conductances in Chinese hamster ovary cells. *Am. J. Physiol. -Cell Physiol.* **267**, C544–C553 (1994).
45. Batista Napotnik, T., Polajžer, T. & Miklavčič, D. Cell death due to electroporation – a review. *Bioelectrochemistry* **141**, 107871 (2021).
46. Chiu, K. P. et al. Pathway aberrations of murine melanoma cells observed in Paired-End DiTag transcriptomes. *BMC Cancer.* **7**, 109 (2007).
47. Potočnik, T., Miklavčič, D. & Maček Lebar, A. Effect of electroporation and recovery medium pH on cell membrane permeabilization, cell survival and gene transfer efficiency in vitro. *Bioelectrochemistry* **130**, 107342 (2019).
48. Sharma, M. et al. pH gradient reversal: an emerging hallmark of cancers. *Recent. Pat. Anticancer Drug Discov.* **10**, 244–258 (2020).
49. Blažič, A., Polajžer, T., Miklavčič, D. & Rems, L. The influence of Lidocaine on cell membrane permeabilization and cell survival after electroporation. In *Proceedings of the 4th URSI Atlantic RadioScience Conference – AT-RASC 2024, (URSI – International Union of Radio Science, Gran Canaria, Spain* (2024). https://doi.org/10.46620/URSIATRASC24/SFXG1870.
50. Zhou, D. et al. Repositioning Lidocaine as an anticancer drug: the role beyond anesthesia. *Front. Cell. Dev. Biol.* **8**, 565 (2020).
51. Li, K., Yang, J. & Han, X. Lidocaine sensitizes the cytotoxicity of cisplatin in breast cancer cells via up-regulation of RARβ2 and RASSF1A demethylation. *Int. J. Mol. Sci.* **15**, 23519–23536 (2014).
52. Ross, J. A. et al. Assessment of the effective tissue concentrations of injectable Lidocaine and a Lidocaine-Impregnated latex band for castration in calves. *Animals* **14**, 977 (2024).
53. Tanaka, E., Yoshida, K., Kawaai, H. & Yamazaki, S. Lidocaine concentration in oral tissue by the addition of epinephrine. *Anesth. Prog.* **63**, 17–24 (2016).
54. McMahon, D. K. et al. C2C12 cells: biophysical, biochemical, and immunocytochemical properties. *Am. J. Physiol. -Cell Physiol.* **266**, C1795–C1802 (1994).
55. Polajžer, T. & Miklavčič, D. Development of adaptive resistance to electric pulsed field treatment in CHO cell line in vitro. *Sci. Rep.* **10**, 9988 (2020).
56. Polajžer, T., Dermol–Černe, J., Reberšek, M., O'Connor, R. & Miklavčič, D. Cancellation effect is present in high-frequency reversible and irreversible electroporation. *Bioelectrochemistry* **132**, 107442 (2020).
57. Polajzer, T., Jarm, T. & Miklavcic, D. Analysis of damage-associated molecular pattern molecules due to electroporation of cells in vitro. *Radiol. Oncol.* **54**, 317–328 (2020).
58. Potočnik, T. & Miklavčič, D. Gene transfer by electroporation with high frequency bipolar pulses in vitro. *Bioelectrochemistry* **140**, 107803 (2021).
59. Miller, Z. A. et al. Lidocaine induces apoptosis in head and neck squamous cell carcinoma through activation of bitter taste receptor T2R14. *Cell Rep.* **42**, 142 (2023).
60. Peng, W., Polajžer, T., Yao, C. & Miklavčič, D. Dynamics of cell death due to electroporation using different pulse parameters as revealed by different viability assays. *Ann. Biomed. Eng.* **52**, 22–35 (2024).

Acknowledgements

This research was supported by Slovenian Research and Innovation Agency (ARIS, programmes P2-0249 and I0-0022, project J2-2503, and Junior Researchers funding), European Union's Horizon 2020 research and innovation program under the Marie Skłodowska-Curie grant agreement No. 893077 (to LR), University of Ljubljana Start-up Research Programme, and by funding from Medtronic. This reserach was partially supported by the European Union and ARIS through NextGenerationEU and NOO funding within project MN-0023. This research

was also partially supported by the European Union's Horizon Europe research and innovation programme within the ERC Starting Grant project No. 101115323 – REINCARNATION. Views and opinions expressed are however those of the authors only and do not necessarily reflect those of the European Union or the European Research Council. Neither the European Union nor the granting authority can be held responsible for them.

Author contributions

A.B.: conceptualization, methodology, formal analysis, investigation, writing—original draft preparation, review and editing, visualization. R.Š.: methodology, formal analysis, investigation, writing—original draft preparation, review and editing, visualization. T.P.: methodology, writing—review and editing. D.M.: writing—review and editing, funding acquisition. L.R.: conceptualization, methodology, formal analysis, investigation, writing—original draft preparation, review and editing, visualization, supervision, funding acquisition. All authors have read and agreed to the submitted version of the manuscript.

Competing interests

D.M. is the inventor of several patents pending and granted, is receiving royalties and is consulting for different companies and organizations, which are active in electroporation and electroporation-based technologies and therapies. Other authors report no conflict of interest.

Additional information

Supplementary Information The online version contains supplementary material available at https://doi.org/10.1038/s41598-025-11695-3.

Correspondence and requests for materials should be addressed to L.R.

Supplementary material

Reassessing lidocaine as an electroporation sensitizer *in vitro*

Anja Blažič[1], Rok Šmerc[1], Tamara Polajžer[1], Damijan Miklavčič[1], Lea Rems[1]*

[1]University of Ljubljana, Faculty of Electrical Engineering, SI-1000 Ljubljana, Slovenia
*Corresponding author (lea.rems@fe.uni-lj.si)

1. Pharmacological activity of lidocaine

In our experiments we used an isotonic lidocaine hydrochloride injection formulation, which is routinely used in clinical practice (vial shown in Fig. S1). To evaluate the pharmacological activity and stability of lidocaine in Tyrode solution, we monitored its ability to inhibit action potentials in S-HEK cells (spiking version of NS-HEK cells). We followed the experimental protocol from Batista Napotnik et. al.[1] Briefly, S-HEK cells, grown in a monolayer within Lab-Tek imaging chamber, were stained with ElectroFluor630 potentiometric dye (Potentiometric Probes, Farmington, CT, USA). A pair of parallel Pt/Ir wire electrodes, with 5 mm inter-electrode distance, was positioned at the bottom of the imaging chamber and the chamber was placed on a stage of an inverted fluorescence microscope (Leica Thunder Imager Live Cell, Leica Microsystems, Germany). Fluorescence images were captured under 635 nm LED excitation with emission detected around 700 nm (DFT51010 filter set) in time-lapse mode using LAS X software (Leica Microsystems): one image every 36 ms, 80 images, 2.8 s total duration of image acquisition. When a pulse was delivered during the time-lapse, the pulse generator was triggered by a TTL signal from the microscope at the 10th image (around 324 ms after the start of the time-lapse). Example of bright-field and fluorescence image of cells is shown in Fig. S2a.

Fig. S1: Lidocaine HCl stock solution (20 mg/ml; 2%; 69.3 mM) prepared by the Pharmacy of the University Medical Centre Ljubljana, Slovenia.

The experiment proceeded as follows. First, we recorded a time-lapse without triggering the pulse, which was later used in image analysis to correct the captured signals for the dye photobleaching. Second, we recorded a time-lapse in which a single 100 µs, 150 V/cm pulse was delivered, which robustly triggered an action potential. We then added lidocaine in the desired concentration and waited for 10 minutes. Finally, we recorded the third time-lapse with pulse delivery (100 µs, 150 V/cm). Control samples were subject to the same experimental steps, just that no lidocaine was added. The captured fluorescence images were processed using a custom Matlab code to extract the relative change in fluorescence from the membranes of all cells in the field of view.[1]

Our results confirmed that 30 µM lidocaine partially inhibited $Na_V1.5$ ion channels and reduced action potential amplitude, as expected based on results from a previous study.[2] In control samples, the peak relative fluorescence change during an action potential was 0.067 ± 0.004, and this decreased to 0.043 ± 0.007 at 30 µM lidocaine (N = 3). At a higher concentration of 10 mM, lidocaine completely abolished action potential generation (Fig. S2b).

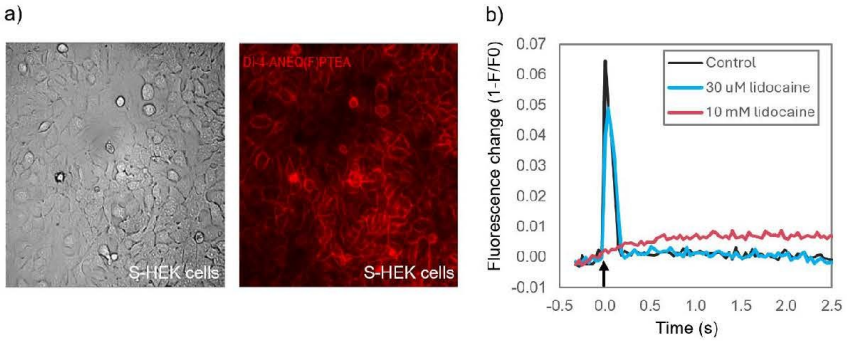

Fig. S2: Confirmation of lidocaine's pharmacological activity in Tyrode solution. a) Brightfield (left) and fluorescence image (right) of S-HEK cells stained with ElectroFluor630 potentiometric dye. b) Graph showing the time course of the relative change in the dye fluorescence indicating generation of an action potential (or absence thereof) in response to pulse application (indicated with arrow). Representative example shows how 30 µM decreased the action potential amplitude, whereas 10 mM lidocaine completely inhibited action potential generation.

2. Pulse waveform

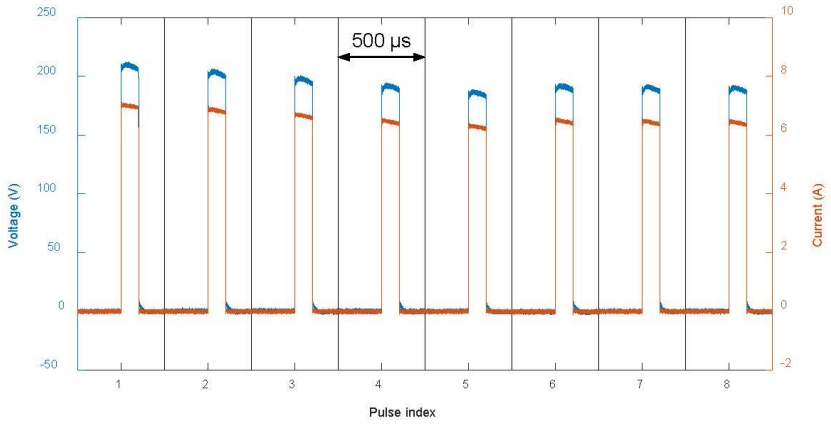

Fig. S3: Measured voltage (blue) and current (red) waveforms for eight consecutive 100 µs pulses delivered at 1 Hz, with the preset applied voltage of 200 V.

References

1. Batista Napotnik, T. *et al.* Genetically engineered HEK cells as a valuable tool for studying electroporation in excitable cells. *Sci Rep* **14**, 720 (2024).
2. Elajnaf, T., Baptista-Hon, D. T. & Hales, T. G. Potent Inactivation-Dependent Inhibition of Adult and Neonatal NaV1.5 Channels by Lidocaine and Levobupivacaine: *Anesthesia & Analgesia* **127**, 650–660 (2018).

3 RESULTS AND DISCUSSION

3.1 DOCTORAL RESEARCH FINDINGS: SUMMARY OF PUBLISHED PAPERS

This section provides an overview of the key findings from the research papers that form the foundation of this doctoral dissertation. Across three independent yet conceptually related studies, electroporation was investigated at different biological levels. The first study focused on elucidating the mechanisms underlying long-term changes in TMV following electroporation, revealing the role of ion channel activity in shaping post-pulse TMV. The second study investigated changes in cell invasion following reversible electroporation in a patient-derived glioblastoma models. The observed increase in invasion was supported by transcriptomic analysis, which revealed gene expression changes related to ion channel activity (among others). This suggests a potential role of ion channels in the observed phenotype, which, however, remains to be confirmed at a functional level. The third study explored whether ion channel modulators could influence electroporation outcomes. We specifically focused on lidocaine, a voltage-gated sodium channel inhibitor, commonly used as an anaesthetic in electroporation-based medical treatments. Each study addressed a distinct biological question using targeted experimental approaches, while collectively contributing to the understanding of electroporation-induced cellular responses.

3.1.1 Ion channel activity as a regulator of long-term changes in TMV after electroporation

The first study, *"Long-term changes in transmembrane voltage after electroporation are governed by the interplay between nonselective leak current and ion channel activation"*, focused on elucidating the biophysical mechanisms responsible for post-pulse changes in TMV. This work was motivated by earlier findings by Burke et al., 2017, who showed that prolonged depolarization in U-87 MG cells exposed to a nanosecond pulse involves complex ion channel activity rather than passive membrane leakage alone. While earlier studies consistently reported that electroporation induces rapid depolarization lasting several seconds to minutes (Batista Napotnik et al., 2024; Burke et al., 2017; Dermol-Černe et al., 2018; Pakhomov et al., 2007a), our study was the first to demonstrate that the initial depolarization phase can be followed by hyperpolarization — a phenomenon observed in U-87 MG but not in the CHO-K1 cell line, and only at 33˚C but not at 25˚C.

We aimed to investigate the sequence of events linking membrane permeabilization, calcium signalling, and TMV dynamics. PI experiments in both cell lines and under both temperature conditions showed that the membrane depolarization phase correlated with the rapid increase in membrane permeability due to pulse exposure and persisted until the membrane almost fully resealed. This confirmed that membrane depolarization was primarily caused by a nonselective leak current across the permeabilized membrane. A transient calcium influx was observed concurrently. Although the calcium transient lasted only about 2 minutes, it served as a critical trigger for the activation of K_{Ca} in U-87 MG cells at 33˚C, which influenced the TMV over the following 20–25 minutes. The K_{Ca} activation resulted in membrane hyperpolarization, as corroborated by theoretical modelling and experiments with ion channel inhibitors.

The theoretical model demonstrated that higher intracellular calcium concentrations lead to stronger hyperpolarization responses and that K_{Ca} channel activity alone could explain the TMV dynamics after membrane resealing. To support these predictions experimentally, U-87 MG cells were pre-treated with three ion channel inhibitors, including Tetraethylammonium (TEA), a broad-spectrum potassium channel blocker; Penitrem A, a selective K_{Ca} channel inhibitor; and Verapamil, a voltage-gated calcium channel blocker. TEA and Penitrem A substantially reduced the amplitude of hyperpolarization, confirming the involvement of K_{Ca} channel activation in shaping the long-term TMV response. However, as hyperpolarization could not be fully abolished by K_{Ca} channel inhibition alone, the contribution of other ion channels — such as chloride channels — cannot be excluded (Catacuzzeno et al., 2011).

Together, the theoretical and experimental data suggest an important role of ion channels in regulating TMV recovery following electroporation in U-87 MG cells. Based on insights from the theoretical model, hyperpolarization was able to develop only after membrane had almost fully resealed, when endogenous ion currents could surpass the electroporation-mediated ionic leak current and effectively shape the TMV. This allowed us to describe a stepwise cascade in U-87 MG cells: initial permeabilization and depolarization, calcium entry, membrane resealing, and finally, channel-mediated hyperpolarization. In contrast, in CHO-K1 cells, which express very few ion channels, the post-pulse membrane depolarization was never followed by hyperpolarization, and it was primarily attributed to nonselective ionic leakage across the permeabilized membrane, rather than to ion channel activity.

Despite successfully detecting dynamic TMV changes over 30 min using the FMP (in the paper, it refers to FLIPR membrane potential; commercially accepted name) dye, the study highlighted considerable methodological limitations in monitoring TMV over such a long period after electroporation. Alternative voltage-sensitive dyes, including ElectroFluor630 and FluoVolt, were found unsuitable due to dye internalization, signal drift, low sensitivity, and phototoxic effects during extended imaging. While the FMP dye performed much better in our experiments, it also presents challenges: its fluorescence relies on a quenching mechanism, which can be disrupted if increased membrane permeability following pulse exposure allows the dye's quencher molecule to enter the cytosol. Although no critical interference was observed under the applied pulsing conditions, the possibility remains that higher pulse amplitudes or different pulse parameters could lead to quencher uptake. Meanwhile, genetically encoded voltage indicators (GEVIs) offer a promising alternative, but their applicability to electroporation studies needs to be tested due to possible perturbation of GEVI's voltage-sensing domains by intense electric fields. These limitations underscore the broader need for improved tools to reliably monitor TMV over extended periods in electroporation studies.

This study highlighted the important role of ion channel activity in shaping TMV recovery and identified K_{Ca} channels as the main factor differentiating the TMV response in U-87 MG glioblastoma (GB) cell line from that of CHO-K1 cell line. Additionally, in the context of GB, the association between membrane hyperpolarization and a less proliferative, more differentiated cell state raised the possibility that changes in TMV could influence tumour cell

behaviour — particularly through the involvement of K_{Ca} channels, which are associated with the regulation of GB invasion (D'Alessandro et al., 2019).

3.1.2 Functional consequences of reversible electroporation: Changes in the invasive behaviour of GB cells

Building on the mechanistic insights from the first study, the second investigation, *"Invasive properties of patient-derived glioblastoma cells after reversible electroporation"* examined whether sublethal electroporation could elicit functional consequences in GB cells that survive the treatment. The first study showed that electroporation-induced TMV changes in U-87 MG GB cells are governed by ion channel activity, particularly K_{Ca} channels (Blažič et al., 2025a). Notably, these channels are linked to the regulation of GB invasion (D'Alessandro et al., 2019). Consequently, the second study aimed to determine whether pulse exposure could influence tumour cell behaviour, with a specific focus on invasion, in a clinically relevant GB model.

This study focused on two patient-derived GB cultures, NIB140 CORE and NIB216 CORE, which were selected after screening five GB cell lines (NIB140 CORE, NIB216 CORE, NIB220 RIM, NIB237 CORE and NIB261 REC) for their intrinsic invasive potential using a transwell invasion assay. The two selected cultures exhibited the highest intrinsic invasion and were chosen to investigate how sublethal electroporation influences tumour cell behaviour. The cells were then exposed to high-frequency biphasic pulses, previously used for irreversible electroporation of brain tumours in canine patients (Latouche et al., 2018; Partridge et al., 2022), and evaluated for membrane permeability, viability and invasive behaviour. Membrane permeability and cell viability were assessed within 4 minutes and after 24 hours of pulse exposure, respectively, using PI staining and flow cytometry. At 1.0 kV/cm, both cell lines showed effective permeabilization, while the majority of cells remained viable. This confirmed that the applied field strength successfully induced reversible electroporation — achieving membrane permeabilization without affecting cell viability. We then assessed changes in invasion 24 hours after exposing cells to 1.0 kV/cm. Both GB cell lines exhibited increased invasion, with NIB140 CORE showing a markedly stronger response — a median 3.74-fold increase in the number of invaded cells compared to sham-treated controls. In contrast, NIB216 CORE showed a more modest but still notable 30 % increase in invasion.

To better understand the molecular basis of this differential response, transcriptomic analysis was performed on both cell lines. In NIB140 CORE, electroporation induced gene expression changes consistent with enhanced invasion, including downregulation of genes involved in extracellular matrix organization and upregulation of genes involved in ion channel activity and passive transmembrane transport (including K_{Ca} channel genes). Notably, these findings align with findings from our previous study using U-87 MG cells, where electroporation-induced calcium (Ca^{2+}) ion influx triggered membrane hyperpolarization via activation of K_{Ca} channels (Blažič et al., 2025a). As mentioned above, these channels are implicated in promoting GB cell invasion (D'Alessandro et al., 2019). In contrast, NIB216 CORE exhibited a transcriptional profile indicative of cytoskeletal disruption and stress-induced alterations in membrane dynamics and intracellular communication, possibly reflecting electroporation-induced changes in membrane plasticity and intracellular communication.

Most preclinical studies on electroporation-based GB therapy have focused on IRE as a non-thermal ablation method, particularly in canine glioma models (Garcia et al., 2011; Latouche et al., 2018; Rossmeisl et al., 2015). Our study underscores a critical challenge for the therapeutic potential of IRE in infiltrative tumours such as GB, if not all exposed cells are ablated. Cells located at the margins of the treatment field may survive but undergo adaptive molecular changes in response to pulse exposure, including enhanced motility and invasive behaviour. Consequently, reversible electroporation may unintentionally promote tumour invasion. It may be possible to mitigate this concern with ECT. ECT combines reversible electroporation with chemotherapeutic agents such as bleomycin or cisplatin, which require membrane permeabilization to access their intracellular targets (Chen J. and Stubbe, 2005; Dasari and Bernard Tchounwou, 2014; Serša et al., 2006). Additionally, electroporation has been shown to transiently disrupt the blood–brain barrier and enhance drug delivery within the central nervous system (Garcia et al., 2012; Lorenzo et al., 2019; Partridge et al., 2022; Sharabi et al., 2019). Collectively, this suggests that combining IRE with targeted cytotoxic or ion channel-modulating agents may represent a safer and more effective strategy than using IRE alone.

Together with the findings from the first study, this work highlights the biological complexity of electroporation responses, demonstrating that pulse exposure can induce transcriptional reprogramming in tumour cells. Importantly, ion channels — initially identified as key regulators of long-term TMV dynamics in U-87 MG cells — were also implicated in the transcriptomic responses of patient-derived GB models following sublethal electroporation. These findings suggest that ion channel modulation could be used to influence electroporation outcome. While it will be interesting to explore the effect of ion channel modulators, particularly inhibitors of K_{Ca} channels on GB cell electroporation, within this dissertation we studied the effects of lidocaine, which has already been proposed as an electroporation sensitizer (Grys et al., 2014; Pan F. et al., 2020; Sherba et al., 2020).

3.1.3 Pharmacological modulation of the electroporation response

The third study, *"Reassessing lidocaine as an electroporation sensitizer in vitro"* investigated whether lidocaine, a clinically approved sodium channel blocker known to affect membrane fluidity, could influence electroporation outcomes. Lidocaine is routinely administered as a local anaesthetic prior to ECT and can also be used before GET, according to current clinical and standard operating procedures (Gehl et al., 2018; Mir et al., 2006). Although previous studies proposed that lidocaine may enhance the efficacy of electroporation-based therapies (Grys et al., 2014; Pan F. et al., 2020; Sherba et al., 2020), their findings were limited by methodological inconsistencies. To address this, our study aimed to rigorously re-evaluate lidocaine's impact on membrane permeabilization and cell survival under well-controlled experimental conditions.

To reflect the diversity of electroporation applications and membrane characteristics, four cell lines were selected. B16-F1 mouse melanoma cells were chosen due to their clinical relevance in ECT of cutaneous tumours (Gehl et al., 2018; Mir et al., 2006), while C2C12 myoblasts served as a representative model for GET (Markelc et al., 2012). CHO-K1 cells, known for their

low endogenous ion channel expression (Gamper et al., 2005), and NS-HEK cells, stably expressing $Na_V1.5$ channels (Batista Napotnik et al., 2024; McNamara et al., 2016; Tian et al., 2023), were used to explore the potential involvement of voltage-gated sodium channels in lidocaine's effects. The experiments were performed both in a low-conductivity electroporation buffer and Tyrode solution, the latter mimicking physiological ionic composition. Lidocaine was tested at two concentrations: 10 mM, reflecting doses used in earlier *in vitro* studies, and 35 mM, corresponding to standard clinical concentrations used for local anaesthesia.

Electroporation was performed using a standard ECT protocol (8 × 100 µs pulses, 1 Hz), and effects on membrane permeabilization and cell viability were assessed. At 10 mM, lidocaine had only modest effects, lowering the electric field threshold for 50 % permeabilization and 50 % survival by no more than 16–18 % in any tested condition. A more pronounced sensitizing effect was observed at 35 mM in B16-F1 cells, where the threshold for IRE decreased by 25-40 %. Interestingly, this cytotoxic effect could not be attributed to enhanced membrane permeabilization, as 35 mM lidocaine had a minimal effect on the threshold for reversible electroporation. Instead, this cytotoxic effect likely involves electroporation-enhanced intracellular accumulation of lidocaine, amplifying its intrinsic toxicity, which was reported in our conference paper (Blažič et al., 2024). Using a simplified computational tissue model, we demonstrated that 35 mM lidocaine could more than double the volume of irreversibly electroporated zone. However, although 35 mM (1 %) lidocaine is clinically injected, the intratumoral concentration achieved several minutes after administration is typically much lower (Ross et al., 2024; Tanaka et al., 2016), raising questions about the translational relevance of these *in vitro* finding. Nevertheless, even modest increases in membrane permeability — particularly in the presence of chemotherapeutic agents such as bleomycin or cisplatin — could enhance drug uptake and improve treatment efficacy in ECT protocols. Thus, further *in vivo* preclinical studies are required to determine the clinical relevance of lidocaine's sensitizing effect.

In the discussion section of our third paper (Blažič et al., 2025b), several mechanisms were proposed to explain how lidocaine modulates membrane permeabilization following electroporation. Possible mechanisms include: (i) reduction of negative membrane surface charge, (ii) interaction with lipid bilayer, (iii) interaction with voltage-gated sodium channels, and (iv) inhibition of membrane-associated ATPases. Of these, the interaction with lipid bilayer appears most plausible; depending on its protonation state, lidocaine can associate with either the bilayer surface or the hydrophobic core, altering properties such as membrane fluidity, elasticity and membrane protein clustering (Bernardi et al., 2009; Park et al., 2012; Yi et al., 2012; Zapata-Morin et al., 2014). Such interactions may increase membrane susceptibility to electroporation, thereby facilitating permeabilization. Moreover, the variations in lipid and protein composition among different cell types could potentially account for the observed cell type–dependent differences in lidocaine's impact on electroporation outcome. Nevertheless, other listed mechanisms could not be completely excluded. The observed effects of lidocaine on cell viability after electroporation are most likely explained by enhanced lidocaine uptake across the permeabilized membrane, amplifying lidocaine's intrinsic cytotoxic effects. This aligns with prior reports of lidocaine's selective toxicity in cancer cells and its broader

anticancer mechanisms — including pro-apoptotic signalling, inhibition of ion transporters, and epigenetic modulation. Together, these findings suggest that lidocaine acts through a multifaceted and cell-type-specific set of pathways (Zhou et al., 2020).

Importantly, our study also highlighted the critical role of experimental parameters — including pH, conductivity, and osmolality — in modulating lidocaine's effects. By carefully controlling these variables, our study enabled a more reliable assessment of lidocaine's true impact on electroporation outcomes compared to preceding *in vitro* studies.

Together, these three studies progress from biophysical mechanisms (regulation of TMV changes 30 minutes following electroporation), through tumour-specific adaptations (GB invasion), to clinically oriented modulation strategies (lidocaine sensitization). Despite their differences in experimental focus, all three studies align in supporting a central insight: electroporation elicits multifaceted cellular responses that extend far beyond the brief window of pulse delivery. These effects — whether through altered ion transport, transcriptomic changes involving ion channels, or modulation of cell behaviour using pharmacological agents —highlight the critical role of ion channels in shaping electroporation outcomes. As key components of passive transport and regulators of cellular excitability, ion channels should be regarded not only as responders but also as potential therapeutic targets in future electroporation research.

3.2 CONNECTING THE DOTS: INTEGRATING OUR RESULTS WITH PREVIOUSLY PUBLISHED WORK

Electroporation induces a cascade of physical and biological responses that cannot be fully explained by the formation of pores in the cell membrane. The following subsections integrate our experimental findings with current literature on how electrical pulses reshape cellular physiology. We begin by examining the TMV regulation after electroporation, highlighting how recovery extends beyond passive leak closure to involve active ion channel participation. We then explore calcium signalling as both a driver and consequence of TMV modulation, linking early ionic disturbances to downstream functional responses in both non-excitable and excitable cells. Finally, we address pharmacological modulation of TMV, demonstrating how ion channel–targeting agents can alter the electroporation outcome and offer potential therapeutic applications.

3.2.1 Regulation of transmembrane voltage after electroporation: A complex interplay between leak current and ion channel activation

Traditional electroporation theory describes membrane permeabilization as the formation of aqueous pores in the lipid bilayer once the induced TMV exceeds a critical threshold — typically between 0.2 and 1 V (Weaver and Chizmadzhev, 1996). Under these conditions, ions and other molecules that are normally impermeable to the lipid bilayer can cross the cell membrane (Kotnik et al., 2019; Tarek, 2005; Tieleman, 2004; Tsong, 1991). Newer findings demonstrate that the increase in membrane permeability caused by electric field exposure is mediated also by lipid peroxidation and formation of pores in oxidatively damaged lesions, as

well as by damage to certain membrane proteins and formation of pores that are stabilized by both lipid and amino acid residues (Rems et al., 2020; Wiczew et al., 2021). After the electric field is removed, these pores generally reseal; pores in the lipid bilayer can close spontaneously within nanoseconds to milliseconds, while oxidatively damaged lesions and damaged membrane proteins can be repaired by cell membrane repair mechanisms. Overall, the membrane resealing typically completes within seconds to minutes after pulse exposure (Dermol-Černe et al., 2018; Pakhomov et al., 2007a). However, the TMV can remain altered even after membrane integrity is restored, as shown in our first study.

Pores formed in the membrane allow rather nonselective transport of ions, which disrupts transmembrane ionic gradients. While the membrane is highly permeable, this nonselective leak current considerably exceeds ionic currents through ion channels and pumps (Batista Napotnik et al., 2024; Ibey et al., 2010). Thus, the membrane unavoidably becomes depolarized, with TMV approaching 0 mV. As the membrane reseals, the ion channels and pumps, which regulate the resting voltage (predominantly the Na^+/K^+-ATPase and potassium channels), can effectively restore the TMV to its resting value. Ion channels and pumps therefore play an essential role in TMV restoration following electroporation. If additional ion channels, which can hyperpolarize the membrane (i.e., make the TMV more negative than its resting value) become activated, hyperpolarization following the initial depolarization becomes possible. We observed this situation in U-87 MG cells, which express various types of ion channels including K_{Ca}. Using calcium and PI imaging, pharmacological inhibition, and theoretical modelling, we demonstrated that this effect arises from a cascade in which transient calcium entry during the pulse delivery activates K_{Ca} channels, which in turn drive prolonged hyperpolarization. This hyperpolarization became evident only after membrane resealing, when the influence of the nonselective leak current diminished and endogenous ion channel activity could govern TMV regulation. Unlike in U-87 MG cells, we observed only transient depolarization in CHO-K1 cells. The latter are not expected to express K_{Ca} channels (at least not abundantly). Our theoretical model confirmed that for cells devoid of K_{Ca} channels, post-pulse TMV restores to its pre-pulse value shortly after the membrane resealing, without following hyperpolarization phase.

3.2.2 Calcium signalling as a driver of TMV modulation and cellular responses following electroporation

Calcium is one of the most versatile and fundamentally important signalling molecules in biology. As a second messenger, it regulates processes ranging from muscle contraction, neurotransmitter release, and cell division to migration, gene expression, and programmed cell death. Its impact results from the pronounced electrochemical gradient across the plasma membrane and from the fact that even small, transient changes in intracellular calcium concentration can engage highly specific and spatially localised signalling cascades (Alberts, 2015; Berridge et al., 2000; Berridge et al., 2003; Brini et al., 2013). In oncology, calcium signalling plays a dual role — supporting physiological processes such as differentiation or apoptosis, but also contributing to malignant behaviours including proliferation, migration, and invasion (Bong and Monteith, 2018; Leclerc et al., 2016; Monteith et al., 2017; Romito et al.,

2022). Consequently, calcium homeostasis has become an important therapeutic target in cancer treatment, with strategies aiming to either disrupt pathological calcium signalling in tumour cells or target calcium-dependent mechanisms to trigger cell death, including calcium electroporation, where high-voltage pulses drive cytotoxic calcium influx leading to ATP depletion and subsequent loss of cell viability (Frandsen et al., 2020). These broad physiological and therapeutic roles make calcium a critical factor when evaluating how electroporation-induced electrical changes translate into biological outcomes.

Within the context of electroporation, calcium influx emerges as a key mediator linking the initial TMV disturbance induced by electrical pulses to a wide range of downstream responses. In non-excitable U-87 MG glioblastoma cells, our work demonstrated that a transient calcium entry following electroporation acts as a trigger for the activation of ion channels, driving a sustained hyperpolarization that persists well beyond the period of membrane permeabilization (Blažič et al., 2025a). This hyperpolarization was detectable only after membrane resealing, suggesting that calcium-dependent channel activity becomes a dominant factor in TMV regulation once passive leak conductance is reduced. Pharmacological inhibition confirmed the involvement of calcium-activated potassium channels in this long-term TMV shift, implicating calcium influx as the initiating event in a cascade that may influence cell phenotype and behaviour.

Beyond our own experimental observations, multiple studies have shown that electroporation can elicit calcium influx not only through pores in the cell membrane but also via direct modulation of endogenous calcium-permeable channels. Voltage-gated calcium (Ca_V) channels are among the best characterized examples: Vernier et al., 2008 demonstrated that a single nanosecond pulse can trigger rapid calcium entry in chromaffin cells, predominantly via L-type channels, with additional contributions from N-type and P/Q-type isoforms, as confirmed by pharmacological blockade. This phenomenon has since been reproduced in other cell types, where calcium transients occurred only in Ca_V-expressing cells, while channel-deficient models such as CHO showed no response under equivalent conditions (Hristov et al., 2018; Nesin et al., 2012). While these studies emphasise the importance of Ca_V and calcium-activated conductance in shaping post-pulse responses in non-excitable cells, their impact is even more pronounced in excitable membranes, where pre-existing electrophysiological machinery can amplify, prolong, or even initiate calcium signals in the absence of detectable membrane permeabilization — a phenomenon reported in cardiomyocytes, neurons, and chromaffin cells exposed to nanosecond pulses, where activation of voltage-gated calcium channels occurs at electric field strengths to low to induce measurable uptake of PI or similar dyes (Pakhomov et al., 2017; Semenov et al., 2015b; Vernier et al., 2008).

In studies from our group published by Batista Napotnik et al., 2024, genetically engineered human embryonic kidney cells were used, expressing $Na_V1.5$ sodium channels and doxycycline-inducible $K_{ir}2.1$ potassium channels — a minimal complementary set required for excitability — referred to as S-HEK cells. They observed that TMV changes and calcium signalling can be achieved even before electroporation becomes detectable by PI uptake in monolayers of S-HEK cells. Pulses with a duration of 100 μs and amplitude somewhat above

the electrostimulation threshold induced weak electroporation, detectable through altered shape of S-HEK action potentials. At the electrostimulation threshold (~126 V/cm), a single pulse triggered a single or multiple action potentials with median duration (full width at half maximum) of ~250 ms. Multiple action potentials were most likely caused by propagation of the action potential along the cell monolayer through endogenous gap junctions expressed in HEK cells, as confirmed by gap junction inhibitor carbenoxolone (unpublished data). At higher fields, action potentials became progressively longer in duration and required more time to recover, ultimately resulting in a sustained depolarization (lasting for ≥3 seconds) (Batista Napotnik et al., 2024, 2025). Theoretical modelling demonstrated that both action potential prolongation and sustained depolarization can be explained by an additional leak current due to electroporation (Batista Napotnik et al., 2024). Indeed, sustained depolarization was also observed at virtually the same electric field strengths in S-HEK's non-excitable counterparts (non-spiking HEK, NS-HEK cells) devoid of $K_{ir}2.1$ channels (Batista Napotnik et al., 2024).

Importantly, alongside changes in TMV (including action potentials), calcium responses were monitored in this study (Batista Napotnik et al., 2024): while a small, single Ca^{2+} peak was observed at low fields in both S-HEK and NS-HEK cells, at intermediate fields (176–200 V/cm) S-HEK cells exhibited a more complex, multi-peak Ca^{2+} response that was absent in NS-HEK cells. The initial peak likely reflects weak electroporation and/or activation of endogenous Ca_V or other calcium-permeable channels, whereas the delayed second peak may arise from additional processes, including activation of endogenous calcium-permeable channels or more intricate pathways such as calcium-induced calcium release (CICR), store-operated calcium entry (SOCE), or intercellular calcium waves. This intriguing biphasic behaviour motivated further investigation. Unpublished work (Batista Napotnik et al., manuscript in preparation, to which I contribute as one of the co-authors) extends these findings by showing that both phases of the calcium signal depend entirely on extracellular calcium, as chelation with EGTA abolished them completely. In contrast, depletion of intracellular stores with thapsigargin did not eliminate the delayed second peak, confirming that endoplasmic reticulum release is not its primary source. Rather than mobilization of internal stores, the late component of the response arises from continued calcium influx across the plasma membrane — perhaps through pores in the cell membrane and/or repeated activation of calcium-permeable channels due to repeated action potential triggering — multiple action potentials were observed in a similar range of electric fields strength as the biphasic calcium response. Given that the biphasic calcium dynamics were not observed in non-excitable NS-HEK cells, it reflects a more complex interplay between changes in TMV (action potentials) and calcium signalling.

Taken all together, early calcium entry may arise either from subtle, weak electroporation that remains undetected by conventional assays such as propidium iodide uptake or from the activation of endogenous calcium-permeable channels. As a result, the response is temporally structured, with calcium signalling and TMV recovery tightly coupled, each contributing to the regulation of the other. This interplay can in turn activate secondary proteins such as K_{Ca} channels, and modulate excitability and downstream signalling pathways, potentially influencing cellular behaviour, such as cell invasion.

3.2.3 Pharmacological modulation of ion channels and its therapeutic potential

Ion channels are transmembrane proteins that form pores in cell membranes, allowing certain ions to pass through them in response to specific stimuli, as part of passive transport that occurs along the concentration gradient from higher to lower ion concentrations. Ion channels can be categorized into six main groups based on the stimuli that trigger their opening or closing: voltage-gated, ligand-gated, stretch, light, pH and heat-activated channels (Neuroscience, 2004). Ion channels are critical for many physiological processes, including neuronal signalling, muscle contraction, cardiac pacemaking, hormone secretion, cell volume regulation, and cell death. Dysfunctions of ion channels are known under common name "channelopathies" and include various pathophysiological conditions, such as muscle dysfunction, kidney disease, epilepsy, and heart disease, making ion channels a valuable target for drug development (Alberts, 2015; Dworakowska and Do, 2000; Kaczorowski et al., 2008).

However, pharmacological modulation of ion channels remains challenging due to the problem of selectivity. Most available drugs have effects beyond their primary targets, and for many channel families, the absence of highly specific inhibitors continues to limit mechanistic interpretation (Alexander et al., 2023). Our own results with lidocaine further illustrate this point: although its primary target are the voltage-gated sodium channels, we observed that electroporation thresholds were altered in a concentration-dependent manner without clear evidence that sodium channel blockade alone was responsible. Instead, lidocaine's broader actions, including its ability to alter membrane fluidity, likely contributed to the observed effects (Blažič et al., 2025). Similar concerns have been raised elsewhere. For instance, verapamil, while commonly used to inhibit L-type calcium channels, also inhibits P-glycoprotein at higher concentrations (Ledwitch et al., 2016). Similarly, tetraethylammonium (TEA), often described as a broad-spectrum potassium channel inhibitor, also affects aquaporins (Yool et al., 2002). These examples demonstrate that ion channel modulators can exert multifaceted effects — beyond direct channel blockade — and may indirectly alter membrane properties.

Despite these limitations, ion channels remain clinically attractive targets. Across therapeutic areas — including cardiac, neurological, and oncologic diseases — ion channels account for ~18 % of small-molecule drug targets (Amin et al., 2010; Bagal et al., 2013; Charlton et al., 2020). In the context of GB, channels like big potassium K_{Ca} channels, voltage-gated calcium channels, or chloride channels have shown potential to impair growth, migration, and invasion (Abed et al., 2023), which is especially interesting based on our results that K_{Ca} channels may contribute to the enhanced invasion observed following electroporation. Taken together, these findings underscore that ion channels represent not only critical regulators of cellular physiology but also promising therapeutic targets whose clinical relevance continues to expand. Consequently, it would be valuable to explore how different ion channel modulators can affect electroporation outcome and whether ion channel modulation could be used in synergy with electroporation treatments.

3.3 FUTURE PERSPECTIVE: ELECTROPORATION-BASED THERAPIES IN GLIOBLASTOMA TREATMENT

The experimental work in this dissertation was designed to investigate fundamental mechanisms of electroporation, specifically the regulation of long-term TMV and the resulting functional responses, including changes in invasion using *in vitro* GB cell line models. The findings presented in this dissertation are directly relevant to the development of electroporation-based GB treatments. However, the hallmarks of GB tumours — diffuse infiltrative growth, marked heterogeneity, and the persistence of treatment-resistant subpopulations — pose major barriers to achieve durable tumour control, with median patient survival remaining around 15 months despite extensive standard therapy, including maximal surgical resection, radiotherapy, and chemotherapy with temozolomide (Grochans et al., 2022; Liu et al., 2024; Obrador et al., 2024; Ostrom et al., 2022). These same features have made GB a focus of several preclinical and early clinical investigations in animal models and veterinary patients, leading to an increasing body of evidence on the potential benefits, limitations, and translational challenges of electroporation-based therapies.

3.3.1 Electroporation-based therapies in glioblastoma treatment: Literature review

Thus far, electroporation-based therapies have shown considerable promise in preclinical glioma models, particularly through non-thermal tumour ablation. In *in vivo* studies, IRE has been applied in canine models with spontaneous gliomas, demonstrating tumour ablation with preservation of surrounding brain structures and, in some cases, long-term tumour control (Garcia et al., 2011; Rossmeisl et al., 2015). In later studies, high-frequency IRE (H-FIRE) protocols have been introduced to reduce neuromuscular stimulation and improve procedural safety (Latouche et al., 2018), yet durable responses were still not achieved uniformly. This highlights the need for further (pre)clinical optimization as well as fundamental research in representative, complex *in vitro* GB models that more closely reflect tumour heterogeneity and microenvironmental complexity.

In parallel, *in vivo* studies in rodent models have demonstrated complete tumour remission in 69 % of cases, performed with bleomycin-based ECT (Agerholm-Larsen et al., 2011), which provided the basis for a phase-1 clinical trial (NCT01322100) investigating ECT as a palliative treatment for brain metastases (Linnert et al., 2012). However, the trial was discontinued due to insufficient patient enrolment. Additionally, electroporation has been shown to transiently disrupt the blood-brain barrier (BBB), at much lower electric field strengths than required for tissue ablation (Garcia et al., 2012; Hjouj et al., 2012; Lorenzo et al., 2019; Sharabi et al., 2019). BBB disruption is associated with disruption of tight junction complexes between endothelial cells mediated by cytoskeletal remodelling (Partridge et al., 2022) and spontaneously recovers within ~4 days post-treatment (Lorenzo et al., 2019; Partridge et al., 2022; Sharabi et al., 2014). This controlled, transient disruption opens new therapeutic possibilities for targeted drug delivery to the brain, either alone or in combination with IRE and/or ECT (Campelo et al., 2023).

Meanwhile, *in vitro* studies have often relied on established (i.e., commercially available) GB cell lines maintained in 2D cultures or embedded in hydrogels or multicellular spheroids, focusing on parameters such as permeabilization and viability. While these models have provided valuable insights into electroporation thresholds (Arroyo et al., 2025; Ivey et al., 2015; Murphy et al., 2022), they fail to capture the complexity of patient-derived tumour biology, cellular heterogeneity, and microenvironmental interactions. For example, Wang et al., 2025 reported reduced invasion of U-87 MG cells after electroporation, an effect linked to downregulation of *SIRT1* and *SIRT2* and impaired mitochondrial function. In contrast, in our study using patient-derived GB cell lines, we observed increased invasion and no significant changes in any *SIRT1–7* genes. These discrepancies likely reflect differences in pulse parameters, experimental conditions, and, perhaps most importantly, the use of immortalized U-87 MG cells versus patient-derived lines. Given the marked transcriptomic differences among GB cell types observed in our study, immortalized cell lines such as U-87 MG have limited ability to reproduce clinically relevant treatment responses, underscoring the importance of patient-derived models for translational electroporation research (Allen et al., 2016).

3.3.2 Electroporation-based therapies in GB treatment: Experimental plan using patient-derived 3D *in vitro* models

The proposed future work builds on the findings of this dissertation by focusing on more complex and representative GB models, such as multicellular spheroids derived from patient GB cell cultures and patient-derived GB organoids. This step is critical for evaluating whether the mechanisms observed in simplified systems translate to biologically and clinically relevant conditions. These advanced models better capture the cellular heterogeneity, structural organization, and microenvironmental context of GB (Seidel et al., 2015), providing a more appropriate platform for evaluating treatment responses and refining electroporation-based therapeutic strategies. A schematic representation of the proposed experimental work is presented in Figure 5.

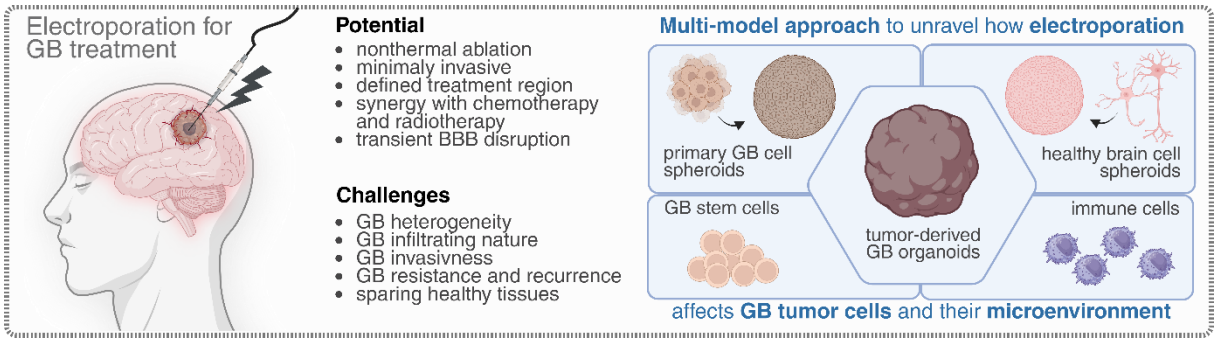

Figure 5: Conceptual framework for studying electroporation in GB treatment. Electroporation offers therapeutic potential for GB through nonthermal ablation, precise targeting of defined treatment regions, potential synergy with chemotherapy and radiotherapy, and transient BBB disruption. However, challenges remain, including tumour heterogeneity, infiltrative growth, invasion, therapeutic resistance and recurrence, and the need to preserve healthy tissues. A multi-model approach incorporating primary GB cell spheroids, GB stem cells, tumour-derived GB organoids, healthy brain cell spheroids, and immune cells would enable a comprehensive investigation of how electroporation influences GB tumour cells and their surrounding microenvironment. Created in BioRender.

Future work should focus on evaluating the effects of electroporation on GB growth and invasion in physiologically relevant 3D models, with the aim of overcoming the limitations of 2D and suspension models used in the present dissertation. This is particularly important given that, when electric pulses are applied *in vivo*, the electric field strength varies spatially, creating distinct regions where cells undergo either irreversible ablation and reversible permeabilization (Davalos et al., 2005), as illustrated in Figure 6. In the treatment of GB, this gradient is particularly relevant due to the tumour's diffuse infiltration into surrounding brain tissue, which implies that many cells will be exposed only to reversible electroporation. Our recent findings raise concerns that cells surviving electroporation might exhibit enhanced tumour invasion. However, these effects may be overcome by ECT, which relies on transient membrane permeabilization to improve intracellular accumulation of poorly permeant cytotoxic agents such as bleomycin or cisplatin (Chen J. and Stubbe, 2005; Dasari and Tchounwou, 2014; Serša et al., 2006), but their efficacy and safety in GB remain to be systematically assessed, since all pre-clinical studies to date have been performed in rodent models inoculated with glioma-derived cells.

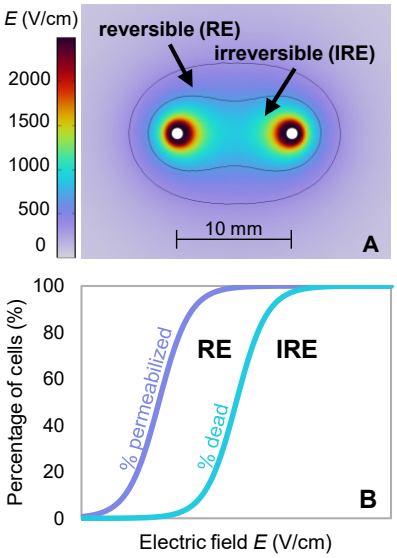

Figure 6: (A) Calculation of the inhomogeneous electric field distribution around a pair of needle electrodes in a tissue, exemplifying how the region of irreversible electroporation is surrounded by a region of reversible electroporation. (B) Schematic representation of how the percentage of permeabilized and dead cells increases with increasing electric field strength. Note that these curves, and the corresponding zones of (ir)reversible electroporation, depend on cell/tissue type and pulse parameters (Cemazar et al., 1998; Miklavčič et al., 2000).

To address these gaps, we propose patient-derived multicellular spheroids as a more realistic *in vitro* platform that preserves tumour heterogeneity, cell–cell interactions, and the structural complexity of GB (Seidel et al., 2015). Spheroids can be prepared and exposed to electric pulses under conditions designed to mimic the heterogeneous electric field distribution observed *in vivo*. Treatment effects can be monitored through 3D viability and invasion assays, and the growth dynamics of spheroids presented in Figure 7. Both reversible and irreversible electroporation settings can be tested, alone and in combination with ECT using bleomycin and/or cisplatin, to identify protocols that effectively suppress spheroid growth and invasion while minimising the survival of potentially more aggressive residual tumour cells. Furthermore, our findings in patient-derived GB models highlight the importance of K_{Ca}

channels in the invasion process, suggesting that their pharmacological targeting using ion channel modulators might represent a promising direction for future investigation (Abed et al., 2023).

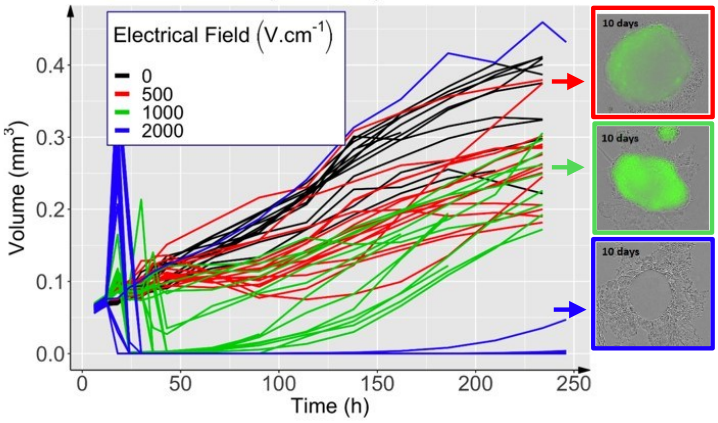

Figure 7: Growth dynamics of spheroids prepared from human colorectal carcinoma cell line (HCT116) following exposure to electric pulses of different amplitudes (Collin et al., 2022).

Finally, we propose to incorporate the diverse tumour microenvironment of GB into these models to capture the interplay between cancer cells, healthy brain cells, and immune components, illustrated in Figure 8. It is important to emphasize that electroporation is the most efficient for immune activation among local ablation strategies (Zhang et al., 2022). Electroporation triggers immunogenic cell death and the release of damage-associated molecular patterns (DAMPs) and tumour antigens (Calvet and Mir, 2016; Justesen et al., 2022; Polajzer et al., 2020; Zhang et al., 2022), which stimulate innate and adaptive immune responses. Additionally, electroporation enhances infiltration of multiple immune cell types, including natural killer (NK) cells (Campelo et al., 2023; Pastori et al., 2024; Zhang et al., 2022), which are of particular interest in GB due to their ability to eliminate tumour cells without prior sensitization and ability to bridge innate and adaptive immunity via secretion of IFN-γ and TNF-α (Breznik et al., 2022). To assess this, we propose co-cultures with naïve or IL-2–activated NK cells to evaluate electroporation-induced immune activation and infiltration of NK cells (Arciga et al., 2025; Ferioli et al., 2024; Justesen et al., 2022; Q. Pan Q. et al., 2020; Yang et al., 2019). Furthermore, we propose to design experiments that will compare NK cells added before or after electroporation, modelling their presence within the tumour or their recruitment post-treatment. These studies will provide insight on whether and to what extent electroporation can act as an immune-stimulating strategy in GB treatment.

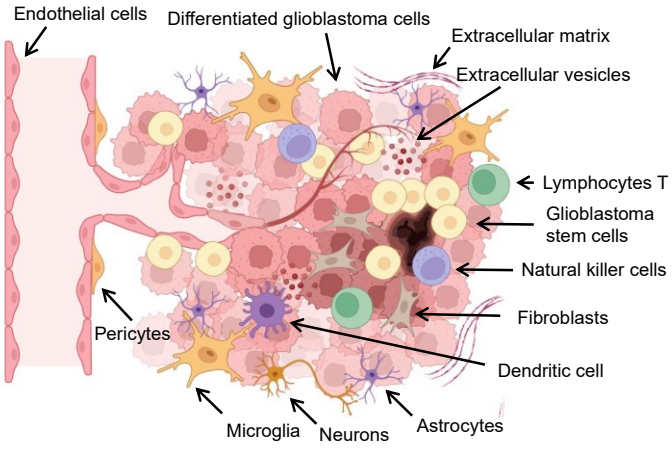

Figure 8: Tumour microenvironment is a complex ecosystem containing different types of cancerous and non-cancerous cells and the extracellular matrix (collagen, laminin, and proteoglycans). Created in BioRender.

Given the pivotal role of glioblastoma stem-like cells (GSCs) in therapy resistance and recurrence, their response to electroporation also warrants detailed investigation, especially since GSCs are typically more invasive than differentiated GB cells (Cheng L. et al., 2011). Interestingly, Ivey et al., 2019 demonstrated that GSCs are as susceptible to H-FIRE ablation as differentiated tumour cells, while both are more susceptible than normal astrocytes — presumably due to differences in nuclear size. However, GSCs were found less sensitive to H-FIRE ablation than neuronal stem cells, highlighting the need for strategies that can target GSCs without damaging healthy neural progenitors. In future work, we propose to systematically assess GSC electrosensitivity, post-treatment self-renewal capacity, and invasion potential using spheroid-based electroporation protocols optimised in earlier experiments. These studies should examine changes in stemness markers (e.g., CD133, SOX2, NOTCH, OLIG2), evaluate clonogenic potential, and assess apoptosis following direct electroporation or exposure to stress signals such as DAMPs released from electroporated GB cells. This approach would clarify whether electroporation-induced tumour cell stress can influence GSC behaviour in ways that promote or inhibit recurrence.

To achieve the most physiologically relevant *in vitro* conditions, we finally propose to utilize patient-derived GB organoids, which represent the highest level of model complexity currently achievable *in vitro*. These organoids closely mimic the architecture, cellular diversity, and microenvironment of human GB, incorporating tumour cells alongside non-malignant components such as endothelial and immune cells (Majc et al., 2024). This complexity enables the study of electroporation effects within a context that reproduces key features of *in vivo* tumour biology, including cell–cell interactions, gradients of nutrients and oxygen, and spatially heterogeneous treatment exposure. We propose to expose the organoids to electroporation parameters established in preceding spheroid experiments (with or without added pharmacological agents), enabling direct comparisons across models of increasing complexity. Treatment effects could be evaluated through comprehensive assessments of cell membrane permeabilization, viability, apoptosis, and invasion, as well as immunofluorescence analyses to identify cell type–specific responses within the organoid. By capturing the interplay between diverse cellular populations and their collective response to pulsed electric fields, this model could provide critical insights into both tumour-directed effects and the potential impact

on the surrounding brain microenvironment, thereby strengthening the translational relevance of the findings.

4 CONCLUSIONS

This doctoral dissertation investigated the regulation of TMV after electroporation and its functional consequences in cells, with a particular focus on the role of ion channels. Across three independent, yet conceptually connected studies, electroporation was explored at multiple biological levels: from the biophysical mechanisms governing TMV changes up to 30 minutes following electroporation, through the tumour-specific adaptations of patient-derived GB cells exposed to reversible electroporation, to the pharmacological modulation of electroporation outcomes using an ion channel modulator, i.e., lidocaine. Together, these studies provide new mechanistic insights into how ion channels shape post-pulse TMV dynamics, demonstrate that surviving tumour cells can acquire a more invasive phenotype after sublethal pulse exposure, and highlight the potential of clinically approved drugs to fine-tune electroporation efficacy. The conclusions from this work can be summarized as follows:

1. A single 100 µs electroporating pulse can lead not only to depolarization but also to sustained hyperpolarization in U-87 MG glioblastoma cells under controlled temperature (33 °C), while this effect is absent in CHO cells, and in both cell lines at room temperature (25 °C). TMV recovery after electroporation of U-87 MG cells follows a stepwise cascade, as shown experimentally and supported by a theoretical model. The sequence of events includes initial membrane permeabilization and depolarization, calcium entry, membrane resealing, and ion channel–mediated hyperpolarization. The hyperpolarization is primarily driven by calcium influx and subsequent activation of K_{Ca} channels, although additional ion channels (e.g., chloride channels) may also contribute.

2. While the FMP dye allowed detection of sustained hyperpolarization, it also presents challenges: its fluorescence depends on a quenching mechanism that may be disrupted if the quencher enters the cytosol during increased membrane permeability, particularly at higher pulse amplitudes or with different parameters. Alternative dyes such as FluoVolt and ElectroFluor630 exhibited major drawbacks (signal drift, internalization, low sensitivity, phototoxicity). These limitations highlight the need for improved TMV monitoring tools, with genetically encoded voltage indicators offering a promising, yet untested alternative for electroporation studies.

3. Reversible electroporation enhances invasion of surviving GB cells in a cell line–dependent manner. In patient-derived GB cell lines (NIB140 CORE and NIB216 CORE), H-FIRE pulses at 1.0 kV/cm increased invasion while minimally affecting cell viability. The effect was cell line–dependent, with NIB140 CORE showing a strong 3.74-fold increase in invasion, and NIB216 CORE a more modest 30 % increase. Transcriptomic profiling revealed distinct adaptive responses to sublethal electroporation. NIB140 CORE cells upregulated genes linked to ion channel activity and extracellular matrix remodelling, indicating invasion-related changes. NIB216 CORE displayed a transcriptional signature consistent with cytoskeletal disruption and stress-induced signalling. Surviving GB cells at the reversible electroporation margins may develop a more invasive phenotype, potentially accelerating tumour progression. This suggests that combining electroporation with

chemotherapeutics or ion channel modulators may represent a better treatment option than relying on IRE alone in infiltrative tumours.

4. Pharmacological modulation can influence electroporation responses. Lidocaine influenced membrane permeabilization and survival in a concentration- and cell type-dependent manner. At 10 mM, effects were modest; at 35 mM (1 %), lidocaine significantly reduced survival in B16-F1 melanoma cells and lowered IRE thresholds. The cytotoxic effect likely resulted from intracellular accumulation of lidocaine during permeabilization in addition to membrane or channel interactions. Theoretical modelling showed that 35 mM lidocaine could expand the IRE zone nearly two-fold. However, the clinical relevance of these *in vitro* findings remain to be tested *in vivo*, since even concentrations of 10 mM exceed those reported in tissues following local administration of lidocaine.

5. Ion channels appear as important regulators of electroporation outcomes. Their importance was shown in shaping long-term changes in TMV following electroporation, and further supported by transcriptional adaptations after sublethal exposure. Thus, ion channels could potentially serve as targets for pharmacological sensitization to enhance or refine electroporation outcomes. Future work should therefore prioritise testing these mechanisms in complex, patient-derived 3D glioblastoma models, such as multicellular spheroids and organoids, to strengthen the translational relevance of the research.

5 ORIGINAL SCIENTIFIC CONTRIBUTIONS

This doctoral dissertation provides novel insights into the regulation of TMV after electroporation and its functional consequences in cells, with a particular emphasis on the role of ion channels. Across three complementary studies, electroporation was investigated at multiple biological levels—ranging from the biophysical mechanisms that shape TMV dynamics immediately after pulse delivery, to adaptive responses in glioblastoma cells, and the impact of pharmacological ion channel modulation on electroporation outcomes.

Long-term changes in transmembrane voltage after electroporation are governed by an interplay between nonselective leak current and ion channel activation. The first study demonstrated that electroporation does not merely induce transient membrane depolarization but can also trigger prolonged membrane hyperpolarization persisting for several minutes after exposure to an external electric field. These long-term changes were found to depend on ion channel activity, in particular calcium-activated potassium (K_{Ca}) channels, as confirmed by experimental measurements and theoretical modelling. The study further highlighted methodological limitations in monitoring TMV over extended periods, since currently available potentiometric dyes exhibit considerable drawbacks when applied to electroporation research.

Electroporation can enhance the invasive potential of surviving glioblastoma cells. The second study investigated how reversible electroporation influences the behaviour of glioblastoma cells that survive electric field exposure. Clinically relevant, patient-derived glioblastoma cell lines were used, providing direct translational value. The results showed that surviving tumour cells may adopt a more invasive phenotype. Transcriptomic analyses revealed altered expression of ion channels and extracellular matrix components, pointing to an adaptive cellular response. This work was the first to clearly demonstrate the potential risks associated with reversible electroporation in the treatment of infiltrative tumours. However, confirming these findings will require additional experiments using more complex and clinically representative 3D models, such as multicellular spheroids or organoids.

Lidocaine, an ion channel modulator used for local anaesthesia, can influence electroporation outcomes in a concentration-dependent manner. The third study explored the pharmacological modulation of cellular responses to electroporation using lidocaine, a clinically approved sodium channel blocker. The results showed that lidocaine could slightly enhance cell permeabilization and more strongly reduce cell survival after electroporation, but these effects were dependent on the applied concentration. Importantly, the concentration at which a pronounced effect on survival was observed (35 mM) is an order of magnitude higher than the concentrations typically present in tissue within minutes after injection. Therefore, the clinical relevance of these findings should be further verified in preclinical or clinical studies.

6 SUMMARY

6.1 SUMMARY

This dissertation explored how electroporation affects the regulation of TMV and how these changes translate into functional and clinically relevant outcomes. Across three interconnected studies, the work progressed from basic mechanisms of TMV recovery to tumour-specific adaptations and pharmacological strategies aimed at modulating electroporation responses. Together, these investigations highlight an important role of ion channels in shaping electroporation outcomes and their potential as therapeutic targets.

The first study clarified the mechanisms underlying long-term (i.e., lasting up to 30 minutes) TMV changes following electroporation. Traditionally, electroporation has been associated with transient membrane permeabilization and depolarization, which is followed by resealing and restoration of the resting TMV. However, our study revealed that a single 100 µs pulse can induce sustained hyperpolarization following the initial depolarization phase in U-87 MG GB cells under controlled temperature conditions (33 ˚C), which was not detected in CHO cells or at room temperature (25 ˚C). This finding challenged the conventional view and built on earlier observations suggesting that post-pulse TMV dynamics cannot be explained by nonselective ion leakage alone (Burke et al., 2017). Through a combination of propidium iodide uptake and calcium imaging, the study confirmed that electroporation triggers a rapid and transient increase in membrane permeability and calcium influx. Importantly, the calcium signal served as a trigger for activating calcium-dependent ion channels, which in turn produced prolonged hyperpolarization after the membrane resealed. A theoretical model supported these findings, demonstrating that calcium-activated conductance alone could account for the observed TMV changes. Pharmacological experiments further validated this mechanism. Inhibitors of K_{Ca} channels reduced the hyperpolarization amplitude, confirming their involvement in shaping TMV recovery. However, the effect could not be fully abolished, suggesting additional contributions from other channels, such as chloride channels (Blažič et al., 2025a).

Building on these mechanistic insights in U-87 MG, the second study investigated whether reversible electroporation alters GB cell behaviour. Using patient-derived GB models, the work examined how cells exposed to sublethal pulse conditions respond in terms of invasion. Two highly invasive GB cultures were selected from a panel of patient-derived lines. When exposed to H-FIRE pulses at 1.0 kV/cm, both models showed effective permeabilization with negligible loss of cell viability, confirming that the treatment was reversible, i.e. sublethal. Remarkably, both cultures displayed increased invasion 24 hours later. The effect was particularly pronounced in one cell line (NIB140 CORE), where it resulted in a 3.74-fold increase in the number of invading cells compared to controls, while the other cell line (NIB216 CORE) showed a more modest increase. Transcriptomic profiling of NIB140 CORE revealed upregulated genes linked to ion transport and extracellular matrix organization, while NIB216 CORE showed signatures of cytoskeletal stress and altered membrane communication. These findings underscore a clinical concern that needs to be further investigated in more clinically relevant 3D models, such as multicellular spheroids and organoids. Nevertheless, our findings

indicate the rationale for combining electroporation with cytotoxic agents, as in electrochemotherapy, or with ion channel-targeting drugs to mitigate pro-invasive behaviour.

The third study examined whether pharmacological agents could be leveraged to modulate electroporation outcomes. Specifically, it revisited lidocaine, a clinically approved sodium channel blocker commonly administered as a local anaesthetic before ECT or GET (Gehl et al., 2018; Mir et al., 2006). Previous studies had suggested that lidocaine could sensitize cells to electroporation, but their conclusions were limited by methodological inconsistencies (Grys et al., 2014; Pan F. et al., 2020; Sherba et al., 2020). To provide a systematic evaluation, four cell lines were selected to represent different clinical and mechanistic contexts: B16-F1 melanoma cells relevant for electrochemotherapy, C2C12 myoblasts as a model for gene electrotransfer, CHO-K1 cells with low ion channel expression, and NS-HEK cells stably expressing $Na_V1.5$ channels. Cells were exposed to standard pulse protocols in both physiological and low-conductivity buffers, with lidocaine tested at 10 mM and 35 mM concentrations. Lidocaine at 10 mM modestly reduced electric field thresholds for permeabilization and survival (<20 %), while 35 mM induced a stronger sensitizing effect in melanoma cells, where irreversible thresholds decreased by up to 40 %. These effects were cell-type dependent, reflecting the complexity of lidocaine's action. A theoretical model further suggested that lidocaine could expand the predicted irreversible electroporation zone, although such high concentrations (35 mM) likely exceed clinically relevant levels. However, even a modest increase in permeability could significantly affect the chemotherapeutic uptake and therefore influence the electroporation efficacy.

Taken together, these three studies outline a coherent trajectory from mechanism to application. The first investigation demonstrated that ion channels are key regulators of TMV recovery following electroporation in U-87 MG glioblastoma cells. The second showed that reversible electroporation can induce transcriptomic reprogramming and promote invasion in patient-derived GB models, again implicating ion channels in the response. The third demonstrated that pharmacological agents such as lidocaine could modulate electroporation outcomes, offering a potential avenue to enhance efficacy or mitigate risks. Overall, these findings demonstrate that electroporation should be regarded not as a brief physical perturbation, but as a biologically active process that recruits complex cellular pathways extending beyond pulse delivery. Most importantly, ion channels play a central role in this response, shaping TMV, influencing cellular behaviour, and offering potential pharmacological targets.

6.2 POVZETEK

6.2.1 Uvod v celično elektrofiziologijo

6.2.1.1 Uvod v celično elektrofiziologijo

Transmembranska napetost (TMN) se nanaša na razliko električnega potenciala prek celične membrane in je temeljna biofizikalna lastnost vseh živih celic. Z vidika fizike je izraz "transmembranska napetost" natančnejši od alternativnega izraza "membranski potencial", saj je razlika električnega potenciala po definiciji napetost. V besedilu bomo zato uporabljali izraz TMN. Pri opisovanju kratkotrajne spremembe v TMN pri vzdražnih celicah, ki jo poznamo pod izrazom "akcijski potencial", pa se bomo držali le-tega izraza zaradi njegove ustaljene rabe v znanstveni literaturi.

Nastanek TMN je posledica selektivne prepustnosti lipidnega dvosloja ter delovanja ionskih kanalov, črpalk in transporterjev, kar povzroči neenakomerno porazdelitev ionov prek plazemske membrane (Alberts, 2015; Hille, 2001). Posledično je notranjost večine evkariontskih celic v mirovanju električno bolj negativna od zunanjosti. Ker se po dogovoru TMN meri od notranjosti proti zunanjosti celice, je TMN negativna, njene vrednosti pa se glede na celični tip gibljejo med -10 in -95 mV (Hille, 2001; Neuroscience, 2004; Wright, 2004). Električno napetost v mirovanju imenujemo kar mirovna transmembranska napetost.

Za celovito razumevanje TMN ni dovolj zgolj osnovna opredelitev, temveč tudi poznavanje njene vloge, ki je različna v vzdražnih in nevzdražnih celicah. V nevzdražnih celicah TMN sodeluje pri uravnavanju celičnega volumna, transporta veziklov in celičnega cikla, medtem ko je v vzdražnih celicah, kot so nevroni, mišične in nevroendokrine celice, nepogrešljiva tudi pri nastanku akcijskega potenciala in prenosu električnih signalov (Alberts, 2015; Blackiston in sod., 2009; Hille, 2001).

Medsebojno delovanje ionskih gradientov, prepustnosti membrane in signalnih poti omogoča, da TMN deluje kot občutljiv pokazatelj fiziološkega stanja celice ter njenega odziva na spremembe v znotrajceličnem in zunajceličnem okolju. Spremembe TMN, prehodne ali trajne, imajo osrednjo vlogo pri uravnavanju celične komunikacije in prilagoditvenih odzivov, vključno s proliferacijo, z diferenciacijo in napredovanjem skozi celični cikel (Alberts, 2015; Blackiston in sod., 2009; Hille, 2001).

6.2.1.2 Celični mehanizmi nastanka in vzdrževanja TMN

Mirovna TMN se vzpostavi in ohranja s kombinacijo aktivnih in pasivnih mehanizmov. Pri tem ima ključno vlogo natrij-kalijeva črpalka, ki z aktivnim transportom ob uporabi adenozin trifosfata (ATP) prenaša tri natrijeve ione (Na^+) iz celice in dva kalijeva iona (K^+) v celico. Tako nastaja neravnovesje, pri katerem se povečuje zunajcelična koncentracija natrijevih ionov (Na^+) in znotrajcelična koncentracija kalijevih ionov (K^+). Ker črpalka iz celice odstrani več pozitivnih nabojev, kot jih vnese, postane notranjost električno negativno nabita. Ta aktivni transport tako vzpostavlja elektrokemični gradient za natrij (Na^+) in kalijeve (K^+) ione, ki predstavlja osnovo mirovne TMN (Alberts, 2015; Kotnik in sod., 2019).

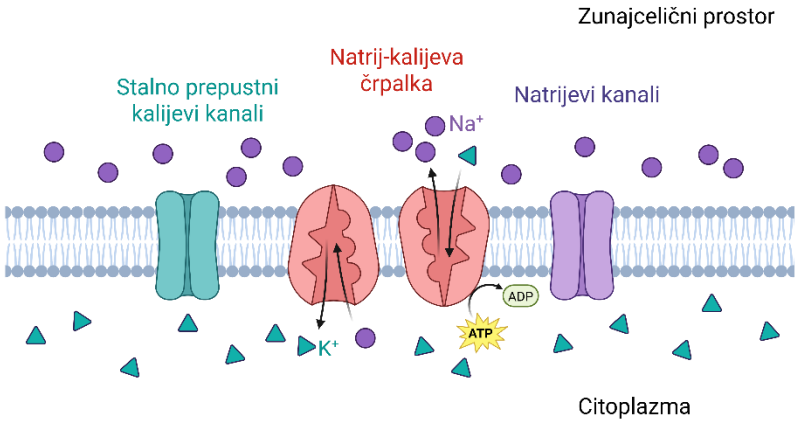

Slika 9: Celični mehanizmi nastanka in vzdrževanja TMN.

Pomemben prispevek k mirovni TMN imajo tudi kalijevi kanali, zlasti tisti, ki omogočajo pasivno uhajanje kalijevih ionov iz celice, t. i. stalno prepustni kalijevi kanali (*angl.* potassium leak channels). Ker je membrana v mirovanju selektivno bolj prepustna za kalijeve (K^+) ione kot za druge ione, se TMN pogosto približa ravnotežni TMN kalija. Uhajanje kalijevih (K^+) ionov iz celice zaradi koncentracijskega gradienta tako dodatno prispeva k vzpostavitvi negativne mirovne TMN (Alberts, 2015; Hille, 2001; Wright, 2004).

Pri regulaciji mirovne TMN sodelujejo tudi navznoter usmerjevalni kalijevi kanali (*angl.* inward-rectifier potassium channels; K_{ir}). Njihovo napetostno odvisno delovanje omogoča omejen iztok kalijevih (K^+) ionov v bližini mirovne TMN, medtem ko se pri bolj depolariziranih napetostih postopoma zapirajo. Na ta način K_{ir} kanali preprečujejo izrazite depolarizacijske premike in prispevajo k vzdrževanju mirovne TMN (Alberts, 2015; Hille, 2001; Wright, 2004).

TMN je kvantitativno opisana z Goldman–Hodgkin–Katzovo enačbo, ki upošteva prepustnost membrane za glavne ione, kalijeve (K^+), natrijeve (Na^+) in kloridne (Cl^-), ter njihove znotrajcelične in zunajcelične koncentracije. Goldman–Hodgkin–Katzova enačba tako predstavlja razširitev Nernstove enačbe, ki opisuje ravnotežno TMN le za posamezni ion, in omogoča celovitejše razumevanje porazdelitve napetosti v celici (Hille, 2001). Ker je membrana v mirovanju najbolj prepustna za kalijeve (K^+) ione, ima prav kalijev gradient največji vpliv na vzdrževanje TMN, medtem ko sta prispevka natrijevih (Na^+) in kloridnih (Cl^-) ionov manj izrazita. Prispevek kalcijevih ionov (Ca^{2+}) k mirovni TMN je običajno zanemarljiv, saj sta njegovi zunajcelični in znotrajcelični koncentraciji znatno nižji od koncentracije kalijevih (K^+), natrijevih (Na^+) in kloridnih (Cl^-) ionov. Vseeno pa kalcij deluje kot eden od ključnih sekundarnih prenašalcev (*angl.* secondary messenger) pri znotrajcelični in medcelični komunikaciji.

Električne lastnosti plazemske membrane določata njena kapacitivnost in upornost. Kapacitivnost izhaja iz dielektričnih lastnosti lipidnega dvosloja in določa, koliko naboja je potrebnega za spremembo TMN. Nasprotno pa je upornost membrane v glavnem odvisna od funkcionalnega stanja ionskih kanalov, ki nadzorujejo hitrost pretoka ionov skozi membrano. Skupaj te električne lastnosti prispevajo k vzdrževanju mirovne TMN in uravnavajo njeno

dinamiko, ki je bistvena za odzivnost celice na zunanje dražljaje, ohranjanje notranje homeostaze ter učinkovito prevajanje signalov in celični transport (Hille, 2001; Wright, 2004).

6.2.1.3 Celični odzivi na spremembe v TMN

TMN ni zgolj pasivna električna lastnost, temveč predstavlja ključni regulator celičnih aktivnosti. Najhitrejše in najbolje pojasnjene spremembe TMN so akcijski potenciali, ki so osnova električnega signaliziranja v vzdražnih celicah. Gre za hitre in prehodne spremembe napetosti na plazemski membrani, ki nastanejo zaradi usklajenega odpiranja in zapiranja napetostno odvisnih ionskih kanalov, predvsem natrijevih, kalijevih in kalcijevih. Akcijski potenciali omogočajo hitro komunikacijo in tako zagotavljajo bistvene fiziološke funkcije, kot so prevajanje živčnih impulzov, krčenje mišic in uravnavanje srčnega ritma. Časovni potek teh dogodkov je tesno povezan z natančno regulacijo TMN, kar poudarja njen osrednji pomen pri delovanju vzdražnih tkiv (Armstrong in Hille, 1998; Hille, 2001).

Poleg hitrih električnih signalov lahko tudi trajnejše ali postopne spremembe TMN pomembno vplivajo na celično delovanje. V celicah v proliferacijski fazi je depolarizacija membrane pogosto povezana z vstopom v celični cikel (Blackiston in sod., 2009; Sachs in sod., 1974; Yang in Brackenbury, 2013), medtem ko je hiperpolarizacija navadno povezana z izstopom iz celičnega cikla ali z diferenciacijo (Sachs in sod., 1974; Sundelacruz in sod., 2009). Spremembe TMN so značilne tudi za apoptozo, kjer iztok kalijevih (K^+) in vdor kalcijevih (Ca^{2+}) ionov delujeta kot zgodnja signala, ki sprožita aktivacijo celične smrti. Ti napetostno-odvisni mehanizmi potrjujejo, da je pomen TMN večplasten: sega od hitrega električnega signaliziranja do dolgoročnega uravnavanja genskega izražanja in presnovnih procesov (Blackiston in sod., 2009; Bortner in Cidlowski, 2007; Franco in sod., 2006).

Širše gledano ionski kanali usklajujejo znotrajcelične in zunajcelične signale ter povezujejo nihanja TMN z različnimi celičnimi odzivi. Uravnavajo ne le električno vzdražnost, temveč tudi procese, povezane s celično smrtjo, medcelično komunikacijo in prilagoditvijo na stres. Zato motnje v izražanju ali delovanju ionskih kanalov vse pogosteje povezujemo s patološkimi stanji, med drugim z rakom, nevrodegenerativnimi boleznimi, epilepsijo in s srčno-žilnimi obolenji (Amin in sod., 2010; Lerche in sod., 2013; Yang in Brackenbury, 2013).

6.2.2 Uvod v elektroporacijo

Elektroporacija, imenovana tudi elektropermeabilizacija, je pojav, pri katerem izpostavitev celic dovolj močnemu zunanjemu električnemu polju povzroči začasno povečanje prepustnosti plazemske membrane. Gre za vsestransko metodo, ki jo je mogoče uporabiti pri praktično vseh vrstah celic, vključno z evkariontskimi celicami, bakterijami in arhejami. Plazemska membrana se obnaša kot tanek dielektrični sloj, kar pomeni, da ločuje naboj na zunanji in notranji strani membrane, zato izpostavitev zunanjemu električnemu polju omogoča nastanek vsiljene TMN. Ko ta doseže dovolj visoke vrednosti, pride do poškodb na ravni plazemske membrane oziroma do nastanka por, ki omogočijo povečan prehod ionov in različnih molekul, med drugim barvil, protiteles, oligonukleotidov, ribonukleinske kisline (*angl.* ribonucleic acid; RNA) in deoksiribonukleinske kisline (*angl.* deoxyribonucleic acid, DNA) (Kotnik in sod., 2019).

V evkariontskih celicah je mirovna TMN običajno med –10 in –95 mV, odvisno od celičnega tipa, kar pomeni, da je notranjost celice električno bolj negativna nabita od njene zunanjosti (Hille, 2001; Neuroscience, 2004; Wright, 2004). Med izpostavitvijo električnemu polju lahko vsiljena TMN preseže več sto milivoltov, kar povzroči strukturne spremembe v membrani (Benz in Zimmermann, 1980). Ali bo elektroporacija reverzibilna ali ireverzibilna, je odvisno od jakosti električnega polja, trajanja, števila in ponavljalne frekvence uporabljenih pulzov ter drugih eksperimentalnih dejavnikov. Pri reverzibilni elektroporaciji se membrana po koncu izpostavitve zaceli, homeostaza se ponovno vzpostavi in celice preživijo, medtem ko pri ireverzibilni elektroporaciji poškodba privede do izgube homeostaze, kar vodi v procese celične smrti, kot je prikazano na Sliki 10 (Kotnik in sod., 2019).

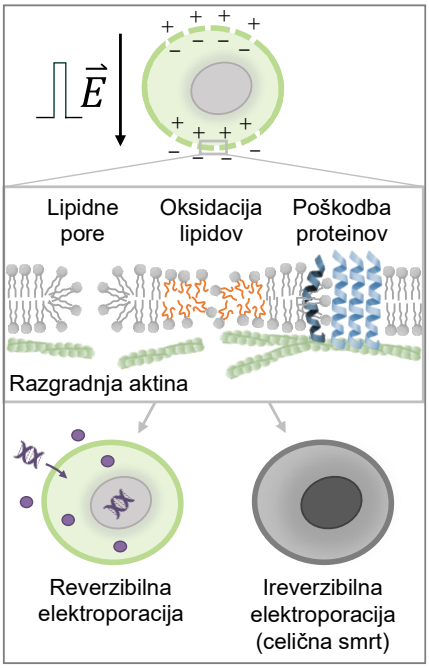

Slika 10: Shematski prikaz učinkov električnega polja na celico, ki lahko vodijo v reverzibilno oziroma ireverzibilno elektroporacijo.

Elektroporacija se uporablja na številnih področjih. V biotehnologiji omogoča elektrotransformacijo, inaktivacijo mikroorganizmov, ekstrakcijo biomolekul ter pospešeno sušenje biomase (Kotnik in sod., 2015). Pomembno vlogo ima tudi v prehrambeni industriji, kjer omogoča izboljšano ekstrakcijo sokov, povečuje izkoristek dragocenih spojin ter optimizira procese, kot so dehidracija, krioprezervacija, biorafinerijski postopki in predelava mesa (Mahnič-Kalamiza in sod., 2014).

Na področju medicine odpira elektroporacija nove terapevtske možnosti, med katerimi so genska elektrotransfekcija oziroma elektroprenos genov, elektrokemoterapija ter netermična ablacija tumorjev ali aritmogenega srčnega tkiva z uporabo ireverzibilne elektroporacije (Chun in sod., 2024b; Geboers in sod., 2020; Lambricht in sod., 2016; Sardesai in Weiner, 2011; Sugrue in sod., 2018; Yarmush in sod., 2014). Natančnost in minimalna invazivnost teh postopkov sta bistveno prispevali k vse širši uporabi elektroporacije v kliničnem okolju.

6.2.3 Raziskovalni cilji naloge

Ob izpostavitvi celice zunanjemu električnemu polju se lipidni dvosloj obnaša kot kondenzator, kar povzroči hitro kopičenje naboja na obeh straneh membrane in posledično povečanje TMN. Vsiljena TMN se vzpostavi s karakterističnim časom polnjena membrane (τ_m), ki znaša od nekaj sto nanosekund do mikrosekund, in je prisotna le med izpostavitvijo zunanjemu električnemu polju (Kotnik in sod., 2010; Pucihar in sod., 2009). Za okroglo celico v homogenem električnem polju vsiljeno TMV (ΔV_m) lahko ocenimo s Schwanovo enačbo:

$$\Delta V_m = \frac{3}{2} E R_{celice} \cos\theta \left(1 - exp(-t/\tau_m)\right) \quad \ldots (3)$$

kjer je:

V_m inducirana transmembranska napetost (V),
E jakost električnega polja (V/m),
R_{celice} polmer celice (m),
θ kot med smerjo električnega polja in točko na celični membrani,
t čas od začetka izpostavitve celic električnemu polju (s),
τ_m časovna konstanta polnjenja membrane (s).

Vsiljena TMN je sorazmerna z jakostjo električnega polja in polmerom celice, največje absolutne vrednosti pa doseže na mestih, kjer je električno polje pravokotno na membrano (θ = 0° in θ = 180°), medtem ko se drugod spreminja sorazmerno s kosinusom kota θ. Če vsiljena TMN preseže kritični prag – običajno med 0,2 in 1 V (Tsong, 1991) – pride v plazemski membrani do nastanka por, ki omogočijo prehod ionov in molekul, ki sicer membrane ne prehajajo. Vrednost vsiljene TMN je odvisna od parametrov, kot so amplituda in trajanje pulza ter velikost in oblika celice. Čeprav vsiljena TMN po koncu pulza hitro upade (s časom praznjenja membrane), lahko povečana prepustnost membrane in njene fiziološke posledice trajajo precej dlje (Kotnik in sod., 2019). Te posledice vključujejo porušenje ionskih gradientov in posledično depolarizacijo membrane. TMN torej ostane spremenjena še nekaj časa po izpostavitvi električnim pulzom.

Dinamiko sprememb TMN po izpostavitvi električnim pulzom so preučevale številne študije. Elektrofiziološke meritve so pokazale, da po izpostavitvi nanosekundnim pulzom nevzdražne celice potrebujejo več kot 15 minut da povrnejo TMN na njeno mirovno vrednost (Pakhomov in sod., 2007). Podobno je bil z uporabo potenciometričnih barvil pokazan pojav podaljšane depolarizacije membrane po izpostavitvi pulzom dolžin 10 ns–10 ms pri različnih tipih celic (Dermol-Černe in sod., 2018). Depolarizacija membrane in spremembe v prožanju akcijskih potencialov so bile opažene tudi pri različnih tipih vzdražnih celic, vključno s kultiviranimi nevroni (Pakhomov in sod., 2017), primarnimi kardiomiociti (Chaigne in sod., 2022; Neunlist in Tung, 1997) in srčnim tkivom (Nikolski in Efimov, 2005). Sprva so podaljšano depolarizacijo pripisovali predvsem neselektivnemu toku, ki nastane zaradi povečane prepustnosti membrane zaradi nastanka por. Kasneje pa je bilo na glioblastomskih celicah U- 87 MG eksperimentalno pokazano, da tudi aktivnost ionskih kanalov igra pomembno vlogo

pri tem procesu. Z zaviralci napetostno odvisnih kalijevih in kalcijevih kanalov ter TRPM8 kanalov so raziskovalci namreč uspeli zmanjšati amplitudo depolarizacije po izpostavitvi celic 10 ns pulzu z jakostjo električnega polja 34 kV/cm pulzu (Burke in sod., 2017).

Ker TMN deluje kot ključen regulator celične aktivnosti, je razumevanje ponovne vzpostavitve njenega ravnovesja po elektroporaciji bistveno za razlago funkcionalnih odzivov celic. Za ta namen je nujno razviti in uporabljati zanesljivo metodologijo, ki omogoča spremljanje dinamike sprememb TMN v minutah po izpostavitvi celic električnemu polju. Metoda vpete krpice membrane (*angl.* patch clamp) ostaja zlati standard za neposredno in zelo natančno merjenje TMN (Liu in Miller, 2020). Vendar je ta metoda invazivna in časovno zahtevna. Njena uporaba v raziskavah elektroporacije je dodatno omejena zaradi tveganja porušitve tesnega stika (*angl.* gigaseal) ob izpostavitvi visokonapetostnim pulzom ter zaradi omejitev parametrov pulzov, ki jih je mogoče dovesti brez poškodb ojačevalnikov (Pakhomov in sod., 2007; Wegner in sod., 2015). Zaradi teh omejitev so se kot neinvazivna alternativa uveljavila fluorescenčna barvila, občutljiva na napetost, ki omogočajo spremljanje TMN v realnem času. Njihova uporaba sega v 70. leta prejšnjega stoletja (Cohen in sod., 1974; Ross in sod., 1977), danes pa jih delimo v dve skupini: (i) počasi odzivna barvila, ki se prenašajo prek membrane z elektroforetskim mehanizmom, pri čemer se njihova fluorescenca spreminja sorazmerno z napetostjo, ter (ii) hitro odzivna barvila, ki se vgradijo v membrano in kažejo napetostno odvisne spremembe fluorescence. Slednja delujejo prek spektroskopskih premikov, orientacije ali dimerizacije, odvisnih od napetosti (Nikolaev in sod., 2023). V primerjavi z metodo vpete krpice membrane ta barvila omogočajo visoko zmogljivo in prostorsko ločeno spremljanje sprememb TMN v populacijah celic in ne le v posameznih celicah. Njihovo uporabo pa omejujejo številne pomanjkljivosti, kot so prerazporeditev barvila zaradi poškodbe membrane, fototoksičnost in fotobledenje, ki jih je treba skrbno upoštevati pri načrtovanju poskusov (Jensen, 2012), še posebej pri elektroporaciji celic.

Če so ionski kanali res ključni pri regulaciji TMN po elektroporaciji, je smiselno preveriti, ali izpostavitev električnemu polju vpliva tudi na spremembe v izražanju genov. Pri komercialno dostopni celični liniji podganjih srčnih mioblastov H9c2 so raziskovalci že pokazali, da elektroporacija vpliva na izražanje podenot natrij-kalijeve črpalke in kalcijeve ATPaze sarkoplazemskega/endoplazemskega retikuluma (*angl.* sarcoplasmic/endoplasmic reticulum calcium ATPase) (Jan in sod., 2024). Prav tako bi bilo zanimivo ovrednotiti vpliv modulatorjev ionskih kanalov na celični odziv po elektroporaciji. To je klinično relevantno zlasti pri bolnikih, ki prejemajo zdravila tarčno usmerjena na ionske kanale (npr. zaviralce natrijevih ali kalcijevih kanalov). Ta lahko spremenijo dinamiko TMN, vnos kalcijevih ($Ca2^{+}$) ionov in prepustnost membrane po pulzu (Lei in sod., 2018; Moller in Covino, 1988; Pan F. in sod., 2020).

Na podlagi opisanega ozadja so bili cilji disertacije oblikovani tako, da celovito naslovijo vpliv elektroporacije na dinamiko TMN in z njo povezane celične odzive. Osredotočili smo se na tri vidike: (i) identifikacijo primernega potenciometričnega barvila za spremljanje sprememb TMN z uporabo fluorescenčne mikroskopije in razjasnitev poteka napetostnih sprememb po izpostavitvi celic električnemu polju, (ii) raziskovanje vpliva modulatorjev ionskih kanalov na spremembe TMN ter njihovo vlogo pri celičnih odzivih, kot sta povečana prepustnost

plazemske membrane in preživetje celic, ter (iii) ugotavljanje, ali elektroporacija povzroča spremembe v izražanju ionskih kanalov in membranskih črpalk, kar bi lahko prispevalo k dolgoročnim spremembam v celičnem vedenju, vključno z invazivnostjo tumorskih celic.

6.2.4 Rezultati in diskusija

6.2.4.1 Aktivnost ionskih kanalov kot regulatorjev dolgoročnih sprememb v TMN po elektroporaciji

V prvi študiji smo se osredotočili na celične mehanizme, ki so odgovorni za spremembe TMN po izpostavitvi celic električnemu polju. Študijo so motivirali rezultati predhodnje raziskave (Burke in sod., 2017), ki so na celicah U-87 MG pokazali, da podaljšana depolarizacija po izpostavitvi nanosekundnemu pulzu ni le posledica neselektivnega prehajanja ionov skozi membrano, temveč vključuje tudi prepleteno aktivacijo ionskih kanalov. Medtem ko so prejšnje študije dosledno poročale, da elektroporacija povzroči depolarizacijo membrane, ki traja nekaj sekund do minut (Burke in sod., 2017; Dermol-Černe in sod., 2018; Pakhomov in sod., 2007a), je naša študija prva pokazala, da lahko začetni depolarizaciji sledi tudi faza hiperpolarizacije, ki traja do 30 minut po izpostavitvi celic električnemu polju (Blažič in sod., 2025a). V naši raziskavi smo pokazali, da lahko en sam 100 µs pulz pri kontrolirani temperaturi (33 °C) v glioblastomskih celicah U-87 MG sproži hiperpolarizacijo, medtem ko tega pojava nismo zaznali v celični liniji pridobljeni iz ovarijev kitajskega hrčka (*ang.* Chinese hamster ovary; CHO) ali pri sobni temperaturi (25 °C). To dodatno dokazuje, da so mehanizmi sprememb TMN po elektroporaciji kompleksnejši od samega neselektivnega toka skozi pore v membrani.

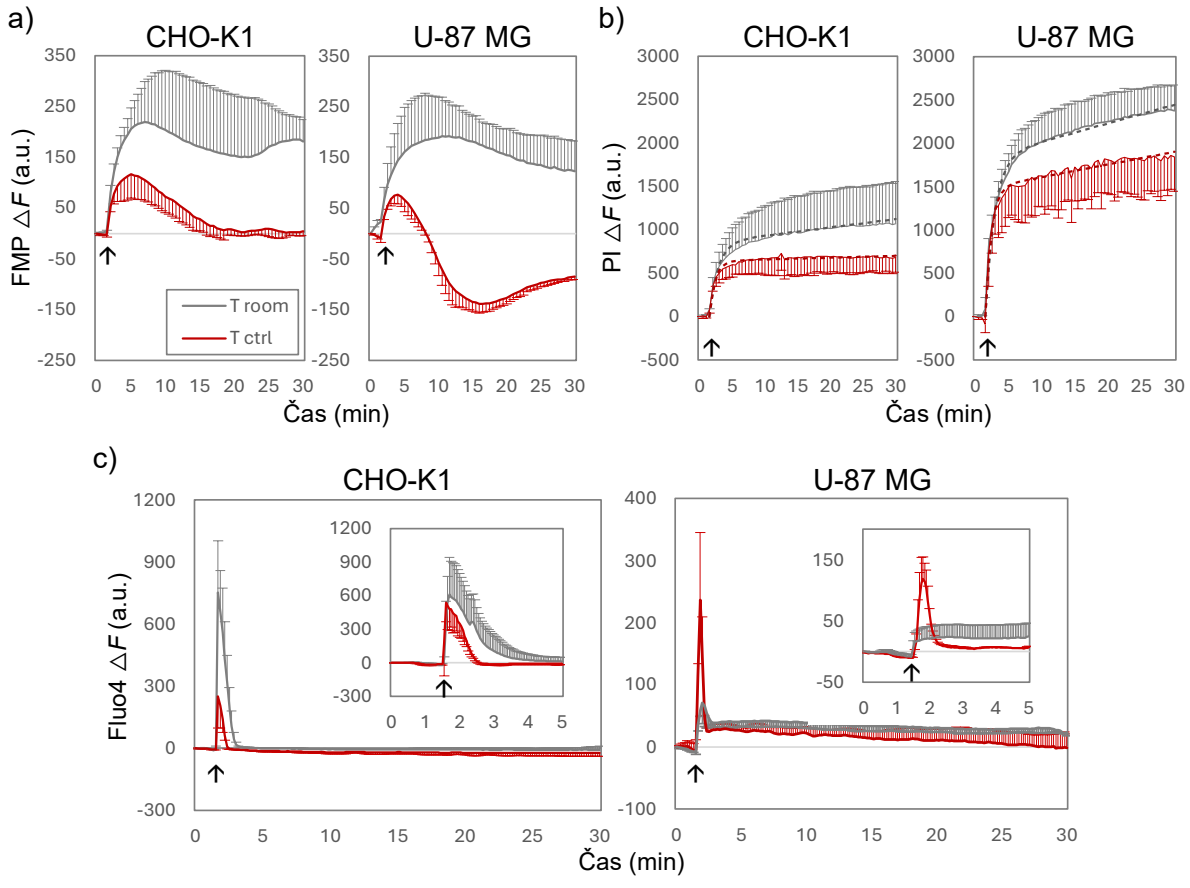

Slika 11: Vpliv temperature na odziv celic po elektroporaciji. Po izpostavitvi enemu pulzu (100 µs, 1,4 kV/cm; čas 1,5 min, označen s puščico) je bil odziv celic spremljan pri sobni (25 °C, sivo) in kontrolirani temperaturi (33 °C, rdeče). Prikazane so povprečne vrednosti iz vsaj 3 poskusov. a) Spremembe v transmembranski napetosti opazovane s fluorescenčnim barvilom FMP (*angl.* FLIPR membrane potential; komercialno uporabljen izraz in izraz uporabljen v članku). b) Povečanje prepustnosti celične membrane opazovano prek vnosa propidijevega jodida (PI) v celice. c) Povečanje znotrajcelična koncentracije kalcija, ki je bilo izmerjeno s pomočjo fluorescenčnega barvila Fluo-4.

Za boljše razumevanje teh sprememb smo uporabili propidijev jodid (*angl.* propidium iodide; PI) kot pokazatelj prepustnosti membrane in barvilo Fluo-4 za spremljanje koncentracije znotrajceličnega kalcija. Rezultati so pokazali hitro povečanje vnosa propidijevega jodida in prehoden dvig koncentracije kalcija takoj po pulzu. Teoretični model je razkril dvofazno dinamiko sprememb v TMN: v zgodnji fazi prevladuje neselektivni tok skozi nastale pore, v kasnejši fazi po celjenju membrane pa postane odločilna aktivacija ionskih kanalov. Prav tako je model pokazal, da je za opaženo hiperpolarizacijo zadostna prisotnost in aktivacija od kalcija odvisnih kalijevih kanalov (*angl.* calcium-activated potassium channels; K_{Ca}). To smo potrdili tudi eksperimentalno z uporabo modulatorjev ionskih kanalov (TEA, penitrem A), ki so izrazito zmanjšali amplitudo hiperpolarizacije. Ker pa hiperpolarizacije ni bilo mogoče popolnoma odpraviti, prispevka drugih kanalov, kot so kloridni ionski kanali, ni mogoče izključiti (Catacuzzeno in sod., 2011).

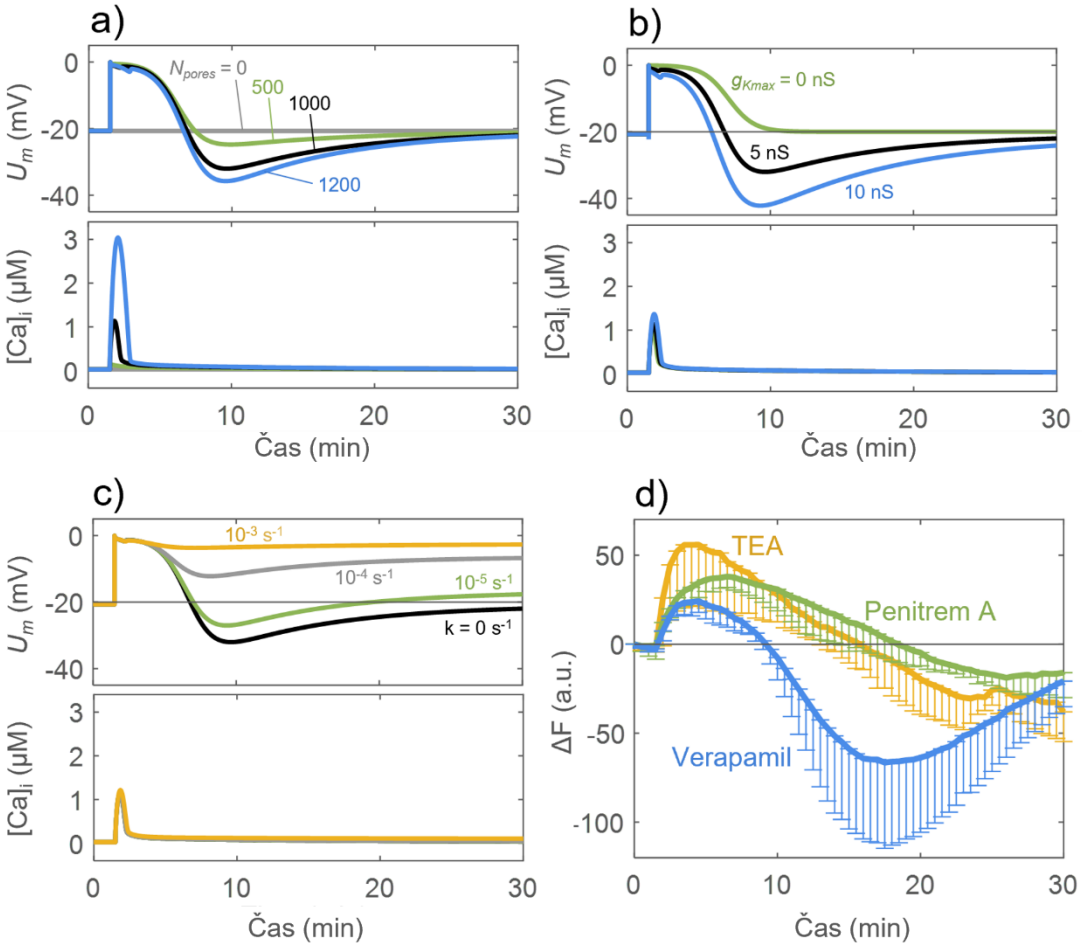

Slika 12: Vpliv od kalcija odvisnih kalijevih kanalov (K_{Ca}) na spremembe TMN po elektroporaciji. a–c) Časovni potek transmembranske napetosti in znotrajcelične koncentracije kalcija, napovedan z modelom pri različnih vrednostih parametrov: a) različno število por, b) različne maksimalne prevodnosti K_{Ca} kanalov, c) različne vrednosti parametra *k*, ki opisuje hitrost celjenja membrane. d) Eksperimentalne meritve sprememb transmembranske napetosti pri celicah U-87 MG po pulzu (100 µs, 1,4 kV/cm) z uporabo fluorescenčnega barvila FMP v prisotnosti zaviralcev ionskih kanalov (TEA, Penitrem A, Verapamil). Podatki so prikazani kot povprečje ± standardni odklon iz treh neodvisnih poskusov.

Študija je hkrati opozorila na metodološke omejitve pri spremljanju dolgotrajnih (30-minutnih) sprememb TMN. Medtem ko je uporabljeno barvilo zanesljivo zaznalo hiperpolarizacijo, sta se FluoVolt in ElectroFluor630 izkazala za manj primerna zaradi bledenja fluorescenčnega signala in nizke občutljivosti, FluoVolt pa tudi zaradi fototoksičnosti. Omejitve FMP barvila ter izzivi pri uporabi genetsko kodiranih napetostnih indikatorjev (*angl.* genetically-encoded voltage indicators; GEVIs) poudarjajo potrebo po razvoju boljših orodij za dolgoročno spremljanje TMN v raziskavah elektroporacije.

Ugotovili smo, da imajo ionski kanali in kalcijeva signalizacija ključno vlogo pri regulaciji dolgotrajnih (do 30 minut) sprememb TMN po elektroporaciji. Povezava med trajno hiperpolarizacijo in manj proliferativnim, bolj diferenciranim stanjem glioblastomskih celic pa nakazuje, da lahko spremembe TMN vplivajo tudi na vedenje tumorskih celic – zlasti prek K_{Ca} kanalov, ki so bili v drugih študijah že povezani z regulacijo invazije glioblastomskih celic (D'Alessandro in sod., 2019).

6.2.4.2 Funkcionalne posledice reverzibilne elektroporacije: Spremembe v invazivnem vedenju glioblastomskih celic

Na podlagi spoznanj iz prve študije smo v drugi raziskavi preučili, ali lahko izpostavitev celic reverzibilni elektroporaciji vpliva na vedenje tumorskih celic, ki preživijo zdravljenje. Prva študija je pokazala, da spremembe TMN v glioblastomskih celicah U-87 MG uravnava aktivnost ionskih kanalov, zlasti K_{Ca} kanalov, katerih aktivnost so predhodne študije že povezale s povečano invazijo glioblastomskih celic po obsevanju (Blažič in sod., 2025a; D'Alessandro in sod., 2019). Posledično nas je zanimalo ali elektroporacija lahko vpliva na invazijo tumorskih celic v klinično relevantnih modelih – primarnih humanih glioblastomskih celicah.

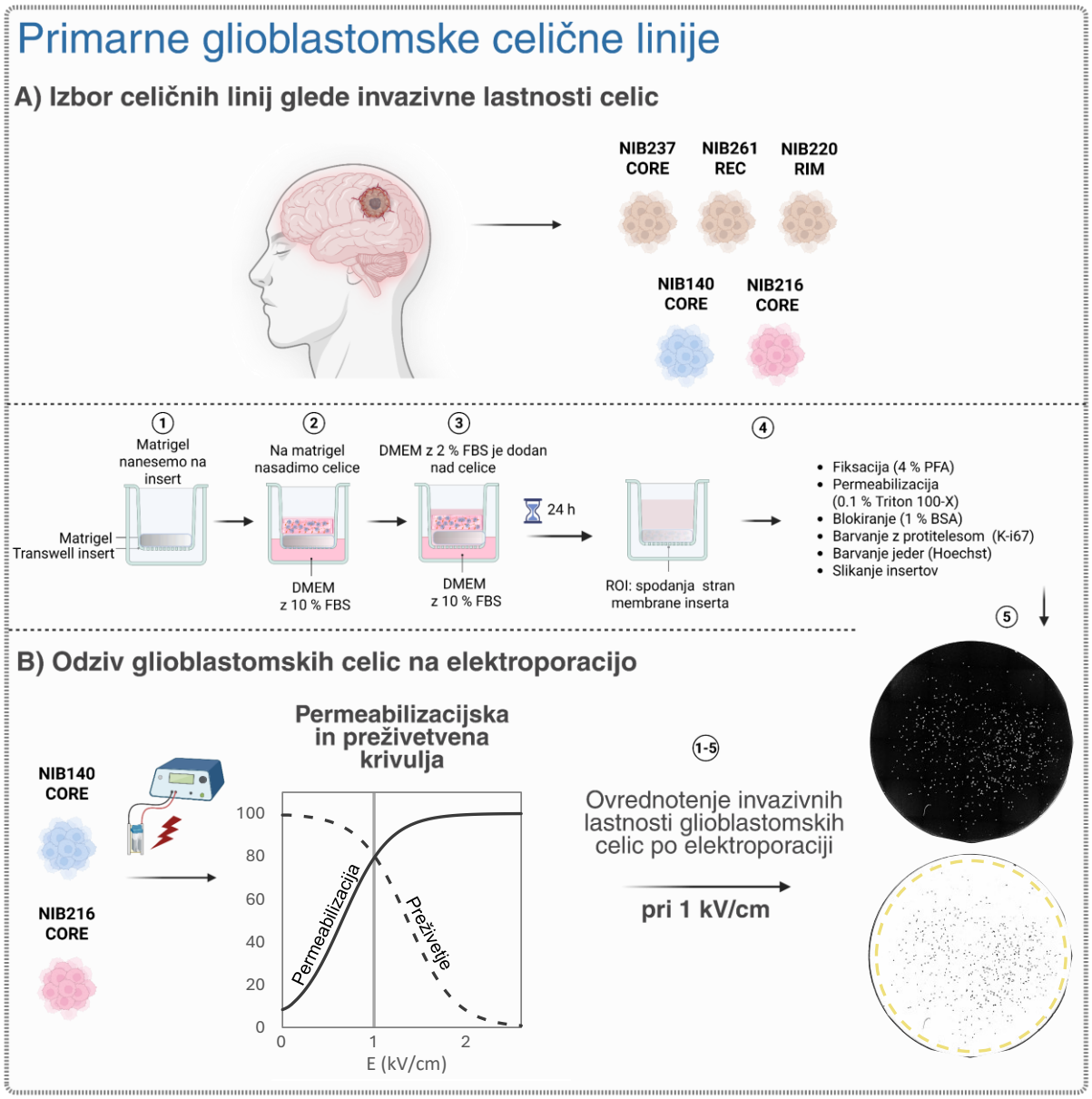

Slika 13: Pregled eksperimentalnega postopka za ovrednotenje vpliva elektroporacije na invazijo glioblastomskih celic, pridobljenih iz pacientov. a) V prvem sklopu smo preverili invazijo petih glioblastomskih celičnih linij brez izpostavitve električnemu polju in na podlagi najvišjega invazivnega potenciala izbrali NIB140 CORE in NIB216 CORE. b) V drugem sklopu poskusov smo celice izpostavili električnemu polju in ovrednotili prepustnost membrane, preživetje celic, presnovno aktivnost ter spremembe v invazivnosti. Invazijo smo določili s pomočjo z migracijskega transwell testa (*angl.* transwell assay), proliferacijo pa z uporabo markerja Ki-67.

Med petimi testiranimi celičnimi linijami sta bili zaradi najvišjega invazivnega potenciala izbrani liniji NIB140 CORE in NIB216 CORE. Obe sta bili izpostavljeni vlakom visokofrekvenčnih bifaznih pulzov dolžine 2 µs pri 1,0 kV/cm. Analiza z propidijevim jodidom in pretočno citometrijo je pokazala učinkovito povečano prepustnost plazemske membrane ob hkratnem ohranjanju preživetja celic, kar potrjuje izpostavitev reverzibilni elektroporaciji. Ocena invazije 24 ur po izpostavitvi celic električnemu polju je razkrila povečano invazivnost v obeh linijah: pri NIB140 CORE je bilo to povečanje izrazito (v mediani 3,74-kratno), medtem ko je NIB216 CORE pokazala skromnejši, a še vedno zaznaven, 30-odstotni porast.

Analiza transkriptoma je osvetlila molekularno ozadje teh razlik. V NIB140 CORE so se pokazale spremembe v izražanju genov; znižanje izražanja genov povezanih z zunajceličnim matriksom in povišano izražanje genov povezanih z ionskimi kanali (npr. *KCNMA1* in *KCNAB1*). Ti izsledki se ujemajo s predhodnimi opažanji iz prve študije, kjer je pri celicah U-87 MG vdor kalcija sprožil hiperpolarizacijo membrane prek aktivacije K_{Ca} kanalov. Nasprotno pa se je pri celični liniji NIB216 CORE izkazalo, da prihaja predvsem do sprememb v izražanju genov citoskeleta in signalizaciji povezani s stresnimi mehanizmi, kar kaže na drugačen prilagoditveni odziv.

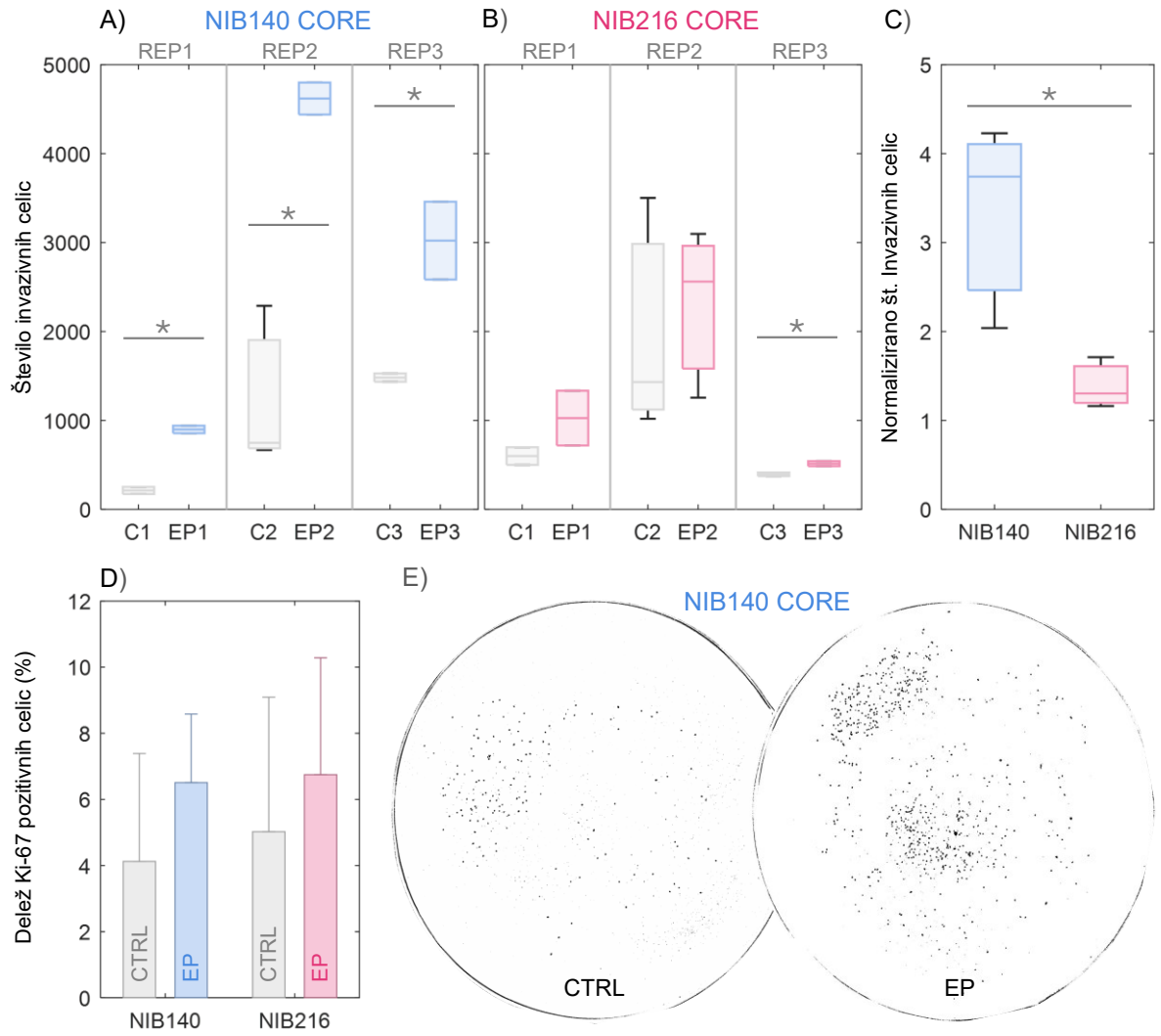

Slika 14: Elektroporacija poveča invazivni potencial glioblastomskih celic, pridobljenih iz pacientov. Lastnost invazije celic smo preverjali 24 ur po elektroporaciji z električnimi pulzi jakosti 1 kV/cm. a-b) Škatlasti diagrami prikazujejo število invazivnih celic glede na posamezno celično linijo: a) NIB140 CORE b) in NIB216 CORE. Siva barva označuje vzorce kontrole, modra (NIB140 CORE) oziroma roza (NIB216 CORE) barva pa tretirane vzorce. Vsaka skupina (REP1–REP3 predstavlja ločeno biološko ponovitev z 2–3 tehničnimi ponovitvami na biološko ponovitev. Vodoravna črta v polju označuje mediano, brki pa prikazujejo celoten razpon vrednosti. c) Relativno povečanje števila invazivnih celic po elektroporaciji v primerjavi s pripadajočo kontrolo. Podatki so prikazani kot povprečje ± SD iz treh bioloških ponovitev. d) Delež Ki-67–pozitivnih (proliferirajočih) celic v kontrolnih in elektroporiranih vzorcih. Vrednosti so v vseh pogojih ostale pod 10 %, kar potrjuje, da opaženo povečanje invazije ni posledica povišane proliferacije. e) Reprezentativna slika maske, dobljene po obdelavi slik,

na kateri so prikazana jedra pobarvana z barvilom Hoechst, ki prikazuje povečano invazijo pri celični liniji NIB140 CORE po elektroporaciji.

Študija opozarja na pomemben terapevtski izziv: celice na obrobju zdravljenega območja, kjer je električno polje nižje, lahko preživijo in se razvijejo v invazivnejši fenotip. V takih primerih reverzibilna elektroporacija namesto zaviranja napredovanja tumorja lahko prispeva k njegovi pospešitvi. To poudarja tveganja uporabe ireverzibilne elektroporacije brez dodatnih sredstev pri infiltrativnih tumorjih, kot je glioblastom (Garcia in sod., 2011; Latouche in sod., 2018; Rossmeisl in sod., 2015). Tveganje bi bilo mogoče zamejiti z elektrokemoterapijo, ki izkorišča reverzibilno elektroporacijo za povečanje vnosa in citotoksičnosti kemoterapevtikov, kot sta bleomicin ali cisplatin (Serša in sod., 2006). Pri tem pa moramo biti pozorni na uporabo zadostne koncentracije kemoterapevtskih sredstev. Poleg tega je pomembno poudariti, da elektroporacija povzroči začasno povečanje prepustnosti krvno-možganske pregrade, kar lahko izkoristimo za izboljšanje vnosa zdravil v centralni živčni sistem (Lorenzo in sod., 2019; Partridge in sod., 2022; Sharabi in sod., 2019).

6.2.4.3 Vpliv modulatorjev ionskih kanalov pri odzivu celic na elektroporacijo

S tretjo študijo smo želeli preučiti, ali zaviralec natrijevih kanalov lidokain lahko vpliva na permeabilizacijo in preživetje celic po elektroporaciji. Lidokain se rutinsko uporablja kot lokalni anestetik pred elektrokemoterapijo in genskim elektroprenosom (Gehl in sod., 2018; Mir in sod., 2006), zato je ključno razumeti, kako lahko vpliva na povečanje prepustnosti membrane in odziv celic pri teh postopkih. Prejšnje raziskave so sicer nakazovale, da bi lidokain lahko povečal učinkovitost terapij, ki temeljijo na elektroporaciji, vendar so bili izsledki teh raziskav omejeni zaradi metodoloških pomanjkljivosti (Grys in sod., 2014; Pan F. in sod., 2020; Sherba in sod., 2020).

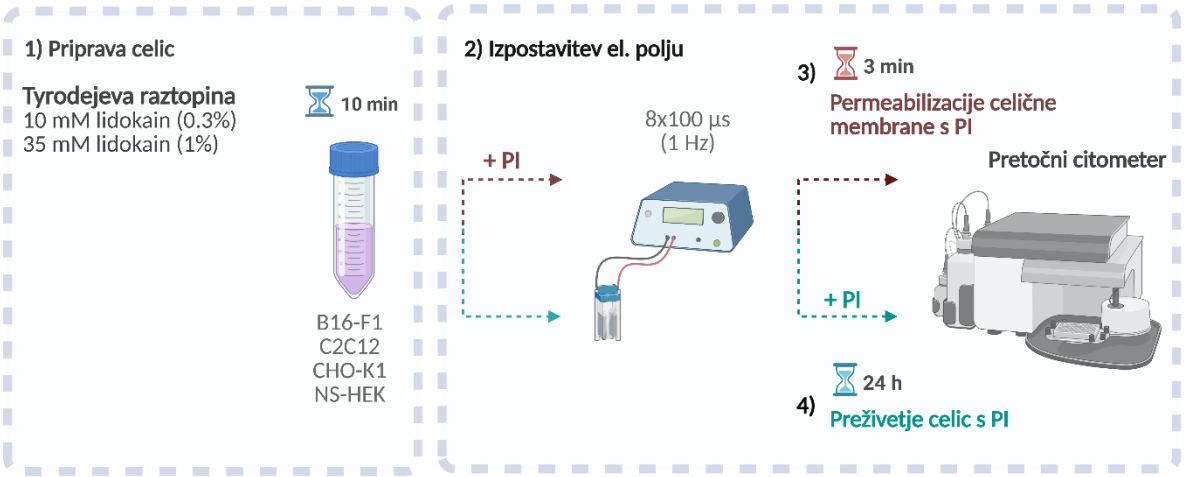

Slika 15: Shema eksperimentalnega načrta. Potek dela je obsegal štiri korake: a) 10-minutna inkubacija celic (B16-F1, C2C12, CHO-K1 ali NS-HEK) v izbranem elektroporacijskem mediju v prisotnosti oziroma odsotnosti lidokaina. b) Izpostavitev osmim električnim pulzom s trajanjem 100 µs pri frekvenci 1 Hz – v prisotnosti propidijevega jodida (PI) za analizo prepustnosti membrane ali brez PI za analizo preživetja celic. c) Določanje prepustnosti membrane z merjenjem vnosa PI 3 minute po elektroporaciji s pretočno citometrijo. d) Določanje preživetja celic 24 ur po elektroporaciji z obarvanjem s PI in štetjem neobarvanih živih celic s pretočno citometrijo. Prepustnost membrane in preživetje celic sta bila ovrednotena na ločenih vzorcih.

V naši raziskavi smo vpliv lidokaina na permeabilizacijo in preživetje ovrednotili v štirih celičnih linijah: B16-F1 – celice melanoma (model za ECT), C2C12 – mioblastne celice (model za GET), CHO-K1 – celice ovarija kitajskega hrčka, ki se odlikujejo po nizki izraženosti ionskih kanalov, in NS-HEK – z genskim inženirstvom razvita celična linija humanih embrionalnih ledvičnih celic (*angl.* human embryonic kidney cells; HEK cells), ki stabilno izražajo natrijeve napetostno odvisne kanale Na$_V$1.5. Poskusi so bili izvedeni v nizkoprevodnem pufru in v Tyrodejevi raztopini. Lidokain je bil testiran v koncentracijah 10 mM (pogosto uporabljena koncentracija v in vitro raziskavah) in 35 mM (1 %, koncentracija raztopine za injiciranje). Elektroporacija je bila izvedena po standardnem pulznem protokolu, uporabljenem pri elektrokemoterapiji, tj. 8 × 100 µs pulzov pri 1 Hz.

Pri koncentraciji 10 mM so bili učinki skromni, saj se je prag električne poljske jakosti potreben za 50 % permeabilizacijo in 50 % preživetje znižal zgolj za 16–18 %. Pri 35 mM pa je lidokain znatno znižal preživetje celic melanoma (B16-F1), kjer se je prag za ireverzibilno elektroporacijo znižal za 25–40 %. Citotoksičnost ni bila neposredna posledica povečane prepustnosti membrane, temveč znotrajcelične akumulacije lidokaina, ki je okrepila njegove toksične učinke opisane v predhodnih raziskavah.

Obstaja več možnih mehanizmov, prek katerih lidokain lahko vpliva na permeabilizacijo membrane pri elektroporaciji, med drugim zmanjšanje površinskega naboja membrane, spremembe v fluidnosti in elastičnosti lipidnega dvosloja ter interakcije z napetostno odvisnimi natrijevimi kanali in membranskimi črpalkami (Grys in sod., 2014; Sherba in sod., 2020; Zhou in sod., 2020). Kljub temu pa natančen mehanizem ostaja nepojasnjen, saj so rezultati pokazali, da je bil odziv med posameznimi celičnimi linijami različen. Poleg tega so se kot pomembni dejavniki izkazali tudi eksperimentalni pogoji, kot so pH in prevodnost medija. V prihodnje bi bilo zato posebej zanimivo raziskati vpliv lidokaina na plazemsko membrano s pomočjo simulacij molekularne dinamike, ki bi omogočile vpogled v njegove interakcije z lipidnim dvoslojem na ravni atomov in molekul.

Da bi ocenili klinično relevantnost pridobljenih rezultatov, smo računsko določili območje reverzibilne in ireverzibilne elektroporacije v poenostavljenem modelu tkiva na podlagi eksperimentalno določenih pragov električne poljske jakosti. Izračuni so pokazali, da lahko 35 mM lidokaina več kot podvoji območje ireverzibilne elektroporacije. Vendar pa ostaja klinična relevantnost teh rezultatov vprašljiva, saj se lidokain po lokalnem injiciranju hitro razredči. Koncentracija lidokaina v tkivu nekaj minut po aplikaciji običajno dosega zgolj nekaj mM. Kljub temu bi lahko že zmerno povečanje prepustnosti membrane zaradi lidokaina lahko znatno izboljšalo privzem kemoterapevtikov v celice in s tem vplivalo na učinkovitost zdravljenja.

6.2.5 Izvirni prispevki k znanosti

Ta doktorska disertacija prispeva nova spoznanja o uravnavanju transmembranske napetosti po elektroporaciji in njenih funkcionalnih posledicah v celicah, s posebnim poudarkom na vlogi ionskih kanalov. V treh med seboj dopolnjujočih se študijah smo elektroporacijo preučevali na več bioloških ravneh – od biofizikalnih mehanizmov, ki določajo dinamiko transmembranske napetosti neposredno po izpostavitvi električnemu pulzu, do prilagoditvenih odzivov tumorskih celic glioblastoma in vpliva lidokaina kot modulatorja ionskih kanalov na izid elektroporacije.

Aktivnost ionskih kanalov je pomemben regulator dolgoročnih sprememb v transmembranski napetosti po elektroporaciji. V prvi študiji smo pokazali, da v glioblastomski celični liniji U-87 MG elektroporacija ne povzroča samo depolarizacije membrane, temveč lahko sproži tudi trajnejšo hiperpolarizacijo, ki vztraja več minut po izpostavitvi celic zunanjemu električnemu polju. Ugotovljeno je bilo, da ima aktivacija ionskih kanalov pomembno vlogo pri tovrstnih spremembah, predvsem od kalcija odvisnih kalijevih kanalov (K_{Ca}), kar je bilo potrjeno tako eksperimentalno kot s teoretičnim modeliranjem. Poleg tega je študija razkrila metodološke omejitve pri spremljanju dolgoročnih sprememb transmembranske napetosti, saj se obstoječa potenciometrična barvila soočajo s številnimi pomanjkljivostmi.

Reverzibilna elektroporacija lahko poveča invazivne procese glioblastomskih celic. V drugi študiji smo preučevali, kako reverzibilna elektroporacija vpliva na vedenje glioblastomskih celic, ki preživijo izpostavljenost električnemu polju. Uporabljeni so bili klinično relevantni modeli – humane primarne glioblastomske celice, pridobljene od pacientov. Rezultati so pokazali, da lahko preživele tumorske celice pridobijo bolj invaziven fenotip. Spremembe v izražanju genov so razkrile predvsem vpletenost ionskih kanalov in spremembe v zunajceličnem matriksu. To delo je prvič jasno opozorilo na potencialna tveganja reverzibilne elektroporacije pri zdravljenju infiltrativnih tumorjev. Vendar pa bo za potrditev teh ugotovitev potrebno izvesti dodatne poskuse z uporabo bolj zapletenih in klinično reprezentativnih 3D modelov, kot so npr. večcelični sferoidi ali organoidi.

Farmakološka modulacija z lidokainom lahko vpliva na učinkovitost elektroporacije. V tretji študiji smo raziskali farmakološko modulacijo odziva celic na elektroporacijo z lidokainom, zaviralcem natrijevih kanalov, ki se uporablja kot lokalni anestetik. Rezultati so pokazali, da lahko lidokain v manjši meri poveča permeabilizacijo celic in v večji meri zmanjša preživetje celic po elektroporaciji, vendar je ta vpliv odvisen od koncentracije lidokaina. Koncentracija lidokaina, pri kateri je bil izmerjen močan vpliv na preživetje celic po elektroporaciji (35 mM), za velikostni razred presega koncentracije, ki se običajno vzpostavijo v tkivu v nekaj minutah po injiciranju. Zato je potrebno klinično relevantnost teh rezultatov preveriti z nadaljnjimi predkliničnimi oz. kliničnimi študijami.

7 VIRI

Abed T., Ganser K., Eckert F., Stransky N., Huber S. M. 2023. Ion channels as molecular targets of glioblastoma electrotherapy. Frontiers in Cellular Neuroscience, 17: 1133984, https://doi.org/10.3389/fncel.2023.1133984

Abidor I. G., Barbul A. I., Zhelev D. V., Doinov P., Bandrina I. N., Osipova E. M., Sukharev S. I. 1993. Electrical properties of cell pellets and cell electrofusion in a centrifuge. Biochimica Et Biophysica Acta, 1152, 2: 207–218, https://doi.org/10.1016/0005-2736(93)90251-t

Agerholm-Larsen B., Iversen H. K., Ibsen P., Moller J. M., Mahmood F., Jensen K. S., Gehl J. 2011. Preclinical validation of electrochemotherapy as an effective treatment for brain tumors. Cancer Research, 71, 11: 3753–3762, https://doi.org/10.1158/0008-5472.CAN-11-0451

Alberts B. 2015. Molecular biology of the cell. Sixth edition. New York, NY, Garland Science, Taylor and Francis Group

Alexander S. P. H., Mathie A. A., Peters J. A., Veale E. L., Striessnig J., Kelly E., Armstrong J. F., Faccenda E., Harding S. D., Davies J. A., Aldrich R. W., Attali B., Baggetta A. M., Becirovic E., Biel M., Bill R. M., Caceres A. I., Catterall W. A., Conner A. C., Davies P., … Zhu M. 2023. The Concise Guide to PHARMACOLOGY 2023/24: Ion channels. British Journal of Pharmacology, 180, Suppl 2: S145–S222, https://doi.org/10.1111/bph.16178

Allen M., Bjerke M., Edlund H., Nelander S., Westermark B. 2016. Origin of the U87MG glioma cell line: Good news and bad news. Science Translational Medicine, 8, 354: 354re3, https://doi.org/10.1126/scitranslmed.aaf6853

Amin A. S., Tan H. L., Wilde A. A. M. 2010. Cardiac ion channels in health and disease. Heart Rhythm, 7, 1: 117–126, https://doi.org/10.1016/j.hrthm.2009.08.005

Arciga B. M., Walters D. M., Kimchi E. T., Staveley-O'Carroll K. F., Li G., Teixeiro E., Rachagani S., Kaifi J. T. 2025. Pulsed electric field ablation as a candidate to enhance the anti-tumor immune response to immune checkpoint inhibitors. Cancer Letters, 609: 217361, https://doi.org/10.1016/j.canlet.2024.217361

Armstrong C. M., Hille B. 1998. Voltage-gated ion channels and electrical excitability. Neuron, 20, 3: 371–380, https://doi.org/10.1016/s0896-6273(00)80981-2

Arroyo J. P., Jacobs E. J., Ahmad R. N., Amin A. J., Verbridge S. S., Davalos R. V. 2025. Characterization of glioma spheroid viability and metastatic potential following monophasic and biphasic pulsed electric fields. Bioelectrochemistry, 165: 109005, https://doi.org/10.1016/j.bioelechem.2025.109005

Aycock K. N., Davalos R. V. 2019. Irreversible Electroporation: Background, Theory, and Review of Recent Developments in Clinical Oncology. Bioelectricity, 1, 4: 214–234, https://doi.org/10.1089/bioe.2019.0029

Azarov J. E., Semenov I., Casciola M., Pakhomov A. G. 2019. Excitation of murine cardiac myocytes by nanosecond pulsed electric field. Journal of Cardiovascular Electrophysiology, 30, 3: 392–401, https://doi.org/10.1111/jce.13834

Bagal S. K., Brown A. D., Cox P. J., Omoto K., Owen R. M., Pryde D. C., Sidders B., Skerratt S. E., Stevens E. B., Storer R. I., Swain N. A. 2013. Ion Channels as Therapeutic Targets: A Drug Discovery Perspective. Journal of Medicinal Chemistry, 56, 3: 593–624, https://doi.org/10.1021/jm3011433

Balantič K., Weiss V. U., Pittenauer E., Miklavčič D., Kramar P. 2023. The role of lipid oxidation on electrical properties of planar lipid bilayers and its importance for understanding electroporation. Bioelectrochemistry (Amsterdam, Netherlands), 153: 108498, https://doi.org/10.1016/j.bioelechem.2023.108498

Batista Napotnik T., Cimperman T., Rems L. 2025. Excitation and electroporation in genetically engineered excitable S-HEK cells exposed to electric pulses of different durations. Scientific Reports, 15, 1: 23451, https://doi.org/10.1038/s41598-025-06989-5

Batista Napotnik T., Kos B., Jarm T., Miklavčič D., O'Connor R. P., Rems L. 2024. Genetically engineered HEK cells as a valuable tool for studying electroporation in excitable cells. Scientific Reports, 14, 1: 720, https://doi.org/10.1038/s41598-023-51073-5

Batista Napotnik T., Polajžer T., Miklavčič D. 2021. Cell death due to electroporation - A review. Bioelectrochemistry (Amsterdam, Netherlands), 141: 107871, https://doi.org/10.1016/j.bioelechem.2021.107871

Benz R., Zimmermann U. 1980. Relaxation studies on cell membranes and lipid bilayers in the high electric field range. Journal of Electroanalytical Chemistry and Interfacial Electrochemistry, 116: 723–739, https://doi.org/10.1016/S0022-0728(80)80301-9

Bernardi R. C., Gomes D. E. B., Gobato R., Taft C. A., Ota A. T., Pascutti P. G. 2009. Molecular dynamics study of biomembrane/local anesthetics interactions. Molecular Physics, 107, 14: 1437–1443, https://doi.org/10.1080/00268970902926238

Berridge M. J., Lipp P., Bootman M. D. 2000. The versatility and universality of calcium signalling. Nature Reviews. Molecular Cell Biology, 1, 1: 11–21, https://doi.org/10.1038/35036035

Berridge Michael J., Bootman M. D., Roderick H. L. 2003. Calcium signalling: dynamics, homeostasis and remodelling. Nature Reviews Molecular Cell Biology, 4, 7: 517–529, https://doi.org/10.1038/nrm1155

Bianchi G., Campanacci L., Ronchetti M., Donati D. 2016. Electrochemotherapy in the Treatment of Bone Metastases: A Phase II Trial. World Journal of Surgery, 40, 12: 3088–3094, https://doi.org/10.1007/s00268-016-3627-6

Blackiston D. J., McLaughlin K. A., Levin M. 2009. Bioelectric controls of cell proliferation: ion channels, membrane voltage and the cell cycle. Cell Cycle, 8, 21: 3527–3536, https://doi.org/10.4161/cc.8.21.9888

Blažič A., Guinard M., Leskovar T., O'Connor R. P., Rems L. 2025a. Long-term changes in transmembrane voltage after electroporation are governed by the interplay between nonselective leak current and ion channel activation. Bioelectrochemistry, 161: 108802, https://doi.org/10.1016/j.bioelechem.2024.108802

Blažič A., Polajžer T., Miklavčič D., Rems L. 2024. The influence of lidocaine on cell membrane permeabilization and cell survival after electroporation. In: Proceedings of the 4th URSI Atlantic Radio Science Conference (AT-RASC), 2024 May 19–24, Gran Canaria, Spain. URSI – International Union of Radio Science, https://doi.org/10.46620/URSIATRASC24/SFXG1870

Blažič A., Šmerc R., Polajžer T., Miklavčič D., Rems L. 2025b. Reassessing lidocaine as an electroporation sensitizer in vitro. Scientific Reports, 15, 1: 25593, https://doi.org/10.1038/s41598-025-11695-3

Bong A. H. L., Monteith G. R. 2018. Calcium signaling and the therapeutic targeting of cancer cells. Biochimica et Biophysica Acta (BBA) - Molecular Cell Research, 1865, 11, Part B: 1786–1794, https://doi.org/10.1016/j.bbamcr.2018.05.015

Bortner C. D., Cidlowski J. A. 2007. Cell shrinkage and monovalent cation fluxes: role in apoptosis. Archives of Biochemistry and Biophysics, 462, 2: 176–188, https://doi.org/10.1016/j.abb.2007.01.020

Breznik B., Ko M.-W., Tse C., Chen P.-C., Senjor E., Majc B., Habič A., Angelillis N., Novak M., Župunski V., Mlakar J., Nathanson D., Jewett A. 2022. Infiltrating natural killer cells bind, lyse and increase chemotherapy efficacy in glioblastoma stem-like tumorospheres. Communications Biology, 5, 1: 436, https://doi.org/10.1038/s42003-022-03402-z

Brini M., Calì T., Ottolini D., Carafoli E. 2013. Intracellular calcium homeostasis and signaling. In: Calcium signaling. Banci L. (ed.). Dordrecht, Springer: 119–168, https://doi.org/10.1007/978-94-007-5561-1_5

Burke R. C., Bardet S. M., Carr L., Romanenko S., Arnaud-Cormos D., Leveque P., O'Connor R. P. 2017. Nanosecond pulsed electric fields depolarize transmembrane potential via voltage-gated K+, Ca2+ and TRPM8 channels in U87 glioblastoma cells. Biochimica Et Biophysica Acta. Biomembranes, 1859, 10: 2040–2050, https://doi.org/10.1016/j.bbamem.2017.07.004

Calvet C. Y., Mir L. M. 2016. The promising alliance of anti-cancer electrochemotherapy with immunotherapy. Cancer and Metastasis Reviews, 35, 2: 165–177, https://doi.org/10.1007/s10555-016-9615-3

Campelo S. N., Lorenzo M. F., Partridge B., Alinezhadbalalami N., Kani Y., Garcia J., Saunier S., Thomas S. C., Hinckley J., Verbridge S. S., Davalos R. V., Rossmeisl J. H. 2023. High-frequency irreversible electroporation improves survival and immune cell infiltration in rodents with malignant gliomas. Frontiers in Oncology, 13: 1171278, https://doi.org/10.3389/fonc.2023.1171278

Casciola M., Tarek M. 2016. A molecular insight into the electro-transfer of small molecules through electropores driven by electric fields. Biochimica et Biophysica Acta (BBA) - Biomembranes, 1858, 10: 2278–2289, https://doi.org/10.1016/j.bbamem.2016.03.022

Casciola M., Xiao S., Apollonio F., Paffi A., Liberti M., Muratori C., Pakhomov A. G. 2019. Cancellation of nerve excitation by the reversal of nanosecond stimulus polarity and its relevance to the gating time of sodium channels. Cellular and Molecular Life Sciences, 76, 22: 4539–4550, https://doi.org/10.1007/s00018-019-03126-0

Casciola M., Xiao S., Pakhomov A. G. 2017. Damage-free peripheral nerve stimulation by 12-ns pulsed electric field. Scientific Reports, 7, 1: 10453, https://doi.org/10.1038/s41598-017-10282-5

Catacuzzeno L., Aiello F., Fioretti B., Sforna L., Castigli E., Ruggieri P., Tata A. M., Calogero A., Franciolini F. 2011. Serum-activated K and Cl currents underlay U87-MG glioblastoma cell migration. Journal of Cellular Physiology, 226, 7: 1926–1933, https://doi.org/10.1002/jcp.22523

Cemazar M., Jarm T., Miklavcic D., Lebar A., Alojz I., Kopitar A. N., Sersa G. 1998. Effect of electric-field intensity on electropermeabilization and electrosensitmty of various tumor-cell lines in vitro. Electromagnetic Biology and Medicine, 17: 263–272, https://doi.org/10.3109/15368379809022571

Chafai D. E., Sulimenko V., Havelka D., Kubínová L., Dráber P., Cifra M. 2019. Reversible and Irreversible Modulation of Tubulin Self-Assembly by Intense Nanosecond Pulsed Electric Fields. Advanced Materials, 31, 39: e1903636, https://doi.org/10.1002/adma.201903636

Chaigne S., Sigg D. C., Stewart M. T., Hocini M., Napotnik T. B., Miklavčič D., Bernus O., Benoist D. 2022. Reversible and Irreversible Effects of Electroporation on Contractility and Calcium Homeostasis in Isolated Cardiac Ventricular Myocytes. Circulation: Arrhythmia and Electrophysiology, 15: e011131, https://doi.org/10.1161/CIRCEP.122.011131

Chakraborty S., Doktorova M., Molugu T. R., Heberle F. A., Scott H. L., Dzikovski B., Nagao M., Stingaciu L.-R., Standaert R. F., Barrera F. N., Katsaras J., Khelashvili G., Brown M. F., Ashkar R. 2020. How cholesterol stiffens unsaturated lipid membranes.

Proceedings of the National Academy of Sciences, 117, 36: 21896–21905, https://doi.org/10.1073/pnas.2004807117

Charlton F. W., Pearson H. M., Hover S., Lippiat J. D., Fontana J., Barr J. N., Mankouri J. 2020. Ion Channels as Therapeutic Targets for Viral Infections: Further Discoveries and Future Perspectives. Viruses, 12, 8: 844, https://doi.org/10.3390/v12080844

Chen J., Stubbe J. 2005. Bleomycins: towards better therapeutics. Nature Reviews Cancer, 5, 2: 102–112, https://doi.org/10.1038/nrc1547

Chen W., Lee R. C. 1994a. Altered ion channel conductance and ionic selectivity induced by large imposed membrane potential pulse. Biophysical Journal, 67, 2: 603–612, https://doi.org/10.1016/S0006-3495(94)80520-X

Chen W., Lee R. C. 1994b. Evidence for electrical shock-induced conformational damage of voltage-gated ionic channels. Annals of the New York Academy of Sciences, 720, 1: 124–135, https://doi.org/10.1111/j.1749-6632.1994.tb30440.x

Chen W., Han Y., Chen Y., Astumian D. 1998. Electric Field-Induced Functional Reductions in the K+ Channels Mainly Resulted from Supramembrane Potential-Mediated Electroconformational Changes. Biophysical Journal, 75, 1: 196–206, https://doi.org/10.1016/S0006-3495(98)77506-X

Chen W., Wu W. 2006. Electric field-induced changes in membrane proteins charge movement currents. Burns: Journal of the International Society for Burn Injuries, 32, 7: 833–841, https://doi.org/10.1016/j.burns.2006.03.012

Chen W., Zhongsheng Z., Lee R. C. 2006. Supramembrane potential-induced electroconformational changes in sodium channel proteins: A potential mechanism involved in electric injury. Burns, 32, 1: 52–59, https://doi.org/10.1016/j.burns.2005.08.008

Cheng L., Wu Q., Guryanova O. A., Huang Z., Huang Q., Rich J. N., Bao S. 2011. Elevated invasive potential of glioblastoma stem cells. Biochemical and Biophysical Research Communications, 406, 4: 643–648, https://doi.org/10.1016/j.bbrc.2011.02.123

Chopinet L., Etienne D., Marie-Pierre R. 2014. AFM sensing cortical actin cytoskeleton destabilization during plasma membrane electropermeabilization. Cytoskeleton, 71, 10: 587–594, https://doi.org/10.1002/cm.21194

Chun K.-R. J., Miklavčič D., Vlachos K., Bordignon S., Scherr D., Jais P., Schmidt B. 2024. State-of-the-art pulsed field ablation for cardiac arrhythmias: ongoing evolution and future perspective. EP Europace, 26, 6: euae134, https://doi.org/10.1093/europace/euae134

Cohen L. B., Salzberg B. M., Davila H. V., Ross W. N., Landowne D., Waggoner A. S., Wang C. H. 1974. Changes in axon fluorescence during activity: Molecular probes of

membrane potential. The Journal of Membrane Biology, 19, 1: 1–36, https://doi.org/10.1007/BF01869968

Collin A., Bruhier H., Kolosnjaj J., Golzio M., Rols M.-P., Poignard C., Collin A., Bruhier H., Kolosnjaj J., Golzio M., Rols M.-P., Poignard C. 2022. Spatial mechanistic modeling for prediction of 3D multicellular spheroids behavior upon exposure to high intensity pulsed electric fields. AIMS Bioengineering, 9, 2: 102–122, https://doi.org/10.3934/bioeng.2022009

Craviso G. L., Choe S., Chatterjee P., Chatterjee I., Vernier P. T. 2010. Nanosecond electric pulses: a novel stimulus for triggering Ca2+ influx into chromaffin cells via voltage-gated Ca2+ channels. Cellular and Molecular Neurobiology, 30, 8: 1259–1265, https://doi.org/10.1007/s10571-010-9573-1

Cvetkoska A., Maček-Lebar A., Polajžer T., Reberšek M., Upchurch W., Iaizzo P. A., Sigg D. C., Miklavčič D. 2023. The Effects of Interphase and Interpulse Delays and Pulse Widths on Induced Muscle Contractions, Pain and Therapeutic Efficacy in Electroporation-Based Therapies. Journal of Cardiovascular Development and Disease, 10, 12: 490, https://doi.org/10.3390/jcdd10120490

D'Alessandro G., Monaco L., Catacuzzeno L., Antonangeli F., Santoro A., Esposito V., Franciolini F., Wulff H., Limatola C. 2019. Radiation Increases Functional KCa3.1 Expression and Invasiveness in Glioblastoma. Cancers, 11, 3: 279, https://doi.org/10.3390/cancers11030279

Dasari S., Bernard Tchounwou P. 2014. Cisplatin in cancer therapy: Molecular mechanisms of action. European Journal of Pharmacology, 740: 364–378, https://doi.org/10.1016/j.ejphar.2014.07.025

Davalos R. V., Mir L. M., Rubinsky B. 2005. Tissue Ablation with Irreversible Electroporation. Annals of Biomedical Engineering, 33, 2: 223–231, https://doi.org/10.1007/s10439-005-8981-8

Dermol-Černe J., Miklavčič D., Reberšek M., Mekuč P., Bardet S. M., Burke R., Arnaud-Cormos D., Leveque P., O'Connor R. 2018. Plasma membrane depolarization and permeabilization due to electric pulses in cell lines of different excitability. Bioelectrochemistry (Amsterdam, Netherlands), 122: 103–114, https://doi.org/10.1016/j.bioelechem.2018.03.011

Dworakowska B., Do K. 2000. Ion channels-related diseases. Ion Channels, 47: 685–703

Ekanem E., Neuzil P., Reichlin T., Kautzner J., van der Voort P., Jais P., Chierchia G.-B., Bulava A., Blaauw Y., Skala T., Fiala M., Duytschaever M., Szeplaki G., Schmidt B., Massoullie G., Neven K., Thomas O., Vijgen J., Gandjbakhch E., Scherr D., … Reddy V. Y. 2024. Safety of pulsed field ablation in more than 17,000 patients with atrial fibrillation in the MANIFEST-17K study. Nature Medicine, 30, 7: 2020–2029, https://doi.org/10.1038/s41591-024-03114-3

Ferioli M., Perrone A. M., De Iaco P., Zamfir A. A., Ravegnini G., Buwenge M., Fionda B., Galietta E., Donati C. M., Tagliaferri L., Morganti A. G. 2024. Clinical Insights and Future Prospects: A Comprehensive Narrative Review on Immunomodulation Induced by Electrochemotherapy. Current Oncology, 31, 10: 6433–6444, https://doi.org/10.3390/curroncol31100478

Franco R., Bortner C. D., Cidlowski J. A. 2006. Potential roles of electrogenic ion transport and plasma membrane depolarization in apoptosis. The Journal of Membrane Biology, 209, 1: 43–58, https://doi.org/10.1007/s00232-005-0837-5

Frandsen S. K., Vissing M., Gehl J. 2020. A Comprehensive Review of Calcium Electroporation—A Novel Cancer Treatment Modality. Cancers, 12, 2: 290, https://doi.org/10.3390/cancers12020290

Gabriel B., Teissié J. 1994. Generation of reactive-oxygen species induced by electropermeabilization of Chinese hamster ovary cells and their consequence on cell viability. European Journal of Biochemistry, 223, 1: 25–33, https://doi.org/10.1111/j.1432-1033.1994.tb18962.x

Gamper N., Stockand J. D., Shapiro M. S. 2005. The use of Chinese hamster ovary (CHO) cells in the study of ion channels. Journal of Pharmacological and Toxicological Methods, 51, 3: 177–185, https://doi.org/10.1016/j.vascn.2004.08.008

Garcia P. A., Pancotto T., Rossmeisl J. H., Henao-Guerrero N., Gustafson N. R., Daniel G. B., Robertson J. L., Ellis T. L., Davalos R. V. 2011. Non-thermal irreversible electroporation (N-TIRE) and adjuvant fractionated radiotherapeutic multimodal therapy for intracranial malignant glioma in a canine patient. Technology in Cancer Research & Treatment, 10, 1: 73–83, https://doi.org/10.7785/tcrt.2012.500181

Garcia Paulo A., Rossmeisl J. H., Robertson J. L., Olson J. D., Johnson A. J., Ellis T. L., Davalos R. V. 2012. 7.0-T magnetic resonance imaging characterization of acute blood-brain-barrier disruption achieved with intracranial irreversible electroporation. PloS One, 7, 11: e50482, https://doi.org/10.1371/journal.pone.0050482

Geboers B., Scheffer H. J., Graybill P. M., Ruarus A. H., Nieuwenhuizen S., Puijk R. S., van den Tol P. M., Davalos R. V., Rubinsky B., de Gruijl T. D., Miklavčič D., Meijerink M. R. 2020. High-Voltage Electrical Pulses in Oncology: Irreversible Electroporation, Electrochemotherapy, Gene Electrotransfer, Electrofusion, and Electroimmunotherapy. Radiology, 295, 2: 254–272, https://doi.org/10.1148/radiol.2020192190

Gehl J., Sersa G., Matthiessen L. W., Muir T., Soden D., Occhini A., Quaglino P., Curatolo P., Campana L. G., Kunte C., Clover A. J. P., Bertino G., Farricha V., Odili J., Dahlstrom K., Benazzo M., Mir L. M. 2018. Updated standard operating procedures for electrochemotherapy of cutaneous tumours and skin metastases. Acta Oncologica (Stockholm, Sweden), 57, 7: 874–882, https://doi.org/10.1080/0284186X.2018.1454602

Graybill P. M., Davalos R. V. 2020. Cytoskeletal Disruption after Electroporation and Its Significance to Pulsed Electric Field Therapies. Cancers, 12, 5: 1132, https://doi.org/10.3390/cancers12051132

Grochans S., Cybulska A. M., Siminska D., Korbecki J., Kojder K., Chlubek D., Baranowska-Bosiacka I. 2022. Epidemiology of Glioblastoma Multiforme-Literature Review. Cancers, 14, 10: 2412, https://doi.org/10.3390/cancers14102412

Grys M., Madeja Z., Korohoda W. 2014. Decreasing the thresholds for electroporation by sensitizing cells with local cationic anesthetics and substances that decrease the surface negative electric charge. Cellular and Molecular Biology Letters, 19, 1: 65–76, https://doi.org/10.2478/s11658-013-0114-z

Hille B. 2001. Ion Channels of Excitable Membranes. 3rd Casebound edition. Sinauer Associates

Hjouj M., Last D., Guez D., Daniels D., Sharabi S., Lavee J., Rubinsky B., Mardor Y. 2012. MRI Study on Reversible and Irreversible Electroporation Induced Blood Brain Barrier Disruption. PLOS ONE, 7, 8: e42817, https://doi.org/10.1371/journal.pone.0042817

Howard B., Haines D. E., Verma A., Packer D., Kirchhof N., Barka N., Onal B., Fraasch S., Miklavčič D., Stewart M. T. 2020. Reduction in Pulmonary Vein Stenosis and Collateral Damage With Pulsed Field Ablation Compared With Radiofrequency Ablation in a Canine Model. Circulation. Arrhythmia and Electrophysiology, 13, 9: e008337, https://doi.org/10.1161/CIRCEP.120.008337

Hristov K., Mangalanathan U., Casciola M., Pakhomova O. N., Pakhomov A. G. 2018. Expression of voltage-gated calcium channels augments cell susceptibility to membrane disruption by nanosecond pulsed electric field. Biochimica Et Biophysica Acta - Biomembranes, 1860, 11: 2175–2183, https://doi.org/10.1016/j.bbamem.2018.08.017

Huang F., Fang Z., Mast J., Chen W. 2013. Comparison of membrane electroporation and protein denature in response to pulsed electric field with different durations. Bioelectromagnetics, 34, 4: 253–263, https://doi.org/10.1002/bem.21773

Ibey B. L., Mixon D. G., Payne J. A., Bowman A., Sickendick K., Wilmink G. J., Roach W. P., Pakhomov A. G. 2010. Plasma membrane permeabilization by trains of ultrashort electric pulses. Bioelectrochemistry, 79, 1: 114–121, https://doi.org/10.1016/j.bioelechem.2010.01.001

Ivey J. W., Wasson E. M., Alinezhadbalalami N., Kanitkar A., Debinski W., Sheng Z., Davalos R. V., Verbridge S. S. 2019. Characterization of Ablation Thresholds for 3D-Cultured Patient-Derived Glioma Stem Cells in Response to High-Frequency Irreversible Electroporation. Research, 2019: 8081315, https://doi.org/10.34133/2019/8081315

Ivey J. W., Latouche E. L., Sano M. B., Rossmeisl J. H., Davalos R. V., Verbridge S. S. 2015. Targeted cellular ablation based on the morphology of malignant cells. Scientific Reports, 5, 1: 17157, https://doi.org/10.1038/srep17157

Jan V., Jusović M., Miklavčič D. 2024. Effects of Electroporation on the Function of Sarco/Endoplasmic Reticulum Ca2+-ATPase and Na+,K+-ATPase in H9c2 Cells. Applied Sciences, 14, 7: 2695, https://doi.org/10.3390/app14072695

Jensen E. C. 2012. Use of Fluorescent Probes: Their Effect on Cell Biology and Limitations. The Anatomical Record, 295, 12: 2031–2036, https://doi.org/10.1002/ar.22602

Justesen T. F., Orhan A., Raskov H., Nolsoe C., Gögenur I. 2022. Electroporation and Immunotherapy—Unleashing the Abscopal Effect. Cancers, 14, 12: 2876, https://doi.org/10.3390/cancers14122876

Kaczorowski G. J., McManus O. B., Priest B. T., Garcia M. L. 2008. Ion Channels as Drug Targets: The Next GPCRs. The Journal of General Physiology, 131, 5: 399–405, https://doi.org/10.1085/jgp.200709946

Kasimova M. A., Lindahl E., Delemotte L. 2018. Determining the molecular basis of voltage sensitivity in membrane proteins. The Journal of General Physiology, 150, 10: 1444–1458, https://doi.org/10.1085/jgp.201812086

Kaźmierska M., Rudzińska M., Jarosz B., Dobrzański Z., Trziszka T. 2012. Changes of the fatty acid composition, cholesterol and cholesterol oxide contents in whole egg after pulsed electric field treatmenta. European Poultry Science, 76, 4: 246–253, https://doi.org/10.1016/S0003-9098(25)00742-8

Kesar U., Markelc B., Jesenko T., Ursic Valentinuzzi K., Cemazar M., Strojan P., Sersa G. 2023. Effects of Electrochemotherapy on Immunologically Important Modifications in Tumor Cells. Vaccines, 11, 5: 925, https://doi.org/10.3390/vaccines11050925

Kinosita K., Tsong T. Y. 1979. Voltage-induced conductance in human erythrocyte membranes. Biochimica et Biophysica Acta (BBA) - Biomembranes, 554, 2: 479–497, https://doi.org/10.1016/0005-2736(79)90386-9

Kotnik T., Pucihar G., Reberšek M., Miklavčič D., Mir L. M. 2003. Role of pulse shape in cell membrane electropermeabilization. Biochimica et Biophysica Acta (BBA) - Biomembranes, 1614, 2: 193–200, https://doi.org/10.1016/S0005-2736(03)00173-1

Kotnik T., Frey W., Sack M., Haberl Meglič S., Peterka M., Miklavčič D. 2015. Electroporation-based applications in biotechnology. Trends in Biotechnology, 33, 8: 480–488, https://doi.org/10.1016/j.tibtech.2015.06.002

Kotnik T., Pucihar G., Miklavcic D. 2010. Induced Transmembrane Voltage and Its Correlation with Electroporation-Mediated Molecular Transport. Journal of Membrane Biology, 236, 1: 3–13, https://doi.org/10.1007/s00232-010-9279-9

Kotnik T., Rems L., Tarek M., Miklavčič D. 2019. Membrane Electroporation and Electropermeabilization: Mechanisms and Models. Annual Review of Biophysics, 48: 63–91, https://doi.org/10.1146/annurev-biophys-052118-115451

Lambricht L., Lopes A., Kos S., Sersa G., Préat V., Vandermeulen G. 2016. Clinical potential of electroporation for gene therapy and DNA vaccine delivery. Expert Opinion on Drug Delivery, 13, 2: 295–310, https://doi.org/10.1517/17425247.2016.1121990

Latouche E. L., Arena C. B., Ivey J. W., Garcia P. A., Pancotto T. E., Pavlisko N., Verbridge S. S., Davalos R. V., Rossmeisl J. H. 2018. High-Frequency Irreversible Electroporation for Intracranial Meningioma: A Feasibility Study in a Spontaneous Canine Tumor Model. Technology in Cancer Research & Treatment, 17: 1533033818785285, https://doi.org/10.1177/1533033818785285

Leclerc C., Haeich J., Aulestia F. J., Kilhoffer M.-C., Miller A. L., Néant I., Webb S. E., Schaeffer E., Junier M.-P., Chneiweiss H., Moreau M. 2016. Calcium signaling orchestrates glioblastoma development: Facts and conjunctures. Biochimica et Biophysica Acta (BBA) - Molecular Cell Research, 1863, 6, Part B: 1447–1459, https://doi.org/10.1016/j.bbamcr.2016.01.018

Ledwitch K. V., Barnes R. W., Roberts A. G. 2016. Unravelling the complex drug–drug interactions of the cardiovascular drugs, verapamil and digoxin, with P-glycoprotein. Bioscience Reports, 36, 2: e00309, https://doi.org/10.1042/BSR20150317

Lei M., Wu L., Terrar D. A., Huang C. L.-H. 2018. Modernized Classification of Cardiac Antiarrhythmic Drugs. Circulation, 138, 17: 1879–1896, https://doi.org/10.1161/CIRCULATIONAHA.118.035455

Lerche H., Shah M., Beck H., Noebels J., Johnston D., Vincent A. 2013. Ion channels in genetic and acquired forms of epilepsy. The Journal of Physiology, 591, Pt 4: 753–764, https://doi.org/10.1113/jphysiol.2012.240606

Linnert M., Iversen H. K., Gehl J. 2012. Multiple brain metastases - current management and perspectives for treatment with electrochemotherapy. Radiology and Oncology, 46, 4: 271–278, https://doi.org/10.2478/v10019-012-0042-y

Liu P., Miller E. W. 2020. Electrophysiology, Unplugged: Imaging Membrane Potential with Fluorescent Indicators. Accounts of Chemical Research, 53, 1: 11–19, https://doi.org/10.1021/acs.accounts.9b00514

Liu Y., Zhou F., Ali H., Lathia J. D., Chen P. 2024. Immunotherapy for glioblastoma: current state, challenges, and future perspectives. Cellular & Molecular Immunology, 21, 12: 1354–1375, https://doi.org/10.1038/s41423-024-01226-x

Lopez A., Rols M. P., Teissie J. 1988. 31P NMR analysis of membrane phospholipid organization in viable, reversibly electropermeabilized Chinese hamster ovary cells. Biochemistry, 27, 4: 1222–1228, https://doi.org/10.1021/bi00404a023

Lorenzo M. F., Thomas S. C., Kani Y., Hinckley J., Lee M., Adler J., Verbridge S. S., Hsu F.-C., Robertson J. L., Davalos R. V., Rossmeisl J. H. 2019. Temporal Characterization of Blood–Brain Barrier Disruption with High-Frequency Electroporation. Cancers, 11, 12: 1850, https://doi.org/10.3390/cancers11121850

Mahnič-Kalamiza S., Vorobiev E., Miklavčič D. 2014. Electroporation in Food Processing and Biorefinery. The Journal of Membrane Biology, 247, 12: 1279–1304, https://doi.org/10.1007/s00232-014-9737-x

Majc B., Habič A., Malavolta M., Vittori M., Porčnik A., Bošnjak R., Mlakar J., Matjašič A., Zupan A., Vidmar M. S., Turnšek T. L., Sadikov A., Breznik B., Novak M. 2024. Patient-derived tumor organoids mimic treatment-induced DNA damage response in glioblastoma. iScience, 27, 9: 110604, https://doi.org/10.1016/j.isci.2024.110604

Markelc B., Tevz G., Cemazar M., Kranjc S., Lavrencak J., Zegura B., Teissie J., Sersa G. 2012. Muscle gene electrotransfer is increased by the antioxidant tempol in mice. Gene Therapy, 19, 3: 312–320, https://doi.org/10.1038/gt.2011.97

Marracino P., Havelka D., Průša J., Liberti M., Tuszynski J., Ayoub A. T., Apollonio F., Cifra M. 2019. Tubulin response to intense nanosecond-scale electric field in molecular dynamics simulation. Scientific Reports, 9, 1: 10477, https://doi.org/10.1038/s41598-019-46636-4

Maxfield F. R., Tabas I. 2005. Role of cholesterol and lipid organization in disease. Nature, 438, 7068: 612–621, https://doi.org/10.1038/nature04399

McCaig C. D., Song B., Rajnicek A. M. 2009. Electrical dimensions in cell science. Journal of Cell Science, 122, Pt 23: 4267–4276, https://doi.org/10.1242/jcs.023564

McNamara H. M., Zhang H., Werley C. A., Cohen A. E. 2016. Optically Controlled Oscillators in an Engineered Bioelectric Tissue. Physical Review X, 6, 3: 031001, https://doi.org/10.1103/PhysRevX.6.031001

Miklavčič D., Šemrov D., Mekid H., Mir L. M. 2000. A validated model of in vivo electric field distribution in tissues for electrochemotherapy and for DNA electrotransfer for gene therapy. Biochimica et Biophysica Acta (BBA) - General Subjects, 1523, 1: 73–83, https://doi.org/10.1016/S0304-4165(00)00101-X

Mir L. M., Gehl J., Sersa G., Collins C. G., Garbay J.-R., Billard V., Geertsen P. F., Rudolf Z., O'Sullivan G. C., Marty M. 2006. Standard operating procedures of the electrochemotherapy: Instructions for the use of bleomycin or cisplatin administered either systemically or locally and electric pulses delivered by the CliniporatorTM by means of invasive or non-invasive electrodes. European Journal of Cancer Supplements, 4, 11: 14–25, https://doi.org/10.1016/j.ejcsup.2006.08.003

Moller R. A., Covino B. G. 1988. Cardiac Electrophysiologic Effects of Lidocaine and Bupivacaine. Anesthesia & Analgesia, 67: 107–114

Monteith G. R., Prevarskaya N., Roberts-Thomson S. J. 2017. The calcium–cancer signalling nexus. Nature Reviews Cancer, 17, 6: 373–380, https://doi.org/10.1038/nrc.2017.18

Muratori C., Pakhomov A. G., Gianulis E., Meads J., Casciola M., Mollica P. A., Pakhomova O. N. 2017. Activation of the phospholipid scramblase TMEM16F by nanosecond pulsed electric fields (nsPEF) facilitates its diverse cytophysiological effects. The Journal of Biological Chemistry, 292, 47: 19381–19391, https://doi.org/10.1074/jbc.M117.803049

Murphy K. R., Aycock K. N., Hay A. N., Rossmeisl J. H., Davalos R. V., Dervisis N. G. 2022. High-frequency irreversible electroporation brain tumor ablation: exploring the dynamics of cell death and recovery. Bioelectrochemistry (Amsterdam, Netherlands), 144: 108001, https://doi.org/10.1016/j.bioelechem.2021.108001

Nesin V., Bowman A. M., Xiao S., Pakhomov A. G. 2012. Cell permeabilization and inhibition of voltage-gated Ca2+ and Na+ channel currents by nanosecond pulsed electric fields. Bioelectromagnetics, 33, 5: 394–404, https://doi.org/10.1002/bem.21696

Nesin V., Pakhomov A. G. 2012. Inhibition of voltage-gated Na+ current by nanosecond pulsed electric field (nsPEF) is not mediated by Na+ influx or Ca2+ signaling. Bioelectromagnetics, 33, 6: 443–451, https://doi.org/10.1002/bem.21703

Neumann E., Schaefer-Ridder M., Wang Y., Hofschneider P. H. 1982. Gene transfer into mouse lyoma cells by electroporation in high electric fields. The EMBO Journal, 1, 7: 841–845, https://doi.org/10.1002/j.1460-2075.1982.tb01257.x

Neunlist M., Tung L. 1997. Dose-dependent reduction of cardiac transmembrane potential by high-intensity electrical shocks. The American Journal of Physiology, 273, 6: H2817-H2825, https://doi.org/10.1152/ajpheart.1997.273.6.H2817

Neuroscience. 2004. 3rd ed. Purves D., Augustine G. J., Fitzpatrick D., Hall W. C., LaMantia A. S., McNamara J. O., Williams S. M. (ed.). Sunderland, Mass, Sinauer Associates, Publishers

Nikolaev D. M., Mironov V. N., Shtyrov A. A., Kvashnin I. D., Mereshchenko A. S., Vasin A. V., Panov M. S., Ryazantsev M. N. 2023. Fluorescence Imaging of Cell Membrane Potential: From Relative Changes to Absolute Values. International Journal of Molecular Sciences, 24, 3: 2435, https://doi.org/10.3390/ijms24032435

Nikolski V. P., Efimov I. R. 2005. Electroporation of the heart. EP Europace, 7, s2: S146–S154, https://doi.org/10.1016/j.eupc.2005.04.011

Obrador E., Moreno-Murciano P., Oriol-Caballo M., Lopez-Blanch R., Pineda B., Gutierrez-Arroyo J. L., Loras A., Gonzalez-Bonet L. G., Martinez-Cadenas C., Estrela J. M., Marques-Torrejon M. angeles. 2024. Glioblastoma Therapy: Past, Present and Future. International Journal of Molecular Sciences, 25, 5: 2529, https://doi.org/10.3390/ijms25052529

Ostrom Q. T., Price M., Neff C., Cioffi G., Waite K. A., Kruchko C., Barnholtz-Sloan J. S. 2022. CBTRUS Statistical Report: Primary Brain and Other Central Nervous System Tumors Diagnosed in the United States in 2015-2019. Neuro-Oncology, 24, Suppl 5: v1–v95, https://doi.org/10.1093/neuonc/noac202

Pakhomov A. G., Bowman A. M., Ibey B. L., Andre F. M., Pakhomova O. N., Schoenbach K. H. 2009. Lipid nanopores can form a stable, ion channel-like conduction pathway in cell membrane. Biochemical and Biophysical Research Communications, 385, 2: 181–186, https://doi.org/10.1016/j.bbrc.2009.05.035

Pakhomov A. G., Kolb J. F., White J. A., Joshi R. P., Xiao S., Schoenbach K. H. 2007a. Long-lasting plasma membrane permeabilization in mammalian cells by nanosecond pulsed electric field (nsPEF). Bioelectromagnetics, 28, 8: 655–663, https://doi.org/10.1002/bem.20354

Pakhomov A. G., Semenov I., Casciola M., Xiao S. 2017. Neuronal excitation and permeabilization by 200-ns pulsed electric field: An optical membrane potential study with FluoVolt dye. Biochimica Et Biophysica Acta - Biomembranes, 1859, 7: 1273–1281, https://doi.org/10.1016/j.bbamem.2017.04.016

Pakhomov A. G., Shevin R., White J. A., Kolb J. F., Pakhomova O. N., Joshi R. P., Schoenbach K. H. 2007b. Membrane permeabilization and cell damage by ultrashort electric field shocks. Archives of Biochemistry and Biophysics, 465, 1: 109–118, https://doi.org/10.1016/j.abb.2007.05.003

Pan F., Vollherbst D. F., Do T., Ridder D. A., Pereira P. L., Kauczor H. U., Macher-Göppinger S., Sommer C. M. 2020. Intra-arterial Injection of Lidocaine as a Cell Sensitizer during Irreversible Electroporation. Journal of Vascular and Interventional Radiology, 31, 5: 831-839.e2, https://doi.org/10.1016/j.jvir.2019.09.029

Pan Q., Hu C., Fan Y., Wang Y., Li R., Hu X. 2020. Efficacy of irreversible electroporation ablation combined with natural killer cells in treating locally advanced pancreatic cancer. Journal of B.U.ON.: Official Journal of the Balkan Union of Oncology, 25, 3: 1643–1649

Park J.-S., Jung T.-S., Noh Y.-H., Kim W.-S., Park W.-I., Kim Y.-S., Chung I.-K., Sohn U. D., Bae S.-K., Bae M.-K., Jang H.-O., Yun I. 2012. The Effect of Lidocaine · HCl on the Fluidity of Native and Model Membrane Lipid Bilayers. The Korean Journal of Physiology & Pharmacology: Official Journal of the Korean Physiological Society and the Korean Society of Pharmacology, 16, 6: 413–422, https://doi.org/10.4196/kjpp.2012.16.6.413

Partridge B. R., Kani Y., Lorenzo M. F., Campelo S. N., Allen I. C., Hinckley J., Hsu F.-C., Verbridge S. S., Robertson J. L., Davalos R. V., Rossmeisl J. H. 2022. High-Frequency Irreversible Electroporation (H-FIRE) Induced Blood-Brain Barrier Disruption Is Mediated by Cytoskeletal Remodeling and Changes in Tight Junction Protein Regulation. Biomedicines, 10, 6: 1384, https://doi.org/10.3390/biomedicines10061384

Pastori C., Nafie E. H. O., Wagh M. S., Mammarappallil J. G., Neal R. E. 2024. Pulsed Electric Field Ablation versus Radiofrequency Thermal Ablation in Murine Breast Cancer Models: Anticancer Immune Stimulation, Tumor Response, and Abscopal Effects. Journal of Vascular and Interventional Radiology, 35, 3: 442-451.e7, https://doi.org/10.1016/j.jvir.2023.11.021

Pavlin M., Leben V., Miklavčič D. 2007. Electroporation in dense cell suspension—Theoretical and experimental analysis of ion diffusion and cell permeabilization. Biochimica et Biophysica Acta (BBA) - General Subjects, 1770, 1: 12–23, https://doi.org/10.1016/j.bbagen.2006.06.014

Peng W., Polajžer T., Yao C., Miklavčič D. 2024. Dynamics of Cell Death Due to Electroporation Using Different Pulse Parameters as Revealed by Different Viability Assays. Annals of Biomedical Engineering, 52, 1: 22–35, https://doi.org/10.1007/s10439-023-03309-8

Perrier D. L., Vahid A., Kathavi V., Stam L., Rems L., Mulla Y., Muralidharan A., Koenderink G. H., Kreutzer M. T., Boukany P. E. 2019. Response of an actin network in vesicles under electric pulses. Scientific Reports, 9, 1: 8151, https://doi.org/10.1038/s41598-019-44613-5

Polajzer T., Jarm T., Miklavcic D. 2020. Analysis of damage-associated molecular pattern molecules due to electroporation of cells in vitro. Radiology and Oncology, 54, 3: 317–328, https://doi.org/10.2478/raon-2020-0047

Potočnik T., Sachdev S., Polajžer T., Maček Lebar A., Miklavčič D. 2022. Efficient Gene Transfection by Electroporation—In Vitro and In Silico Study of Pulse Parameters. Applied Sciences, 12, 16: 8237, https://doi.org/10.3390/app12168237

Pucihar G., Kotnik T., Miklavčič D. 2009. Measuring the Induced Membrane Voltage with Di-8-ANEPPS. Journal of Visualized Experiments, 33: 1659, https://doi.org/10.3791/1659

Pucihar G., Kotnik T., Miklavcic D., Teissié J. 2008. Kinetics of transmembrane transport of small molecules into electropermeabilized cells. Biophysical Journal, 95, 6: 2837–2848, https://doi.org/10.1529/biophysj.108.135541

Rems L., Miklavčič D. 2016. Tutorial: Electroporation of cells in complex materials and tissue. Journal of Applied Physics, 119, 20: 201101, https://doi.org/10.1063/1.4949264

Rems L., Kasimova M. A., Testa I., Delemotte L. 2020. Pulsed Electric Fields Can Create Pores in the Voltage Sensors of Voltage-Gated Ion Channels. Biophysical Journal, 119, 1: 190–205, https://doi.org/10.1016/j.bpj.2020.05.030

Rems L., Viano M., Kasimova M. A., Miklavčič D., Tarek M. 2019. The contribution of lipid peroxidation to membrane permeability in electropermeabilization: A molecular dynamics study. Bioelectrochemistry, 125: 46–57, https://doi.org/10.1016/j.bioelechem.2018.07.018

Ringel-Scaia V. M., Beitel-White N., Lorenzo M. F., Brock R. M., Huie K. E., Coutermarsh-Ott S., Eden K., McDaniel D. K., Verbridge S. S., Rossmeisl J. H., Oestreich K. J., Davalos R. V., Allen I. C. 2019. High-frequency irreversible electroporation is an effective tumor ablation strategy that induces immunologic cell death and promotes systemic anti-tumor immunity. eBioMedicine, 44: 112–125, https://doi.org/10.1016/j.ebiom.2019.05.036

Romito O., Guéguinou M., Raoul W., Champion O., Robert A., Trebak M., Goupille C., Potier-Cartereau M. 2022. Calcium signaling: A therapeutic target to overcome resistance to therapies in cancer. Cell Calcium, 108: 102673, https://doi.org/10.1016/j.ceca.2022.102673

Ross J. A., Roche S. M., Beaugrand K., Schatz C., Hammad A., Ralston B. J., Hanson A. M., Allan N., Olson M. 2024. Assessment of the Effective Tissue Concentrations of Injectable Lidocaine and a Lidocaine-Impregnated Latex Band for Castration in Calves. Animals, 14, 6: 977, https://doi.org/10.3390/ani14060977

Ross W. N., Salzberg B. M., Cohen L. B., Grinvald A., Davila H. V., Waggoner A. S., Wang C. H. 1977. Changes in absorption, fluorescence, dichroism, and birefringence in stained giant axons: Optical measurement of membrane potential. The Journal of Membrane Biology, 33, 1: 141–183, https://doi.org/10.1007/BF01869514

Rossmeisl J. H., Garcia P. A., Pancotto T. E., Robertson J. L., Henao-Guerrero N., Neal R. E., Ellis T. L., Davalos R. V. 2015. Safety and feasibility of the NanoKnife system for irreversible electroporation ablative treatment of canine spontaneous intracranial gliomas. Journal of Neurosurgery, 123, 4: 1008–1025, https://doi.org/10.3171/2014.12.JNS141768

Ruarus A. H., Vroomen L. G. P. H., Puijk R. S., Scheffer H. J., Zonderhuis B. M., Kazemier G., van den Tol M. P., Berger F. H., Meijerink M. R. 2018. Irreversible Electroporation in Hepatopancreaticobiliary Tumours. Canadian Association of Radiologists Journal, 69, 1: 38–50, https://doi.org/10.1016/j.carj.2017.10.005

Ruiz-Fernández A. R., Campos L., Villanelo F., Garate J. A., Perez-Acle T. 2023. Protein-Mediated Electroporation in a Cardiac Voltage-Sensing Domain Due to an nsPEF Stimulus. International Journal of Molecular Sciences, 24, 14: 11397, https://doi.org/10.3390/ijms241411397

Ruiz-Fernández A. R., Campos L., Villanelo F., Gutiérrez-Maldonado S. E., Perez-Acle T. 2021. Exploring the Conformational Changes Induced by Nanosecond Pulsed Electric Fields on the Voltage Sensing Domain of a Ca2+ Channel. Membranes, 11, 7: 473, https://doi.org/10.3390/membranes11070473

Sachs H. G., Stambrook P. J., Ebert J. D. 1974. Changes in membrane potential during the cell cycle. Experimental Cell Research, 83, 2: 362–366, https://doi.org/10.1016/0014-4827(74)90350-4

Sardesai N. Y., Weiner D. B. 2011. Electroporation delivery of DNA vaccines: prospects for success. Current Opinion in Immunology, 23, 3: 421–429, https://doi.org/10.1016/j.coi.2011.03.008

Schmidt B., Bordignon S., Neven K., Reichlin T., Blaauw Y., Hansen J., Adelino R., Ouss A., Füting A., Roten L., Mulder B. A., Ruwald M. H., Mené R., van der Voort P., Reinsch N., Kueffer T., Boveda S., Albrecht E. M., Schneider C. W., Chun K. R. J. 2023. EUropean real-world outcomes with Pulsed field ablatiOn in patients with symptomatic atRIAl fibrillation: lessons from the multi-centre EU-PORIA registry. Europace: European Pacing, Arrhythmias, and Cardiac Electrophysiology: Journal of the Working Groups on Cardiac Pacing, Arrhythmias, and Cardiac Cellular Electrophysiology of the European Society of Cardiology, 25, 7: euad185, https://doi.org/10.1093/europace/euad185

Schwab A., Stock C. 2014. Ion channels and transporters in tumour cell migration and invasion. Philosophical Transactions of the Royal Society B - Biological Sciences, 369, 1638: 20130102, https://doi.org/10.1098/rstb.2013.0102

Seidel S., Garvalov B. K., Acker T. 2015. Isolation and culture of primary glioblastoma cells from human tumor specimens. Methods in Molecular Biology, 1235: 263–275, https://doi.org/10.1007/978-1-4939-1785-3_19

Semenov I., Xiao S., Kang D., Schoenbach K. H., Pakhomov A. G. 2015a. Cell stimulation and calcium mobilization by picosecond electric pulses. Bioelectrochemistry, 105: 65–71, https://doi.org/10.1016/j.bioelechem.2015.05.013

Semenov I., Zemlin C., Pakhomova O. N., Xiao S., Pakhomov A. G. 2015b. Diffuse, non-polar electropermeabilization and reduced propidium uptake distinguish the effect of nanosecond electric pulses. Biochimica et Biophysica Acta (BBA) - Biomembranes, 1848, 10, Part A: 2118–2125, https://doi.org/10.1016/j.bbamem.2015.06.018

Sengel J. T., Wallace M. I. 2016. Imaging the dynamics of individual electropores. Proceedings of the National Academy of Sciences, 113, 19: 5281–5286, https://doi.org/10.1073/pnas.1517437113

Serša G., Čemažar M., Miklavčič D., Rudolf Z. 2006. Electrochemotherapy of tumours. Radiology and Oncology, 40, 3: 163–174

Sharabi S., Bresler Y., Ravid O., Shemesh C., Atrakchi D., Schnaider-Beeri M., Gosselet F., Dehouck L., Last D., Guez D., Daniels D., Mardor Y., Cooper I. 2019. Transient blood-brain barrier disruption is induced by low pulsed electrical fields in vitro: an analysis of permeability and trans-endothelial electric resistivity. Drug Delivery, 26, 1: 459–469, https://doi.org/10.1080/10717544.2019.1571123

Sharabi S., Last D., Guez D., Daniels D., Hjouj M. I., Salomon S., Maor E., Mardor Y. 2014. Dynamic effects of point source electroporation on the rat brain tissue. Bioelectrochemistry, 99: 30–39, https://doi.org/10.1016/j.bioelechem.2014.06.001

Sherba J. J., Hogquist S., Lin H., Shan J. W., Shreiber D. I., Zahn J. D. 2020. The effects of electroporation buffer composition on cell viability and electro-transfection efficiency. Scientific Reports, 10, 1: 3053, https://doi.org/10.1038/s41598-020-59790-x

Silkunas M., Silkuniene G., Pakhomov A. G. 2024. Real-time imaging of individual electropores proves their longevity in cells. Biochemical and Biophysical Research Communications, 695: 149408, https://doi.org/10.1016/j.bbrc.2023.149408

Sugrue A., Maor E., Ivorra A., Vaidya V., Witt C., Kapa S., Asirvatham S. 2018. Irreversible electroporation for the treatment of cardiac arrhythmias. Expert Review of Cardiovascular Therapy, 16, 5: 349–360, https://doi.org/10.1080/14779072.2018.1459185

Sundelacruz S., Levin M., Kaplan D. L. 2009. Role of Membrane Potential in the Regulation of Cell Proliferation and Differentiation. Stem Cell Reviews and Reports, 5, 3: 231–246, https://doi.org/10.1007/s12015-009-9080-2

Tanaka E., Yoshida K., Kawaai H., Yamazaki S. 2016. Lidocaine Concentration in Oral Tissue by the Addition of Epinephrine. Anesthesia Progress, 63, 1: 17–24, https://doi.org/10.2344/15-00003R2.1

Tarek M. 2005. Membrane Electroporation: A Molecular Dynamics Simulation. Biophysical Journal, 88, 6: 4045–4053, https://doi.org/10.1529/biophysj.104.050617

Teissié J., Ramos C. 1998. Correlation between electric field pulse induced long-lived permeabilization and fusogenicity in cell membranes. Biophysical Journal, 74, 4: 1889–1898, https://doi.org/10.1016/S0006-3495(98)77898-1

Teissie J., Tsong T. Y. 1980. Evidence of voltage-induced channel opening in Na/K ATPase of human erythrocyte membrane. The Journal of Membrane Biology, 55, 2: 133–140, https://doi.org/10.1007/BF01871155

Tian H., Davis H. C., Wong-Campos J. D., Park P., Fan L. Z., Gmeiner B., Begum S., Werley C. A., Borja G. B., Upadhyay H., Shah H., Jacques J., Qi Y., Parot V., Deisseroth K., Cohen A. E. 2023. Video-based pooled screening yields improved far-red genetically encoded voltage indicators. Nature Methods, 20: 1082–1094 https://doi.org/10.1038/s41592-022-01743-5

Tieleman D. P. 2004. The molecular basis of electroporation. BMC Biochemistry, 5: 10, https://doi.org/10.1186/1471-2091-5-10

Tsong T. Y. 1991. Electroporation of cell membranes. Biophysical Journal, 60, 2: 297–306, https://doi.org/10.1016/S0006-3495(91)82054-9

Vernier P. T., Levine Z. A., Gundersen M. A. 2013. Water Bridges in Electropermeabilized Phospholipid Bilayers. Proceedings of the IEEE, 101, 2: 494–504, https://doi.org/10.1109/JPROC.2012.2222011

Vernier P. T., Sun Y., Chen M.-T., Gundersen M. A., Craviso G. L. 2008. Nanosecond electric pulse-induced calcium entry into chromaffin cells. Bioelectrochemistry, 73, 1: 1–4, https://doi.org/10.1016/j.bioelechem.2008.02.003

Vižintin A., Miklavčič D. 2022. The electropermeome: cellular response to electroporation. Slovenian Medical Journal, 91: 11–12, https://doi.org/10.6016/ZdravVestn.3267

Wang S., Chen J., Chen M.-T., Vernier P. T., Gundersen M. A., Valderrábano M. 2009. Cardiac myocyte excitation by ultrashort high-field pulses. Biophysical Journal, 96, 4: 1640–1648, https://doi.org/10.1016/j.bpj.2008.11.011

Wang X., Hong T., Liu G., Rao J., Shi F., Wang H., Guo J., Zhuang J. 2025. High-frequency irreversible electroporation suppresses invasion and metastasis by targeting SIRT1/2 in highly invasive tumor cells: an in vitro study. Bioelectrochemistry, 166: 109036, https://doi.org/10.1016/j.bioelechem.2025.109036

Weaver J. C., Chizmadzhev Yu. A. 1996. Theory of electroporation: A review. Bioelectrochemistry and Bioenergetics, 41, 2: 135–160, https://doi.org/10.1016/S0302-4598(96)05062-3

Wegner L. H., Frey W., Silve A. 2015. Electroporation of DC-3F Cells Is a Dual Process. Biophysical Journal, 108, 7: 1660–1671, https://doi.org/10.1016/j.bpj.2015.01.038

Wiczew D., Szulc N., Tarek M. 2021. Molecular dynamics simulations of the effects of lipid oxidation on the permeability of cell membranes. Bioelectrochemistry, 141: 107869, https://doi.org/10.1016/j.bioelechem.2021.107869

Wright S. H. 2004. Generation of resting membrane potential. Advances in Physiology Education, 28, 1-4: 139–142, https://doi.org/10.1152/advan.00029.2004

Xiao D., Tang L., Zeng C., Wang J., Luo X., Yao C., Sun C. 2011. Effect of actin cytoskeleton disruption on electric pulse-induced apoptosis and electroporation in tumour cells. Cell Biology International, 35, 2: 99–104, https://doi.org/10.1042/CBI20100464

Yang L., Craviso G. L., Vernier P. T., Chatterjee I., Leblanc N. 2017. Nanosecond electric pulses differentially affect inward and outward currents in patch clamped adrenal chromaffin cells. PloS One, 12, 7: e0181002, https://doi.org/10.1371/journal.pone.0181002

Yang M., Brackenbury W. J. 2013. Membrane potential and cancer progression. Frontiers in Physiology, 4: 185, https://doi.org/10.3389/fphys.2013.00185

Yang Y., Qin Z., Du D., Wu Y., Qiu S., Mu F., Xu K., Chen J. 2019. Safety and Short-Term Efficacy of Irreversible Electroporation and Allogenic Natural Killer Cell Immunotherapy Combination in the Treatment of Patients with Unresectable Primary Liver Cancer. CardioVascular and Interventional Radiology, 42, 1: 48–59, https://doi.org/10.1007/s00270-018-2069-y

Yarmush M. L., Golberg A., Serša G., Kotnik T., Miklavčič D. 2014. Electroporation-based technologies for medicine: principles, applications, and challenges. Annual Review of Biomedical Engineering, 16: 295–320, https://doi.org/10.1146/annurev-bioeng-071813-104622

Yi Z., Nagao M., Bossev D. P. 2012. Effect of charged lidocaine on static and dynamic properties of model bio-membranes. Biophysical Chemistry, 160, 1: 20–27, https://doi.org/10.1016/j.bpc.2011.08.007

Yool A. J., Brokl O. H., Pannabecker T. L., Dantzler W. H., Stamer W. D. 2002. Tetraethylammonium block of water flux in Aquaporin-1 channels expressed in kidney thin limbs of Henle's loop and a kidney-derived cell line. BMC Physiology, 2, 1: 4, https://doi.org/10.1186/1472-6793-2-4

Younes S., Mourad N., Salla M., Rahal M., Hammoudi Halat D. 2023. Potassium Ion Channels in Glioma: From Basic Knowledge into Therapeutic Applications. Membranes, 13, 4: 434, https://doi.org/10.3390/membranes13040434

Zapata-Morin P. A., Sierra-Valdez F. J., Ruiz-Suárez J. C. 2014. The interaction of local anesthetics with lipid membranes. Journal of Molecular Graphics and Modelling, 53: 200–205, https://doi.org/10.1016/j.jmgm.2014.08.001

Zhang N., Li Z., Han X., Zhu Z., Li Z., Zhao Y., Liu Z., Lv Y. 2022. Irreversible Electroporation: An Emerging Immunomodulatory Therapy on Solid Tumors. Frontiers in Immunology, 12: 811726, https://doi.org/10.3389/fimmu.2021.811726

Zhao M. 2009. Electrical fields in wound healing-An overriding signal that directs cell migration. Seminars in Cell & Developmental Biology, 20, 6: 674–682, https://doi.org/10.1016/j.semcdb.2008.12.009

Zhou D., Wang L., Cui Q., Iftikhar R., Xia Y., Xu P. 2020. Repositioning Lidocaine as an Anticancer Drug: The Role Beyond Anesthesia. Frontiers in Cell and Developmental Biology, 8: 565, https://doi.org/10.3389/fcell.2020.00565

ACKNOWLEDGEMENTS

First and foremost, I would like to express my deepest gratitude to my supervisor Assist. Prof. Dr. Lea Rems for her continuous support, guidance, and encouragement throughout my doctoral studies. Her scientific insight, patience, and willingness to engage in thoughtful discussion have shaped this thesis in many ways. Working with her has been a privilege, and I am sincerely grateful for her trust, dedication, and kindness.

I would also like to thank Prof. Dr. Damijan Miklavčič, the Head of the Research Programme, for his support and for giving me the opportunity to enroll in the PhD programme and to work on many exciting and meaningful projects.

I would like to thank the commission for assessment and defence: Prof. Marko Kreft, Ph.D. (President), Prof. Gregor Serša, Ph.D. (Member), and Assoc. Prof. Alenka Maček Lebar, Ph.D. (Member), for reviewing my dissertation and for their constructive comments, valuable suggestions, and insightful feedback.

My sincere thanks go to all my colleagues and former colleagues at the Laboratory of Biocybernetics for creating a supportive, friendly, and stimulating research environment. I would especially like to thank Lana Balentović, Tamara Polajžer, Tina Cimperman, Tina Turk, and Zala Vidic for the many discussions, shared challenges, and countless moments of laughter that brightened my days. I am grateful that we have met.

I am deeply thankful to my family for their support, encouragement, and belief in me throughout this journey. A heartfelt thank you also goes to my dear friend Tina Anželj, whose kindness, support, and unwavering belief in me — especially in the moments when I doubted myself the most — have meant more than words can express.

Finally, I want to express my profound gratitude to Benjamin for his support, patience, and understanding. Thank you for celebrating every day with me and for finding joy in all the small victories. Your presence has made this path lighter, and I am truly grateful.

ANNEXES

ANNEX A

Acceptance confirmation for publication in Radiology and Oncology

From: RadioloncolJurnal@radioloncol.com <RadioloncolJurnal@radioloncol.com>
Sent: Monday, September 29, 2025 17:14
To: Rems, Lea <lea.rems@fe.uni-lj.si>
Subject: [R&O] Editor Decision

Anja Blažič, Bernarda Majc, Metka Novak, Barbara Breznik, Lea Rems:

We have reached a decision regarding your submission to Radiology and Oncology, "Reversible electroporation enhances invasive properties of patient-derived glioblastoma cells".

Our decision is to: Accept Submission

Please cite this paper as soon and often as possible. Then it will be highly cited by others.

Please note that Radiology and Oncology (http://www.degruyter.com/view/j/raon) is an open access journal, as well as on PubMed (PubMed Central) (http://www.ncbi.nlm.nih.gov/pubmed) and journal's web page (www.radioloncol.com).

Therefore all articles are subject to payment of 1500 EUR + VAT publication fee and will not be published until its payment.

Currently the payment is possible only via Bank transfer. Therefore, send us to the email address: mklemencic@onko-i.si and vkaluza@onko-i.si the following data for preparation of the invoice: name, institution, postal address, VAT

We greatly appreciate that you chose Radiology and Oncology for publication of your valuable work.

Gregor Serša

Editor in chief

ANNEX B

Research data management plan

Research data management plan

Name of the doctoral student: Anja Blažič
Doctoral programme and scientific field: Bioscience, Cell sciences
Proposed title of the doctoral dissertation: Changes in transmembrane voltage regulation due to cell electroporation

Type of data and methods used for data collection or production

1. What data will be collected or produced?
   Experimental data in form of images and numerical data (tables).
2. **How will new data be collected or produced and/or how will existing data be re-used for the purposes of your doctoral thesis?**
   Images of cells in vitro were acquired by optical microscopy using commercial software adapted for the microscope used (i.e., LasX software – Leica Microsystems). Spectrophotometric measurements of absorbance were performed for cell viability studies using dedicated software (i.e., Magellan software – Tecan Trading AG). In addition, flow cytometry data were collected using an Attune NxT Flow Cytometer (Thermo Fisher Scientific), which detected fluorescence emission from labeled cellular markers. The acquired data were analyzed using the corresponding Attune NxT Software for gating, quantification, and export of fluorescence intensity values.
   I did not use existing data for my doctoral thesis.
3. **Will you be dealing with sensitive data? If yes, how will you ensure compliance with ethical requirements when producing and/or creating data?**
   The research involved patient-derived glioblastoma cell lines that had been previously established, anonymized, and stored within the Slovenian GlioBank managed by the National Institute of Biology (NIB). Patients or their authorized representatives had signed informed consent forms in accordance with the Declaration of Helsinki. The collection and processing of tumour tissue material were approved in advance by the National Medical Ethics Committee of the Republic of Slovenia (approval numbers 92/06/12, 0120-190/2018-4, 0120-190/2018-26, 0120-190/2018-32, and 0120-190/2018-35). Since all ethical approvals and patient consents were obtained prior to this doctoral research, no new ethical approvals were required. All data used in the thesis were fully anonymized, and no personal or identifiable patient information was handled.

How data will be stored and protected during research for a doctoral thesis

1. **How will data be stored?**
   Raw data, as well as the results of their postprocessing, is stored on cloud and local hard drive and backed up on a server maintained by the Laboratory of Biocybernetics at the University of Ljubljana, Faculty of Electrical Engineering.
2. **If you will be dealing with sensitive data, how will you keep it safe and secure? (Move to the next question if not applicable)**
   Not applicable.

Long-term data availability and storage

1. **In which data repository will you store the data for the long term after the completion of the research work and make it accessible in accordance with the requirement of Article 50 of the Regulations on Doctoral Studies of the UL?**
   The published research papers have been deposited on the Repository of the University of Ljubljana. In addition, raw RNA-sequencing data have been deposited and are publicly available in the Gene Expression Omnibus (GEO) repository under the accession number GSE305017.
2. **Do you plan to restrict access to the data for a certain period? If yes, please explain the reasons for this (e.g. for intellectual property or patent protection, or other reasons).**
   No.